GALILEO:

EXPLORATION OF JUPITER'S SYSTEM

NASA

GALILEO:

EXPLORATION OF JUPITER'S SYSTEM

1. Report No.	2. Government Accession No.	3. Recipient's Catalog No.
NASA SP-479		

4. Title and Subtitle	5. Report Date
Galileo: Exploration of Jupiter's System	June 1985
	6. Performing Organization Code
7. Author(s)	8. Performing Organization Report No.
T.V. Johnson et al.	
	10. Work Unit No.
9. Performing Organization Name and Address	
Jet Propulsion Laboratory Pasadena, California	11. Contract or Grant No.
	13. Type of Report and Period Covered
12. Sponsoring Agency Name and Address	Special Publication
Office of Space Science and Applications National Aeronautics and Space Administration Washington, DC 20546	14. Sponsoring Agency Code

15. Supplementary Notes

16. Abstract

This book presents the scientific objectives of the Galileo mission to the jovian system. Topics discussed include the history of the project, our current knowledge of the system, the objectives of interrelated experiments, mission design, spacecraft, and instruments. The management, scientists, and major contractors for the project are also given.

17. Key Words (Suggested by Author(s))	18. Distribution Statement
Galileo Jupiter	Unclassified - Unlimited

19. Security Classif. (of this report)	20. Security Classif. (of this page)	21. No. of Pages	22. Price
Unclassified	Unclassified		

N-305

For sale by the National Technical Information Service, Springfield, Virginia 22161

NASA SP-479

GALILEO:

EXPLORATION OF JUPITER'S SYSTEM

C. M. Yeates, Jet Propulsion Laboratory
Galileo Science Manager

T. V. Johnson, Jet Propulsion Laboratory
Galileo Project Scientist

L. Colin, Ames Research Center
Galileo Probe Scientist

F. P. Fanale, University of Hawaii
Satellite Working Group Chairman

L. Frank, University of Iowa
Magnetospheric Working Group Chairman

D. M. Hunten, University of Arizona
Atmospheric Working Group Chairman

NASA Scientific and Technical Information Branch 1985
National Aeronautics and Space Administration
Washington, DC

Library of Congress Cataloging in Publication Data
Main entry under title:

Galileo : exploration of Jupiter's system.

(NASA SP ; 479)
1. Galileo Project. I. Yeates, C. M. II. Galileo Project. III. Series.
QB661.G35 1985 523.4'5 84-16638

For sale by the Superintendent of Documents, U.S. Government Printing Office, Washington, D.C. 20402

Acknowledgments

This book is the result of a great deal of work by many people connected with Project Galileo. We thank all our colleagues on the various Galileo science teams for providing information in their disciplines and for numerous suggestions and reviews of several versions of the manuscript.

We would like to acknowledge the leadership provided by John Casani, Galileo Project Manager, without whose constant encouragement this book would never have been completed.

Contents

chapter 1 THE MISSION OF GALILEO

The outer solar system begins somewhere in the asteroid belt, beyond Mars. The first major outpost of this vast realm is Jupiter, the giant planet. Orbiting at a mean distance of 778 million km from the Sun, Jupiter is the largest of the Sun's family of planetary companions, having a volume approximately 1000 times that of Earth. Jupiter is not merely a single large planet, however; it is the central object and master of a complex system involving four large moons, at least twelve smaller satellites, a ring system, and a powerful magnetic field that influences an immense region of space filled with charged particles of all varieties. It is the archetype of the "miniature solar systems" common to the outer parts of our planetary system—Saturn and Uranus have comparable systems, while Neptune and Pluto possess at least satellites.

Exploration of the outer reaches of our solar system began when the Pioneer 10 spacecraft, launched in 1972, flew past Jupiter in 1973, followed by Pioneer 11 about a year later. The Pioneers' visits were followed in 1979 by the spectacular reconnaissance missions of the two Voyager spacecraft. These terrestrial emissaries, extensions of our Earth-bound senses across more than half a billion kilometers of space, revealed intriguing details about Jupiter's variegated clouds, the large satellites, and the magnetic fields and charged particles surrounding the planet. Long-standing problems were resolved or seen in a new light, many discoveries were made, and totally new questions were raised as the jovian system proved to be even more complex and its members more interrelated than we had previously suspected. Intriguing new worlds of enormous complexity were viewed closely for the first time—volcanically active Io, heavily cratered Callisto, strangely marked Ganymede, and cracked Europa. Through the eyes of Voyager, astronomers saw strange planetary surfaces unlike anything previously envisioned, except perhaps in speculative fiction. Complicated electromagnetic phenomena were encountered in the vast natural laboratory of plasmas and interacting forces that surrounds the giant planet and encompasses many of its large satellites. The jovian system revealed by these preliminary explorations suggested new dimensions of fundamental studies about planets, satellites, the interplanetary medium, and the formation of systems around stars.

But the flyby missions of the Voyagers and the earlier Pioneers could not provide the in-depth long-term measurements needed to resolve the many new questions their discoveries raised. We are still a long way from having the answers required to understand our origins and to meet a very basic human need—obtaining a credible explanation and description of the causes and effects

leading to a solar system and a planet on which life could evolve so highly that it could question its own mode of origin. All civilizations have attempted to answer that question, and of all humankind we today have the best opportunities to probe this issue. One tool that we will use to press this inquiry is a product of our highest technology and advanced scientific capabilities, Project Galileo.

Project Galileo is an innovative, challenging deep-space mission—the most complex flown by the National Aeronautics and Space Administration (NASA) since the Viking program at Mars in 1976. The Galileo spacecraft (figs. 1 and 2) consists of a probe vehicle to penetrate deep into the maelstrom of Jupiter's atmosphere and an orbiter vehicle to traverse the complex magnetosphere of the planet for many months, to observe the planet's changing cloud patterns and atmospheric structure, and to closely scrutinize the major Galilean satellites, those planet-sized worlds that have proven to be so different from the inner planets of the solar system. Project Galileo will be our first chance to make an in-depth study of the jovian system. This is an important distinction. Early deep-space probes were considered "Venus missions" or "Mars missions," but Galileo is not really planet specific—it is a comprehensive survey of the entire jovian system.

Overall project management for Galileo resides with the California Institute of Technology's Jet Propulsion Laboratory in Pasadena, California, which is building the orbiter. Ames Research Center in Mountain View, California, has responsibility for the probe, to be supplied by the Hughes Aircraft Company and the General Electric Company. In addition to the many components built by aerospace firms across the United States, the Federal Republic of Germany is constructing the orbiter's main propulsion system, two complete scientific instruments, and major elements of several others. These are being supplied to NASA free of charge under a cooperative agreement between the United States and the Federal Republic of Germany.

This book details the scientific questions to be addressed by the Galileo mission and discusses how the Galileo spacecraft, mission design, and scientific experiments will work together to unravel the secrets of the jovian system. The first four chapters explore our knowledge of the atmospheres, satellites, and magnetosphere and detail Galileo's projected contributions. Chapters 5 to 7 give a more technical review of mission design, the spacecraft, and the science instruments. Table 1 details the science payload.

History

Project Galileo had its genesis during the mid-1970s, when space scientists and NASA mission planners were considering the next steps in outer planet exploration. By that time Pioneers 10 and 11 had flown past Jupiter, but the Voyager spacecraft had not been launched. Choosing Jupiter as the obvious next target (it is the most readily accessible of the giant planets), space scientists and mission planners realized that an advanced mission should incorporate two vital elements: a probe to descend into the atmosphere and a relatively long-lived orbiter to study the planet, its satellites, and the vast expanse of the jovian magnetosphere. Such a mission was developed by NASA and approved by Congress in 1977. Although originally called Jupiter Orbiter-Probe, the program was soon renamed Project Galileo to honor the Italian astronomer who discovered the four large satellites of Jupiter that now bear his name.

Galileo was designed to be the first American planetary mission to ride the space shuttle, a decision that subsequently proved troublesome. When development and schedule problems plagued the shuttle and upper-stage rocket during 1979-1982, the Galileo Project underwent a number of frustrating and costly delays in launch date, originally slated for January 1982. The configuration evolution caused by these delays is shown in figure 3. Now, with the shuttle operational and the development of a modified, more powerful Centaur upper-stage rocket underway, Galileo is scheduled for launch in May 1986.

Getting There

For launch, the Galileo spacecraft, orbiter plus probe, will be attached to the top of a modified Centaur rocket, the same basic hydrogen-fueled upper stage that was used for the Surveyor, Viking, Pioneer, and Voyager launches. This time, however, instead of being mounted in turn on a

Figure 1. The Galileo spacecraft—orbiter and probe—on the way to the giant planet Jupiter and an in-depth exploration of the complex jovian planetary system.

larger, first-stage booster rocket, the entire spacecraft–Centaur combination will be loaded into the shuttle's cargo bay for its trip into Earth orbit. Figure 4 shows the launch sequence. After achieving orbit, the astronauts will open the cargo bay doors and deploy the rocket and its precious payload (fig. 5). At this stage Galileo will resemble a butterfly emerging from its cocoon, with all its appendages, booms, and antennas still folded up to fit within the dimensions of the cargo bay. Once the deployment is accomplished, the shuttle will back away to a safe distance, about four nautical miles, and the Centaur's computer will take over the launch sequence. Approximately 45 minutes after deployment, as the Centaur enters the proper "window" in space and time for injection into an interplanetary Jupiter transfer trajectory, the rocket's computers will command the engines to ignite and Galileo will be on its way toward the giant planet.

After successful injection on its path toward Jupiter, the Galileo spacecraft will still have a series of complex steps to perform to transform itself into a functioning planetary robot. Still attached to the now spent Centaur, the spacecraft will be spun up slowly to about 0.1 rpm for stabilization, and the interplanetary "butterfly" will begin to spread its wings as its main antenna—a fine gold-plated

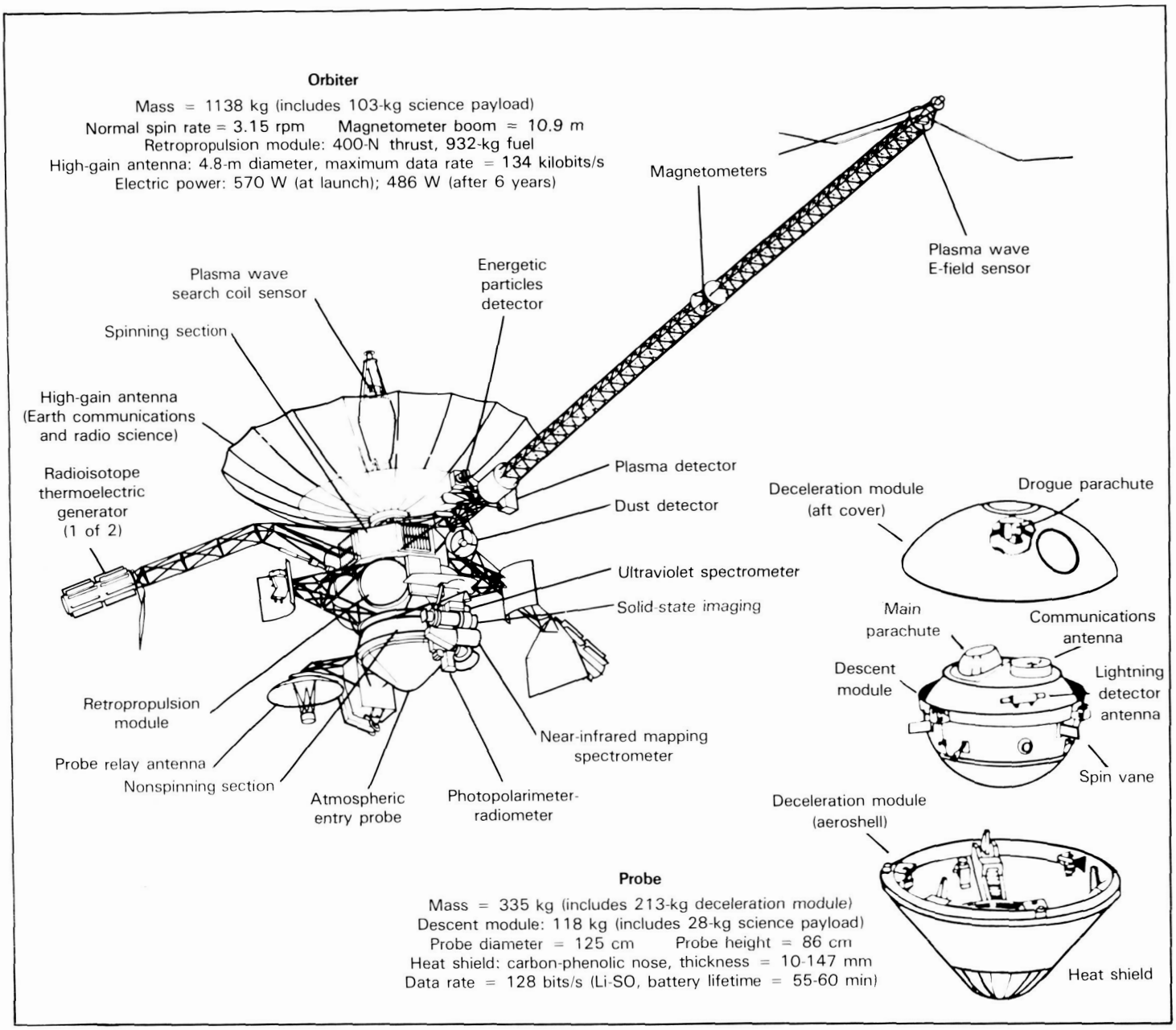

Figure 2. Galileo orbiter and probe.

mesh supported by an umbrella-like structure—unfolds and the three main booms snap into place. The spacecraft will then be spun up to 3 rpm. The final step in freeing the spacecraft from Earth will occur when the metal band attaching the spacecraft to the spent rocket is fractured by an explosive ring. From that point, Galileo will be an independent entity, and the long process of checking out its various systems and functions and preparing for arrival at Jupiter will begin.

Galileo will arrive in the vicinity of Jupiter after an interplanetary transit of a little more than two years (fig. 6). Figure 7 presents a schedule of major mission events. One hundred and fifty days before its arrival at Jupiter, the probe will be separated from the orbiter and will head straight for the planet, while the orbiter will back off to fly in formation as both spacecraft drop into the jovian gravity well.

Finally, some time in late 1988, the pair will reach their destination and begin a flurry of intense activities (fig. 8). As the orbiter passes within 1000 km of the volcanic moon Io, the probe will plunge toward the swirling cloud tops girdling Jupiter's equator. A few hours later the orbiter will reach a point 230 000 km from the planet and begin relaying to Earth precious data being radioed by the probe as it descends by parachute into the atmosphere. About an hour after the probe completes its transmission, the orbiter's retrorocket will

burn for about 46 minutes. This firing, in combination with the gravitational effect of the close Io flyby, will ease the orbiter into a long, looping jovian orbit with a period of 200 days.

As the spacecraft recedes from Jupiter along this path, scientists will have already begun to analyze the hour-long spurt of data gathered by the probe, and our in-depth exploration of the jovian system will be truly underway. In the next 20 months, the orbiter will orbit Jupiter eleven times, making a close flyby of a Galilean satellite in each orbit, using the gravity of the satellites to adjust its flight path, and studying the planet and its rings, satellites, and magnetosphere.

Scientific Objectives

The entire design of the Galileo mission is dictated by the many-faceted and interrelated nature of the jovian system (appendix C and fig. 9). Subsequent chapters detail our current knowledge concerning the three major components of the system: the planet, the major satellites, and the magnetosphere. These chapters also outline some of the main questions in these areas and the advances that we hope to make with the many Galileo investigations.

Most of Galileo's science goals are underlaid by our view of Jupiter as a system that holds clues to conditions in the early solar system at the time of planet formation 4.6 billion years ago, the processes that initially modified and shaped the newly formed planetary bodies, including Earth, and the processes that are still active today, ranging from volcanic activity on Io to astrophysical plasma processes in the vast magnetosphere. Also, although most investigations can be classified as relating to atmospheric, satellite, or magnetospheric

Science Objectives of the Galileo Mission

Atmosphere

- Determine the chemical composition
- Determine the structure to a depth of at least 10 bars
- Determine the nature of the cloud particles and location and structure of cloud layers
- Determine the radiative heat balance
- Investigate the circulation and dynamics
- Investigate the upper atmosphere and ionosphere

Satellites

- Characterize the morphology, geology, and physical state of the surfaces
- Investigate the surface minerology and surface distribution of minerals
- Determine the gravitational and magnetic fields and dynamic properties
- Study the atmospheres, ionospheres, and extended gas clouds
- Study the magnetospheric interactions of the satellites

Magnetosphere

- Characterize the energy spectra, composition, and angular distribution of energetic particles throughout the magnetosphere to 150 R_J
- Characterize the vector magnetic fields throughout the magnetosphere to 150 R_J
- Characterize the plasma energy spectra, composition, and angular distribution throughout the magnetosphere, including plasma wave phenomena, to 150 R_J
- Investigate satellite–magnetosphere interactions

Table 1. Galileo's Scientific Payload

Experiment	Mass (kg)	Range	Objectives
Probe			
Atmospheric Structure Instrument (ASI)	4	Temp.: 0-540 K Pres.: 0-28 bars	Determine temperature, pressure, density, and molecular weight as a function of altitude
Neutral Mass Spectrometer (NMS)	11	Covers 1-150 AMU	Determine chemical composition of atmosphere
Helium Abundance Detector (HAD)	1	Accuracy: 0.1%	Determine relative abundance of helium
Nephelometer (NEP)	5	0.2-20-μm particles, as few as 3/cm^3	Detect clouds and infer states of particles (liquid versus solid)
Net-Flux Radiometer (NFR)	3	6 infrared filters from 0.3 to >100 μm	Determine ambient thermal and solar energy as a function of altitude
Lightning and Energetic Particles (LRD/EPI)	2	Fisheye lens sensors; 1 Hz-100 kHz	Verify the existence of lightning and measure energetic particles in inner magnetosphere
Orbiter			
Solid-State Imaging (SSI)	28	1500-mm, f/8.5 800 x 800 CCD, 8 filters, 0.47° field of view	Map Galilean satellites at roughly 1-km resolution, and monitor atmospheric circulation over 20 months while in orbit around planet
Near-Infrared Mapping Spectrometer (NIMS)	18	0.7-5.2-μm range, 0.03-μm resolution	Observe Jupiter and its satellites in the infrared to study satellite surface composition, jovian atmospheric composition and temperature
Ultraviolet Spectrometer (UVS)	4	1150-4300 angstroms	Measure gases and aerosols in jovian atmosphere
Photopolarimeter-Radiometer (PPR)	5	Discrete visible and near-infrared bands, radiometry to >42 μm	Determine distribution and character of atmospheric particles; compare flux of thermal radiation to incoming solar levels
Magnetometer (MAG)	7	32-16,384 gammas	Monitor magnetic field for strength and changes
Energetic Particle Detector (EPD)	9	Ions: 0.020-55 MeV Electrons: 0.015-11 MeV	Measure high-energy electrons, protons, and heavy ions in and around jovian magnetosphere
Plasma Detector (PLS)	12	1 eV to 50 keV in 64 bands	Assess composition, energy, and three-dimensional distribution of low-energy electrons and ions
Plasma Wave (PWS)	6	6-31 Hz, 50 Hz-200 kHz, 0.1-5.65 MHz	Detect electromagnetic waves and analyze wave-particle interactions
Dust Detector (DDS)	4	10^{-16}-10^{-6} g, 2-50 km/s	Measure particles' mass, velocity, and charge
Radio Science (RS): Celestial Mechanics	—	S- and X-band signals	Determine mass of Jupiter and its satellites (uses radio system and high-gain antenna)
Radio Science (RS): Propagation	—	S- and X-band signals	Measure atmospheric structure and objects' radii (uses radio system and high-gain antenna)

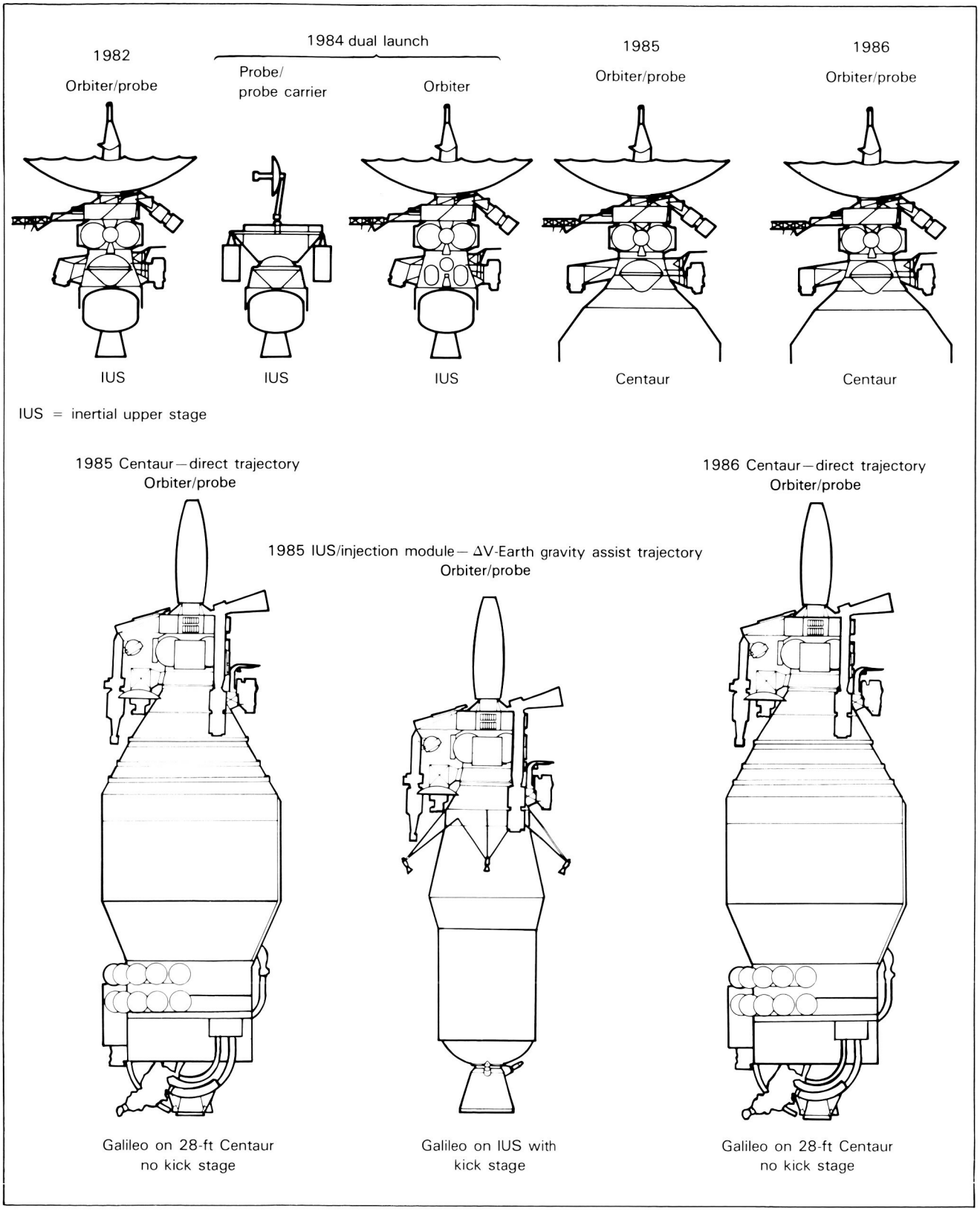

Figure 3. Configuration contrasts for the various mission designs resulting from adapting the mission to different launch modules and launch dates.

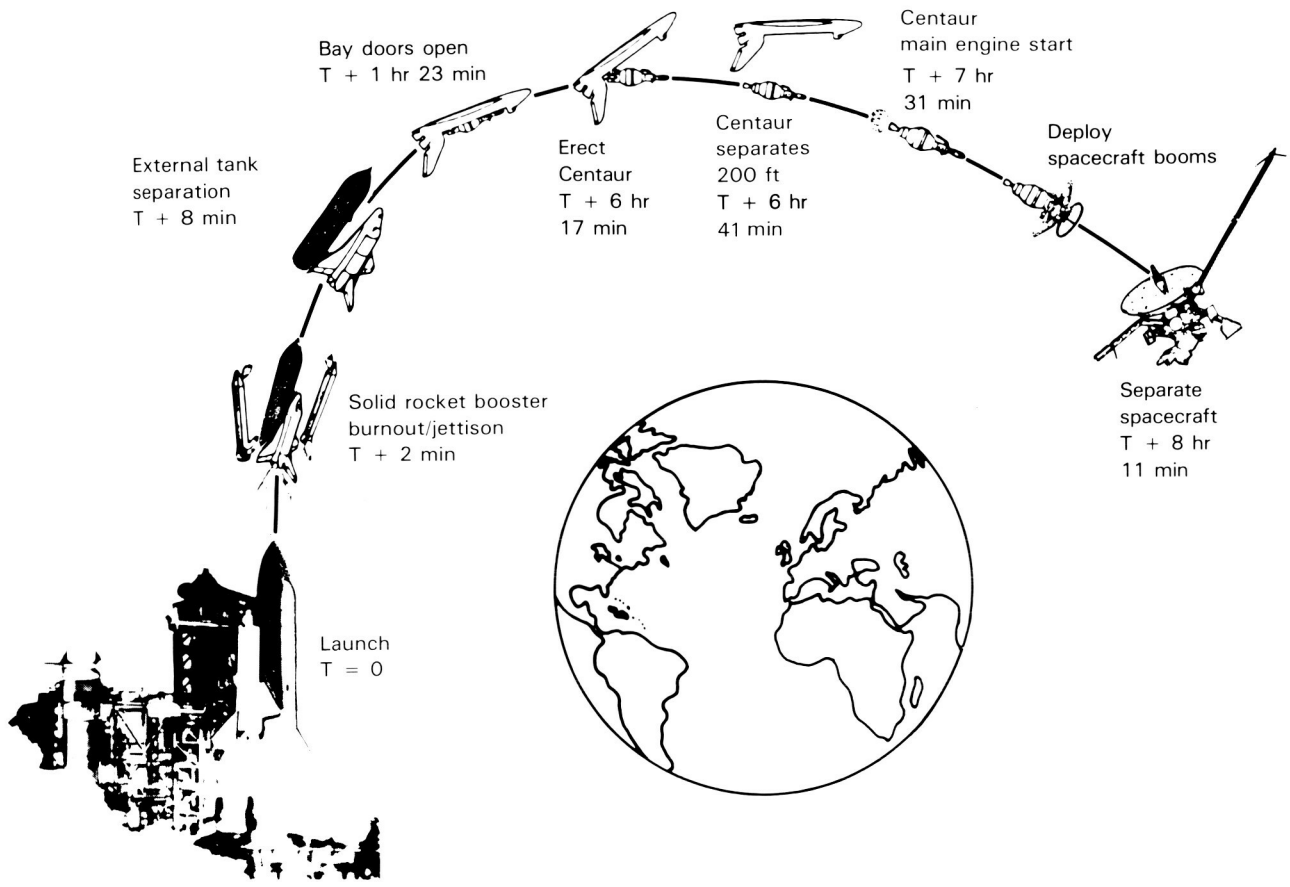

Figure 4. Launch deployment sequence.

science, it should be recognized that these areas are frequently very closely related, either directly by the processes that link them or indirectly through inferences about one or more of them drawn from study of another.

Origins

At the heart of our hopes to learn more about the early solar system from study of the jovian system are the similarities and the differences between this system and the solar system as a whole. The obvious analogy between the planets orbiting the Sun and the large moons circling Jupiter was in fact one of the most important conceptual aspects of the discovery of the moons by Galileo in 1610, leading to acceptance of the Copernican Sun-centered theory. However, our modern discoveries and understanding of the system suggest that this analogy is both more profound and more complicated than a mere similarity in the appearance of the orbits of the planets and satellites. We now know that early Jupiter was in many ways Sun-like or star-like. Even now, it is composed almost entirely of hydrogen and helium under extreme temperatures and pressures. Although it was too small to achieve the critical values of temperature and pressure necessary to ignite the fusion processes that power the stars, Jupiter apparently was quite hot and luminous during a brief period in its early history and still emits about twice as much energy as it receives from the Sun, as residual heat energy still flows out of the planet's deep interior. (This was true of Saturn only to a token extent.) Since the satellites are believed to have formed some time during this period of high luminosity, their strikingly different characteristics have been explained as a function of their proximity to Jupiter, just as the inner planets are affected by their positions near the early Sun.

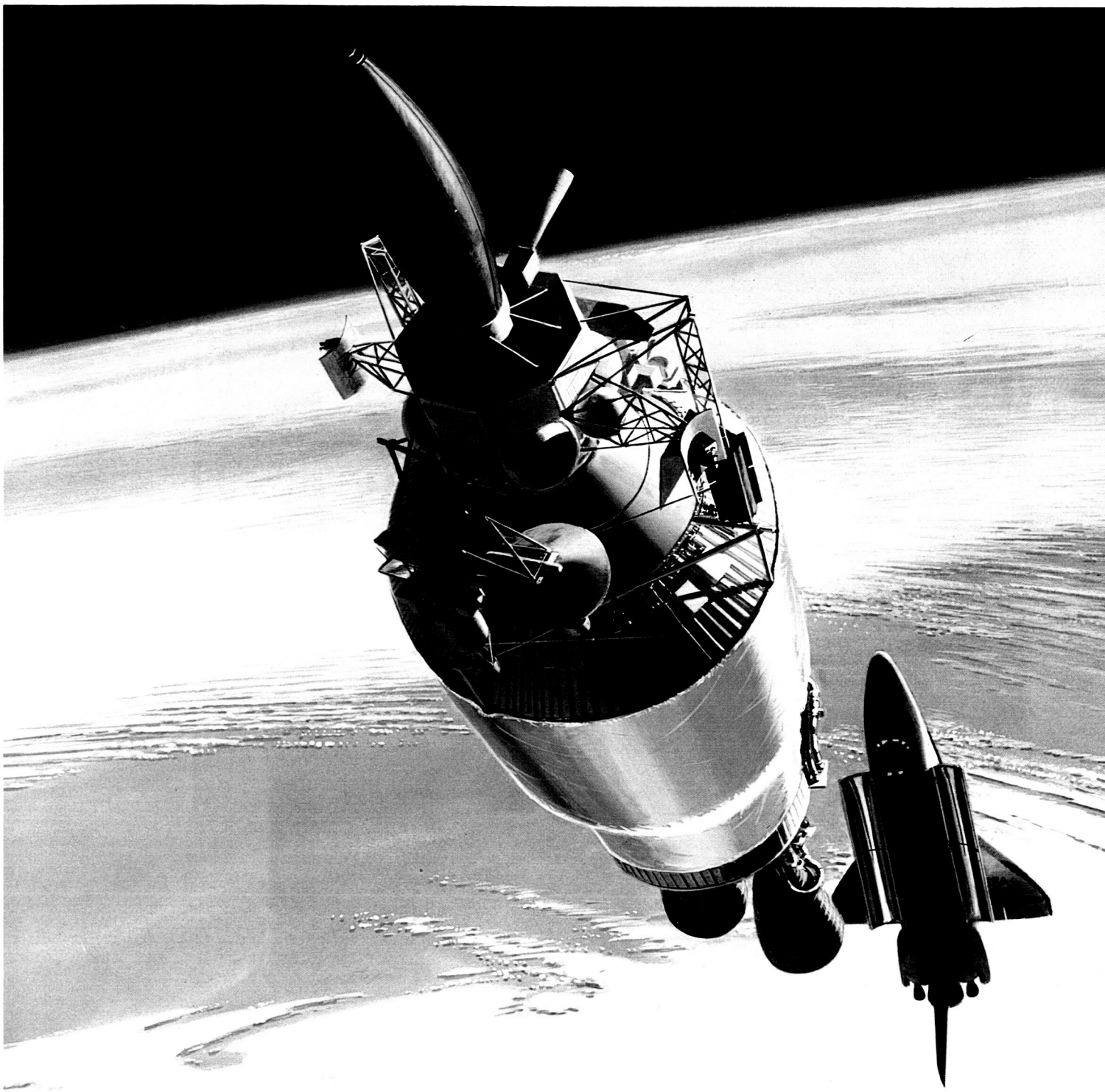

Figure 5. Shuttle-Centaur deployment. (Photo courtesy of General Dynamics/Convair)

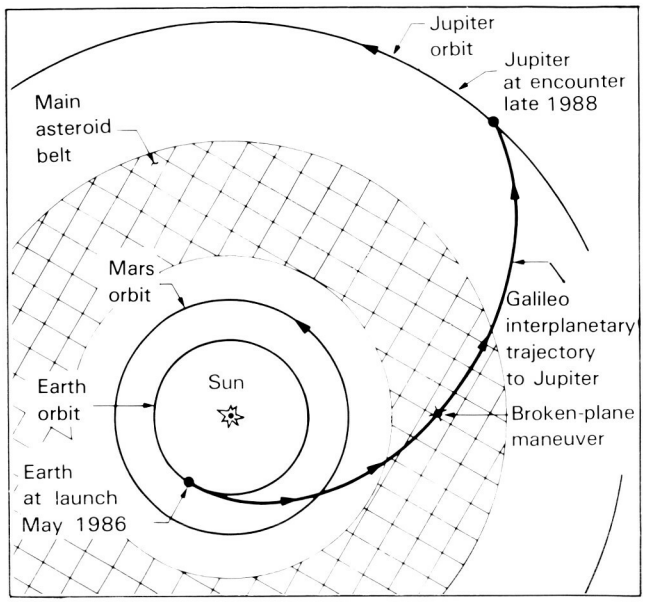

Figure 6. Trajectory to Jupiter showing location of a broken-plane maneuver to arrive at Jupiter above the ecliptic plane as required for mid-1980 trajectories.

Figure 7. Major mission events.

1986	May - Launch
1987	February - Broken-plane maneuver
1988	July - Probe release
	December - Encounter/Jupiter orbit insertion/relay
1989	July - First flyby of Ganymede
	October - Second flyby of Ganymede
	November - First flyby of Callisto
1990	January - Third and fourth flybys of Ganymede
	February - First flyby of Europa
	March - Second flyby of Europa
	May - Third flyby of Europa
	June - Second flyby of Callisto
	July - Fifth flyby of Ganymede
	October - End of tour

There obviously are not one-to-one relationships between the processes which formed the planets and those which formed Jupiter's satellite system. Different time scales, the smaller distances involved, and the effects of the details of Jupiter's formation and early evolution may have caused profound differences in chemical and physical processes affecting the formation of the satellite system. Although we suspect that Jupiter dominated conditions in its local vicinity, many other processes occurring in the early solar nebula, such as the intense bombardment by planetesimals that is believed to have occurred about 3.5 billion years ago, also would have altered conditions around Jupiter. In spite of these inevitable complications, however, we expect to learn much about the conditions in the primitive solar nebula and the effects of various planet formation processes from a study of Jupiter's atmosphere and the satellites. In particular, we believe that the composition of Jupiter's atmosphere, its major and minor components and isotopic ratios, may tell us about the original star stuff from which all the planets formed. Our current knowledge concerning the atmospheric composition and the formation of satellites, along with some of the many investigations in these areas we expect to undertake with the Galileo mission, is discussed in chapters 2 and 3.

The Planet

In addition to giving us clues about the conditions in the early solar nebula, Jupiter's atmosphere is a major area of study in its own right. We are interested in the current state of the atmosphere, the composition of its clouds, the variation of temperature and pressure with depth, the strength of the winds, the driving forces behind its meteorology, and the characteristics of the lightning that Voyager observed flashing on the night side of the planet. Answers to these and other questions will not only tell more about Jupiter as a planet, but will also advance our understanding of the nature of all planetary atmospheres, including our own. Chapter 2 discusses the atmospheres in detail.

The Satellites

The nature of the satellites, particularly their composition, tells us many things about the conditions around Jupiter during the period of planet

formation. The satellites are also, of course, individual worlds, each with its own unique characteristics and history. As such, they provide us with a fascinating set of natural "experiments" concerning the effects of initial conditions, size, energy sources, meteorite bombardment, and tectonic processes on the way planets evolve. From volcanically active, sulfurous Io to cold, battered Callisto, the Galilean satellites provide the Galileo mission with rich material for planetologic study. Some of what we hope to learn from the satellites is discussed in chapter 3, along with studies of the other material orbiting Jupiter: small satellites, dust, and rings.

The Magnetosphere

Jupiter possesses the strongest magnetic field and most complex magnetic environment of any planet known. The magnetosphere is that huge volume of space in which the jovian field dominates the environment, excluding for the most part the effects of the outflowing solar wind. The scale of this structure is truly impressive, enclosing a volume many times larger than the Sun; if it were visible from Earth it would appear to the eye as large as the full Moon. Inside the magnetosphere we find complex structures filled with electrons, protons, and the charged ions of oxygen and sulfur. Some of these particles, particularly the oxygen and sulfur, originate at Io and are continuously injected into a doughnut-shaped region surrounding Jupiter known as the Io torus. Ions in this torus radiate immense amounts of ultraviolet energy. The energy is continually replenished by magnetospheric processes that heat the torus ions. These ions and others from the solar wind and perhaps the ionosphere of Jupiter are spread throughout the magnetosphere and are subject to various acceleration and diffusion processes. Many

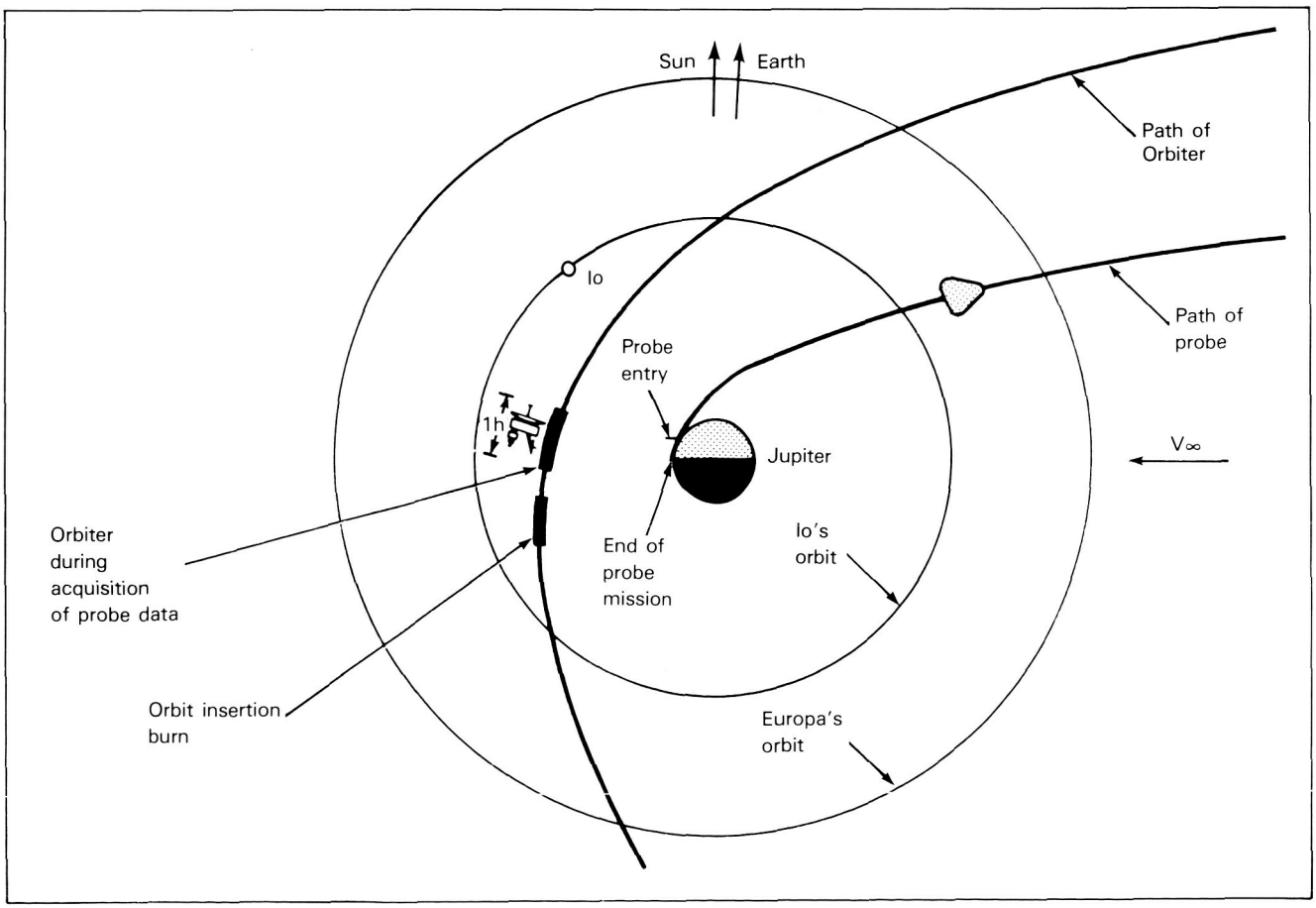

Figure 8. Arrival geometry.

of these processes have been studied on a smaller scale in Earth's magnetosphere; some are unique to Jupiter; all are of great interest to scientists attempting to understand the complex interplay of magnetic forces and matter throughout the universe. Jupiter is in effect a relatively convenient laboratory of astrophysics, where once again nature will provide us with many answers if we can ask the right questions. Chapter 4 details our current understanding of magnetospheric phenomena and addresses the many investigations Galileo will carry out to further our understanding of this complex part of the jovian system.

Finally, although we have many detailed ideas about what we expect Galileo to accomplish, it should be remembered that the most exciting results from exploratory missions are frequently totally unanticipated. Galileo, with its array of sophisticated instrumentation (fig. 2) and two-year mission about Jupiter, is designed to give us excellent opportunities to investigate the unexpected.

Investigations of Opportunity

Any time we send a spacecraft out from Earth, particularly on as long as voyage as Galileo's, opportunities arise to perform science investigations not directly related to the main objectives of the mission. These opportunities usually result from the fact that the spacecraft must traverse vast reaches of interplanetary space before arriving at its destination, from the long duration of the mission, or from some fortuitous combination of spacecraft and planetary geometry. As with previous missions, Galileo will attempt to take advantage of a number of these "investigations of opportunity."

Gravity Wave Detection

One of the opportunities recognized at the time experiments were selected for Galileo is the possibility of using certain types of radio tracking data to search for gravity waves propagating through the solar system. This investigation takes advantage of the great distance of the Galileo spacecraft from Earth during most of its mission and the tremendous sensitivity of the tracking data from NASA's Deep Space Network. Gravity waves have never been unambiguously detected by physicists, although they are a necessary consequence of Einstein's theory of general relativity; the problem lies in the fact that these waves are "coupled" in an extremely weak way to ordinary matter and only very violent astrophysical events are capable of perturbing the space-time continuum sufficiently to produce waves of detectable amplitude. Events of the necessary scale, such as the collapse of massive black holes or a collision of galaxies, are believed to be relatively infrequent and thus difficult to "catch" with short-lived experiments.

Galileo's gravity radiation experiment relies on the fact that a large-amplitude gravity wave passing through the solar system will produce an anomalous doppler signal as the distance between the spacecraft and the ground station varies ever so slightly. The greater accuracy of such doppler measurements has been further enhanced on Galileo by modifications in the X-band radio receiver. Even with this improved sensitivity, Galileo will only be able to detect waves from the most violent types of astrophysical catastrophes. For example, the Galileo search could marginally detect gravitational radiation resulting from the collision of two massive black holes in the center of our own Milky Way galaxy. The chances of actually seeing such signals are regarded as very small by most experts; however, there remain tremendous uncertainties in many of the theoretical estimates of these probabilities and the amplitudes of the resulting gravity waves. If the Galileo search does detect something, it will be an event of great significance for the entire astrophysical science community, and even if the results are negative, they can be used to set new upper limits on the frequency and amplitudes of possible gravity wave phenomena as well as to refine techniques for even more sensitive experiments in the future.

Cruise Science

Any planetary spacecraft with magnetospheric instrumentation usually attempts to make measurements of the interplanetary medium, the solar magnetic field, and the solar wind structure on its way to its final destination. These measurements are useful for both continuing study of this medium and providing needed instrument performance and calibration information prior to beginning the main portion of the mission. Although not originally included as part of the Galileo mission, such measurements are now planned. This results in part from the requirements

ORIGINAL PAGE
COLOR PHOTOGRAPH

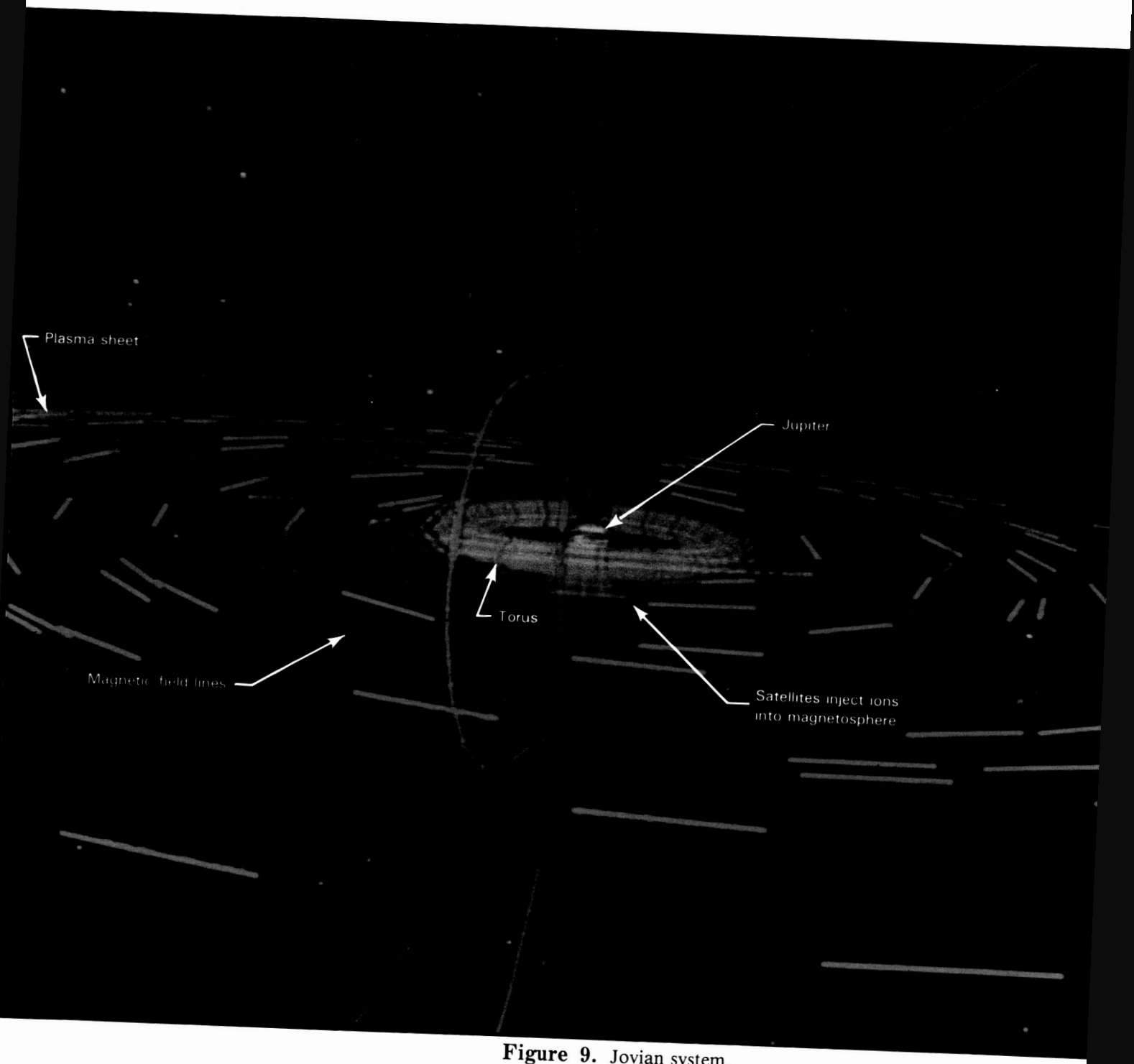

Figure 9. Jovian system.

for calibration data and in part from the development of an agreement with the Federal Republic of Germany that provides for periodic tracking of Galileo using a German tracking station and the provision of the data records to all interested experimenters.

Asteroid or Comet Encounters

Since the Galileo spacecraft will cross the asteroid belt en route to Jupiter, it is not unreasonable to expect that a close flyby of one or more of the asteroids might be possible. A preliminary search for such possibilities has been carried out using computer catalogs of main-belt asteroids, comets, and Earth-crossing asteroids, about 4000 possible targets in all. From this initial search, several promising targets have been identified, including Amphitrite, an S-class asteroid. This asteroid could in principle be approached very closely by Galileo if the spacecraft's trajectory were altered somewhat from the optimum path to Jupiter. No decision has been made about whether to make an attempt; the effects of the extra fuel expenditure on other Galileo science objectives and the cost and risk to the mission of performing such a flyby have still to be evaluated in detail. Meanwhile, further opportunities are being sought, and Galileo may well have an opportunity to take a close look at an asteroid in late 1986 or early 1987.

Mission Design and the Orbital Tour

While the probe's success is keyed to its ability to penetrate the jovian atmosphere, the orbiter's success depends on its unique trajectory, which provides for unprecedented new measurements. Once captured by Jupiter's gravity, the orbiter would repeat its initial 200-day orbit if nothing were done; this would allow several Voyager-like passes through the system before the spacecraft "died" from radiation effects or actually dropped at its low point into the atmosphere due to gravitational perturbations of the Sun. For Galileo to be utilized more effectively during its limited lifetime, the orbital period must be shortened and the spacecraft targeted to make very close flybys of the Galilean satellites.

If this had to be accomplished by rocket propulsion, the mission would be impossible—too much fuel (and weight) would be required to do the necessary maneuvers in Jupiter's strong gravitational field. Fortunately, mission designers have found a way to fly a very demanding, complicated mission using little fuel. They will manage this trick by employing the gravity-assist technique that successfully redirected the Voyagers and other spacecraft as they swung by various planets along their routes.

In the case of Galileo, a celestial 11- or 12-cushion billiard shot will be set up, using the gravity of the massive Galilean moons to modify the orbiter's course during each pass. This simultaneously sends the craft on toward the next encounter and provides extremely close approaches to the satellites for scientific measurements. As a result, the entire "satellite tour" can be flown so that rockets need supply only about 100 m/s of velocity change—60 times less than what would be needed without the satellites' help!

Chapter 5 provides an in-depth look at how this complex mission is designed and how it responds to the numerous requirements placed on it by the science objectives.

The Spacecraft and Instruments

To accomplish the many objectives of Galileo's jovian exploration, some new concepts in spacecraft design and instrumentation are required. Based on earlier Pioneer, Voyager, and Mariner systems, Galileo also takes advantage of the latest microcomputer electronics, improved solid-state imaging systems for both the visual and infrared portions of the spectrum, and very-high-speed entry technology for the probe.

For the orbiter, one important innovation is its "dual spin" design, with the antenna and certain instrument booms rotating about three times per minute while another instrument platform and the spacecraft's aft portion remain fixed in inertial space. This means that the orbiter can easily accommodate both magnetospheric experiments (which perform best when rapidly swept through large angles) and telescopic remote sensing experiments (which require very accurate and stable pointing). Also, instead of utilizing a central computer as did previous planetary spacecraft, Galileo uses dozens of microcomputers scattered among its subsystems and experiments to provide unprecedented operational flexibility.

On its spinning portion, the orbiter has instruments to measure Jupiter's magnetic field, the charged particles and plasmas trapped in the

magnetosphere, and the electromagnetic and electrostatic waves propagating through this environment. One new instrument will examine the frequency and paths of micrometeoroids near Jupiter. Investigators will use the spacecraft's radio system to probe Jupiter's atmosphere and to search for atmospheres on the satellites. In general, these newer instruments have greater sensitivity, energy range, and angular resolution than their Voyager counterparts.

The nonspinning portion carries four instruments on a pointable mounting boom (the scan platform) that are all new in one way or another. A photopolarimeter-radiometer will measure the polarization of light scattered from Jupiter's clouds and the satellites' surfaces, and its infrared channels will sound the atmosphere and measure satellite temperatures. An ultraviolet spectrometer will operate from wavelengths of 1150 to 4300 angstroms (from just below the radiation from neutral hydrogen in the Lyman-alpha band to the blue end of the visible spectrum). The near-infrared mapping spectrometer is a newly developed instrument designed to map the satellites in 200 spectral channels and discern any compositional variation across their surfaces. It will also study cloud structure and gas composition in the jovian atmosphere.

The most familiar scan-platform instrument—a TV camera—is also included. Its optical portion (actually a telescope with a focal length of 1500 mm) is a Voyager spare, but the sensor electronics are entirely new. Instead of using a conventional TV vidicon tube, Galileo's camera has a charge-coupled device at its focal plane. The charge-coupled device is a 1 cm^2 silicon "chip" containing 640 000 individual diode sensors in an 800 by 800 array. It is over 100 times more sensitive than Voyager's vidicons and can "see" out to about 9000 angstroms in the near infrared.

Galileo's probe is similar in concept to those on the 1977 Pioneer Venus mission, incorporating experiments to measure temperature and pressure along the descent path, locate major cloud decks, and analyze the chemistry of atmospheric gases. In addition, the probe will attempt to detect and study jovian lightning both by looking for optical flashes and by listening for the radio "static" they generate. The latter detector will also measure high-energy electrons close to Jupiter just prior to atmospheric entry.

Slowing the probe as it "hits" the atmosphere presents a crucial engineering challenge. Unlike the Pioneers' relatively low entry speed at Venus (12 km/s), the Galileo probe will be greatly accelerated by Jupiter's immense gravitational pull and will strike the atmosphere at about 50 km/s—more than 160 000 km/hr! Its deceleration to about Mach 1—the speed of sound—should take just a few minutes and will cause a tremendous buildup of heat in the probe's protective covering. These entry conditions, far more severe than those faced by returning Apollo astronauts, cannot be simulated in conventional wind tunnels. New facilities at NASA's Ames Research Center were required to test heat shield materials, which make up approximately half the overall weight of the probe.

On the brighter side, once it survives its fiery entry, the probe will operate in a more benign environment than did its Pioneer predecessors. It will not have to cope with corrosive sulfuric acid clouds or the furnace-like temperatures at Venus' surface. Jupiter's atmosphere is primarily hydrogen and helium, of little consequence to the spacecraft or its parachute, and for most of the descent the probe will be immersed in gases at or below room temperature. Eventually, however, it will sink below the visible clouds, where rising pressure and temperature will take their toll.

More detailed information about the spacecraft design is found in chapter 6; instruments are discussed individually in chapter 7.

chapter 2 ATMOSPHERES

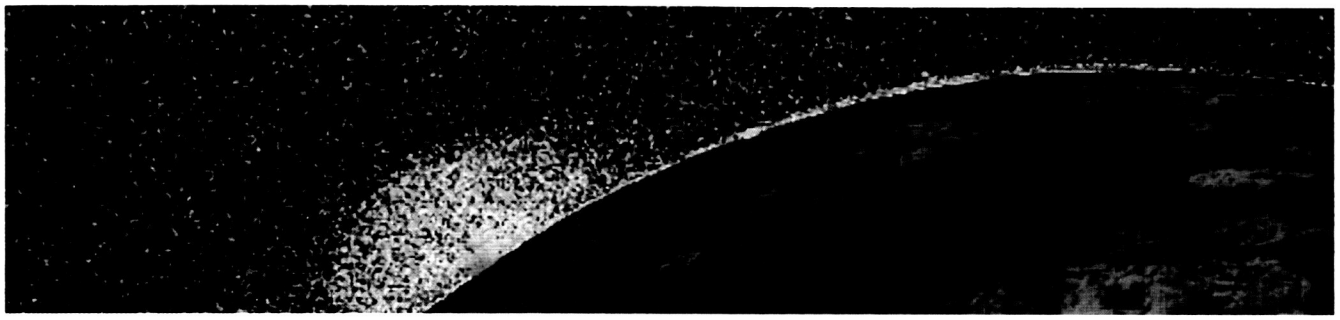

Jupiter is the prototype of the four "jovian planets," grouped with Saturn, Uranus, and Neptune. Although each is unique, as a group they differ sharply from the terrestrial planets in that they are much larger but have much smaller mean densities. Mercury, Venus, Earth, Moon, and Mars can all be regarded as composed of a varying mixture of rock and iron. Similar material probably is buried in the cores of the jovian planets, but it is surrounded by huge envelopes of gas, principally hydrogen and helium. Small proportions of the hydrides of carbon, nitrogen, and oxygen [methane (CH_4), ammonia (NH_3), and water (H_2O)] are also present. All three are observed in Earth-based spectra of Jupiter, but the less volatile ones (H_2O and NH_3) disappear from view in the other, colder planets, undoubtedly because they condense to form clouds at levels too deep to be seen.

Some of these clouds are readily visible from Earth and have been studied in detail by the Voyagers (fig. 10). A wide range of meteorologic phenomena has been studied from Earth and other spacecraft and will be studied further by Galileo. Figure 11 summarizes current ideas about the clouds and deeper levels.

The term "structure" for an atmosphere refers to a description of pressure, density, and temperature as functions of height. Cloud density and composition are sometimes included. Once the composition is known, most of the other quantities can be derived from the temperature profile, along with the equation of state, represented in many cases by the ideal gas law (the relationships among temperature, pressure, and volume obeyed by an idealized gas).

The following sections correspond to the three areas discussed above: composition, meteorology, and structure. A fourth section discusses satellite atmospheres. In each area the present state of knowledge is summarized; the major open questions are then discussed, along with Galileo's expected contributions to their solutions.

Composition

Early measurements of the ratios of helium (He), carbon (C), and nitrogen (N) to hydrogen (H) at Jupiter gave values close to those for the Sun and, along with the obvious rarity of rock and iron relative to gas, encouraged the view that the compositions of Jupiter and the Sun are indeed identical. The Voyager results for He are still in agreement with this concept, but current analyses of Jupiter's methane spectrum show an overabundance of carbon compared to solar values by a factor of 2 to 3. Similar factors are derived from gravity data for the rocky core. Water, on the other

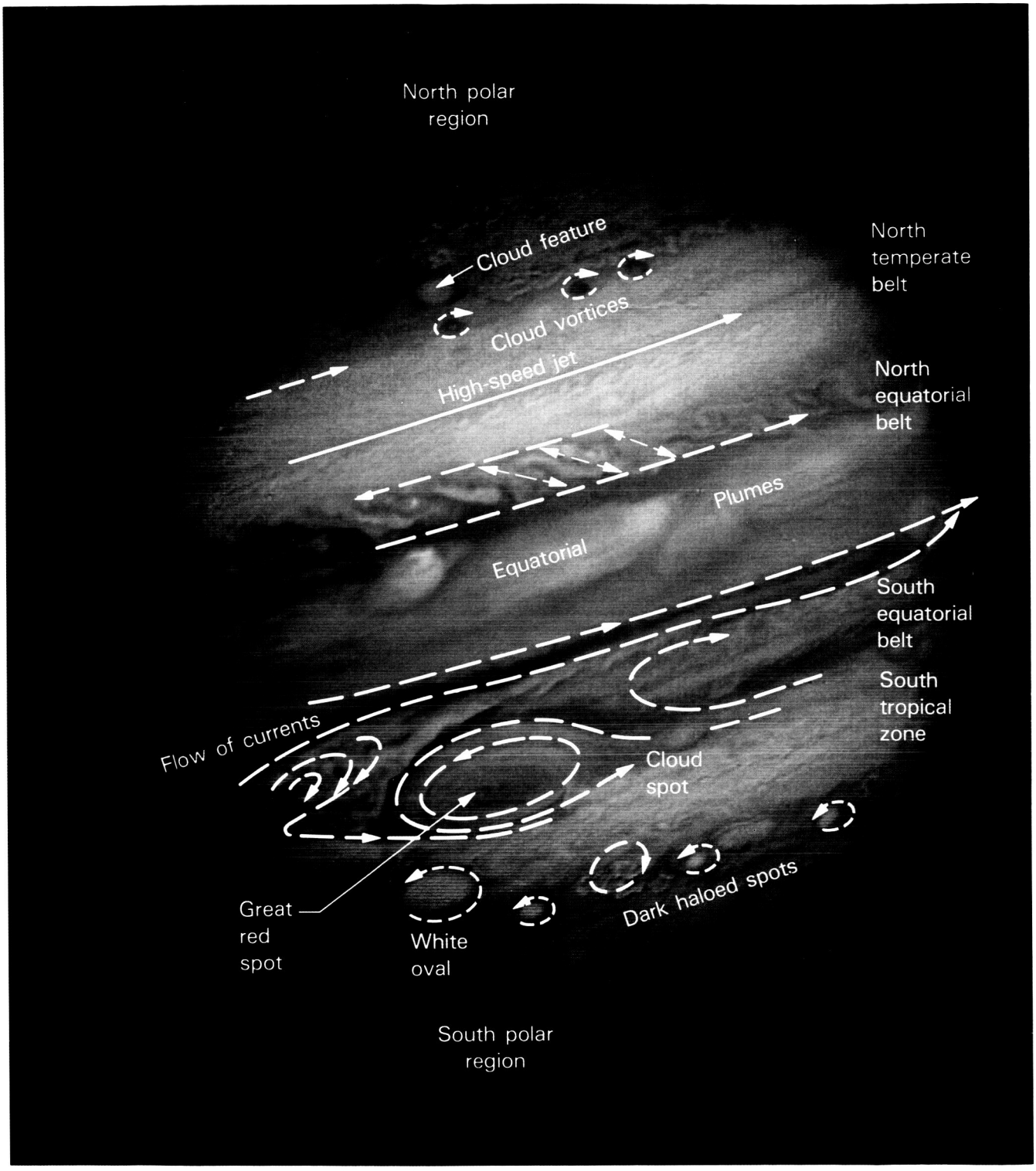

Figure 10. Observed close up, the patterns of the clouds provide much information about the complex dynamics of the jovian atmosphere.

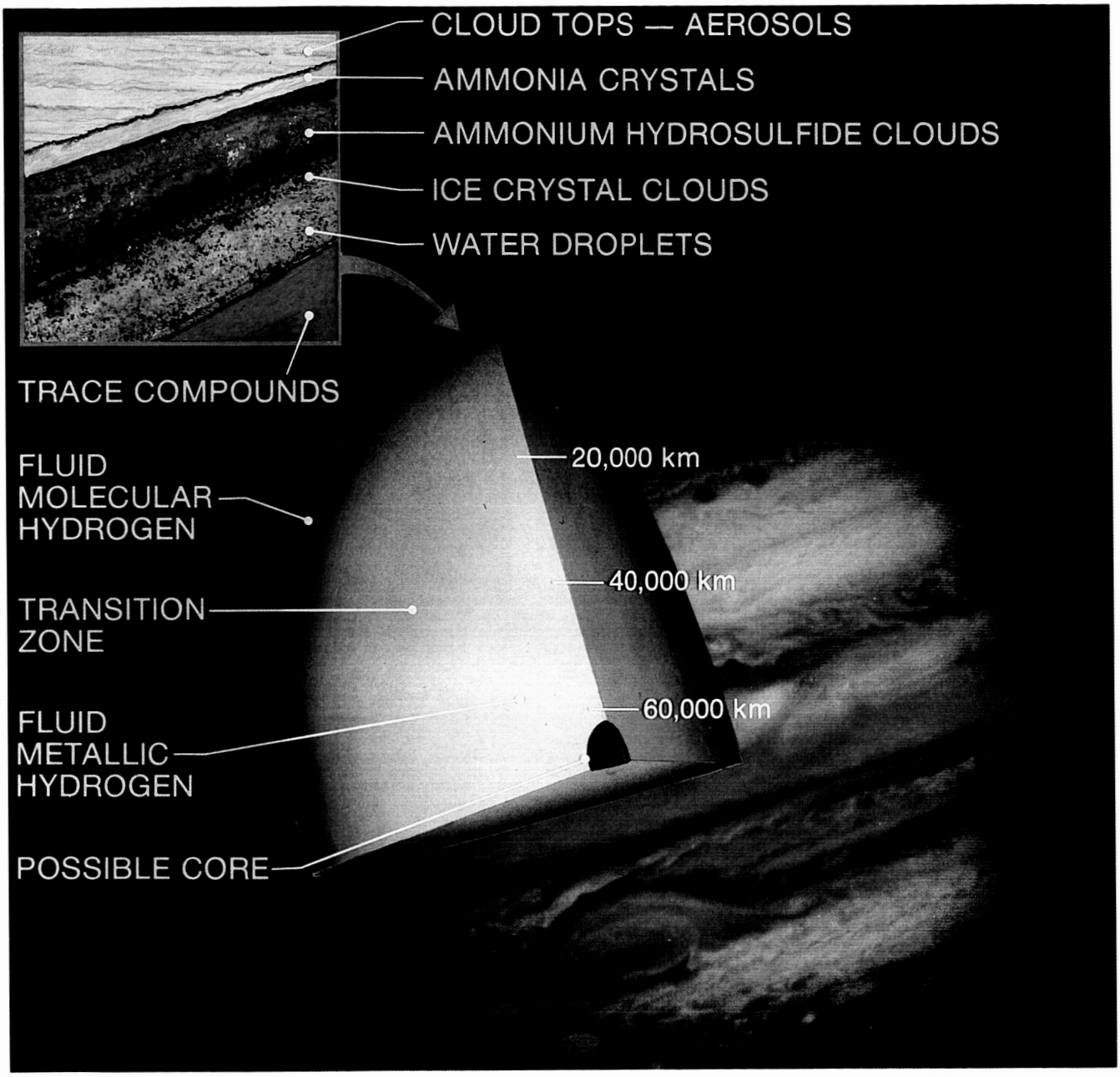

Figure 11. Theoretical cross-section of Jupiter indicates current concepts of the structure of the interior and the atmosphere and identifies the cloud layers. The probe will drop through the cloud layers indicated in the inset.

hand, is apparently underabundant by more than a factor of 100. This molecule can be seen, however, in only a few special cloud-free regions which undoubtedly contain strong downdrafts and which would therefore be expected to have dried out. The average H_2O abundance is thus still very uncertain. The NH_3 abundance in the visible atmosphere is also greatly affected by cloud formation, and although ammonia can be detected at radio frequencies at deeper levels, the mixing ratio remains uncertain.

Theoretical studies of cloud formation in an atmosphere of solar composition predict three main cloud layers above the pressure range of 10 to 20 atmospheres (figs. 11 and 12). Near 0.6 atmosphere there should be a "cirrus" of ammonia crystals. At about 6 atmospheres, a dense cloud of water and ice is predicted, and in between these layers there may be a cloud of ammonium hydrosulfide (NH_4HS).

Important clues to the origin of a planet come from isotopic ratios, which are only very slightly affected by the planet's subsequent chemical evolution. Two such ratios have been measured for Jupiter: carbon 13 to carbon 12, which is the same as on Earth, and deuterium (heavy hydrogen) to hydrogen, which requires a rather uncertain correction in the mathematical analysis but is found to be only one-fifth the terrestrial value. Low values are also seen in other parts of the galaxy and may represent the initial ratio for the solar system. Noble (inert) gases are of even greater interest, but their isotopic ratios cannot be measured remotely from space.

A number of molecules, of which ethane (C_2H_6) is typical, are detected in the infrared. There is also a pervasive high-altitude aerosol, or smog, which darkens the whole planet in the ultraviolet. Such substances are expected to be produced from methane by the action of solar ultraviolet light. Lightning has also been suggested from time to time as an energy source for similar processes, but most scientists doubt that the strength of this source is at all competitive with direct sunlight.

A persistent mystery is the nature of the agent that colors the clouds. The yellow color may be due to phosphorus, sulfur compounds, or some unspecified organic compounds.

Generally speaking, the methods of remote sensing have reached their limits in the area of composition. Quantitative spectroscopy is frustrated by the need to allow for clouds whose structure and properties are poorly known and inhomogeneous. Little information can be obtained below the cloud level. Many constituents of great interest, especially N_2 and the noble gases, cannot be detected at all. These considerations were crucial when the Galileo mission was formulated with an entry probe as an integral part of the concept. The principal analytic instrument on the probe is a mass spectrometer. Because of the particular cosmologic importance of helium, there is another instrument,

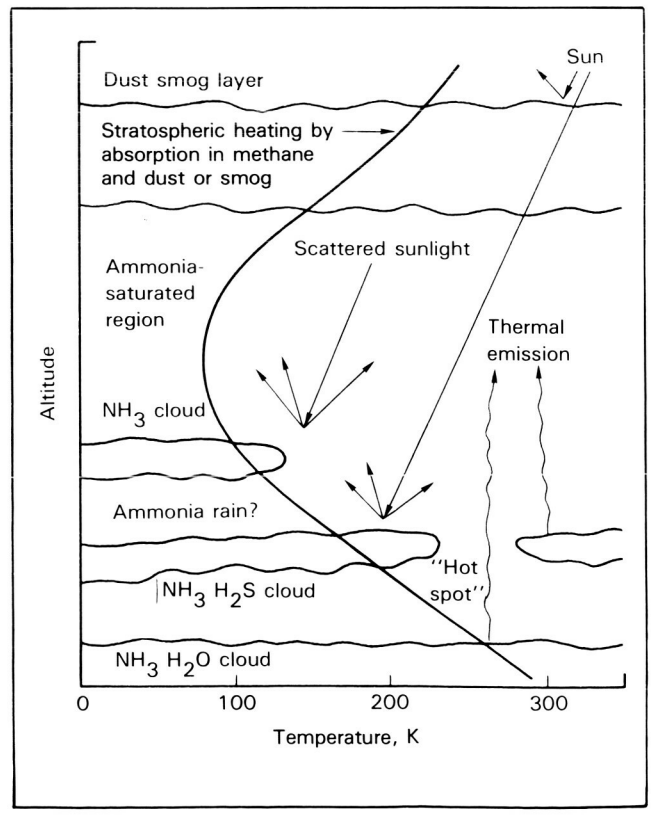

Figure 12. Radiation absorption and emission processes in the jovian atmosphere. Incident sunlight is scattered by atmospheric molecules (Rayleigh scattering) and reflected by clouds. Thermal emission in the NIMS spectral range emanates from the lower clouds and atmospheric molecules. As this sunlight or thermal radiation traverses the atmosphere, absorption by the molecules produces characteristic spectral signatures.

the helium abundance detector, devoted to this one measurement. Descriptions of both instruments may be found in chapter 7.

The neutral mass spectrometer measures neutral gas species by ionizing them in an electron beam and selecting particular ion masses by a carefully tailored combination of fixed and oscillating electrical fields. The necessary high vacuum is produced by pumps within the instrument. The gas is introduced through a very small aperture or "leak" after passing through a complex, miniaturized plumbing and valving system. An approximation of the expected composition, expressed for solar abundances, is presented in tables 2 and 3. The minimum detectable mixing ratio, or fraction of gas present, is about 10^{-8}, but may be considerably greater at some masses because of residual gas in the instrument or other ions of the same mass. The third column in the tables indicates some of these potential problems and likely remedies. For example, ammonia is very scarce at high altitudes, so molecules with which it interferes are best measured there. The instrument measures three kinds of samples: the unprocessed atmosphere, a sample with all but noble gases removed, and a sample of complex molecules from which the rest of the gas has been removed. Such molecules may therefore be measured even if their original mixing ratio was well below 10^{-8}. In the noble gas sample, the proportions should be: helium, 1.0; neon, 1.7×10^{-3}; argon, 6.3×10^{-5}; krypton, 2×10^{-8}; xenon, 3 to 20×10^{-9}. Excellent isotopic ratios should be obtained for the three lightest gases and at least abundances for krypton and xenon.

Table 2. Gross Atmospheric Composition

Dominant Isotope

Gas	Mixing Ratio	Interference/ Solution[a]
Molecular hydrogen	0.89	
Helium	0.11	
Water	1.47×10^{-3}	
Methane	0.83×10^{-3}	Ammonia/height dependence
Ammonia	1.74×10^{-4}	
Hydrogen sulfide	2.83×10^{-5}	
Argon-36	1.77×10^{-6}	Hydrogen sulfide/ fragmentation, purification
Neon-20	0.66×10^{-4}	

Isotope Ratios Accessible in this Range

Ratio	Expected Value	Interference/ Solution
D/H	1.5×10^{-5}(?)	
$^{3}He/^{4}He$	1.4×10^{-5}(?)	HD/ionizing energy, hydrogen removal
$^{18}O/^{16}O$	2.1×10^{-3}	Ne/ionizing energy
$^{13}C/^{12}C$	1.1×10^{-2}	NH_3/measure early
$^{15}N/^{14}N$	3.6×10^{-3}	
$^{22}Ne/^{20}Ne$	1.2×10^{-1}(?)	
$^{34}S/^{32}S$	4.4×10^{-2}	Ar/pattern, energy
$^{38}Ar/^{36}Ar$	1.9×10^{-1}	H_2S/measure early

[a]Solutions refer to sequences of measurements and/or techniques of operating the mass spectrometer.

Table 3. Less Abundant Species

New Species

Gas	Mixing Ratio	Interference/ Solution[a]
Phosphine	6×10^{-7}	Hydrogen sulfide/ measure early, pattern
Hydrochloric acid	6×10^{-7}	Argon, hydrogen sulfide/pattern, ionizing energy
Hydrogen fluoride	6×10^{-8}	Neon, water/ionizing energy, pattern

Isotope Ratios Accessible in this Range

Ratio	Expected Value	Interference/ Solution
$^{20}Ne/^{21}Ne$	329(?)	
$^{35}Cl/^{37}Cl$	3.1	Argon, hydrogen sulfide/ionizing energy, altitude
$^{32}S/^{33}S$	125	Phosphine/pattern, ionizing energy

[a]Solutions refer to sequences of measurements and/or techniques of operating the mass spectrometer.

The helium abundance detector is an interferometer that measures the refractive index of an atmospheric sample after trace gases have been removed. The measurement is accurate enough to give the helium mole fraction to 0.1 percent of the total, much more accurate than can be expected from a mass spectrometer.

No matter how deep it goes or how sophisticated its instruments, the probe will sample only one place on Jupiter. Instruments on the orbiter will be used to determine the context of the entry location and to relate the results to the rest of the planet. The principal tools will be images in all available passbands, near-infrared spectral maps from the near-infrared mapping spectrometer, and polarimetry by the photopolarimeter-radiometer related mainly to cloud struture. The ultraviolet spectrometer will explore the atmosphere mainly at altitudes much higher than those feasible for most of the probe measurements. Species that can be monitored with the near-infrared mapping spectrometer include ammonia, phosphine, water vapor, and germanium. Methane can be observed but is not expected to be variable, since it mixes well. Galileo will also search for molecules that so far have not been found in the jovian atmosphere.

A radio occultation will occur shortly after probe entry and Jupiter orbit insertion. The occultation will sound the atmosphere at nearly the same latitude as the probe but at a considerably different longitude. Nevertheless, these results should be extremely valuable for comparison with, and extension of, the probe data.

Meteorology

Jupiter is over ten times the diameter of Earth and spins about two and a half times faster. These differences are reflected in the visual appearances of the two planets. On Earth, the cloud patterns at middle latitudes are dominated by cyclonic storms, with a generally circular or spiral pattern. On Jupiter, the basic pattern is one of belts (less cloudy) and zones (more cloudy) arranged parallel to the equator (fig. 10). At a finer level of detail there are anticyclonic features, notably the Great Red Spot (fig. 13). Other local features, such as white ovals, brown barges, and white plumes, are of special interest. From these we may be able to learn much about atmospheric dynamics and cloud physics and composition. The Great Red Spot, for instance, may involve convection that brings material up from depths which are far from conditions of local thermochemical equilibrium. The equatorial plumes could be a type of cirrus anvil cloud arising from moist penetrative convection. The brown barges are holes in the clouds through which measurements can be made to relatively great depths.

The Voyager images produced a wealth of data on the horizontal flows at cloudtop level for latitudes to 60° north and south and on correlations with horizontal variations in cloud structure. Cloud-tracked winds indicate both horizontal variations in cloud structure and horizontal shear between zonal currents which appear conducive to the development of barotropic eddies. Measured eddy motions between zonal currents, if interpreted two dimensionally, appear to be able to accelerate the high-speed jetstreams observed in the atmosphere. Wave phenomena are apparent on a wide variety of length scales, from a series of equatorial plumes circling the entire planet and very large white anticyclones (thousands of kilometers across) in the middle latitudes down to periodic cloud forms with wavelengths of tens of kilometers. The most important limitation in all of the Voyager meteorologic data is, however, that they are essentially confined to one atmospheric level. This arises because Voyager's imaging system observed over broad spectral ranges confined to the visual part of the spectrum and because the planet is completely covered with clouds.

A tremendous variety is seen in the texture of the cloud tops, and the differences are correlated with local features such as ovals and with large-scale structures such as the equatorial region jets and reversing currents. Correlations between global and local scales include the regular spacing of plume clouds in the equatorial region. The images also show that the Great Red Spot and the white ovals are anticyclonic, while the dark barges and some of the irregular features preceding and trailing the ovals are cyclonic. Voyager imaging provided an extensive descriptive catalog of the morphology of the cloud tops and correlations with local and global dynamic behavior.

Lightning on Earth is produced by charges generated and separated in cumulonimbus clouds (ice-water convective clouds initiated by vertical moist static instability). Collisions between water and ice cause some particles to become charged

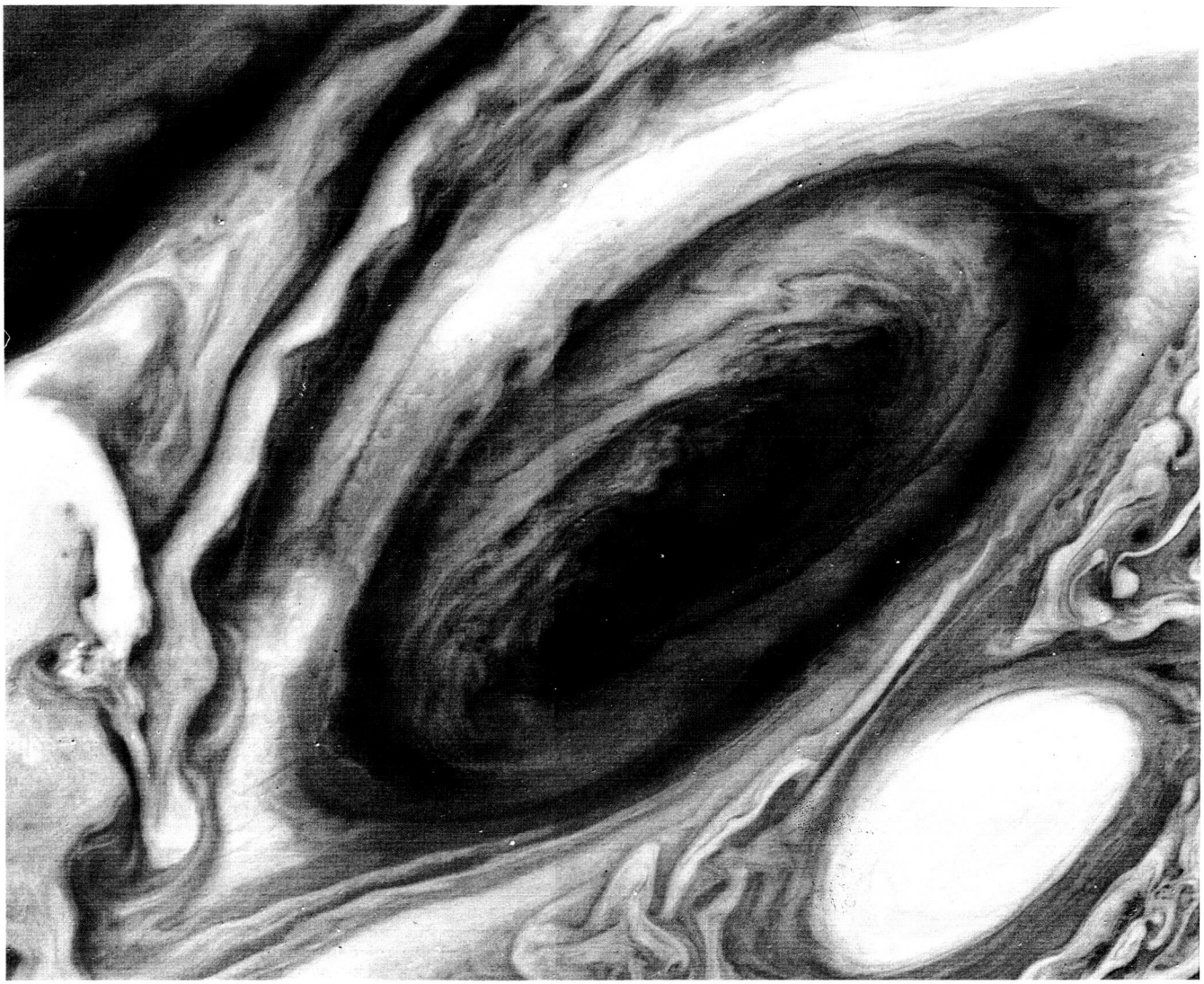

Figure 13. The Great Red Spot is an example of local features of the jovian atmosphere, the study of which is important to understanding the dynamics involved on a planetary as well as a local scale.

positively and others to become charged negatively. Most lightning discharges in Earth's atmosphere occur within a cloud cell and neutralize tens of coulombs of charge. Cloud-to-ground lightning transfers negative charge from the bottom of the cloud to Earth's surface.

A similar dynamic regime may exist on Jupiter and may be responsible for the lightning detected by Voyager (figs. 14 and 15). That lightning does occur on Jupiter implies that vertical instabilities occur, and this has important implications for the large-scale atmospheric dynamics at the levels where the flashes occur. Questions now concern the frequency and global distribution of the lightning flashes and the sizes of individual storms and their locations. More details will be furnished by the lightning and radio emission detector on the probe. The range of detection by this instrument is estimated to be about 10 000 km from the probe's entry point. The data will be obtained during the entire descent of the probe, below the jovian ionosphere, and inside and below dense cloud

systems. The lightning and radio emission detector will provide information about the radio frequency noise spectrum, and will record statistics on the pulse amplitudes, widths, spacing, and shapes. The number and location of the lightning cells, the scale size of the cloud turbulence, and evidence for precipitation can then be deduced. Comparisons with terrestrial lightning characteristics will provide information about the energy content of the jovian lightning discharges.

Virtually all current results that pertain to horizontal winds are strictly two dimensional in nature. However, atmospheric dynamics depend on vertical differences in physical and chemical properties of the atmosphere and on the full three-dimensional patterns of fluid motion that compensate any imbalance of energy, particularly from equator to pole and from interior to exterior. An important contribution of Galileo imaging will be to probe the critical third dimension of Jupiter's static and dynamic structure. This will be made possible by the spectral capabilities of the new imaging device.

The Galileo camera will observe Jupiter throughout a wider range of wavelengths than possible before. Representative and special regions of Jupiter's atmosphere will be selected for detailed

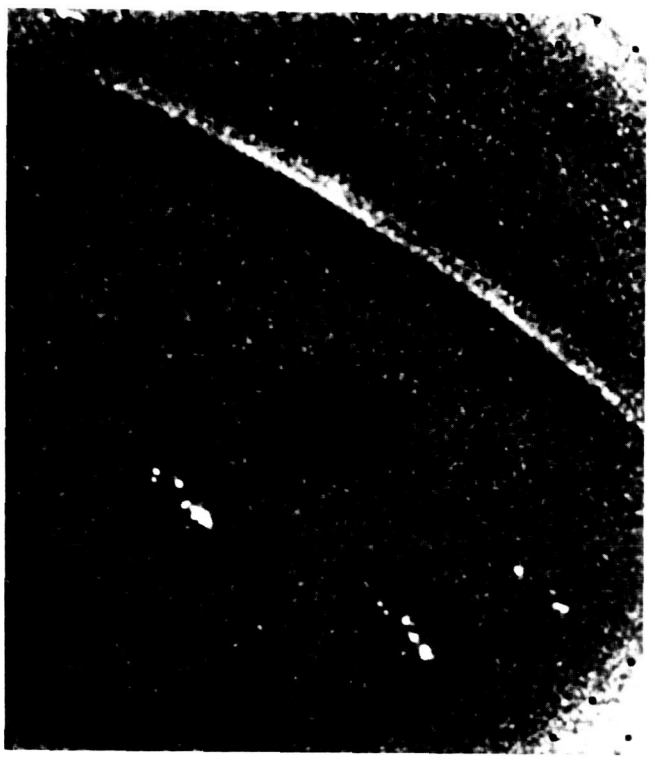

Figure 14. The Voyager spacecraft discovered lightning flashes and auroral emissions on Jupiter's night side.

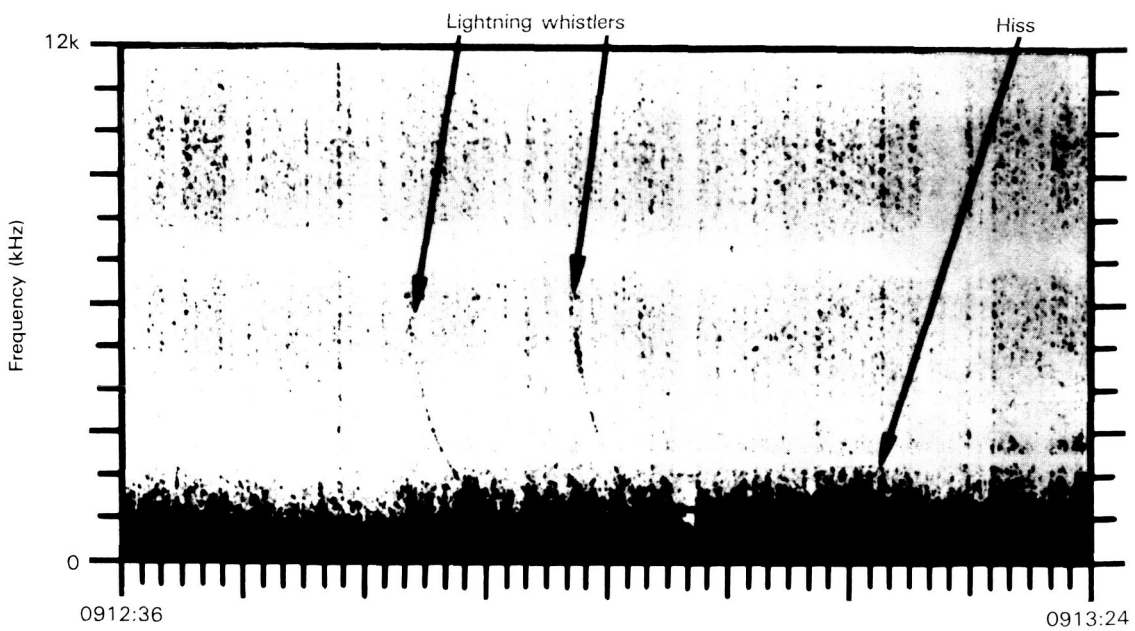

Figure 15. Voyager 1 observed whistlers from lightning in the jovian atmosphere on March 5, 1979, at 5.8 R_J.

study. Each region will be viewed through three or four filters every ten minutes during a period of several hours while the rotation of the planet carries the region across the face of Jupiter from morning to evening. To find out how the observed motions and inferred vertical structure change over long periods, the sequence will be repeated six or seven hours later, when the same region can be viewed again from the spacecraft. These picture sequences will be made when the spacecraft is close to Jupiter on the sunlit side, and they will resolve features as small as 30 km across. They will also be used to produce short color movies so that the motions can be readily appreciated and studied.

By using the different camera filters, we will be able to identify distinct cloud layers below the visible cloud tops. For example, the response of the charge-coupled device to near-infrared radiation (less than 10 000 angstroms) makes it possible to obtain images in spectral "windows" where absorptions due to methane modify the effective altitude being imaged. Photographs in the strongest methane band at 8900 angstroms will provide details of the atmosphere at a level above the widespread ammonia clouds. Those taken at the weaker 7250-angstrom band will show ammonia cloud features and permit observations between the clouds to levels at which the jovian atmosphere is at a higher pressure than Earth's atmosphere at sea level. In other regions of the visible spectrum, the camera will record light reflected from still greater depths, providing there are breaks in the cloud cover. By comparing pictures of the same region photographed at different wavelengths and from different geometries, we should be able to piece together the scale height of Jupiter's atmosphere—a three-dimensional view of the atmosphere involving the relationship between density and temperature at a scale of resolution that is of fundamental significance in the dynamics of the jovian atmosphere.

Jupiter's atmosphere is driven by temperature differences that arise from a combination of absorbed sunlight and heat that percolates upward from the inner regions of the planet. The local energy input from the Sun can be determined by measuring the reflectivity of the jovian cloud systems and their distribution around the planet. Since it is known how much sunlight is striking the planet, a good measure of the amount of reflected light, combined with the photopolarimeter-radiometer's measurement of the thermally emitted radiation, can determine the planetary energy budget. The reflected light can be measured by both the photopolarimeter and the charge-coupled device.

To understand the planet's meteorology, atmospheric scientists need a comprehensive, synoptic view of Jupiter's general circulation at high spatial resolution. In principle, Galileo could serve as a weather satellite of Jupiter to provide this synoptic view. It will systematically take pictures at several wavelengths throughout the 20-month tour and for whatever extended time may be available afterward. Such pictures will provide a wealth of information for studying the full range of dynamic phenomena that characterizes Jupiter's atmosphere. Atmospheric processes on a variety of scales, ranging from the huge belts, zones, and spots down to features only 10 or 20 km across (fig. 16), may participate in changes on time scales ranging from minutes to centuries. Telescopic views from Earth provide data on only the largest features. The Space Telescope will sample Jupiter at smaller spatial scales (approximately 240 km across), but it may not always be scheduled with the frequency needed to provide data about events taking place relatively quickly and that are known to be important to our understanding of the jovian atmosphere. Galileo could provide such data down to very small spatial scales and over times extending from minutes to years. Galileo's remote sensing instruments will provide complementary coverage. Figure 17 shows the relative sizes and shapes of the fields of view of these instruments.

Despite constraints placed on the use of the camera and the spacecraft by other mission requirements, Galileo will observe Jupiter for extended periods throughout the mission and will gather as much synoptic data as possible. Occasionally, maps of the cloud features will be produced at moderately high spatial resolution for comparison with data of the same region obtained by other instruments. Special attention will be paid to particular features of unusual shape or behavior. The Great Red Spot, dark barges, plumes, circulating currents, shear regions, and other known phenomena of interest will be studied using the vertical structure sequences.

All the pictures taken during the mission will be pieced together in an attempt to understand the dynamic modes through which Jupiter's energy is

redistributed within the atmospheric layers. Cyclones, anticyclones, fronts, jet streams, convective thunderstorms, and other processes are active in Earth's atmosphere. Some of these modes may also operate on Jupiter, but there may be others of equal or greater importance. There are fundamental questions in fluid dynamics concerning the interactions of these modes, the manner in which they are manifested, and the conditions necessary for their development.

Convective motions are of particular interest because of their role in the cyclonic features. However, these studies may be hampered for several reasons. For example, if the vertical shear is strong enough, instabilities that appear as organized roll patterns may superficially resemble convective turbulence. In addition, convective modes are most likely to occur in the polar regions, which cannot be observed well from Galileo's equatorial orbit.

So-called baroclinic instabilities, analogous to those that form cyclones in Earth's atmosphere and draw energy from large-scale horizontal differences in temperature combined with wind shear, are widespread on Jupiter. In regions of large horizontal variations in wind velocity, these instabilities may become dominant. Attempts to understand Voyager data in terms of pre-Voyager theoretical

Figure 16. Dynamic regimes on Jupiter.

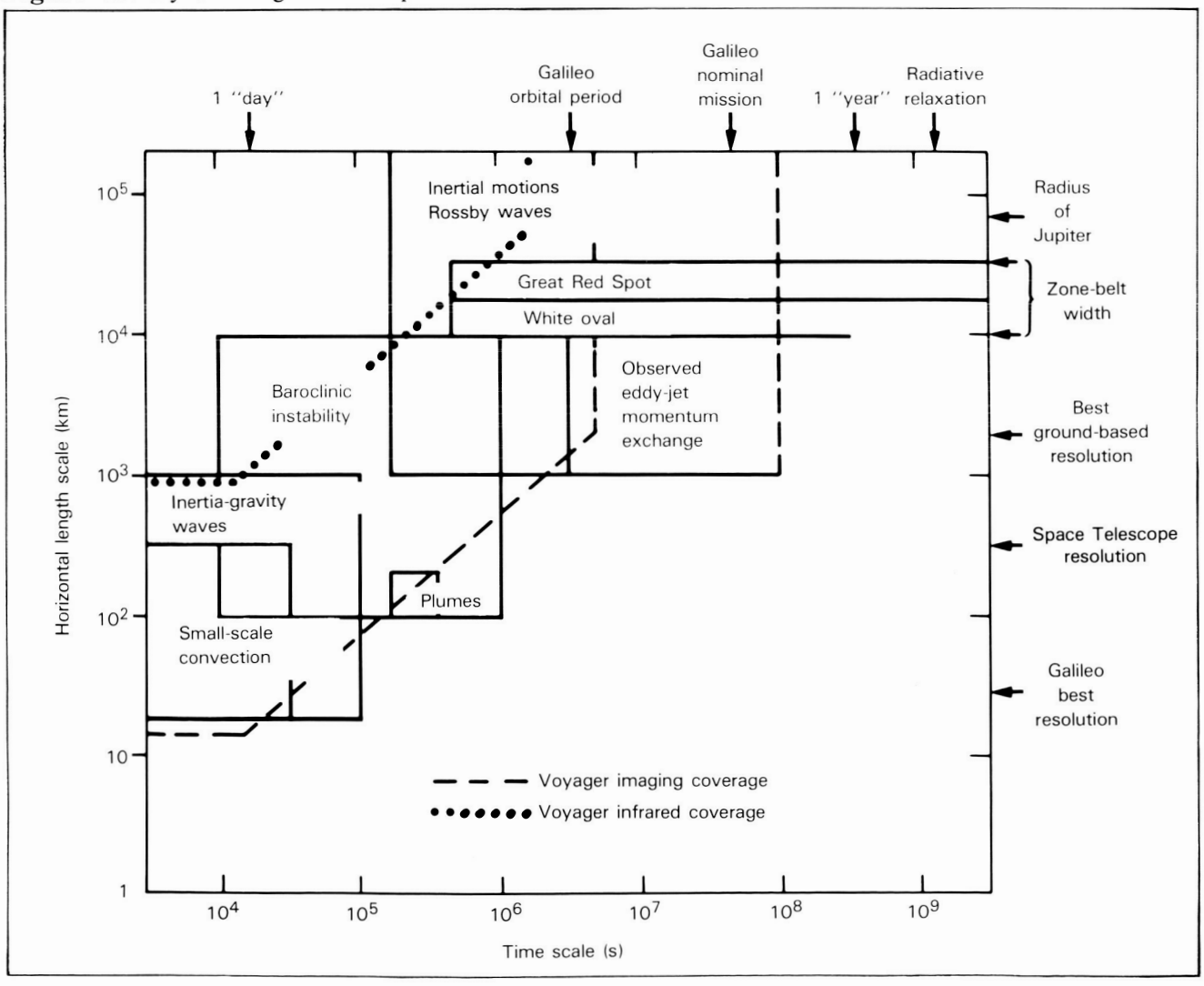

concepts have shown the partial applicability of some of the early ideas. However, Jupiter's atmospheric circulation is still not clearly understood. Galileo has many questions of dynamics to address, and we are likely to obtain the answers only by making the most refined observations of which Galileo is capable.

The Galileo experiments build substantially on the science and hardware experience gained from the Voyager missions. For example, the 1500-mm narrow-angle telescope, shutter, and filter systems of the Voyager imaging system are used with minor modifications for Galileo. The Galileo imaging experiment also includes several innovations in camera design. First, unlike Voyager, Galileo carries only one high-resolution camera. Second, Galileo's system has a hard-wired capability for data compression and for pixel summation of the video data stream. Third, and perhaps most significant, a cooled, solid-state detector replaces the slow-scan vidicons used in most earlier planetary missions. The Galileo imaging experiment will not only provide an in-depth scientific exploration of the remarkable phenomena discovered by Voyager, but will also provide opportunities for discovery of new phenomena by virtue of the properties of the new detector and by the nature of the orbiter's tour. For example, the charge-coupled device will be able to image the night side of Jupiter for lightning strokes, airglow, and meteoric fireballs. Further details on the camera system are given in chapter 7.

The near-infrared mapping spectrometer will investigate the important areas of chemical composition, atmospheric structure, nature of the clouds, energy balance, and atmospheric motions. The radiation received from the atmosphere in the spectral range of the instrument has two components—reflected solar radiation and thermal radiation from the lower atmosphere. Spectral maps obtained by the mapping spectrometer will provide information on composition, cloud properties, and thermal properties. Since the maps will be obtained over large parts of the atmosphere, the instrument will characterize atmospheric properties on a global scale. The 500-km resolution is several times better than that obtainable with Earth-based telescopes. The experiment can also study regions of the jovian spectrum that cannot be observed from Earth because of absorption by the terrestrial atmosphere.

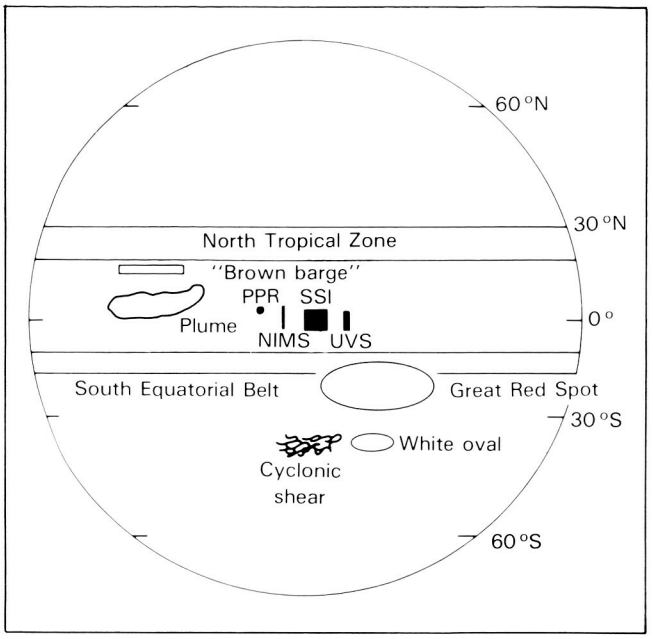

Figure 17. Sizes of instrumental fields of view for a spacecraft at a distance of 10 planetary radii from Jupiter. The solid-state imaging (SSI) field is the frame size consisting of 800 by 800 elements. The near-infrared mapping spectrometer (NIMS) has 20 elements in a line as shown. The ultraviolet spectrometer (UVS) and photopolarimeter-radiometer (PPR) fields of view are also shown. The sizes of the features, such as the Great Red Spot, depicted on the planet are as seen at the center of the jovian disk, that is, directly below the spacecraft.

As noted above, the probe's measurements will accurately determine the chemical composition at one location and for a short time only. However, for many atmospheric species, temporal and spatial variations are expected to be governed by meteorologic conditions. An obvious example of such variability on other planets is the distribution of water vapor in the terrestrial and martian atmospheres.

Structure and Clouds

Our current view of the structure of part of the atmosphere is given in figure 12, which covers a pressure range from 7 atmospheres (bars) to a few millibars; the temperature minimum is at about 100

millibars. The region above this minimum is the stratosphere, where temperatures rapidly become very uncertain. They may rise, as shown, to over 200 K or level off at 170 K. Various sources of information have gone into this temperature profile: 1 to 10 bars, radiometry from Earth; 0.1 to 1 bar, thermal infrared radiometry from Earth and Voyager; 0.01 to 1 bar, radio occultations of Pioneers and Voyagers; 1 microbar, stellar occultation observed from Earth.

The ionosphere and very high atmosphere have also been measured by radio occultation and by occultation (or eclipse) of the Sun observed by the Voyager ultraviolet spectrometer. In these upper regions the temperature rises steeply to a variable value, typically around 1000 K.

The cloud structure is considerably more uncertain, and the heights of the cloud layers rest mainly on theory—they are predicted to lie at the temperature levels where their assumed constituents are expected to condense.

Ground-based observations of infrared radiation from Jupiter at wavelengths of 5 μm indicate that there are holes in the upper cloud layer through which radiation can emerge from hot regions deeper in the atmosphere. The belts appear to be warmer than the zones and features such as the Great Red Spot. The hottest features observed are associated with blue-gray areas in the North Equatorial Belt. For an area near the center of the disk, including the Equatorial Region and the North and South Equatorial Belts, the 5-μm brightness exhibits a strong peak at a temperature of 250 K and two weaker ones at temperatures of 225 and 200 K. This suggests emissions from distinct layers in the atmosphere. If absorption and reemission above the radiating levels are taken into account, the temperatures of the three radiating levels, evidenced by the 5-μm peaks, are calculated as 292, 225, and 140 K, approximately. The visual appearance of the regions supports these calculations; namely, blue corresponds to no clouds, brown corresponds to clouds at 225 K, and white corresponds to clouds at 140 K overlying clouds at 225 K. However, other models of cloud layering could also fit the 5-μm data, and the Galileo orbiter's remote sensing instruments will help unscramble the choices.

The high-altitude smog is inferred from the fact that Jupiter is rather dark in the ultraviolet, even though none of the known gases absorb ultraviolet radiation. The effect of the smog has also been seen in photometry of satellite eclipses. Similar smog is seen on Saturn and especially on Titan, where conditions are favorable for the conversion of methane to more complex hydrocarbons. The absorbed solar energy is converted to heat in the atmosphere and is responsible for the "warm" temperatures shown near the top of figure 12. Additional heating is contributed by methane absorptions in the near infrared.

For the lower, denser atmosphere there are two principal heat sources: conversion of the remaining solar energy and heat from the interior of Jupiter. The excess of emitted over absorbed energy was established by Earth-based measurements and refined by the Voyagers; it is almost a factor of 2. It is believed to be due to a remnant of the heat generated by Jupiter's original accretion (see fig. 21). Most of the solar energy is absorbed between 1 and 3 bars. Between them, the two heat sources maintain a temperature gradient very close to the adiabatic (constant heat) value (about -1.9 K/km) from levels far deeper than we can ever probe up to 1 bar or slightly less. The upper part of this region is shown by the straight line in figure 12. The upper boundary is roughly the source region for the infrared radiation to space that balances the convective heat input from below.

The atmospheric structure instrument on the probe measures temperature, pressure, and acceleration. A complete interpretation of the data requires knowledge of the mean molecular weight of the atmospheric gases, which will be derived from the mass spectrometer and supplemented at very high altitudes by the ultraviolet spectrometer. Starting at very high altitude and low density (10^{-14} g/cm^3; number density, 10^{10}/cm^3) the deceleration of the probe is used as a measure of the density. With knowledge of the mean molecular weight and use of the principles of hydrostatic equilibrium, we can derive the temperature profile. The mass of the probe and heat shield must also be known; sensors in the heat shield are used to measure its rate of ablation. The upper part of figure 18 shows similar results from Pioneer Venus. Measurement of the ablation rate terminates when the velocity becomes subsonic and the parachute is opened (at Mach 1). Pressure and temperature are then measured directly, as shown for Venus in the lower part of figure 18. If the mean molecular weight is independently known, these measurements are

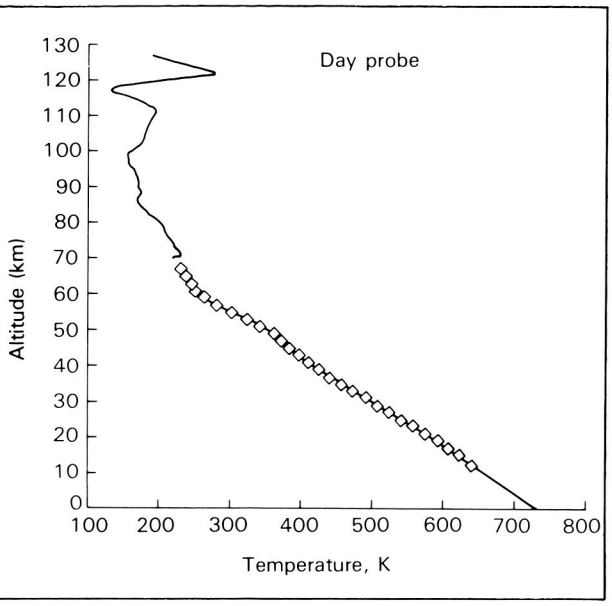

Figure 18. Temperature profile measured in the atmosphere of Venus by the atmospheric structure instrument on the Pioneer Venus day probe. Points indicate descent mode data. The solid line was determined from accelerations measured during high-velocity entry and extends into the lower thermosphere.

redundant and a cross-check is possible. Such experiments have demonstrated high precision and accuracy in the past, sufficient, for example, to demonstrate to meteorologists the presence on Venus of layers with subadiabatic lapse rates and on Mars of wave structure in the stratosphere.

During much of the tour, the Galileo orbits are poorly suited for use of the radio occultation technique, because the spacecraft will pass very far behind Jupiter and frequently will not be occulted at all. Even if it is, the accuracy of the results, particularly at the higher pressures, will be degraded by the large distance. Attempts will be made, however, to obtain the best structure data possible from the available occultations. Voyager data indicate considerable variability in the lower stratosphere; there is therefore no assurance that the probe measurements of this region will be representative.

The principal instrument for measuring clouds on the probe is a nephelometer, a device that sends out short flashes of light and measures the returned signal at several angles. Considerable information is therefore obtained, not only on the density of the clouds, but also on the properties of the particles (see the Venus results in fig. 19). The mass spectrometer will measure the changing composition as the vapor molecules begin to appear during penetration of a layer. If the condensate is abundant enough, the signature of its vaporization heat will appear in the temperature profile. Even if the condensate is not abundant enough to be detected by a discrete signature, the temperature at which a cloud appears is highly diagnostic of what is condensing.

The orbiter's remote sensing instruments (imaging, near-infrared mapping spectrometer, photopolarimeter, and ultraviolet spectrometer) will be used in support of the probe data. Even more important, the probe results will serve as "ground truth" or "cloud truth" to calibrate the analysis for vertical cloud structure of similar data from other parts of Jupiter. The near-infrared mapping spectrometer can also investigate the composition and vertical structure of clouds and the atmospheric temperature profile. Such work makes use of the broad spectral coverage applied to small areas of Jupiter.

The net flux radiometer on the probe will measure the difference between the upgoing and downgoing infrared fluxes. During the first part of the descent, the probe will be in late-afternoon sunlight, and the remaining solar input will be measured. At depths greater than a few bars, it is expected that only the internal heat flux will remain, but it cannot be directly measured because an increasing part of the total is carried by convection; the net flux radiometer measures only the radiative part. Several filters are used to select wavelength channels that give information on the composition, especially the crucial H_2O abundance. Little energy can be radiated through the clouds in wavelength regions that are opaque due to H_2O absorption, and the energy is forced to flow at other wavelengths. Although the precision of such a measurement is low, it should be free of systematic error and will be a valuable check on the results from the mass spectrometer.

Satellite Atmospheres

The four Galilean satellites are all massive enough to retain atmospheres, but they are undoubtedly very tenuous. Sulfur dioxide (SO_2) was

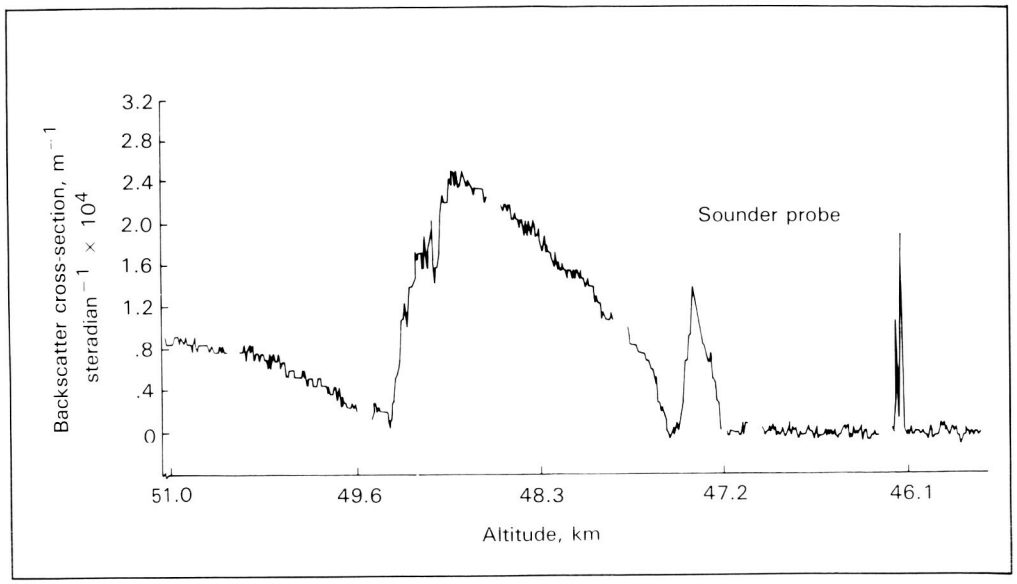

Figure 19. Signal measured in the backscatter channel of the Pioneer Venus nephelometer instrument as a function of altitude as the Venus probe descended through the atmosphere. Similar types of profiles are expected for the Galileo probe's nephelometer experiment.

detected on Io by Voyager, and the atmosphere of Io probably contains mainly SO_2 and its dissociation products, including O_2. There is also a large and energetic plasma torus containing ions of sulfur and oxygen, as well as some neutral gas. The torus might be regarded as an extension of Io's ionsphere but can better be treated as part of the magnetosphere (chapter 4). Europa, Ganymede, and Callisto all have water ice exposed on their surfaces and must certainly have small quantities of water vapor, as well as O_2, produced from it. Hydrogen escapes rapidly, and oxygen more slowly. The Voyager ultraviolet spectrometer set an upper limit to the density of Ganymede's atmosphere in a stellar occultation; the small quantities of gas allowed by this limit are still consistent with expectations from theory. The Galileo ultraviolet spectrometer is sensitive at longer wavelengths than Voyager's instrument and may be able to detect emissions from these thin media, stimulated by solar radiation or electron impacts.

The information about Io is much more substantial, but a considerable range of interpretations is consistent with the data. The SO_2 seen by Voyager could represent an atmosphere but could equally well have been from a volcanic plume. Ionospheres were detected at both limbs by radio occultation of Pioneer 10, but the samples may not have been representative. Finally, large quantities of gas must be in transit to supply the torus. On the night side, most of the SO_2 must freeze to the surface; if any significant atmosphere remains, it is probably O_2. In any case, Io's atmosphere is probably anything but uniform. Again, the Galileo ultraviolet spectrometer may be able to detect airglow emissions that will help to tie down the atmosphere density and its day to night variation.

chapter 3 SATELLITES, RINGS, AND DUST

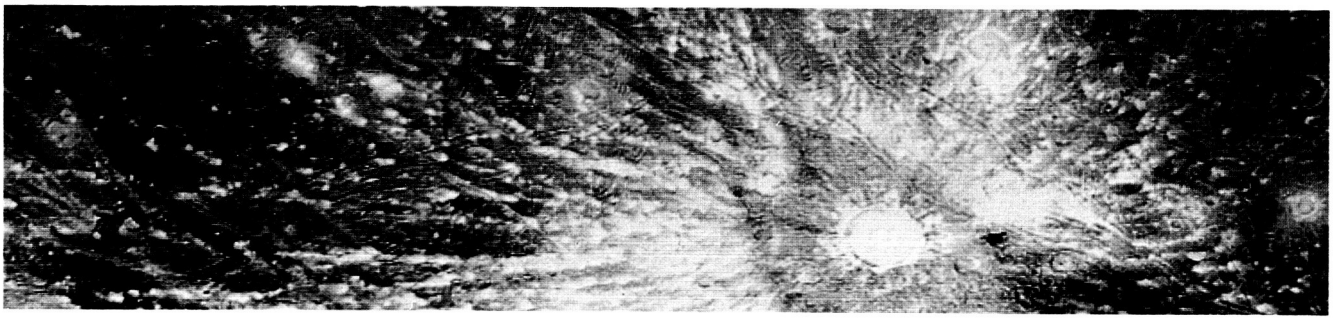

The jovian system is in some ways a smaller replica of the solar system. It consists of massive gaseous Jupiter with a retinue of satellites ranging from worlds the size of the terrestrial planets, down through asteriod-sized bodies, to micron-sized dust and ring particles. Although all multiple satellite systems look like small solar systems, the analogy is profoundly justified in the case of the jovian system. Jupiter, in its earliest history, was a "weak star" and created a temperature gradient in the gas cloud from which its moons formed that strongly influenced this composition and later evolution. In addition to their importance as part of a miniature solar system, several of the larger satellites have undergone extensive individual geologic evolution like that which has affected the terrestrial planets. In one case, that of Io, the intensity of geologic evolution is greater even than that which has characterized Earth.

The satellites of Jupiter fall into several groups (fig. 20): the large worlds Io, Europa, Ganymede, and Callisto and several groups of much smaller bodies. The four large regular satellites are called the Galilean satellites because they were first seen by the astronomer Galileo in 1610. Four small satellites—Adrastea, Metis, Amalthea, and Thebe—orbit Jupiter closer than Io, the innermost of the Galilean satellites. Very close to Jupiter are the orbiting particles that comprise Jupiter's faint ring system. At least two small satellites, discovered by Voyager, orbit very close to the outer edge of the ring.

The rest of Jupiter's satellites are irregular and fall into two main groups: an inner cluster that consists of small satellites (in posigrade orbits) that circle Jupiter at roughly 11.5 million km and an outer group that orbits Jupiter at roughly twice that distance. The outer satellites move in intricate retrograde orbits, making one circuit of the planet in about two years. They are so far from Jupiter that if you could stand on the surface of Amalthea you would need a small telescope to detect them. Posigrade orbits are those in which bodies revolve in the same direction as Earth in its orbit, that is, counterclockwise as viewed looking down on the north pole. Retrograde motion is oppositely directed. All the planets of the solar system revolve about the Sun in a posigrade direction, and most also have posigrade rotation. The major exceptions to this rule are Uranus, whose axis is severely tilted, and Venus, which has retrograde rotation. However, there are numerous examples of retrograde motion among the various satellites.

The Galilean satellites are large enough to appear as measurable disks when viewed by telescope from Earth, but the largest Earth-based telescope cannot reveal details on the surfaces of any of them. All four satellites are in synchronous rotation, keeping one face turned constantly toward Jupiter, as the Moon does to Earth. These satellites

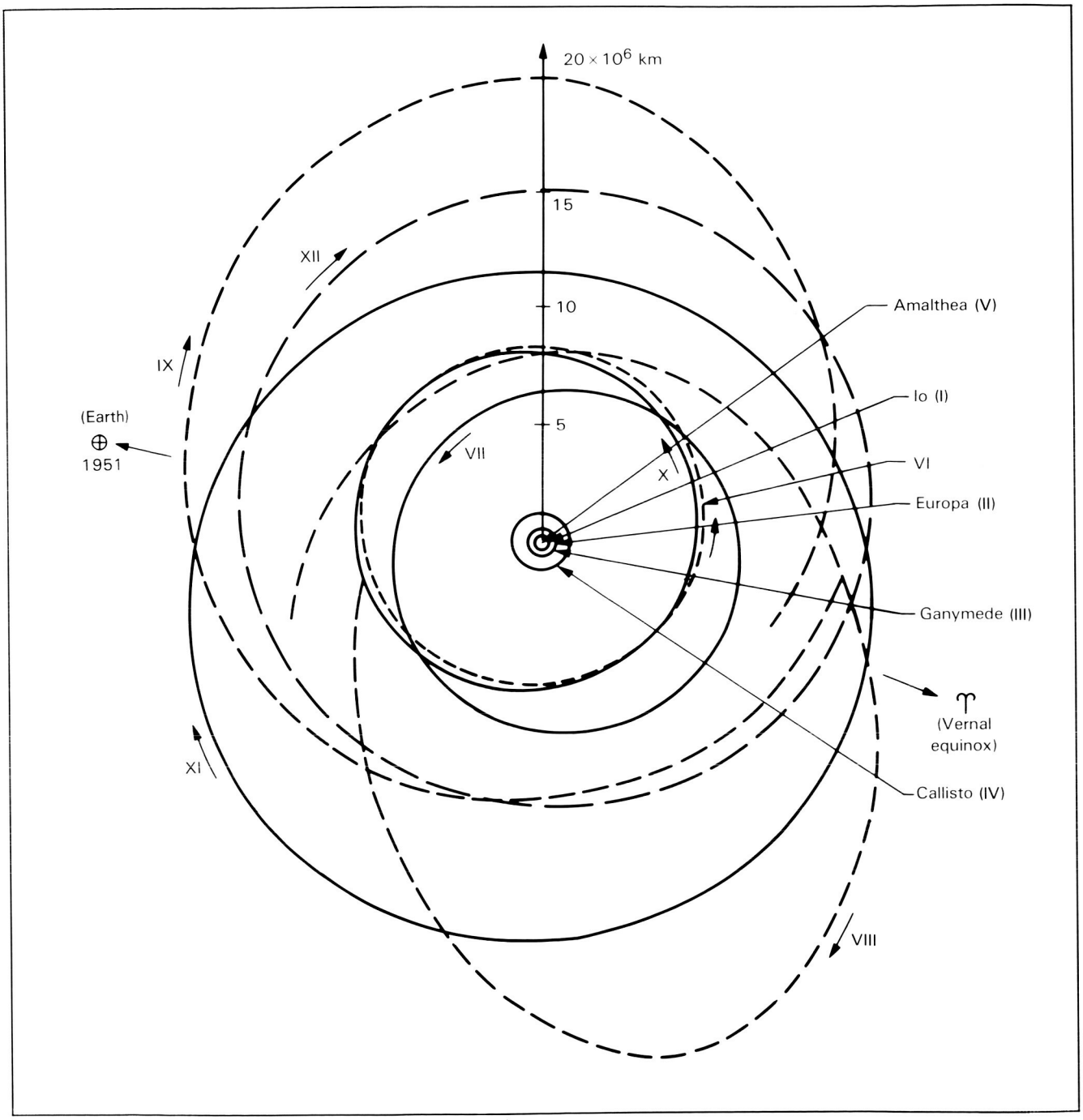

Figure 20. The satellites of Jupiter reduced to the ecliptic plane (1951 epoch) to show the four major groups—the Galilean satellites (I to IV), the inner posigrade cluster (XIII, VI, X, and VII), the outer irregular cluster (XII, XI, VIII, and IX), and the four small satellites inside the orbits of the Galilean satellites (XIV, XVI, V, and XV).

are locked in resonance in their orbits—two periods of revolution of Io about Jupiter are almost equal to one of Europa, and two of Europa are almost equal to one of Ganymede.

The Galilean satellites were first imaged from spacecraft by the Pioneers, but the low resolution did not reveal significantly greater detail than images obtained from Earth. When each of the four satellites was imaged in detail by Voyager spacecraft, however, remarkably varied levels of geologic activity were discovered.

Formational History

First we consider the importance of the satellites as members of a small-scale solar system. Our theories of the origin of the solar system, and of any other possible planetary systems, all assume that planetary bodies form from a gaseous nebula of essentially uniform composition—the material of the primordial nebula from which the Sun and all other bodies of the solar system originated about 4.6 billion years ago. As the material from which planets form condenses and the planets begin to aggregate from it, their bulk composition is determined. Terrestrial planets such as Earth were deprived of most of the light elements because those remained in the gas phase during planetary condensation, but the stronger gravitational fields of larger planets such as Jupiter were able to hold on to the light elements. A key to understanding differences among planets is how heat from a central body, such as the Sun or Jupiter, produced compositional differences among the objects that formed around it by preventing, to various degrees, the condensation of volatile compounds. Most studies of the formation of Jupiter's satellites have concluded that Io, Europa, Ganymede, and Callisto were formed by the same processes in the jovian nebula that led to the formation of planets within the primordial solar nebula. The satellite system exhibits characteristics similar to those of the solar system (fig. 21). Several billion years ago Jupiter was much hotter than it is now (fig. 22). Its fierce heat prevented condensation of ices in the inner part of the presatellite cloud, and this left the inner satellites denser than the outer satellites. Io, the innermost of the four Galilean satellites, is most dense—3.5 g/cm^3. Europa, the next satellite, is also "rocky" but has an outer crust of water ice and a density of 3.04 g/cm^3. Ganymede and Callisto, the outer two satellites, have densities of about 1.8 g/cm^3, which suggests that they are two-thirds ice in bulk and only one-third silicate rock.

Although Jupiter never put out more than one-hundredth the heat of the present Sun (fig. 22), the satellites were profoundly affected by it because they are much closer to Jupiter than even the planet Mercury is to the Sun. For example, when Io first formed it was probably receiving as much energy from Jupiter as Earth currently receives from the Sun.

Geologic Evolution and Current State

Not only did Jupiter influence the "starting points" of the four Galilean satellites by controlling their initial composition, the planet continues to influence their subsequent evolution by pumping tidal energy into their interiors: the enormous gravitational field of Jupiter raises tides on the satellites, and tidal energy can be dissipated as heat within the satellites if these tides vary with time. The amount of heating varies dramatically among the big satellites, depending on how their orbits change due to the gravitational tugs of the other moons. Io receives the most internal heating because its interaction with Europa causes continual changes in tidal amplitude and position. Io's violent volcanic activity is driven by this energy source. In addition to contributing to Io's intense volcanism, tidal heating may sustain a liquid water ocean under the icy crust of Europa. Callisto, which receives virtually no tidal heating, has a surface much like Earth's Moon, with shoulder-to-shoulder cratering; this is evidence of bombardment from space soon after the satellite's formation and of few subsequent changes over eons of time.

Io

One of the most startling discoveries by the Voyager spacecraft was the presence of erupting sulfurous volcanoes on Io (figs. 23, 24, and 25). The huge plumes of eight geyser-like eruptions observed during the relatively brief periods of the two flybys indicate that Io is remarkably volcanic, much more so than Earth. It is seemingly the most volcanically active body of the solar system. Evidence for sulfur as a major element in Io's chemistry comes from several sources: the colors

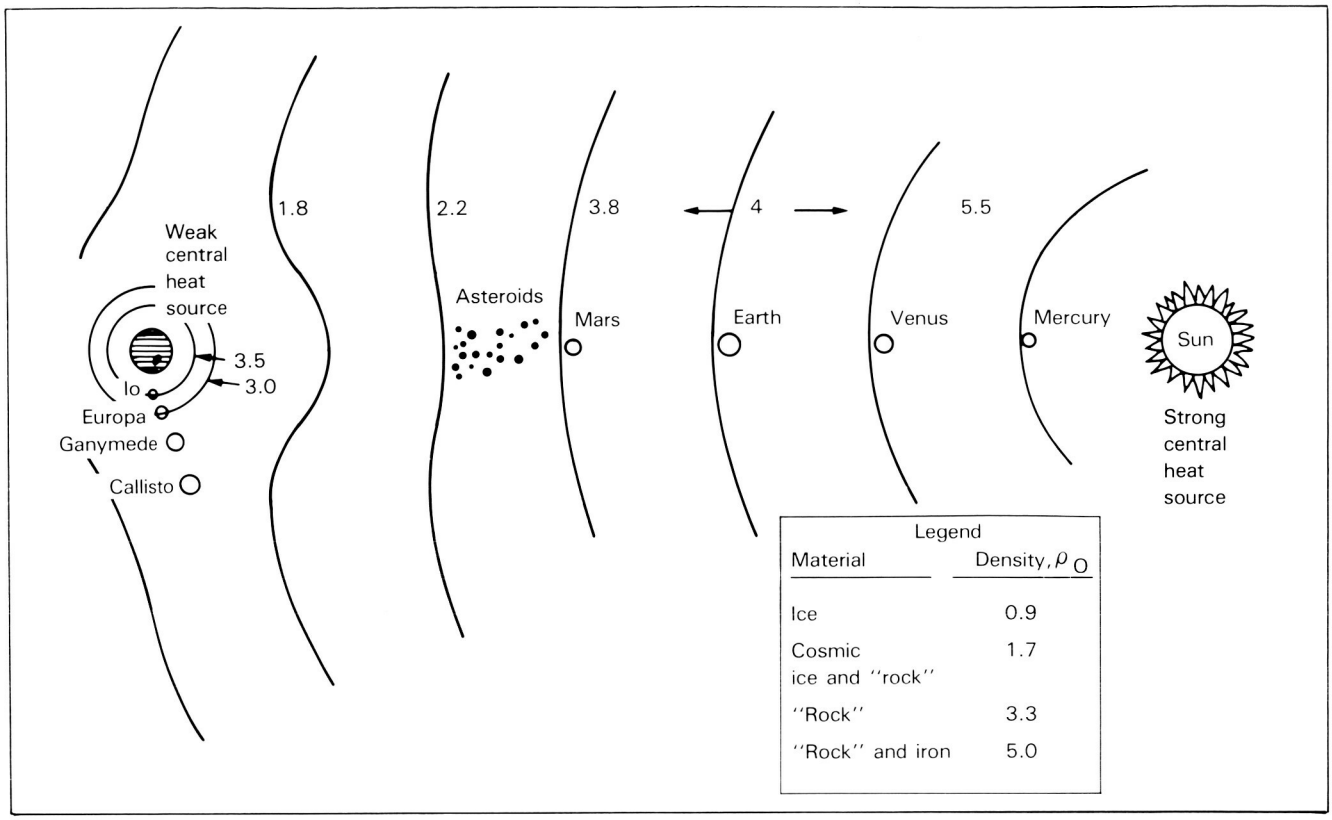

Figure 21. The satellite system of Jupiter reflects some of the characteristics of the solar system in that the central heat source was responsible for depleting volatile gases from the inner worlds of each system.

Figure 22. During its evolution Jupiter has changed from a very hot central body to its present relatively cool condition. In the early stage of its history Jupiter emitted sufficient energy to affect the density gradient of the Galilean satellites.

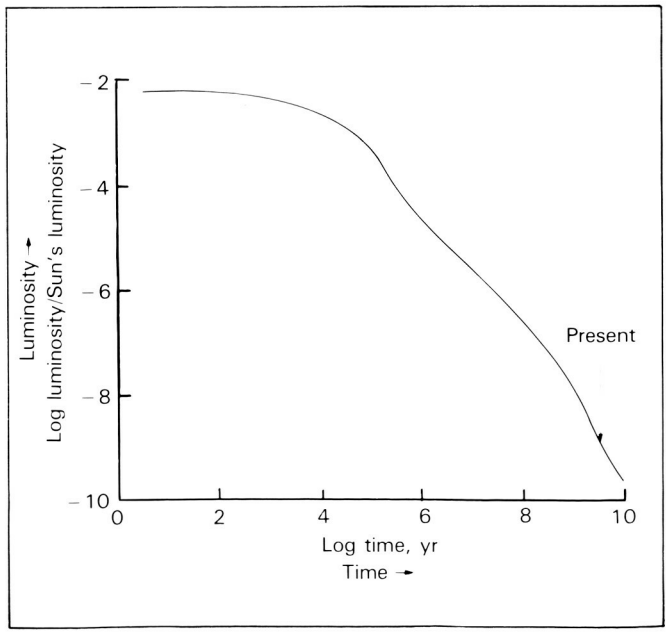

are appropriate for sulfur allotropes (an allotrope is an element in two or more different forms, usually in the same phase) formed at the observed temperatures, Voyager detected gaseous sulfur dioxide (SO_2) over one volcanic area, frozen SO_2 has been identified on the surface via Earth-based telescopic spectra, and sulfur and oxygen ions dominate the surrounding magnetospheric plasma.

Voyager observed active volcanic plumes, an abundance of volcanic calderas and flows on the surface, and several hot spots. Although there are many circular volcanic caldera seen on the images

Figure 23. One of the most startling Voyager discoveries was the presence of volcanic eruptions on Io. Here the plume from one of the eruptions is visible on the limb of Io.

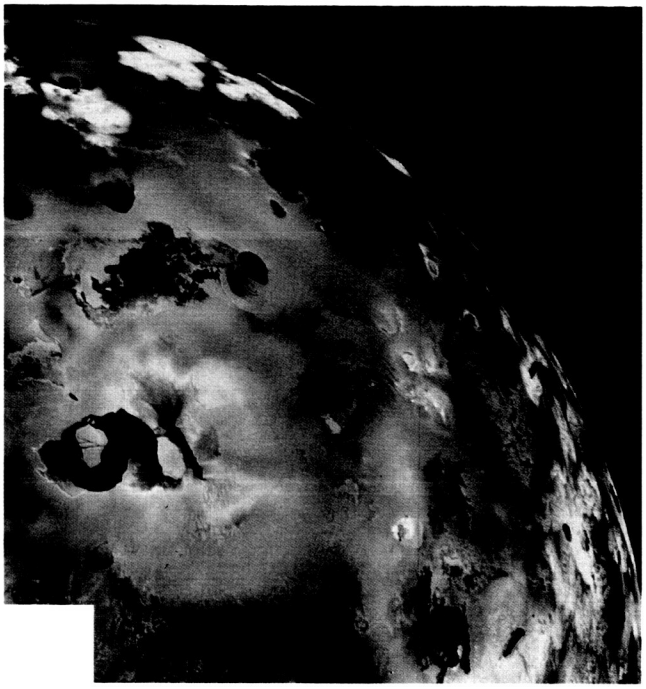

Figure 24. Loki plumes emerge from the ends of a linear black fissure some 200 km long. The D-shaped black patch below the Loki fissure may be a lava lake. It remains to be established whether the lava is sulfur or silicate. Most of the surface of the lake has a temperature of about 300 K, which is 170 degrees higher than the temperature of the surrounding terrain. The image is a Voyager 1 mosaic processed by a technique developed by Alfred S. McEwen of the U.S. Geological Survey in which high-resolution images contribute spatial detail and low-resolution images contribute color data.

of Io, Voyager detected no impact craters on this satellite. It appears that material expelled from volcanic vents and flows continually resurfaces Io. While the enormous rate of volcanic activity is well established, its precise nature is poorly understood. Particularly important are the questions of overall eruption rates and the relative roles of silicates, sulfur, and SO_2. Many of the surface features—except for the occasional mountains—may be of sulfur. However, the surface may be composed of both silicates and sulfur, with silicates providing the structural strength. Considerable uncertainty also exists concerning the relative roles of explosive volcanism, exemplified by the plumes, and quiet effusion of lava, as indicated by the numerous flows visible on the surface.

Many flows in the Voyager pictures appear to have alteration zones around their periphery. These may be caused by condensation on the surrounding terrain of volatiles such as sulfur dioxide and sulfur outgassed from the lava. Other explanations are possible, however.

There is general agreement that tidal heating is responsible for the active volcanoes on Io. The solid rocky crust may be no thicker than 20 km. While much of this crust may be made of silicates, the evidence on surface composition suggests there is an uppermost layer a few kilometers thick that is heavily enriched with elemental sulfur and sulfur compounds. However, if basaltic volcanism dominates, as has been argued by some geologists, the sulfur layer may be even thinner. The interior of Io is at least partially molten and is believed to consist of ferromagnesium silicates, with perhaps a core

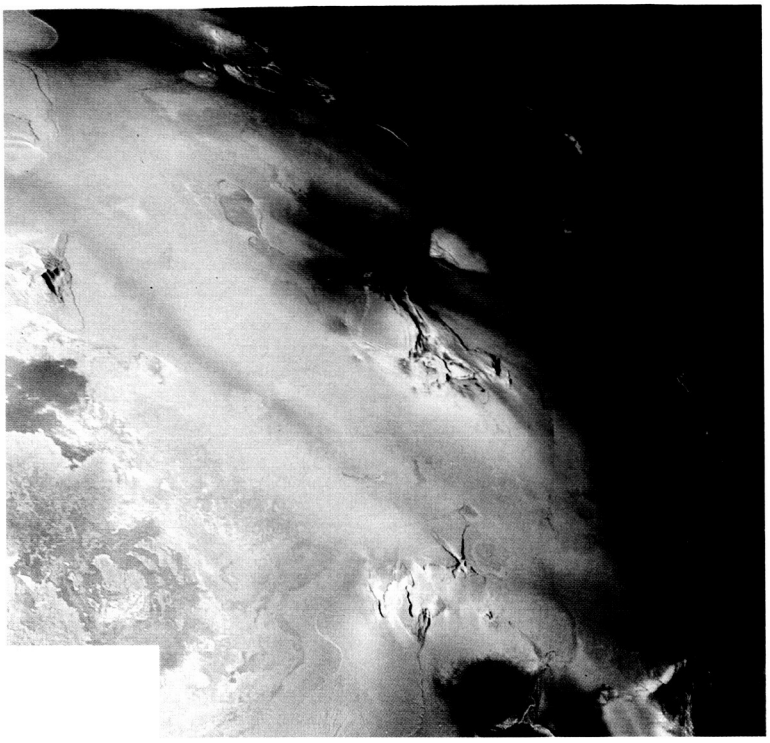

Figure 25. Pele is the largest geyser-like eruption observed in Io so far. The plume is visible above the limb of the Moon; it ascends to a height of about 300 km. Markings and flows are evidence of past eruptions. This view of Pele was made by Voyager 1; it is a mosaic produced by McEwen's technique. When Voyager 2 arrived four months after Voyager 1, Pele was inactive.

rich in iron sulfide. Perhaps elemental sulfur was produced by dissociation of iron sulfide and "floated" up to form the crust while iron sulfide and iron sank to form a core.

Io is also surrounded by a huge cloud of neutral sodium that is thought to be sputtered from its surface or atmosphere by atomic charged particles in the jovian magnetosphere. Moreover, it is highly probable that the ions of sulfur and oxygen observed throughout the entire jovian magnetosphere originate from the atmosphere or surface of Io by similar processes. Studies of the torus and neutral cloud thus have direct bearing on Io's surface composition and atmospheric processes. Calculations suggest that Io must have possessed considerable water in bulk when it formed; apparently the water was lost to space early in the satellite's history, perhaps by similar magnetospheric interactions.

Europa

The density of Europa combined with the presence of a bright icy surface indicates that it is a dominantly silicate body with a thin icy crust, perhaps up to 100 km thick. Its most distinctive geologic feature is a network of intersecting dark and light linear streaks (figs. 26 and 27). The dark streaks, which are about 10 percent darker than the surrounding terrain, are fairly straight, vary in width from about 3 to about 70 km, and are up to several thousand kilometers long. They appear to have little or no topographical relief. The light streaks are smaller than the dark ones. They appear to be ridges about 10 km wide and a few hundred meters high. They also form scallops or cusps with smooth curves that repeat regularly on a scale of one to several hundred meters.

These streaks may be surface manifestations of several tectonic processes that have deformed the ice-rich crust of this satellite. Folding in response to compression might have formed the light ridges, while fracturing in response to either compression or tension might have formed the dark streaks. The satellite has very few impact craters, which suggests a process of degradation such as viscous relaxation of an ice-rich crust or a process of surface rejuvenation such as volcanism or flooding by liquid water released from the interior through fractures.

The possibility of a liquid water ocean beneath the surface ice is plausible theoretically as well, because, although Europa receives far less tidal heat than Io, it may receive enough to keep water from freezing if it were originally liquid. Early theories of Europa's structure regard it as having a thick ice crust through which heat is transported to the surface by conduction rather than by solid-state convection. Even with radioactivity as the only heat source, these models permit liquid water to exist below 40 km. Voyager found Europa's density to be 3.03 g/cm^3, which allows for the possibility of a thick ice crust. (If Europa's density had been the same as that of denser silicates, only a thin ice crust could have been considered.) The absence of large-scale topography also suggests that the crust cannot be very thin. Now, with a thick-crust model and with tidal heating thought to be much greater than radioactive heating, the chances for a liquid zone seem stronger than before.

If the cracks on Europa represent crustal expansion during freezing of a 100-km-deep water shell, much more crustal expansion would be required. However, if the ice were deposited layer by layer at the base of an ice crust over a period of time, the expansion required to produce the

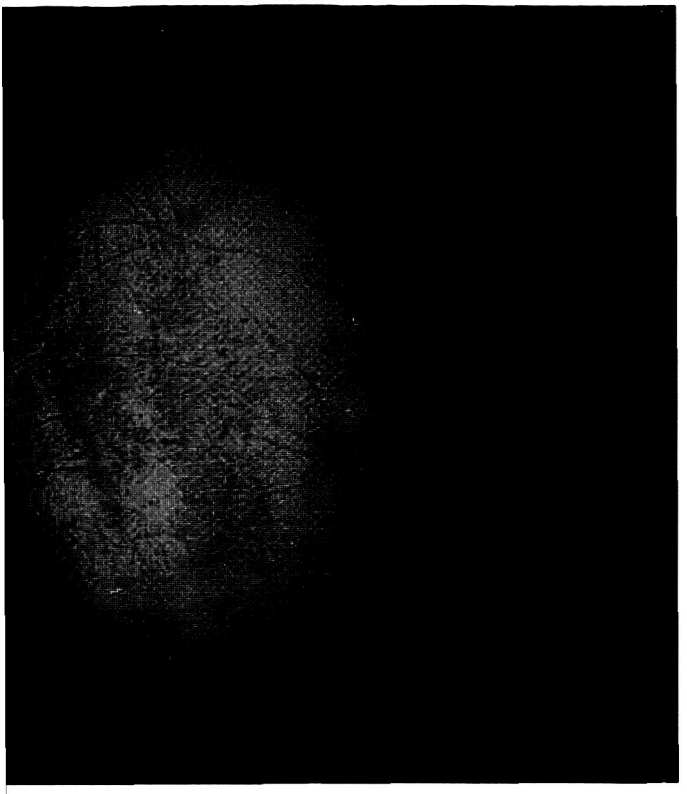

Figure 26. The intriguingly smooth surface of Europa is marred by a network of intersecting dark and light linear streaks which suggest that material from the interior continues to resurface this satellite.

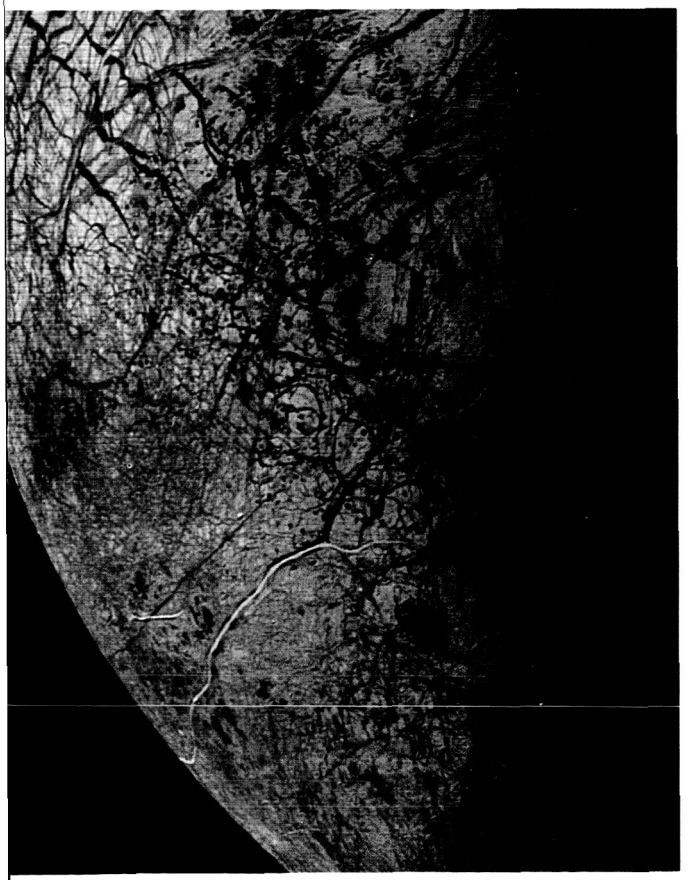

Figure 27. Complex patterns on the icy surface of Europa may be cracks filled with dark material welling up from the interior. Very few impact craters can be seen, suggesting that active processes are still modifying Europa's surface.

observed features could be obtained. In this case it is conceivable there would be no liquid zone because entrapment of the tidal heating to sustain the liquid depends, in part, on the presence of liquid in the first place.

All models proposed to explain the surface features of Europa assume that the streaks express crustal failure from stresses induced by tidal forces or by convection deeper in the interior. One theory suggests that as tidal forces slowed the spin of the satellite, the equatorial bulge relaxed and caused distinctive latitudinal variation in stress. Radial tides then became effective and formed concentric fracture patterns around those areas on Europa pointing directly toward and directly away from Jupiter. Another idea that has been considered includes the dehydration of the interior, which could have produced global expansion, with mantle convection adding a nonuniform stress. Whatever their cause (and multiple causes are thought to have produced multiple sets), these surface markings are unique among the planetary surfaces observed so far in our solar system. Closer inspection of their form and patterns is required before we can develop a clear picture of how the interior and the surface of Europa have evolved. Europa was the least studied of all the Galilean satellites because of the nature of the Voyager trajectory. It is likely that closer observation will definitely answer many of our questions about this satellite, including the exciting possibility of a crustal subsurface "ocean."

Ganymede

The density of Ganymede (1.93 g/cm^3) suggests that this satellite is composed largely of ice. The crust can be divided into two components—dark areas of densely cratered terrain and bright bands of more sparsely cratered, grooved terrain (figs. 28 and 29). Within the latter are closely spaced, almost parallel grooves, most of which are crudely organized into long curvilinear sets but which also form equidimensional blocks or

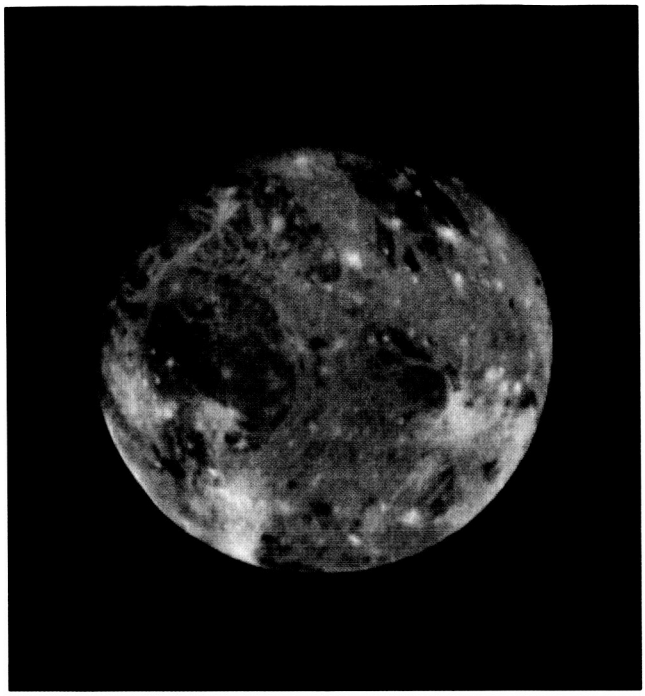

Figure 28. Each Galilean satellite is unique. Ganymede has two distinctive surface types—old cratered terrain and grooved and modified terrain.

fan-shaped arrays. Different sets intersect to form a variety of reticulate patterns. This grooved terrain appears to have been formed by tectonic processes that fractured and faulted the crust over a considerable period of time early in the history of the satellite, modifying or destroying the older cratered terrain. Although relatively young with respect to the darker regions, the grooved terrain is more heavily cratered than the lava plains of the Moon.

One of the major geologic questions about Ganymede concerns the origin of the grooved terrain. A former silicate-rich crust might have foundered into a water mantle, with consequent oozing of water or ice to the surface. One mechanism for this could be disruption of the lithosphere as a result of internal expansion following phase changes in the constituent ice. Another possibility is glacier-like convection in the ice-rich mantle and rafting of lithospheric blocks, analogous to the plate tectonics of Earth. Answers to these questions may possibly be obtained by mapping distribution patterns of the grooved terrain, patterns of displacements, and details of the zones of intersection between different belts of this terrain.

Another important question about Ganymede is how the viscoelastic properties of the crust evolved. The Voyager images show bright circular features with little relief in many parts of Ganymede. These features have been called palimpsests. They look like ancient craters that have merged back into the surface. Detailed observations of these features are needed to determine the deformational properties of the satellite's crust and whether these properties have changed with time. Such information is important for studying the thermal evolution of Ganymede's interior.

Callisto

Callisto is the most heavily cratered Galilean satellite, and it is the only body larger than 1000 km in diameter in our solar system that has not undergone extensive resurfacing since impacts molded its surface (figs. 30 and 31). Crater densities in the solar system are generally two or three times as great as those in the most heavily cratered parts of Ganymede. Callisto's surface is clearly very ancient. Some large palimpsests are present. An extensive but degraded impact basin named Valhalla is 600 km in diameter and surrounded by closely spaced concentric rings. Clearly, Callisto's geologic history has been more passive than that of Ganymede.

Most of the information about impact craters gathered since the beginning of the space age involves craters in silicate materials of the inner planets and the Moon. Both Ganymede and Callisto offer new opportunities to study craters in nonsilicate icy materials. The origin of central pits in craters on Ganymede and Callisto is unknown. They are probably intimately related to energy partitioning during impacts, an important matter for understanding the mechanism responsible for all kinds of cratering.

Craters on both of these large icy satellites provide clues to their thermal history. Large, old craters are very degraded; smaller, younger craters have shallow or domed floors; and small, young craters are bowl shaped. Many craters have undergone some form of degradation, depending on their age and size. The ultimate shapes of craters are probably strongly controlled by the thickness of the lithosphere of each satellite.

Ganymede and Callisto are thought to have

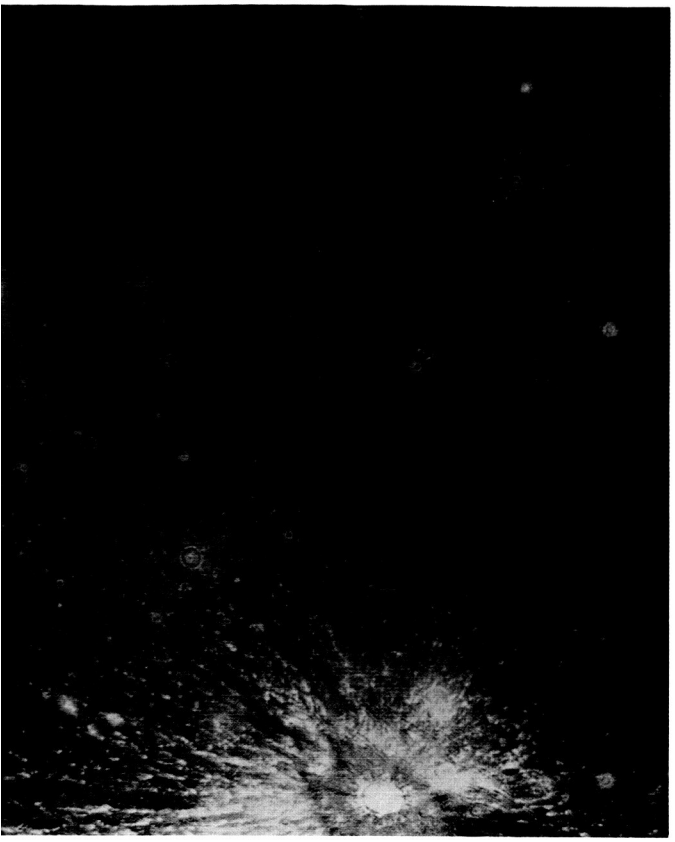

Figure 29. Plate tectonics appear to be moving crustal plates on Ganymede, but there is still evidence of meteoroid impacts.

accreted from a 2:1 mixture of water-ice and primitive meteoritic material rich in volatile gases, similar to carbonaceous chondritic meteorites. Before Voyager, we thought that internal differentiation, in which light materials floated toward the surface and dense materials sank toward the center, could have been complete for Ganymede and Callisto because of radioactive heating alone. This would have resulted in an inner rocky core and an initially convecting and liquid water mantle capped by a thin crust of ice. In these theories, differences between the thermal histories of Ganymede and Callisto caused different crustal freezing histories and hence different abilities to preserve the original mixture of silicates and ice in portions of the crust that did not melt. Also, within the lunar-sized silicate cores of these satellites, any possible assemblage of "carbonaceous-chrondritic" mineral would probably have been thermally metamorphized into a higher-temperature assemblage of silicate. The icy crusts envisioned by the theorists are believed to become unstable with respect to solid-state convection and to transport heat much more rapidly than by solid-state conduction. Consequently, in these models the entire liquid mantle freezes very early in the planet's history. This viewpoint was generally accepted before the Voyager data became available. It is still unknown whether the dark material coloring the ice is primitive carbonaceous material or whether that material fell to the center and was replaced by contaminants from meteorites and dust hitting the surface.

Although the basic theories discussed above have remained intact, the Voyager data (fig. 32) caused the differences between Ganymede and Callisto to emerge as a somewhat more intriguing problem. While the difference in density was shown to be only about 8 percent, Voyager confirmed that the difference in albedo between these two satellites arises from a much more active tectonic history on Ganymede than on Callisto. The role of tidal heating might account for the difference in the longevity of surface activity on the

Figure 30. The outermost of the Galilean satellites, Callisto, is a heavily cratered world, which seems to indicate that its surface has not changed greatly over billions of years, in sharp contrast to the other Galilean satellites.

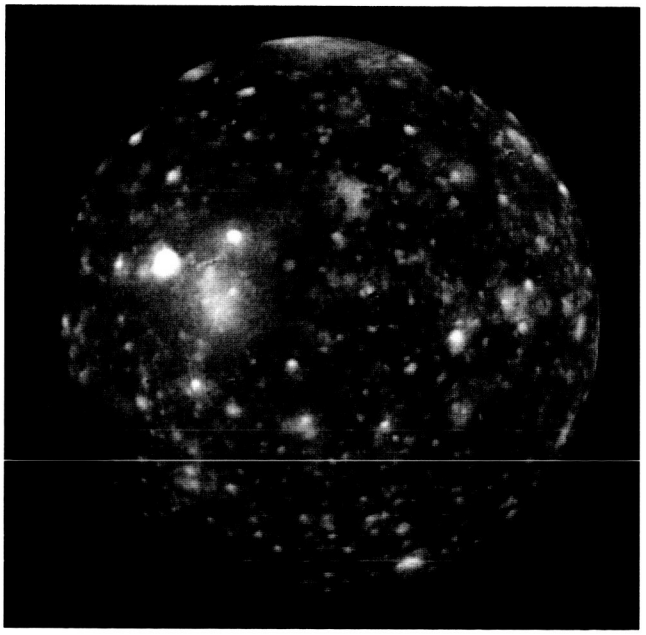

two satellites, since Ganymede is much closer to Jupiter than is Callisto. This heating might have extended the period during which Ganymede had a thin lithosphere and hence surface activity, but only by about 100 million years. Accretional heating differences are not great, although they also favor a more active Ganymede. If Ganymede has a much larger silicate core than Callisto, radioactive heating might account for the differences. This could stretch Ganymede's heating period to 500 million years. Coupled with tidal and accretional heating, the effect could be sufficient for Ganymede's lithosphere to express endogenic activity for 1 billion years after the lithosphere of Callisto. This would exempt the presently visible surface from the bombardment with rocky material that apparently affected the most ancient surfaces of the solar system. The grooved terrain might also have been a result of this freezing of Ganymede's mantle. The general absence of very large craters on the oldest terrain of Ganymede supports the view that Ganymede started with a liquid mantle and a solid crust no more than 10 km thick.

The small-scale topography of these objects is also a subject of considerable interest. Monostatic (using the same stationary antenna to transmit and receive) radar studies of the Galilean satellites from Earth reveal that the satellites are fundamentally different from the Moon and the terrestrial planets in terms of their radar scattering properties. Although they have very high radar reflectivities on the average, the outer three Galilean satellites do not show the strong radar return from the center of their disks that is the most prominent feature in the radar signatures of the Moon and the terrestrial planets. The surfaces of the Galilean satellites may have a basically different fine-scale structure because of the presence of ice. However, even the polar ice caps of Mars scatter radar more like the surfaces of the Moon and the terrestrial planets and unlike the Galilean satellites.

In summary, the most important issues related to the current state of the satellites include the nature of Io's volcanism and the composition of its crust; the possible existence of liquid H_2O zones in Europa, Ganymede, and Callisto; and the tectonic processes that have produced such diversity in the geologic evolution of their crusts.

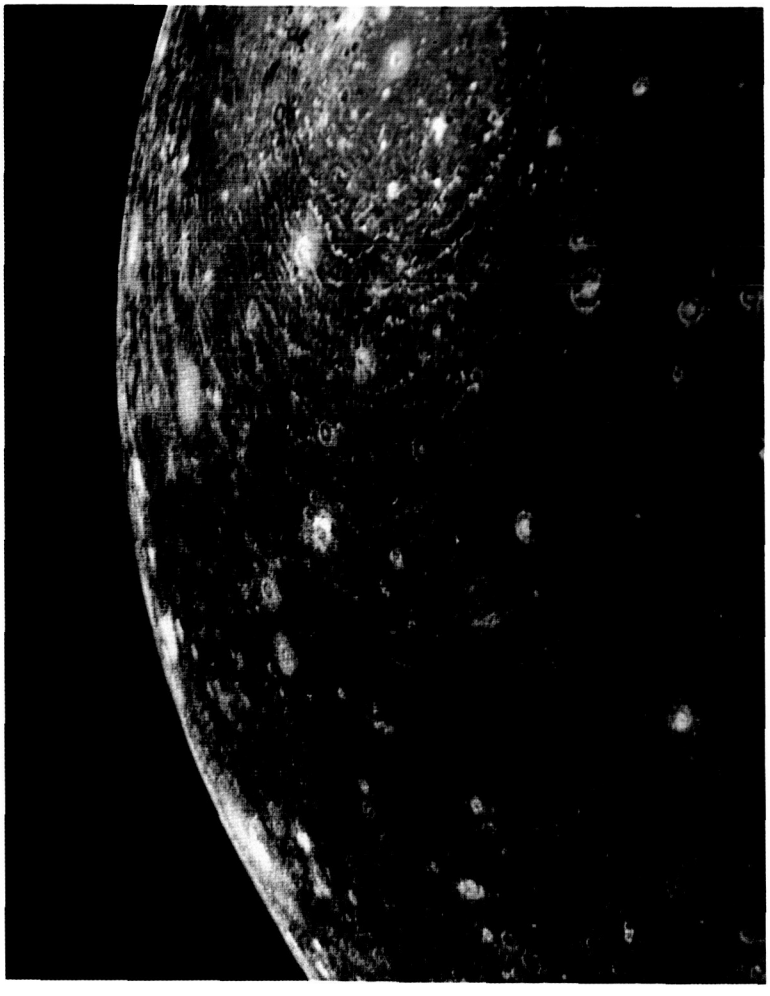

Figure 31. Concentric shock waves ripple out from the center of Callisto's Valhalla impact crater.

Small Satellites, Rings, and Dust

Collectively, Amalthea and the recently discovered small satellites are called the inner satellites to distinguish them from the Galilean satellites (Io, Europa, Ganymede, and Callisto) and the outer satellites (J6 through J13).

The first spacecraft observations of Amalthea were made by Voyager 1 in March 1979. Essentially all of our current knowledge of the physical characteristics of Amalthea comes from a few observations made by Voyagers 1 and 2, although the satellite's approximate size and the fact that it is a very dark, red object were deduced from Earth-based observations. Amalthea is an irregular body with dimensions of 270 by 165 by 150 km. The

satellite is not ellipsoidal in shape. The blunt end of the axis points toward Jupiter, and as far as can be determined from the Voyager data, the satellite is in synchronous rotation, as expected from dynamic theory. Its mean orbital distance is 181 300 km, and its albedo is far lower than those of the Galilean satellites, only about 0.05.

In the Voyager images of Amalthea, discrimination of surface features is limited, yet two very large craters, Pan (90 km in diameter) and Gaea (70 km in diameter), are clearly visible, and some half-dozen smaller craters are suspected. In addition to craters, ridges are evident, as is some complex, trough-like topography near the crater Pan. Local relief on the satellite reaches 20 km. Pan is at least 8 km deep, and Gaea is probably twice as deep.

Assuming a mean density of 3 g/cm^3, surface gravity on Amalthea ranges from about 5 to 7 cm/s^2. This is roughly a factor of 5 higher than on the satellites of Mars, but approximately a factor of 20 less than on the Moon. One expects that all

Figure 32. Data from Voyager provided better insight into the interior and surface composition of the Galilean satellites but raised many new questions.

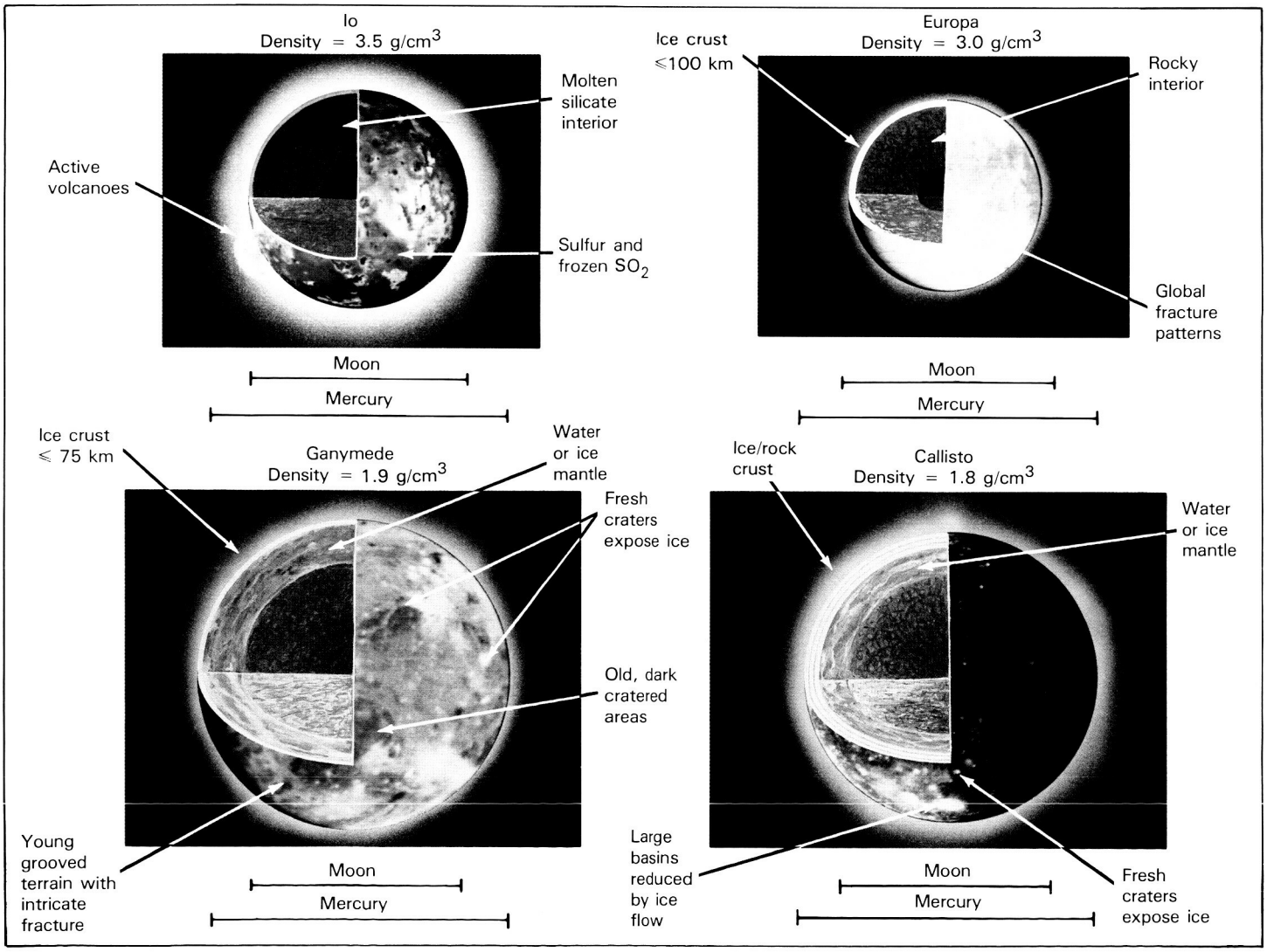

craters on rocky bodies the size of Amalthea will be bowl shaped. The deposition of ejecta blankets on this satellite should be intermediate between the situation on the Moon and on the satellites of Mars. Amalthea should have developed an abundant regolith—like that of the Moon, but unlike that of small asteroids—that may contain abundant, impact-generated glass.

The color and reflectance characteristics (darkness and redness) of Amalthea may be affected by the satellite's extreme environment. Prolonged exposure to charged particles in the jovian magnetosphere, contaminants such as sulfur from Io, and high-velocity micrometeoroids might combine to darken and redden Amalthea's surface material. Laboratory measurements on mixtures of carbonaceous materials with sulfur allotropes provide good (but not necessarily unique) matches to the red spectrum and low albedo of the satellite.

An inner satellite, Adrastea (1979J1), with a diameter of about 25 km, was discovered at the outer edge of Jupiter's ring. The surfaces of Adrastea and other small objects suspected to exist near the ring may well be a source for ring particles. Adrastea may also interact dynamically with the ring particles in a manner similar to that of the small satellites near the edges of Saturn's rings.

The second inner satellite, Thebe (1979J2), was discovered during analysis of Voyager photographs in the spring of 1980. A comparatively large object, it orbits at a mean distance of 3 Jupiter radii (R_J). (Jupiter's equatorial radius is 71 398 km.) Its diameter is 80 $\pm$ 10 km, and its reflectance is comparable to that of Amalthea.

The third of the inner satellites, Metis (1979J3), was discovered in the late summer of 1980 while additional images of Adrastea were being sought. This new satellite orbits close to the outer edge of the ring at a mean distance of 1.8 R_J. Its diameter is 40+ km, and its reflectance is also comparable to that of Amalthea.

Both Adrastea and Metis appear to be intimately connected with Jupiter's ring. It is even possible that these two objects represent the two largest lumps of a whole spectrum of fragments. While most of the ring consists of small, micrometer-sized particles, some kilometer-sized objects could well exist but have not been detected. Continued erosion of these larger chunks may resupply the small particles needed to maintain the ring.

Three major components of the ring (fig. 33) can be identified: a bright ring with a sharp outer edge at about 1.81 R_J and a more diffuse edge at about 1.72 R_J, a faint ring extending from the inner edge of the bright ring to the surface of Jupiter, and a faint halo of material extending some 104 km above the ring plane which we believe indicates electromagnetic effects on small ring particles. All discussions of ring particles so far assume that the particles are dark like Amalthea and the inner satellites. While this assumption is reasonable, no definitive measurements exist to prove this point. Also, no definitive information concerning the color of the ring particles exists.

The environment of the inner satellites and the rings is severe. The surfaces are exposed to high doses of energetic ions, protons, and electrons in the jovian magnetosphere and high-velocity micrometeoritic bombardment, as well as probable contamination by gas and dust from Io. For instance, the surface of Amalthea is subjected to fluxes of 10^8 particles/cm^2/s of protons in the 1 to 10 MeV range. Absorption of protons and electrons by the satellite is readily apparent in the Pioneer 10 and 11 particles and fields data. However, although Pioneer did detect effects later found to be related to the rings, no particles and fields measurements directly pertinent to the inner satellites were obtained on these missions.

In addition to high doses of protons and electrons, the inner satellites are subjected to impacts by heavy ions—mostly sulfur (S), oxygen (O), and sodium (Na)—diffusing away from Io. Any material injected into the inner side of the Io torus will tend to diffuse toward Jupiter and thus interact effectively with the inner satellites and the ring. Small charged dust particles may be removed from the immediate vicinity of Io by the sweeping action of Jupiter's magnetic field and eventually reach the ring. In the case of Amalthea, such material will impact the surface at 60 km/s. Uncharged micrometeoroids originating outside the jovian system will impact the surface with average velocities near 40 km/s. Thus, the spectrophotometric characteristics of the surface may have been profoundly altered by the environment. The unusual red color and low albedo of Amalthea could be the result of the high doses of electrons, protons, heavy ions, and especially of sulfur-bearing dust from Io, in which case the smaller inner satellites and the larger particles in the ring

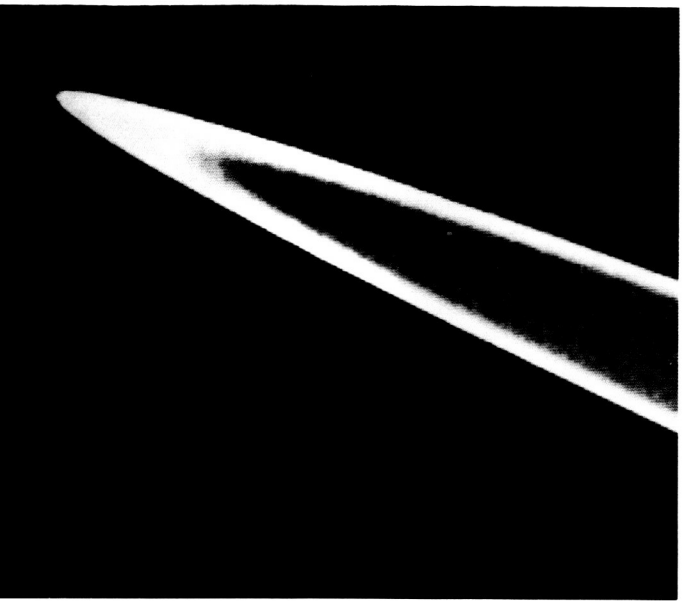

Figure 33. This striking view of Jupiter's ring was recorded by Voyager 2 in 1979 at a distance of 1.5 million km. The unexpected brightness is probably due to forward scattering of sunlight by small ring particles. Seen within the inner edge of the brighter ring is a fainter ring which may extend all the way down to Jupiter's cloud tops.

should have similar colors and albedos. Another interesting possibility is that the unusual spectrophotometric properties of Amalthea are due to the production of sulfur-bearing glasses in the surface layer.

Available data indicate that all inner satellites and the particles in the ring are dark. Perhaps further analysis of Voyager data may permit us to test whether the colors of these objects are also similar. More likely, we will have to wait until more data, particularly spectral albedo measurements of the inner satellites, become available. Thus, the inner satellites are not only of great interest as primordial relics, but are also of great interest as probes of the peculiar magnetospheric environment and as catchalls for a peculiar planetary mass transfer process.

Solid-Body Science Studies

Four optical remote sensing science instruments will be mounted aboard a steerable scan platform appended to the orbiter's despun section. They have been designed to provide complementary data.

Imaging: Surface Geology

The Galileo imaging experiment will lead to improved understanding of almost every aspect of jovian satellite geology. The highly successful Voyager mission revealed the geologic style of each of the satellites and raised crucial questions regarding their evolution. With Galileo we will begin systematic exploration of each of the bodies and address some of the questions raised by Voyager data. These imaging tasks will be accomplished by means of increased mission flexibility, passes 20 to 100 times closer than Voyager, a 20-month encounter sequence, and a camera with spectral resolution and range, light sensitivity, and photometric fidelity that are significantly improved over those flown on the Voyager spacecraft due to advances in the state of the art. Pertinent instrument parameters are given in chapter 7.

The special excitement of the Galileo imaging experiment derives in part from our ability to observe the changing face of Io over a period of two years, obtain our first high-resolution images of Europa, and complement Voyager's satellite coverage at even higher resolutions. Additional highlights of Galileo's imaging experiment include guidance from the results of both Voyager and prior Galileo passes; greater light sensitivity for studies of dark sides, Callisto, and the irregular satellites; better spectral resolution; and a more diagnostic spectral range reaching into the infrared. The importance of a single parameter, resolution, is worth illustrating from a qualitative point of view: resolution improvements over Voyager for Galileo result from a combination of improved encounter characteristics and camera improvements. Such resolution improvements—exceeding a factor of about 2 or 3—can result in both a quantitative change in our understanding of geologic processes and a radical qualitative change in our perception of the overall character or "physical personality" of an object. Figure 34 illustrates how enhanced resolution will aid in identifying the processes that can be inferred from morphology.

Io. Among the key issues concerning Io's surface geology are the global distribution and chronology of volcanism, the styles of volcanism,

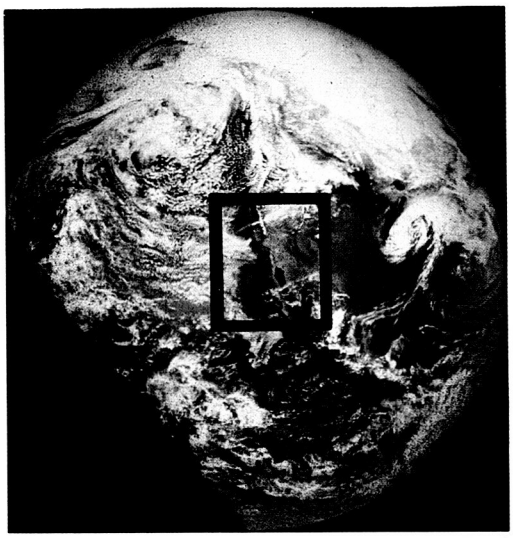

Diameter: ~12,800 km

Earth

(a) Apollo 17, December 1972, Hasselblad camera

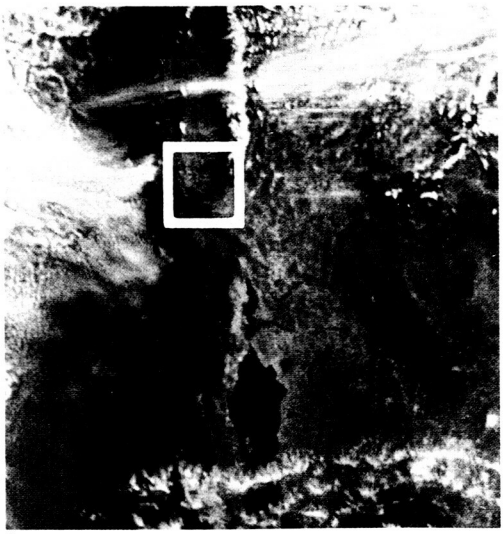

Area: ~2000 × ~2000 km

(b) Apollo 17, December 1972, Hasselblad camera

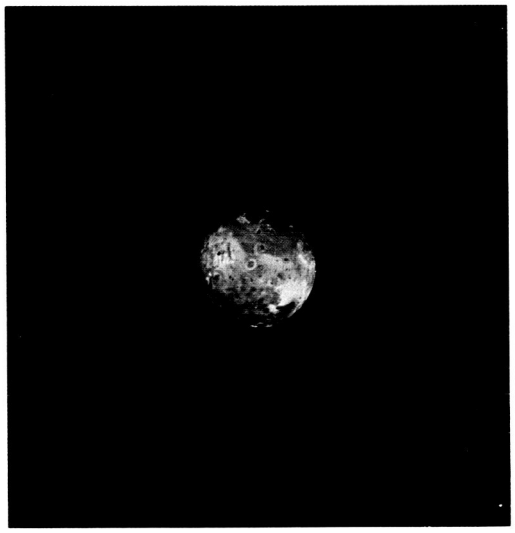

Diameter: ~3600 km

Io

(e) Voyager 1, March 1979, vidicon imaging system

Area: ~1800 × ~1800 km

Resolution: ~5 km/lp

(f) Voyager 1, March 1979, wide angle vidicon imaging system

Figure 34. Both high-resolution images of specific features and lower-resolution images of broad areas are necessary to understand the "regional context" of the surface of a planetary body. These pairs of images at similar resolutions and areal coverage compare Earth with Io in an attempt to illustrate the expected resolution enhancement by the Galileo mission. Areas covered in succeeding images are outlined in the preceding images.

Earth (photo a) and Io (photo e) are shown here in relative scale to each other. In this photograph of Earth, one can study the gross structure of the surface but little can be said about the topography or geologic processes of the planet. Similarly, in the Io image, one is struck by its multicolored patches, but the boundaries between these areas are fuzzy and little can be deduced about Io's geologic processes. There seem to be no impact craters as one would normally expect to see.

In images b and f, the resolution is about 5 kilometers. On Earth (photo b), one can no longer see an entire continent. Some topographical details are visible, yet there is little information about Earth's geologic processes. In photo f, one can start to see geologic detail on Io such as volcanic calderas (left center) and mountains (lower right). (Geologic features such as these are much larger on Io than on Earth.)

Photo c is a LANDSAT image of an area of the western United States stretching from Lake Tahoe (upper left) to Lake Mead (lower right) at about 1 kilometer resolution. This resolution is comparable to the very best Voyager images of Io. It is now possible to see different types of geologic structure and to infer some of the geologic processes that are occurring in this region. Lakes, rivers, and erosional patterns can be clearly identified. The different colors of the regions indicate

ORIGINAL PAGE
COLOR PHOTOGRAPH

Area: 480 × 480 km
Resolution: 1 km/lp

(c) LANDSAT multispectral scanner, processing by U.S. Geological Survey

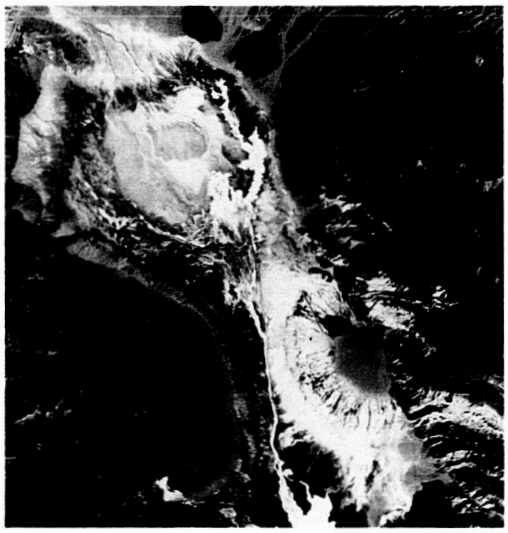

Area: 24 × 24 km
Resolution: 50 m/lp

(d) LANDSAT thematic mapper, processing by U.S. Geological Survey

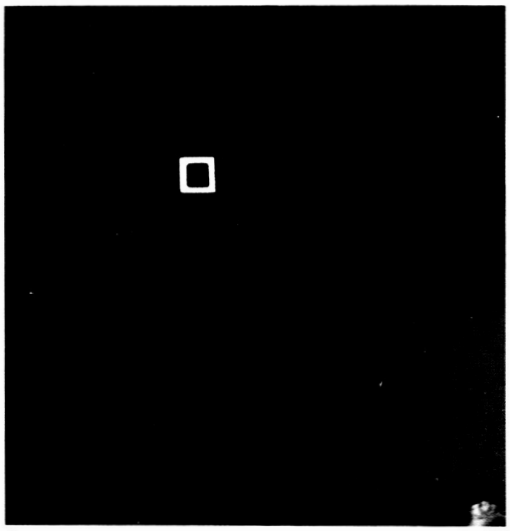

Area: 400 × 400 km
Resolution: 1 km/lp

(g) Voyager 1, March 1979, vidicon imaging system

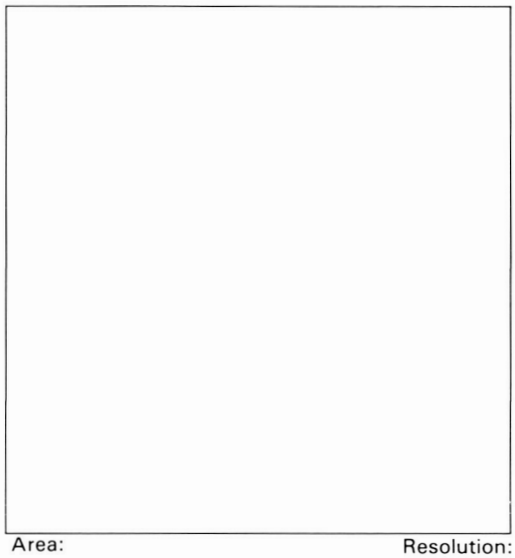

Area: 8 × 8 km
Resolution: 20 m/lp

(h) Typical Galileo frame size, 1988–1990, charge coupled device in solid-state imaging system

that they are composed of different materials. With additional study of this image, one could determine the relative ages of the various parts of this region and could deduce its geologic history. Photo g is representative of the very best Voyager pictures of Io; only a few pictures were obtained at this resolution. This picture is typical of Galileo's resolution for at least 50 percent of the surfaces of the Galilean satellites. Details of flow features on the flanks of Maasaw Patera are now visible, including the scarp that extends around the dark flow features. This provides information about the tectonic setting of Maasaw Patera. One can now see that in some cases color differences are superimposed on the topography, indicating that the colors are caused by a relatively thin covering of materials overlying a surface constructed by other forces.

Photo d, a LANDSAT photo of an area at the center of photo c, has a resolution of 50 meters and is typical of the very best resolution that will be obtained by Galileo. The detail in this picture allows studies of the erosional processes occurring in this region. Studies of the outwash patterns and their paths down the sides of the mountains can reveal a great deal about the sequence of geologic events. The physical state of the outwash materials (e.g., loose or consolidated) can be estimated from the topography. Differences in the color and brightnesses of the outwashed material suggest differences in the composition or particle sizes of the materials. From this, one can estimate how fast the materials were washed down from the mountains—gradually or catastrophically—and if other geologic processes redistributed these materials after they were deposited on the slopes of the mountains. Photo h must remain blank until Galileo flies by Io in 1988, but the very best resolution will be about 20 meters, allowing studies of portions of each of the Galilean satellites in images as detailed as photo d.

mineralogic and chemical changes in the composition of effused material with time, and the relationship between the bulk composition and global geophysical evolution of Io and its surface volcanism and tectonics.

Galileo's imaging experiment will make a variety of observations pertinent to these issues. Comparison of the surface conditions with what was observed by Voyager will lead directly to a better determination of eruption rates. Repeated moderate-resolution imaging observations of Io's surface will occur over a period of two years from about the orbit of Europa. New flows, as well as areas in which the former topography has been buried by plume debris, may be identified. In addition, the capability to resolve craters smaller than 100 m will place much narrower constraints on resurfacing rates than is now possible with the 1 to 5 km data. The combination of crater data (if any) and differencing (exacting comparison) with Voyager pictures may thus result in identification of areas in which volcanic activity has occurred in the eight years since Voyager, as well as areas in which little activity has occurred for millions of years. The silicate-sulfur controversy discussed earlier may be resolved partly on the basis of detailed surface morphology. The shape of lava flows depends to a large extent on the properties of the erupted lava. Detailed examination of flow dimensions, shapes, and subsidiary features such as lava channels, tubes, and levees will give an indication of the variety of eruptive styles, place constraints on lava composition, and possibly allow us to distinguish sulfur flows from silicate ones. Particularly important will be the vertical dimensions. Flow thickness depends strongly on its rheology; hence lava composition can be inferred from vertical dimensions. Caldera depths are limited by the strength of the surface materials—again by composition. Special emphasis will therefore be placed on acquiring quantitative information on topography.

Many flows appear to have alteration zones around their peripheries. These zones may be caused by condensation of volatile gases (SO_2, S) outgassed from the lava, but there are other possible explanations. Study of the zonal colors and their relations to the surrounding features should narrow the possibilities.

The main contribution of solid-state imaging (SSI) to understanding plume dynamics will be with respect to plume stability and scattering properties. We will be observing Io after a lapse of several years and will readily establish whether the plumes observed by Voyager are still active or whether an entirely new set has formed. We will also be able to determine from the topography and albedo markings whether other plumes formed in the interim and died out. Furthermore, by continually monitoring plume activity for two years we will determine whether activity is episodic, periodic, or continuous and on what time scale—all of which is essential for understanding plume mechanics and the overall energy dissipation system for the entire body. Much of the value of the SSI experiment will be synergistic with compositional [near-infrared mapping spectrometer (NIMS)] and radiometric (photopolarimeter-radiometer) mapping (see below). It will put that data in a morphologic context. The compositions suggested by SSI data will surely be tentative and dependent on confirmation from NIMS data. However, the imaging experiment has the best chance of isolating almost pure spectral components. Thus, it will help us understand how to begin to identify individual components from the high-resolution NIMS reflection spectra. Conversely, compositional identification with the multifilter SSI system will be backed up by the NIMS system with a 200-element infrared spectrum at a spacial resolution several times lower than that of the SSI system (discussed in the next section). The SSI experiment also has the best chance of associating compositional with morphologic boundaries; this is a key way to answer genetic questions.

Europa. Among the key questions concerning Europa's geology are the following. How many components of the prominent fracture patterns are there, and what is the chronology and genesis of each? What are the detailed characteristics of the stripes, and what are the relationships between the various surface morphologic features we might expect to see (e.g., cracks, cusps, and ridges of various ages) and their compositions? How thick is the ice crust, and what lies beneath (liquid H_2O? volcanically active silicate?)? Have there ever been floods of liquid H_2O on the surface? What is the global energy history, and how has it been affected by jovian tidal stresses or more familiar energy sources? How old is the surface, and how do the various surface areas relate to each other? Has

Europa's surface been affected by external meteoritic and atomic particle bombardment?

Galileo imaging has the potential to resolve or at least shed additional light on the question of how Europa has evolved by:

- Adding to coverage in the polar regions to observe fracture patterns. Extensional features (e.g., graben or other depressions) would support tidal despinning models; compressional features such as ridges would support the expansion-convection model.
- Acquiring high-resolution images that would permit identification of small impact craters and so place tighter constraints on the timing of tectonic and resurfacing rates.
- Acquiring high-resolution and/or stereo images of the various streaks to provide a better definition of their morphology and sequence of formation. Such definition would place further constraints on various tectonic models and may reveal changes in style and composition of aqueous and other eruptions with time.

In summary, both the zonal structure and the surface geology on Europa are unique among the planetary objects observed so far in the solar system. Better definition of the surface morphology and distribution of compositional units will lead to improved understanding of how the interior and the surface of the satellite have evolved.

Ganymede. Among the key issues to be addressed by the imaging experiment on Ganymede is the origin of "renewed" or tectonically modified terrain (as opposed to what appears to be terrain relics from the last stages of accretional bombardment) and its relationship to the energy history of the planet.

To understand the formation mechanics of this renewed or "grooved" terrain, we must study its distribution pattern, the pattern of displacements (rift, shear, or compression together with directions), the detailed morphology of zones of interaction between different belts, and the morphology of the grooves themselves. Galileo will contribute in all of these areas by increasing the area of the planet that is covered at useful resolution and by acquiring high-resolution samples in appropriate areas.

A second question with respect to Ganymede, and one not entirely unconnected with the grooved terrain, concerns the evolution of the viscoelastic properties of the crust. In many parts of Ganymede we see palimpsests, bright circular features with little relief. These appear to be ancient craters that have undergone recovery by some form of creep. The size and age give indications of the rheologic properties of the early crust. Additional clues to the viscoelastic properties of the crust are provided by the shape of impact craters, particularly the presence and absence of central peaks and central pits, and the dimensional relations between various crater features such as depth and diameter. By assembling data on the size and frequency distribution of palimpsests, assessing their ages by the number of superposed craters, and assembling detailed data on crater shapes and sizes of constituent features, the SSI experiment will yield a better understanding of the deformational properties of the Ganymede crust and how they have changed with time. This in turn will allow us to infer more about the thermal evolution of the interior.

Callisto. The photometric data obtained by the imaging experiment will allow comparison of the spectral reflectance of individual tiny areas on Ganymede, equal to a single picture element, with those on other objects and laboratory samples. This will allow us to answer questions such as, "Is the most pristine part of the ancient crater on Ganymede the same as terrain on Callisto?" Here the imaging must be linked with the considerably lower spatial resolution but much higher spectral resolution (and greater wavelength range) data from NIMS to form compositional maps.

The main problems to be addressed by the imaging experiment on Callisto have to do with cratering processes and the possibly primordial nature of portions of the surface and the materials on it. Much of the experimental, theoretical, and observational data on impact craters concerns silicates. High-resolution views of Callisto will provide a wealth of new data on primary shapes of craters on icy bodies, data which are essential for the theoretical and experimental modeling of such craters. Recognition of impact melt deposits in or around craters on Ganymede and Callisto would aid greatly in constraining such calculations and would serve as a point for comparison with craters on the rocky terrestrial planets. In a related area,

the origin of central pits seen in craters on Ganymede and Callisto (and parts of Mars) is unknown, although numerous hypotheses have been advanced. Because these features are probably intimately related to energy partitioning during impacts, the importance of how central pits form cannot be overemphasized – not only in terms of cratering in ice, but in the general context of impact cratering.

As on Ganymede, the crater population contains a record of the satellite's thermal history. Large old craters are palimpsests, smaller younger craters have shallow or domed floors, and small young craters are bowl-shaped. Clearly, many craters have undergone some form of recovery (return to preimpact states), and the degree of recovery depends on the age and size of the crater. Mapping the distribution of the different classes of craters may allow us to date the various stages in the development of the lithosphere and compare the timing of the like stages of Ganymede.

Since Callisto's surface is the oldest and least modified surface we have viewed in detail, the nature of the nonicy and possibly primordial material is of great interest. Since there appears to be some global physical asymmetry on Callisto, we must determine whether the nonicy material is indeed indigenous to Callisto or is merely infall. It could well be unmodified primordial material in either case. Detailed studies of photometric properties of the darkest material and its morphologic relationship to lighter material could be crucial to understanding the history of the nonicy component. Again, synergism with NIMS is apparent, with imaging providing information on the physical placement of nonicy material and the nature of the contacts with ice, while the NIMS experiment may possibly provide specific absorption band identification.

Amalthea and Inner Satellites. Additional coverage of Amalthea at resolutions comparable to the best obtained by Voyager will enable us to determine more accurately the shape of this irregularly shaped satellite, as well as to chart its largest surface features more completely. Additional spectrophotometric coverage of the bright spots should help in unraveling their compositional nature, while comparisons with the other inner satellites may help distinguish between endogenic and exogenic effects.

Although selection of a tour trajectory has not been completed, it appears certain that several passes near the orbit of Europa (9.5 R_J) will occur. While it is true that the spacecraft will make one pass close to Io during insertion into Jupiter orbit, it is unlikely that much attention will be paid to the inner satellites during this very busy period. Fortunately, given the likelihood of repeated observations from 10 R_J (perijove), it may be shown that the Galileo coverage of the inner satellites will be comparable in resolution to the Voyager coverage of Amalthea: 8 to 9 km/line pair (a line pair refers to the CCD array of columns and rows).

Thus, we can expect to learn a great deal about Amalthea and the other inner satellites from Galileo. We should be able to determine the shapes, rotation states, accurate albedos, and colors. Color is especially important in light of the possibility that all the inner surfaces are being polluted with material from Io. We predict that the surfaces of all the inner satellites are dark and red like that of Amalthea. The Galileo experiment will greatly extend the spectral coverage of the inner satellites. The imaging experiment alone will provide high-quality photometric data between 0.4 and 1.0 μm, while the NIMS may extend this coverage out to 5 μm, at least in the case of Amalthea. It will be especially important to compare the spectrophotometric characteristics of the small ring particles and the associated satellites (Adrastea and Metis).

Imaging: Bulk Composition and Internal Zonation

Along with radio tracking, the imaging experiment will also make major contributions to our knowledge of the bulk composition, internal zonation, and physical state of the satellites. Knowledge about the size and shape of a satellite, together with its mass and gravitational moments, can provide evidence of internal differentiation or orbital evolution and constrain models of internal structure and composition.

Interesting questions include the following. Are the interiors of these satellites homogeneous or differentiated? Are they in hydrostatic equilibrium? Do they possess cores? What size? One major source of information on internal structure and physical state is the radio tracking experiment (see below). However, another major contribution comes from imaging: accurate measurements of

radii and shape should be made, and measurements of principal moments of inertia of the satellites are very important along with the tracking data to constrain models of internal structure.

Since the Galileo encounters are flybys, the quality (resolution) of the pictures will vary from region to region over the surfaces of the satellites. Thus, the accuracy of the radii measurements will vary; in some areas, however, an accuracy of 1 to 3 km should be possible. In other areas, the accuracy will drop to a few kilometers. The mean radii should be well determined and radii of the best-fit ellipsoids measured to an accuracy of a few kilometers.

Mapping Spectrometry: Mineral Mapping and Radiometry

To understand the chemical composition and physical state of the satellites, knowledge of the minerals or phases present on the surfaces is required, along with the distribution of such compositional units in relationship to the surface geology and morphology.

Vast differences between surface composition and bulk composition seem to be as much the rule as the exception among solar system objects. Nonetheless, our experience has shown that knowledge of surface mineral distribution and its relationship to surface geology, when combined with other information, usually provides many clues to the formational conditions and evolutionary history of the object as a whole. The classes of minerals that are known or suspected to be on the satellites include ice and frosts, various forms of sulfur and sulfides, salts, primary igneous rock-forming minerals (for example, iron-bearing silicates), products of alteration by water (clays), and possibly carbonaceous compounds. Knowledge of the mineral composition and distribution on a satellite surface provides some of the most useful evidence for studying formation history and subsequent evolution. This is so because the phases, or minerals, present reflect not only the assemblage of chemical elements incorporated into the forming satellite, but also (for example) a record of the chemical evolution of the interior reservoirs from which the materials were sequentially derived. For this reason, the Galileo payload includes the NIMS, described in chapter 7. The objective of mapping the satellite's surface mineral distribution is best served by a synergistic combination of the NIMS and imaging experiments, and the anticipation of this postencounter blending of the data has influenced the design of both of these instruments and the mission.

The Galileo NIMS investigation represents a new philosophy in remote sensing on planetary spacecraft. It combines, in one experiment, moderate to high spectroscopic and imaging capabilities (chapter 7) and utilizes the infrared region out to 5.0 μm, which is highly diagnostic of both atmospheric and surface species. Although the experiment philosophy is new, this instrument has not required new development, being simply the marriage of a telescope with a spectrometer. This instrument capability, coupled with the orbital coverage provided by the Galileo mission, allows unique geologic investigations of the jovian satellites, along with a broad range of studies of Jupiter's atmosphere. The objectives of the infrared spectrometer experiment are to map mineral compositional units on the surfaces of the jovian satellites and to characterize the mineral content of these units.

Specifically, one can contrast the capabilities of the NIMS experiment with classic imaging experiments and pure spectroscopic investigations. For imaging experiments, as exemplified by Galileo's imaging system, one obtains a very high spatial resolving power—a factor of 25 better than the NIMS experiment—but limited spectral information. The SSI camera contains only seven spectral channels and one broadband channel. Therefore, the imaging system will be able to make high spatial resolution multispectral images, but detailed spectroscopic characterization will depend on NIMS. In contrast to the customary imaging system, previous spectral investigations have been directed toward very high spectral resolution at the expense of spatial information. Consequently, such measurements have been directed toward global properties or constrained to individual localized features.

The longest wavelength achievable by the imaging experiment is 1.1 μm. The NIMS spectral range of 0.7 to 5.2 μm includes many of the spectral features of materials that might be expected to occur on the satellite surfaces. (It should be noted, however, that the NIMS spectral range was designed to overlap that of the imagery to facilitate the synergistic "blending" of data, as indicated above.) Sunlight that is reflected from the surface

shows spectral features, or absorption bands, due to molecular and lattice vibration transitions, which are often diagnostic of composition, banding, and lattice structure. Examples of some absorption bands and an example of the sharp contrast in whole-disk spectra shown by the Galileo satellites are given in figure 35. If one considers the extreme variability exhibited by these objects, it becomes clear that the type of "whole-disk" spectral information shown in the figure, although largely unambiguous, would be greatly enhanced if the composite whole-disk spectra could be broken down into these components. Recent laboratory studies also suggest that information concerning such parameters as grain size and intimacy of mixing can often be gleaned from the spectra along with the phase identification.

Regardless of detailed mineral identifications, spectral classification of compositional units and mapping of these units over the satellite surfaces are powerful tools for understanding satellite geologic processes. These studies are enhanced when compositional unit maps are combined with images and data from other scan platform experiments.

A crucial point is that Earth-based observations have already revealed many deep absorption bands on the satellites, despite the fact that only hemisphere spectra are available. This implies the possibility that when NIMS resolves the hemisphere into many thousands of spectral elements, many spectral features which are mated, suggestive, or even imperceptible in the whole-disk spectra may become exceedingly strong owing to the concentration of particular mineral components in that particular field of view. Even when operating at the highest spatial resolution, the field of view is apt to include several components. This is where imaging of the same field will be of great interpretive value for NIMS.

Thermal emission from the hot spots on Io can also be used by NIMS to investigate the satellite. The warm "lakes" and calderas radiate in the infrared, and a portion of this emission occurs in the NIMS spectral range. The distribution and characteristics of these hot spots will be investigated during the Io flyby and on each subsequent orbit. The latter measurements, when obtained near perijove, will be performed at a spatial resolution of about 300 km on Io's surface, a size comparable to some of the larger hot spots. This will be useful for understanding the energy outflow from Io and its time and space variations—especially when combined with the photopolarimeter-radiometer data (see below).

During the 20-month period of orbital operations, multiple passes of Europa, Ganymede, and Callisto will occur. With these frequent observations, NIMS will be able to map large areas of each satellite. By the end of the mission, roughly half of the surface of each of these three satellites will be spectrally mapped at a resolution of about 25 km or better. In addition, NIMS will obtain spectra of Amalthea and perhaps Jupiter's ring and two of the outer satellites, J6 and J7.

The NIMS resolution of Io at perijove, attained repeatedly during the course of the mission, is 300 km. This means that the evolution of Io's local or regional surface composition can be monitored with high spectral resolution by NIMS for two years and correlated with variation in thermal emission as observed by NIMS and from Earth.

Ultraviolet Spectrometry: Atmospheric and Surface Studies

The ultraviolet spectrometer (UVS) will identify atomic and molecular gases in the atmosphere of the satellites and their distribution in altitude and location. The UVS is sensitive to small quantities of H, O, N, C, S, N_2, NO, C_2, Mg, CO, SO_2, N_2^+, CO^+, CO_2^+, and Mg^+. It will identify those constituents on the surface which are ultraviolet active (e.g., SO_2, NH_3, O_3) and obtain some information as to physical characteristics such as grain size. It will also measure plasma torus properties, including emissions from multiply ionized oxygen and sulfur as observed by Voyager.

The ability of the Galileo UVS to measure relatively small spatial domains increases the chances of finding local concentrations of ultraviolet-active substances. Already, even in whole-disk spectra, the Earth-orbital International Ultraviolet Explorer satellite has identified spectra features associated with frozen SO_2 on Io and longitudinally mapped them and was able to identify features associated with implanted sulfur on Europa and torus emission features beyond the wavelength range of Voyager. The Galileo UVS will be able to map these in detail. The ability of the UVS to measure atmospheric species with good

ORIGINAL PAGE
COLOR PHOTOGRAPH

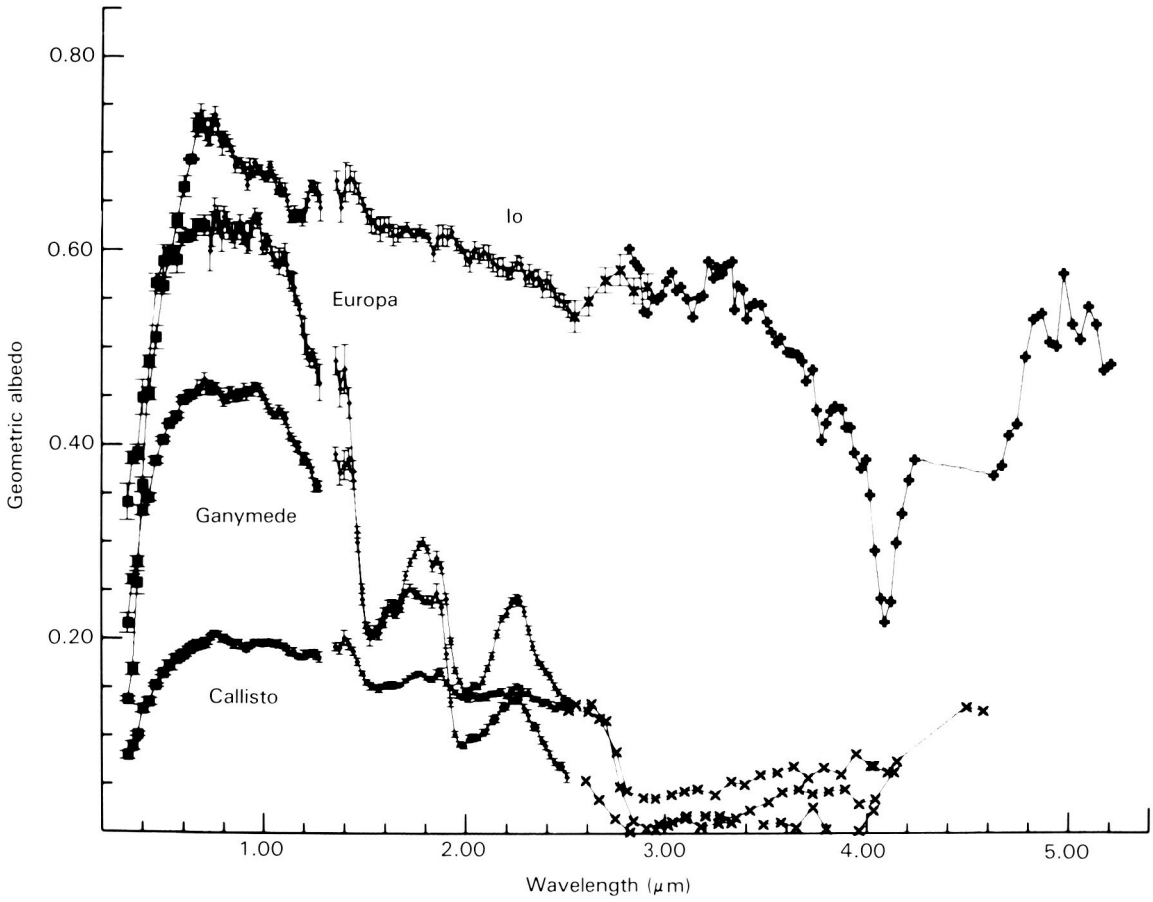

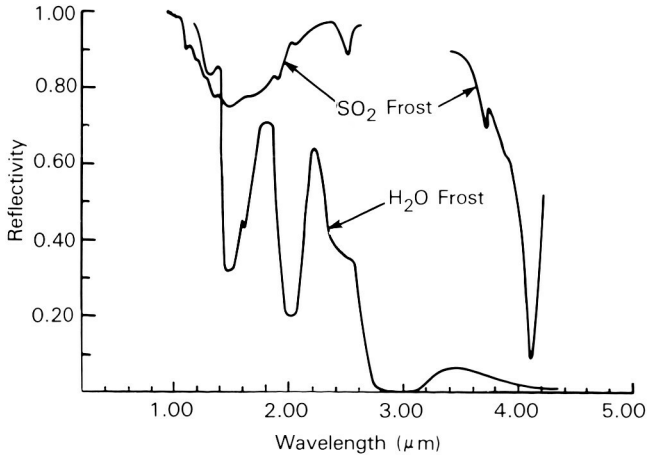

Figure 35. Telescopic spectra of the Galilean satellites of Jupiter (upper panel) compared to laboratory measurements (lower). The full-disk spectrum of Io at the top shows an infrared absorption band at 4.1 μm. Laboratory measurements shown below indicate that this band corresponds to sulfur dioxide (SO_2), which may occur on Io's surface as a frost or adsorbed species. The spectra of the outer Galilean satellites—Europa, Ganymede, and Callisto—show absorption features similar to the laboratory spectrum of water frost. The infrared region of the spectrum is highly diagnostic for characterization of surface materials.

vertical spatial resolution may help us to understand not only the escape rates but also the processes that have propelled the molecules into the atmosphere (e.g., thermal versus sputtering).

During the 20-month mission, the UVS will map changes in frozen and absorbed SO_2 coverage on Io from about 10 R_J and correlate these data with variations in torus emissions and the general fields and particles environment as measured by the fields and particles instruments.

The UVS spectral coverage is from 1150 to 4300 angstroms. The addition of some 300 spectral bands in this range complements the eight charge-coupled device camera filters in the visible and nearest infrared, as well as the 200 NIMS visible and infrared bands, and virtually assures identification of any spectrally active species that is a major constituent of any spatial domain on the order of tens of kilometers. Instrument characteristics are given in chapter 7.

Photopolarimetry-Radiometry: Thermal Structures

The fourth instrument on Galileo's scan platform is the photopolarimeter-radiometer (PPR). This instrument is capable of measuring surface temperatures, heat flow, emissivity, and thermal inertia for the areas within its field of view. On a close flyby, this field of view could provide 2.5-km resolution! We will learn much about global heat flow on Io and the role of discrete sources. Also, we will investigate the crustal structure in volcanic areas via heat flow mapping to gain insights into the mechanisms of volcanism. Synoptic observations of Io made from distances near Europa's orbit over 20 months will allow correlation of both regional and global heat flow with regional and global changes in albedo, depth of absorption bands in the ultraviolet and infrared, torus ion population, and other expected regional and global variations. In addition, passive thermal measurements on all the satellites will greatly augment our understanding of the thermophysical properties and from that, the textural nature of the near-surface materials. Finally, the instrument will measure albedo and photometric functions of the material, thereby complementing compositional measurements by the NIMS, UVS, and SSI instruments.

The PPR complements the thermal measurements made by NIMS and is the only instrument on Galileo that can measure the normal thermal emission of absorbed sunlight from the Galilean satellites. Thus, the PPR is necessary for any direct measurements of surface temperature and the thermophysical properties of the surfaces.

Io and its volcanic hot spots present a special case of great scientific interest. For spots much hotter than the ambient background, measurements of thermal emission can be made by NIMS, with its higher spatial resolution and its imaging capability, as well as with the PPR. Indeed, if the spots are at a temperature of 400 K or higher, more of their energy will fall within the spectral range of NIMS than of the PPR. During the initial close flyby of Io, both instruments will do an excellent job, and together they can give a comprehensive picture of thermal radiation from hot spots over a wide spectral range. Later in the tour, when encounters take place at much greater distances, both instruments lose capability. Generally, however, NIMS remains more sensitive to hot-spot radiation than does the PPR for all encounters and spot sizes, and for the more distant encounters and the small spots, the ability of the PPR is quite limited.

Particles and Fields

Magnetometry

The study of any induced or intrinsic magnetic fields associated with the satellites will be important for our understanding of the interior structure composition and dynamics of the satellites; the way that magnetospheric particles impinge on and affect the evolution of satellite surfaces and atmospheres, including temporal variations; and fundamentals of physics of magnetic field generation in solid objects of the solar system.

Along with other properties, the Galilean satellites may have global or regional magnetic fields arising from dynamo activity, fossil magnetization, or electrical induction. These factors involve a key class of parameters in defining the internal intrinsic physical and chemical states of the satellites. Our understanding of the various means of creating such planetary magnetic fields is limited, since this is a relatively new area of study.

Of the three means of magnetization mentioned above, dynamo action due to self-regenerated magnetic fields arising from coupled

convective (and conducting) fluid motions and preexisting magnetic fields in planetary interiors has the longest history and is generally dealt with in the most detail. For the Galilean satellites, the possibility of such dynamo activity is mediated strongly by the exotic interior constituents thought to be present, with water (probably salty) being a possible ingredient of the interiors of at least Ganymede and Callisto. Even for Io, the density appears low for any expectation of a substantial fraction of iron, the most common high-conductivity material. Nevertheless, even subregenerative dynamo activity appears possible for these objects; this increases the likelihood that there is a global magnetic field due to dynamic processes in the interiors. Alternatively, the fact that the Moon is endowed with a spectrum of local and regional magnetic fields increases the possibility that a similar form of fossil magnetization is present on one or more of the jovian satellites. Finally, electromagnetic induction cannot be ruled out as a dynamic source of magnetic fields in the neighborhood of the Galilean satellites.

For these three main classes of field sources, fundamental constraints on the internal physical and chemical constitution prevail. In all cases, the presence of magnetic fields associated with the satellites implies strong but still poorly understood constraints on heat flux, internal thermal regimes including heat sources, and internal chemistry. Of equal interest is the effect on the neighborhood of these objects if a global magnetic field is present, for such a field will couple the planet and its atmosphere (and especially ionosphere) to the ambient jovian magnetospheric plasma.

The chances of detecting a dynamo field associated with Ganymede and Callisto may be slight. First, these objects may be frozen throughout because of the efficiency with which solid-state convection removes heat from the interiors. There is a possibility that salts may have been extensively leached from the interior, lowering the melting point. Obviously, incipient crystalization of the interior will concentrate these salts in solution. However, preliminary estimates are that only a small deep liquid zone might exist in each in equilibrium, with radiogenic heat production and loss if solid-state convection is effective in the overlying solid ice. Even if the zone were augmented, say by concentration of uranium and potassium in the liquid or by inefficiency of convection in the overlying solid, it is not clear whether a dynamo field would be detectable. This is so because, for example, sea water conductivity would probably have to be augmented by several orders of magnitude to produce an effective dynamo fluid. The question is still open, however. A detectable dynamo field on Io seems more likely because Io's interior is probably extremely hot and sustains an average surface heat flow over an order of magnitude greater than that of Earth. The high-density material we would expect to find in Io's deep material would probably be mainly FeS rather than Fe, based on chemical considerations. If so, the conductivity would be almost three orders of magnitude less than that of molten Fe. Thus, the difference would presumably have to be made up by much more vigorous convection than in the deep Earth, for example, for Io to have a strong field. Perhaps Io's enormous tidal input could satisfy this requirement. Also, the theory suggests the requirements for generating and sustaining a dynamo field are much less when the object is itself situated within a strong magnetosphere such as that of Jupiter. Finally, there is the possibility of permanent magnetization of these objects. Mercury was not expected to have a field because of its solid interior, but it does. The Moon's crust also exhibits substantial permanent paleomagnetism, as do the oceanic and continental crusts of Earth (although global properties of such rock magnetism—as opposed to specimen properties—are generally overridden by Earth's strong global field). In summary, satellite magnetic fields may be studied from Galileo and may reveal much concerning the composition, state, and dynamics of their interiors.

Plasma Experiment

The interaction between jovian magnetospheric particles and the satellites' surfaces puts satellite surface material into the magnetosphere. This material in turn is ionized and returns to the satellite surface with sufficient energy to eject still more surface material. Thus, the satellites are bombarded with their own surface material as well as with material initially derived from Jupiter or the Sun. Some satellite material is completely ejected, resulting in loss from the satellite, and some simply receives enough energy to be launched on a trajectory such that it reimpacts the satellite elsewhere. The latter can strongly affect population of the atmosphere—especially on satellites or parts of

satellites where thermal processes are relatively unimportant because of the low vapor pressure curves of the available materials or because of the low temperatures.

In steady state, there is a population of satellite-derived material around the satellites. Line emission from the Io torus can even be detected and the torus mapped from Earth. In situ orbital compositional measurements of satellite surface material is therefore possible. In principle, such plasma measurements constitute an exceedingly powerful "cross constraint" on surface compositional models, because all the other tools at our disposal on Galileo are oriented toward phase composition, with elemental composition as an indirect fallout. In contrast, the plasma measurements examine directly the elemental (ionic) composition of the plasma and only indirectly the nature of the surface phase from which it derived. The plasma instrument can measure electrons and ions from 1 eV to 50 keV, as well as identify and measure fluxes of the major species derived from satellite surfaces: Na^+, K^+, and S^+, as well as the dominant ambient species, H^+, He^+, and He^{2+}. In general, the radial distributions of satellite-derived ions and Jupiter/Sun-derived ions are quite different and distinguishable.

Energetic Particles Detector

The energetic particles detector will also help to study satellite-derived materials. In the case of the weak saturnian magnetosphere, for example, most of the particles measured by Voyager's energetic particles detector in the inner portion were oxygen ions derived from the satellites. In addition to direct measurement of the satellite-derived materials, shadowing by the satellites will reveal the nature and intensity of the bombarding flux to which their surfaces are subjected. Information on other means of ion loss from the magnetosphere will elucidate loss fluxes from the satellite sources. The detector measures electrons and protons greater than 20 keV and heavier ions greater than 100 keV/nucleon as a function of energy, angle, and particle species.

Dust Detector

The overall objective of the dust detection investigation is the exploration of the physical and dynamic properties of small dust particles in the jovian environment with masses between 10^{-16} and 10^{-6} g. The parameters to be studied include the mass, speed, flight direction, and charge of individual particles. The impact rate, size distribution, angular distribution, and charge will be determined with respect to the jovian distance, the distance from the satellites, and the magnetospheric coordinates.

The primary specific objectives are:

- to search for evidence of "rings" of particles in jovian orbits, in addition to the ring observed by Voyagers 1 and 2.
- to search for the particles responsible for generating both the visible ring and any other rings that may be found; to determine whether the ring particles are secondary ejecta from a minor moon (or moons). If not, then a science objective will be to determine the true origin of the rings.
- to examine the hypothesis that there is a Jupiter-orbiting population of dust particles not in rings that may have derived from mutual collisions of Jupiter's outer moons.
- to search for the large flux increase of interplanetary meteoroids that is expected to be caused by the powerful gravitational field of Jupiter and to search for similarly concentrated interstellar grains.
- to search for evidence of particles ejected from, or levitated above, the Galilean moons.
- to evaluate the relative importance of the processes of volcanic ejection, impact-induced ejection, and electromagnetic removal or levitation of particles from the moons.
- to measure charges on the particles and to understand the charging causes.
- to search for evidence of electrostatic disruption of dust balls in the jovian magnetosphere.
- to evaluate dust trajectories within the jovian magnetosphere.
- to correlate the spatial structure of the radiation belts with the dust distribution.
- to evaluate how albedo variations on the jovian moons may be caused by variable impacting dust populations.

Radio Science Studies

The radio science experiment on Galileo can contribute to understanding of the satellites in two main ways: it can provide (via occultation) information on the structure of tenuous satellite atmospheres, and it can provide evidence on the internal structure of the satellites. Also, the radio science experiment can provide valuable information on the plasma population in the ionized torus around Io and its time variation, which may correlate with variations in such parameters as volcanic activity and heat flow over the duration of the mission.

Radio Propagation Experiments

Radio occultations by the Galilean satellites are possible in principle during the Galileo orbiter's tour and would be important for several investigations. While it is not expected that any of the satellites have atmospheres of sufficient density to be measured in this way, at least one has a detectable ionosphere. The Pioneer 10 occultation experiment found a well-developed ionosphere on Io. There is probably a close connection between the ionospheric characteristics, the level and nature of concurrent volcanic emissions from Io, and the density and other features of the Io torus. Additional ionospheric measurements will give information on the vertical and longitudinal distribution of neutral species and temporal variations, as well as the interaction of magnetospheric radiation with the neutral species. Such information is needed for modeling the processes that supply and control Io's atmosphere. No occultation measurements have been made of the other Galilean satellites, which may also have detectable ionospheres, but if they do, the source is probably different from that of Io. For example, measurable ionospheres might be formed from the dissociation products of water derived by sublimation from icy surfaces. The best chance for an atmosphere of thermal origin may be on Callisto, the satellite with generally the warmest surface.

Radio occultation measurements would also provide accurate values for the radii of the Galilean satellites. These results would contribute to the determination of more precise values for their average densities, which in turn are important to theories concerning satellite origin and evolution.

Additional radio propagation experiments with Galileo will include attempts to detect Jupiter's ring, which occulted Voyager 1 after the spacecraft's exit from atmospheric occultation. While no signal perturbation was detected, these results helped determine definitive upper limits on the sizes of the particles in this ring. Several additional attempts at detection should be made with Galileo, since the ring characteristics may vary with time and because the radio technique is quite sensitive and indicative of fundamental ring characteristics whenever a signal change can be measured. For example, the Voyager 1 radio occultation by Saturn's rings showed rich detail throughout and successfully measured the F ring, even though its normal optical depth (at the radio wavelength) was only about 0.01.

Celestial Mechanics Experiments

Celestial mechanics experiments may be described in terms of measurements made with the orbiter itself as it probes gravitational fields in Jupiter's environment. The radio system serves as the sensor for small gravitational perturbations on the trajectory, which in turn can be used to infer the structure of the gravitational fields of Jupiter and its satellites. Also, we will measure the relativistic time delay in radio ranging during solar conjunctions and improve our knowledge of the orbits of Jupiter and the Galilean satellites. Using one-way doppler data, referenced to the spacecraft's ultrastable oscillator, we will measure the general relativistic redshift in the gravitational field of Jupiter.

Perhaps the most significant result of the celestial mechanics experiments will be a measurement of the second-degree harmonics in the gravitational fields of Ganymede, Io, and Europa. This aspect of the investigation will receive considerable emphasis. At least two encounters each with Ganymede and Europa and one encounter with Io will make it possible to determine differences in the principal moments of inertia of the satellites with an error an order of magnitude less than the expected size of the differences, at least for Ganymede. With this information we will use the fact that the satellites respond to comparable perturbations from rotation and tides to discriminate among an assortment of plausible interior models.

We will also be able to determine the degree of central compression in the satellites and whether the satellites are totally differentiated with respect

to rock and ice or homogeneous throughout, and in addition obtain information on chemical composition and physical states in the interiors. While the Pioneer and Voyager spacecraft determined the mass and mean densities of the Galilean satellites and thereby provided clues to their chemical composition, the Galileo orbiter will approach the satellites at close enough range to discriminate between the total mass of the satellite and higher-order terms in the gravitational field. It is these higher-order terms that yield detailed information on internal conditions in the satellite.

The Galileo orbiter will provide improved knowledge of the orbits of Jupiter and the Galilean satellites. The new data from Galileo, which will be combined with ground-based data and Voyager data, will be limited only by the accuracy of the orbit determination of the orbiter. Experience with similar analyses on Mars orbiters and Mercury flybys indicates that the reduced-range data to the center of mass of Jupiter or a satellite during a close flyby can be determined to about 150 meters. Such data are important to an overall program to improve knowledge of the orbital motions of the entire solar system for experimental relativity. In addition, new orbital data on the Galilean satellites will yield information on the orbital energy distribution among these satellites and on some of the dynamic forcing terms, which are important for understanding the orbital evolution of the satellites since their formation. Galileo will establish tighter observational bounds on the secular acceleration of Io's mean orbital motion, which in turn can be used to deduce the character of the heat flow from Io by tidal heating. Current observational bounds leave some question as to whether Io is constantly in a state of high activity, as evidenced by the Voyager observations of volcanism, or whether such activity is episodic.

The degree of internal differentiation of the four Galilean satellites is an important clue to their interior composition and also provides a clue to the abundance of radionuclide, tidal heating, and accretional heating contributions; mechanisms of heat transport; and the general history of planetary energetics. By measuring the response of a rotating planet to its centrifugal potential, we can deduce information about its degree of central condensation, when hydrostatic equilibrium is assumed. Because the Galilean satellites all rotate synchronously with their orbital period, it would at first seem unlikely that the resulting equatorial bulge would be detectable over nonhydrostatic contributions to the gravity field. In fact, the orbital periods are short enough that this is not necessarily the case. Furthermore, the tidal distortion due to Jupiter is comparable in magnitude to the rotational distortion. Since the rotational and tidal responses are, to an excellent approximation, separately excited and separately measurable, we can deduce the degree of central condensation in the interior of a satellite in two independent ways and thus verify the assumption of hydrostatic equilibrium. This assumption is expected to hold for a low-density satellite such as Ganymede, and thus it will be possible to use the second-degree harmonics determined from the orbiter as important boundary conditions on the interior models.

The Galileo orbiter will be used to determine the zero-order gravitational moment (mass) of the four Galilean satellites, or actually the product of the gravitational constant and the mass gravitational moment. In addition, because of the planned close approaches of the orbiter to the surfaces of the satellites, it will be possible to determine the next significant higher gravitational moments as well, namely, the product of G with differences in the principal moments of inertia of the satellites, $G(B-A)$ and $G[C-(A+B)/2]$. Past missions to Jupiter have been sensitive only to the mass, so Galileo will provide the first measurements of these principal moment differences to an accuracy of better than 10^6 km^5/s^2, and as a result information will be obtained on the internal structure and composition of the satellites. For example, the expected size of these higher-order gravitational moments varies from about 5×10^6 to 3×10^7 km^5/s^2 for Ganymede, depending on the degree of differentiation of rock and ices in the deep interior. The expected range of values can be predicted based on the known response of a satellite to its own rotation and to the distortions of the body of the satellite by tides raised by Jupiter. In the absence of these two forces the satellite would be spherical, no matter what the nature of its internal structure, and only the mass would be needed to define its gravitational field. However, because of the rotational and tidal distortions, the gravitational field deviates from a spherical shape, and as a result subtle disturbances are set up in the flyby orbit which can be interpreted in terms of the principal moment differences defined above. The measured

magnitude of the moment differences then yields the internal structure of the satellite by means of physical models generated by computer simulation.

The expected range of the principal moment differences, expressed in terms of what will actually be measured by means of disturbances in the orbit of the Galileo orbiter during the flyby, for Ganymede are illustrated in figure 36 along with a series of curves showing the expected accuracy of the measurement as a function of the two most important flyby parameters, the radius of closest approach to the center of the satellite and the flyby velocity. Actually, for a given satellite tour, we have very little control over the flyby velocity, so the important design parameter is the flyby distance, although to a lesser extent the viewing angle of the flyby as viewed from Earth and the inclination of the flyby orbit to the equator of the satellite are also important. In general, a near-polar orbit will determine one component of the gravitational field, $G[C-(A+B)/2]$, while a near-equatorial orbit will determine the other component, $G(B-A)$; thus, the determination of both components requires at least two flybys of the satellite.

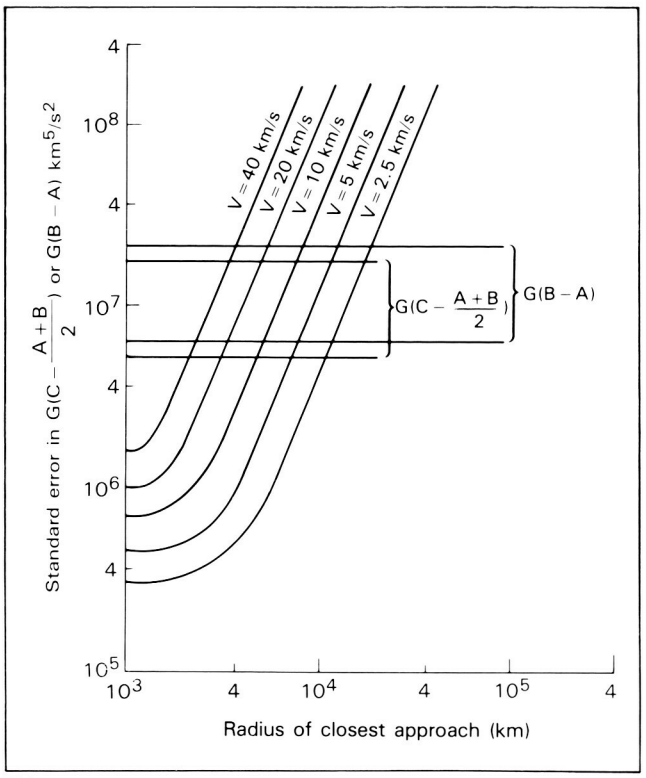

Figure 36. Measurement errors for different flyby parameters at Ganymede. The errors are assumed to be the same for both zonal and longitudinal harmonics. Horizontal lines show maximum and minimum predicted values for hydrostatic equilibrium.

As indicated in figure 36, it is possible to perform a very significant gravity experiment on Ganymede with the Galileo mission. The error curves are essentially the same for all the Galilean satellites, but the size of the expected coefficients varies with rotation and orbital distance for each satellite. For Io it is possible to perform an interesting gravity experiment, but only one flyby of Io is planned, a near-equatorial pass before the orbit insertion phase of the mission. Fortunately, if only one flyby is available, it is far better to have an equatorial pass than a polar pass, in which a clear separation of the rotational and tidal distortion is impossible. Therefore, we expect to obtain important information from the Io flyby, although not of the high quality expected from Ganymede, for which we will have at least one equatorial and one near-polar pass.

Finally, we must deal with the question of possible departures from hydrostatic equilibrium. A principal diagnostic factor of nonhydrostatic behavior is an inconsistency between the separately determined values of gravity moments or values of these quantities that lie completely outside the plausible range. Based on the size of known nonhydrostatic moments for the Moon, the large rotational and tidal distortions of Io should so completely dominate its figure and gravitational field that nonhydrostatic behavior should not present a problem. For Europa there is a possibility that we will measure only nonhydrostatic components and that little information will be obtained on the interior. In this case, the value of the measurement will lie in its ability to provide information on the magnitude of stresses in the surface layers of Europa. The two outer satellites, Ganymede and Callisto, are expected to be close to hydrostatic equilibrium because of their high ice content and liquid interiors.

In summary, the Galileo flybys of Io and Ganymede should provide effective probes of their interior structures. The flybys of Europa may provide similar information about that satellite, or

they may provide measurements of nonhydrostatic components in the gravity field. For Callisto, because of its greater distance from Jupiter, the gravitational field should appear essentially spherical to the flyby trajectory, and a determination of interior conditions is doubtful. The flybys of Callisto primarily provide a test for gross departures from hydrostatic equilibrium.

chapter 4 THE MAGNETOSPHERE

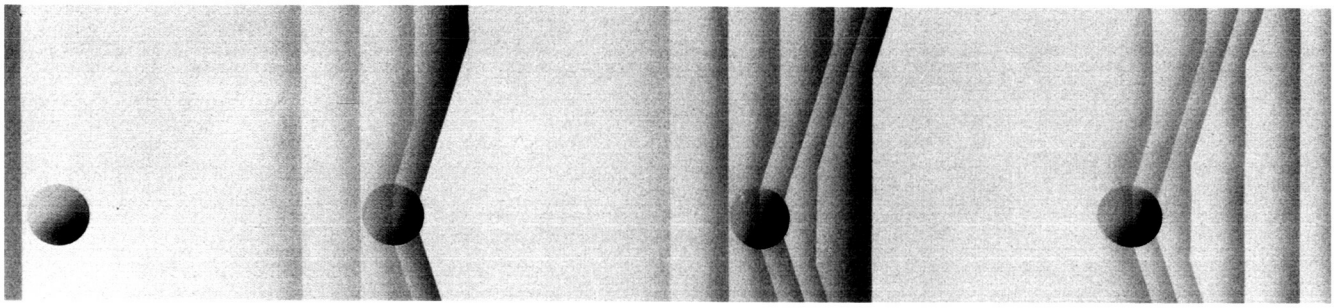

Previous Findings

Jupiter, with its very rapid rotation rate and strong magnetic field, presents an opportunity to investigate exotic physical processes taking place in an enormous volume of space around the planet—processes that cannot easily be duplicated in laboratories on Earth. The jovian magnetosphere—a vast swarm of energetic particles and gases moving in the magnetic field of the planet—is dominated by rotational effects. The power necessary to drive the planet's radiation belts, magnetosphere, and a torus of ions in the orbit of Io comes largely from Jupiter's rotational energy. At Earth, in contrast, the solar wind—the high-velocity stream of protons and electrons from the Sun—provides the energy for our planet's magnetosphere. Jupiter, in fact, resembles rapidly rotating stellar objects such as pulsars, although its rotation rate is much less and its magnetic field is much weaker than those of a pulsar. However, the study of the jovian magnetosphere can provide insight into many astrophysical phenomena that cannot be observed directly in any other way.

Data gathered during the early flybys of the Pioneer spacecraft indicated that there are three main regions of the jovian magnetosphere (fig. 37). The magnetic field of Jupiter dominates the inner magnetosphere, a region extending to about 20 times the radius of the planet. In the middle magnetosphere, from about 20 to about 60 Jupiter radii, the magnetic field is severely distorted by the trapped plasma. The outer magnetosphere beyond 60 Jupiter radii exhibits significant irregularities in both the magnitude and direction of the planetary magnetic field. The solar wind interacts on a vast scale with particles and fields to give rise to a complex and dynamic conflict between magnetic forces originating in the planet and those forces carried by the solar wind itself (fig. 38).

A torus of dense plasma was found by the Pioneer spacecraft at jovicentric radial distances of about 3 to 11 R_J, near the magnetic equator in the magnetosphere. The telemetry from Pioneer's plasma analyzer presents difficulties in interpretation, since the electrometer responses were near those corresponding to the measurement limits of the instrument. Thus, the ion species could not be positively identified, although the angular distributions of the ions clearly display the effects of corotation with the planet. To estimate the ion number densities and temperatures, the ions were assumed to be protons. The fact that these are heavy ions, such as S^+ and SO_2^+, is evident in the later Voyager measurements. With the assumption that the primary ions were protons, the corresponding densities ranged from about 100/cm^3 at 3 R_J to 1/cm^3 at 14 R_J. The thickness of the plasma

What Is a Magnetosphere?

When the supersonic ionized gases flowing outward from the Sun (the solar wind) arrive at the vicinity of the planets in the solar system, various types of interactions are possible, depending on the strength and orientation of a planet's magnetic field and its rotation rate. If the planet has a sufficiently large magnetic field, it forms a cavity in the solar wind. The region inside this cavity is dominated by the planet's environment, its magnetic field, and a swarm of energetic particles and gases. The low-energy ions, protons, and electrons are called plasma. This region is called the magnetosphere, and the boundary between the magnetosphere and the solar wind is the magnetopause. A bow shock is necessarily formed in the solar wind upstream from the magnetopause. A low-energy plasma, largely concentrated within a few planetary radii of the equatorial plane, is distributed throughout the magnetosphere, thus forming a plasma sheet through which concentrated electric currents flow (the current sheet). In the direction away from the Sun the magnetosphere is drawn out in a long magnetotail by the drag of the solar wind. At Jupiter the plasma within the magnetosphere tends to rotate along with the rotating magnetic field of Jupiter. If it rotates at the same speed it is referred to as rigid corotation. Processes within the magnetosphere cause the plasma to rotate at less than rigid corotation speeds in some regions.

sheet at 15 R_J is about 2 R_J. The calculated temperatures are 100 to 400 eV. The Pioneer plasma analyzers detected a moderate maximum of ion densities near the Io flux tube at radial distances of 5.9 to 6.5 R_J at the magnetic equator.

Observations with the plasma and medium-energy charged particle instruments on the Voyagers provided further insight into the nature of the jovian magnetospheric plasmas. Heavy ions from the volcanic eruptions on Io were found to be the dominant constituents of the great torus of plasmas in the inner magnetosphere. For example, the principal heavy ions detected by Voyager 1 at 5.3 R_J near the magnetic equator are S^+ (69 percent), O^+(21 percent), S^{2+} (2.4 percent), and O^{2+} (1.5 percent). Identification of these ion species is possible due to the high speed of corotation relative to ion thermal speeds (random motions due to the ion's energy in the field compared to its motion with the field). At increasing radial distances, identification of ions becomes more difficult and uncertain as the ion temperature increases, and clear maxima in ion intensities as functions of energy are not detected. Heavy ions are observed with the plasma instrument to jovicentric radial distances of 40 R_J. However, at the larger distances the corotation of the plasmas is sufficient to give the ions kinetic energies above the energy range of the plasma instrument, which is 6 keV. The energy of a rigidly corotating O^+ ion at 30 R_J is 10 keV. Measurements with the medium-energy particle detector, which has an energy threshold of 30 keV, show that the heavy ion populations extend to the magnetopause near the magnetic equator.

The maximum densities of thermal ions in the jovian magnetosphere are located near the Io orbit. These densities are 3000/cm^3. Densities decrease rapidly with increasing radial distances to values of 1 to 10/cm^3 at radial distances of 10 to 20 R_J. Beyond these radial distances and in the plasma sheet the ion densities range from 10^{-3} to 1/cm^3. Above or below the plasma sheet the densities are as low as 10^{-5} to 10^{-4}/cm^3.

There is a large gradient in the ion temperatures on the planet side of the torus near the Io orbit. The ion temperature decreases rapidly from 40 eV at 6 R_J to 1 eV at 5 R_J. For the bulk of the plasma torus at 6 to 8 R_J the ion temperatures

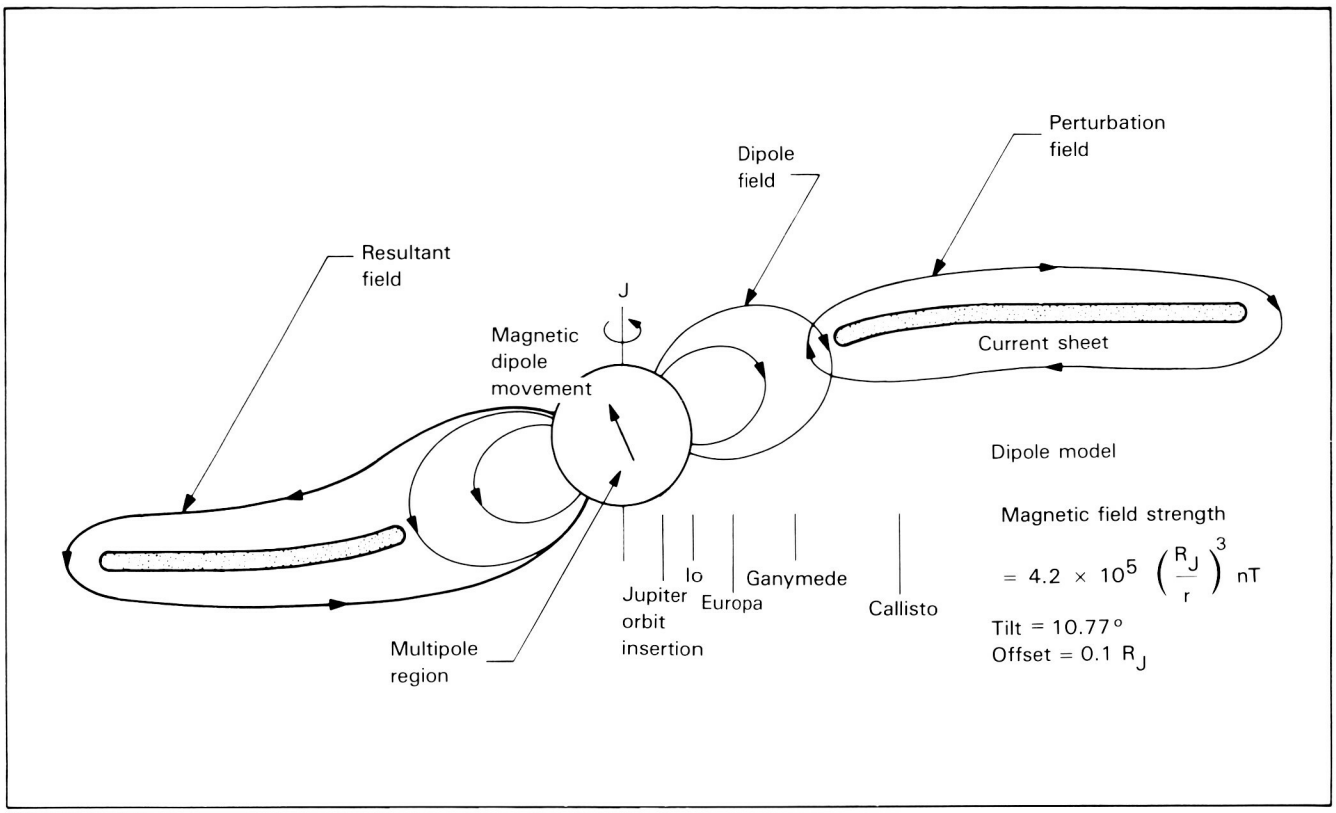

Figure 37. The magnetic field of Jupiter dominates the inner magnetosphere, one of the three major regions. The positions of the Galilean satellites in this region are shown on one side of the planet to relate their orbital radii to the scale of the inner magnetosphere. All interact strongly with this region of particles and fields.

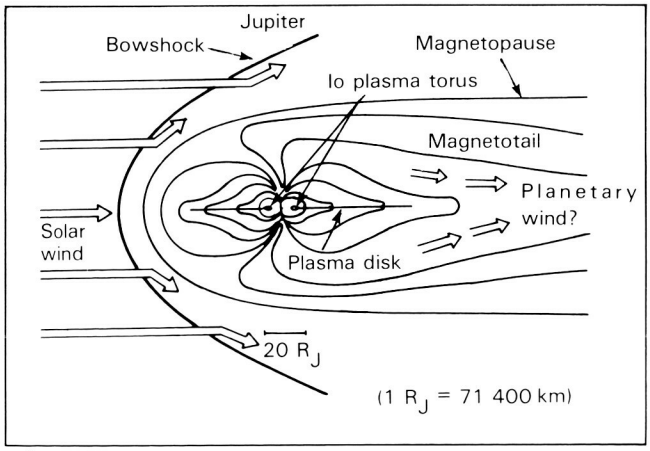

Figure 38. There are complex and dynamic interactions among the solar wind, the magnetosphere, the planet's magnetic field, the Galilean satellites, and other inner satellites.

are 40 to 100 eV. At larger radial distances in the plasma sheet the ion temperatures increase until typical temperatures are 20 to 40 keV at 30 to 100 R_J. Electron temperatures are most suitably described in terms of a two-component plasma, hot and cold. The cold electron temperatures are 10 to 100 eV over the radial distance range of 6 to 40 R_J near the magnetic equator. At the inner edge of the torus, these electron temperatures decrease precipitously to 0.5 eV, coincident with the decrease in ion temperatures noted above. The hot component of the electron velocity distribution is generally less dense than the cold component. For example, the density of the hot component at 8 R_J is 1 percent of the total number density and increases to 50 percent at 40 R_J. The characteristic temperature of these hot electrons is 1 keV. The temperatures of electrons and ions in the plasma sheet are cooler relative to those detected above and below the plasma sheet.

The plasmas are observed to corotate rigidly

with Jupiter to radial distances of about 20 R_J. At distances of 20 to 40 R_J the corotation speed is significantly less than that expected from rigid corotation by factors of 2 or less. At radial distances exceeding 40 R_J the plasmas are again observed to rigidly corotate occasionally, as inferred from measurements with Voyager's medium-energy particle detector. However, flow speeds at these larger radial distances are less than the rigid corotation speeds by factors of 10 or less at other times. Beyond radial distances of 130 R_J in the dawn side of the jovian magnetosphere the ion flows become directed generally anti-Sunward, with a strong flow along directions that are radially outward from the planet. This phenomenon is called the magnetospheric wind. At the lesser radial distances of Io's orbit, Voyager's plasma instrument detected a perturbation in the direction of bulk flow from that corresponding to rigid corotation as the spacecraft passed near the Io magnetic flux tube. Magnetic field measurements also indicate the presence of a strong, magnetically field-aligned current.

Observations during the Pioneer flybys of Jupiter revealed that the giant planet's magnetosphere (fig. 39) is an extensive and highly dynamic reservoir of charged particles. The Pioneer results also provided valuable insights into several physical phenomena operating in the magnetosphere of Jupiter, such as interactions between electromagnetic waves and energetic particles (wave–particle interactions) and radial diffusion of these charged particles. The Voyager mission to Jupiter confirmed the Pioneer results, and Voyager's much improved instrumentation to detect and measure energetic ions yielded fundamental advances in knowledge of this dynamic magnetosphere. There are unusually large numbers of oxygen and sulfur ions in the magnetosphere, with comparatively few carbon ions and a small number of sodium ions. Both sodium and sulfur abundances are much greater in comparison to their relative abundance in the spectrum of the solar wind ions flowing outward from the Sun, showing that many of the particles in the jovian magnetosphere are supplied by the satellites, particularly Io.

Three different ion sources have been identified for the magnetospheric plasma: the Sun, the jovian ionosphere, and the large jovian satellites. In the outer magnetosphere the ions of helium, carbon, nitrogen, oxygen, neon, manganese, silicon, and iron probably originate from the solar wind. Closer to Jupiter, the ions of sulfur, sodium, and oxygen probably originate from Io and its plasma torus. Energetic molecular hydrogen, H_2 and H_3, also has been found in the jovian magnetosphere. The energetic H_3 is most likely of ionospheric origin, while the H_2 may come from the ionosphere and possibly from the moons. Comparison of data obtained by the flybys of the two Voyager spacecraft indicates that the ion population in the magnetosphere varies considerably with time.

Beyond 10 Jupiter radii, the pressure of the energetic ion particles exceeds that of the magnetic field. Thus, the energetic ions play an important role in determining the dynamics of the jovian magnetosphere. The presence of a large particle pressure at the jovian magnetopause is completely different from conditions at Earth, where the magnetic pressure is the important force balancing the solar wind. Interaction with the solar wind is thus very different at Jupiter than at Earth.

Io affects the environment of Jupiter in ways other than its gravitational pressure in the jovian system. Before spacecraft flew by the giant planet, Io was known to affect radio emissions from Jupiter and to possess a sodium cloud that moved around Jupiter in the vicinity of this satellite. Later, a torus of plasma encircling Io was found (fig. 40) in which there are ionized atoms of sulfur and oxygen. These ions are believed to be associated with the volcanic eruptions on Io. Temperatures of these ions reach 60 000 K–ten times that at the surface of the Sun. How the composition and number of ions in this torus vary with time is still unknown. Observations from Voyager show that Io's volcanoes are probably a source of sulfur dioxide. This gas escapes into space, where it becomes dissociated into sulfur and oxygen and ionizes to form the ring-like cloud of neutral and ionized gases along Io's orbit. As Jupiter spins, its magnetic field also spins, pulling the charged particles along with it. If they reach the same spin rate as Jupiter, they become corotating, and the speed of corotation increases with increasing distance from the planet. Jupiter thus accelerates the ions to high velocities, and the major energy input to the Io torus comes from Jupiter's rotational energy. Evidence from Pioneer and Voyager suggests substantial variations of the torus density with time that may be related to the level of volcanic activity on Io.

The combined observed energy dissipation due to ultraviolet radiation from the torus, from aurorae on Jupiter, and from the magnetospheric wind appears to be greater than can be supplied by rotational energy transferred into the Io torus. Where the additional energy comes from is a puzzle. If energy transfer occurs over a greater volume than the torus, then these regions must rotate more slowly than the corotation rate. Otherwise, the magnetic field could not supply sufficient energy to the ions.

The Voyager spacecraft provided an initial survey of the plasma wave and radio emissions

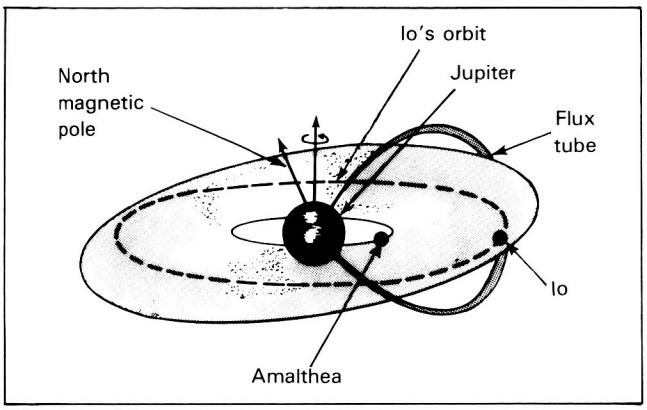

Figure 40. A torus of plasma surrounds Jupiter like a doughnut at about the distance of the orbit of Io but inclined in that orbit to the plane of the planet's magnetic equator.

Figure 39. Jupiter's magnetosphere is created by the planet's powerful magnetic field holding ionized particles of the solar wind away from the planet. As these particles are spun out by the centrifugal force of Jupiter's high-speed rotation, they drag the magnetic field with them. Jupiter's magnetosphere has an average diameter of 14 million kilometers. If its magnetosphere could be seen from Earth at a distance of half a billion miles it would occupy 2° of sky, compared to the Sun's 0.5° of sky.

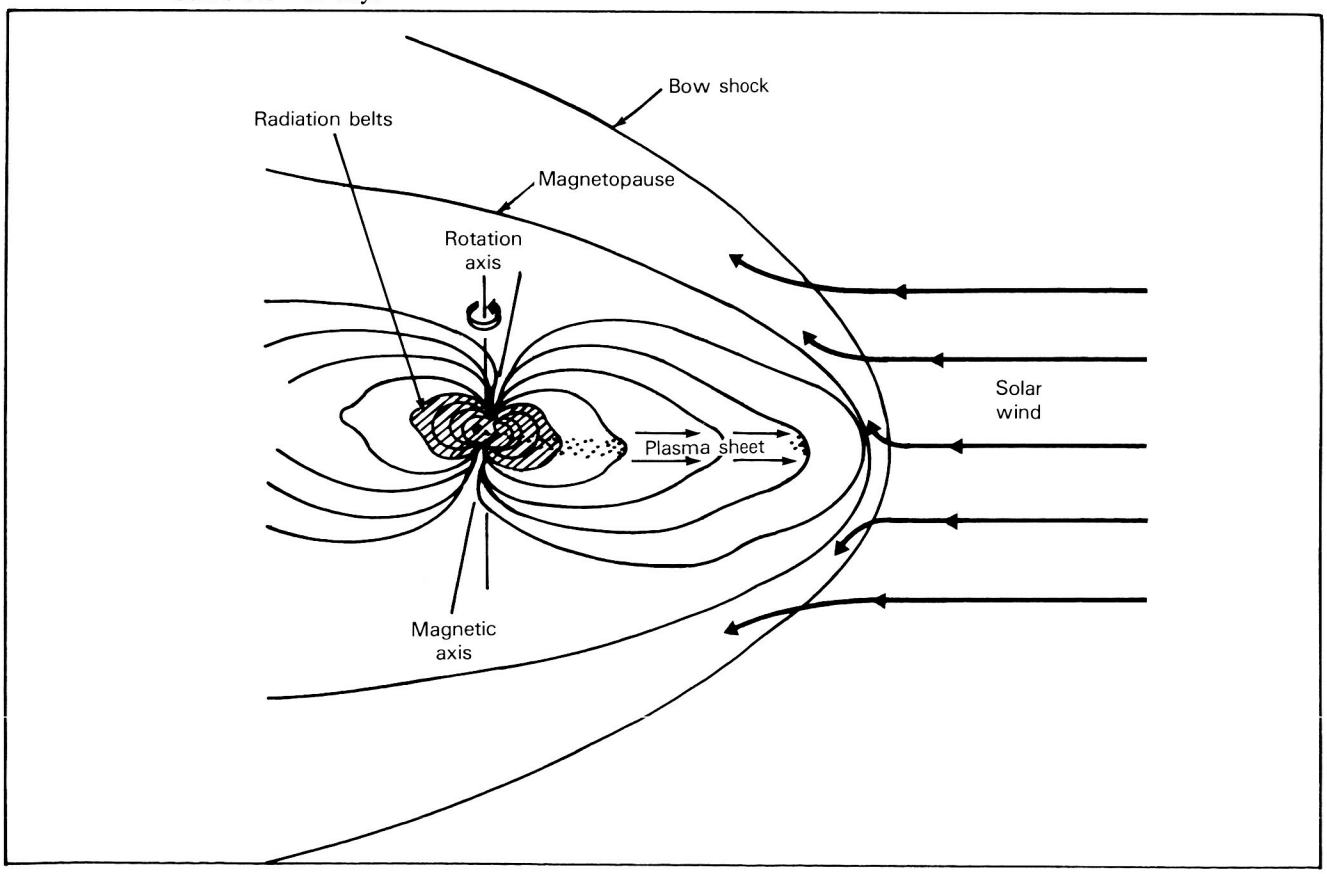

from this plasma torus. At the inner edge of the torus, Voyager 1 detected plasma wave emissions known as whistler-mode auroral hiss emissions. In Earth's magnetosphere these emissions are normally found only in association with low-energy (100 eV to 10 keV) electron beams and field-aligned currents in the auroral regions. The implication of the observations at Jupiter is that similar electron beams and field-aligned current systems must be present at the inner edge of the plasma torus. Such beams and current systems would have significance for our understanding of the transfer of energy between the plasma torus and the jovian ionosphere and the occurrence of aurora where the jovian magnetic field lines that pass through Io intersect the jovian atmosphere (fig. 41). The jovian decametric (wavelengths between 1 and 10 dm) radio emissions are believed to be generated along the Io L shell* at a radial distance at which the electron gyrofrequency is equal to the wave frequency. It is important to be able to confirm this by making direction-finding measurements from an orbiting spacecraft within the jovian system. More puzzling is a complex decametric arc structure for which no single theory has yet received broad acceptance.

Both the Pioneer and the Voyager spacecraft made measurements in the innermost region of the jovian magnetosphere within 4 Jupiter radii above the cloud tops. The most prominent findings were those of the very close encounter of Pioneer 11 at 1.6 planetary radii. Increase in particle flux with decreasing distance from the planet is not monotonic but instead has a more complex "shell-like" structure that depends on the energy and species of the particle. The interpretation is that particles diffusing inward are absorbed by solid materials, such as the dust particles in the jovian ring. Similar absorption of energetic charged particles by the satellites, also known as "sweeping," at larger radial distances has been observed by the Pioneer and Voyager spacecraft.

Despite the many exciting discoveries by Pioneer and Voyager about the environment of Jupiter, there are important questions about major physical processes observed in the jovian magnetosphere that remain unanswered. The sequence of movie frames in figure 42 depicts some of the dynamics in the magnetosphere.

The Io torus, shown to scale in yellow, is centered about the orbit of Io and is essentially a plasma composed of electrons and oxygen and sulfur ions that have been spewed off from Io and trapped by Jupiter's magnetosphere (fig. 42a). The torus corotates with Jupiter at a speed of approximately 60 km/s relative to Io. The plane of the torus is tilted with respect to the jovian ecliptic (and the orbit of Io) due to the effect of Jupiter's magnetic field on the plasma. This view of the torus is along an axis perpendicular to Jupiter's rotational axis. The two arrows protruding through Jupiter are Jupiter's rotational and magnetic axes, the latter being tilted and offset from Jupiter's rotational axis. The three white elliptical lines surrounding Jupiter and the torus are the orbits of the outer three Galilean satellites, Europa, Ganymede, and Callisto. The orbit of Io can be seen faintly within the torus. The radial contours within the torus represent observed density gradients (in intervals of 500 cm^{-3}), with the densest portion (approximately 2500 cm^{-3}) toward the center of the torus. Note that this is a simulation and that in reality there is no "sharp boundary" between the torus and the rest of the magnetosphere. However, the plasma density does drop rapidly at the boundaries shown.

Highlighted by green "dashes" is an orthogonal view of the "warped" jovian plasma sheet (shown roughly to scale). The plasma sheet (fig. 42b) is a relatively dense, cold plasma within Jupiter's magnetosphere, confined to approximately ± 2 to 5 R_J from the magnetic equator. As with the Io torus, the boundaries of the plasma sheet are, in reality, not sharp. The matter in the plasma sheet is largely supplied by plasma from the Io torus, although the density of the plasma sheet is lower by factors of 100 to 1000 than that of the torus. The plasma sheet differentially rotates with Jupiter's magnetic field and is tilted and warped with respect to both the jovigraphic and the jovian magnetic equatorial planes. The plasma sheet is sometimes called the jovian plasma disk, and is geometrically congruous to, and nearly coincident with, the jovian current sheet, a thick region of electrical current that (differentially) rotates with Jupiter. The jovian current sheet produces a magnetic field throughout the magnetosphere that

*Current theory supposes a series of "shells" in Jupiter's magnetosphere. The shells are three-dimensional surfaces defined by a given magnetic field intensity and are labeled moving outward from Jupiter's equator.

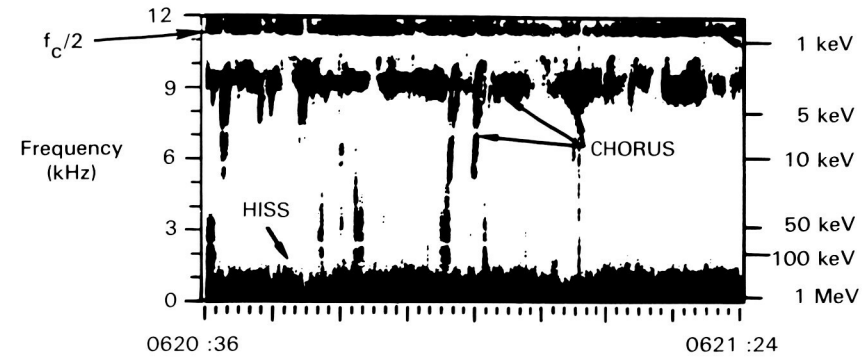

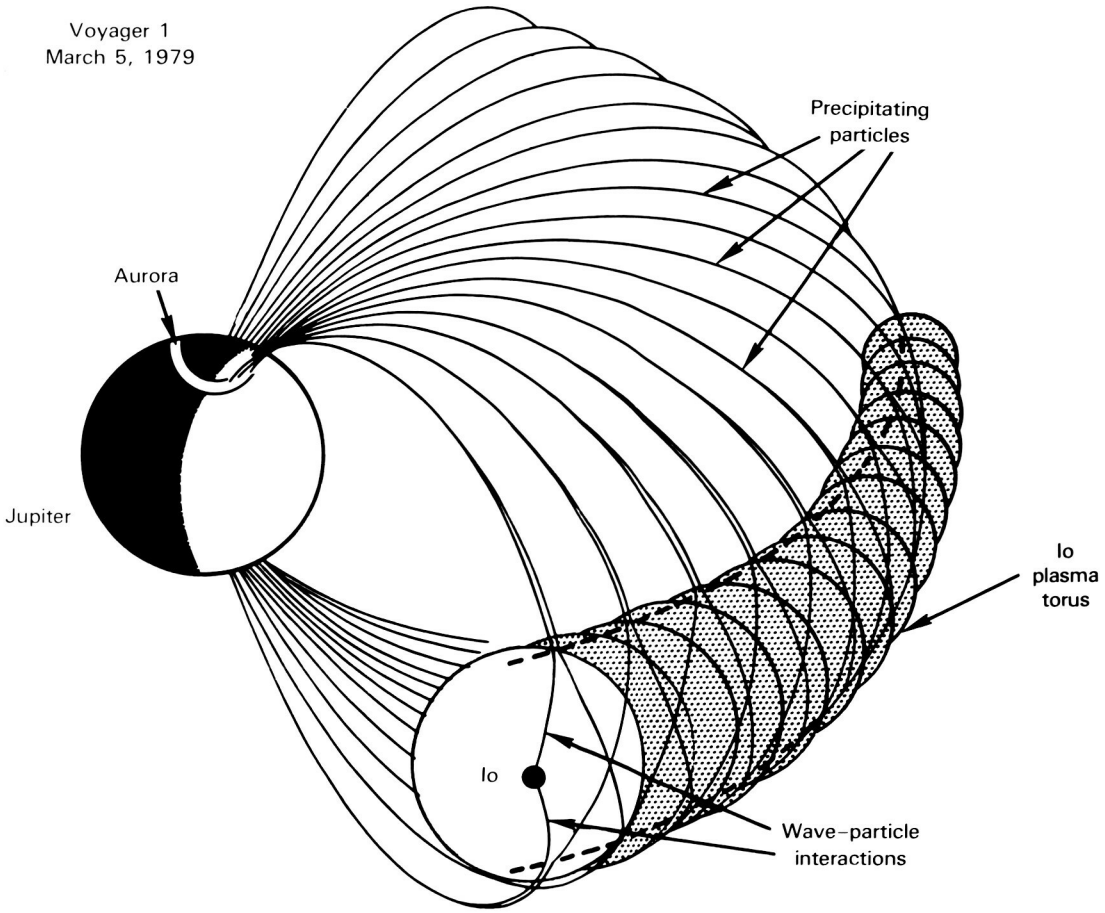

Figure 41. Aurorae are probably caused by precipitating particles from the Io plasma torus. (F_c, electron cyclotron frequency)

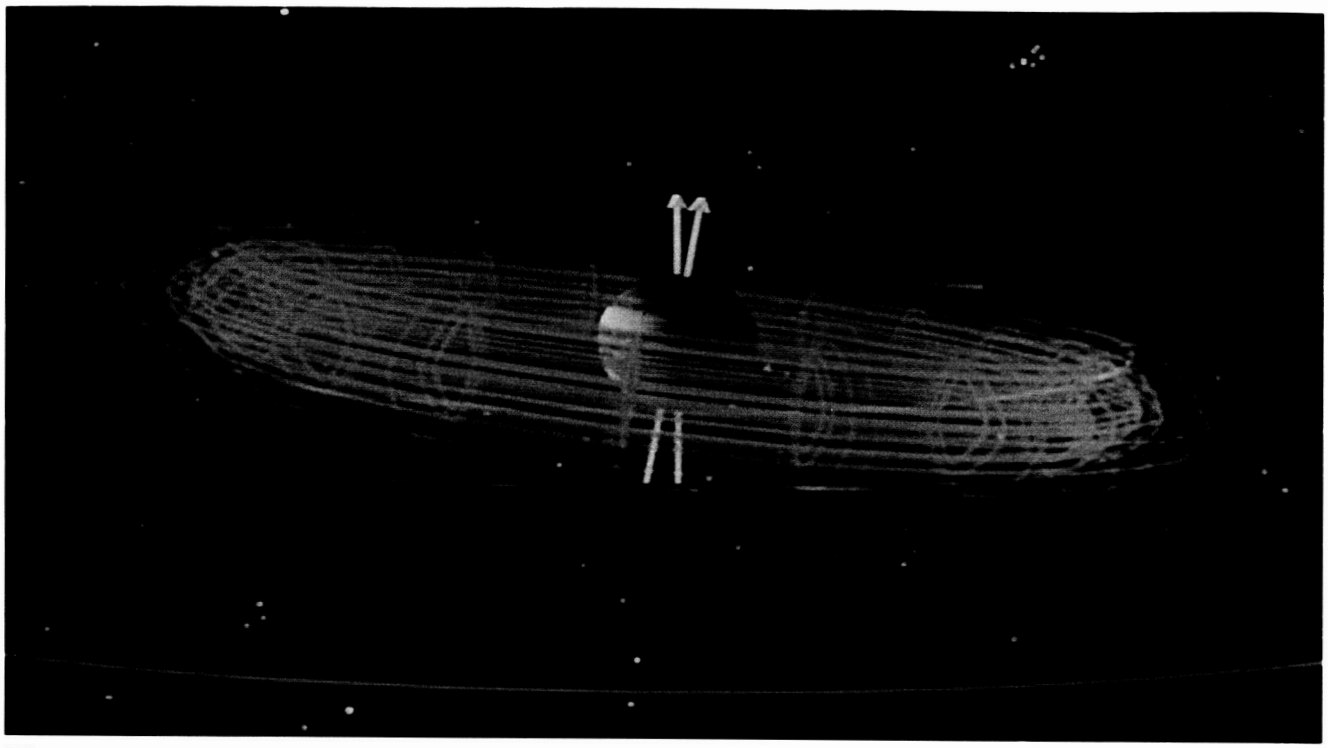

Figure 42. (a) The Io torus, shown to scale in yellow.

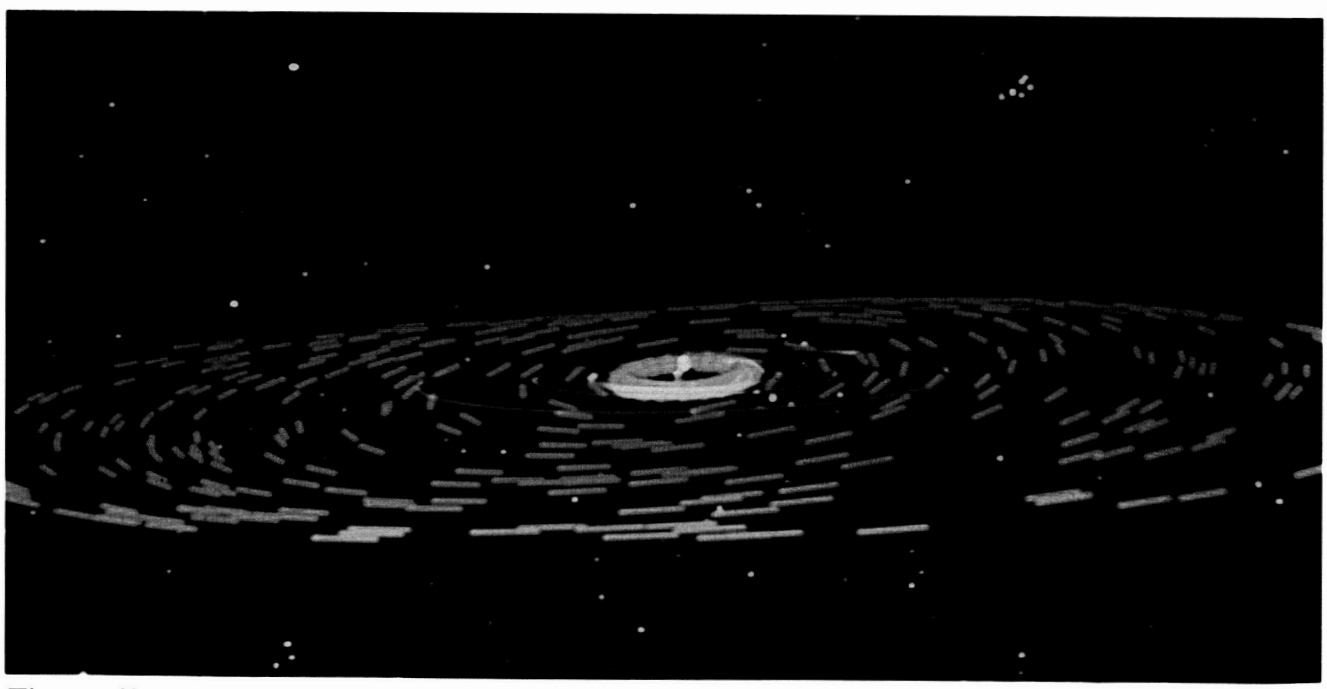

Figure 42. (b) Orthogonal view of the "warped" jovian plasma sheet shown roughly to scale.

dramatically distorts the otherwise nearly dipole jovian magnetic field.

Figure 42c presents a global view of Jupiter's magnetosphere, from a model generated by R. J. Walker, University of California at Los Angeles. The blue lines represent the magnetic field lines of Jupiter, swept back by the action of the solar wind, a hot, ionized gas (plasma) flowing radially outward from the Sun. The apparent parabola-shaped boundary of the magnetosphere is called the magnetopause. The space inside of the magnetopause is dominated by Jupiter's magnetic field. Although in this view some of Jupiter's magnetic field lines appear to terminate, this is an artifact of the computer simulation. In reality they either close upon themselves or connect with the solar wind magnetic field (not shown).

Figure 42d depicts a numerical simulation of an energetic ion (shown in red) spiraling around Jupiter's magnetic field lines near the orbit of Io. The simulation was performed by J. G. Luhmann, University of California at Los Angeles. The motion of the ion is traced as it reflects from Jupiter's magnetic poles.

Figures 42e and f present two views of the solar wind interaction with Jupiter's magnetosphere. The solar wind (shown in yellow) blows outward from the Sun at approximately 400 km/s. Jupiter's magnetic field acts as an obstacle to the (supersonically flowing) solar wind, and a shockwave called the "bow shock" is formed upstream of the magnetosphere. The bow shock can be seen here as a parabolic curve in the solar wind. The magnetic field lines are distorted and

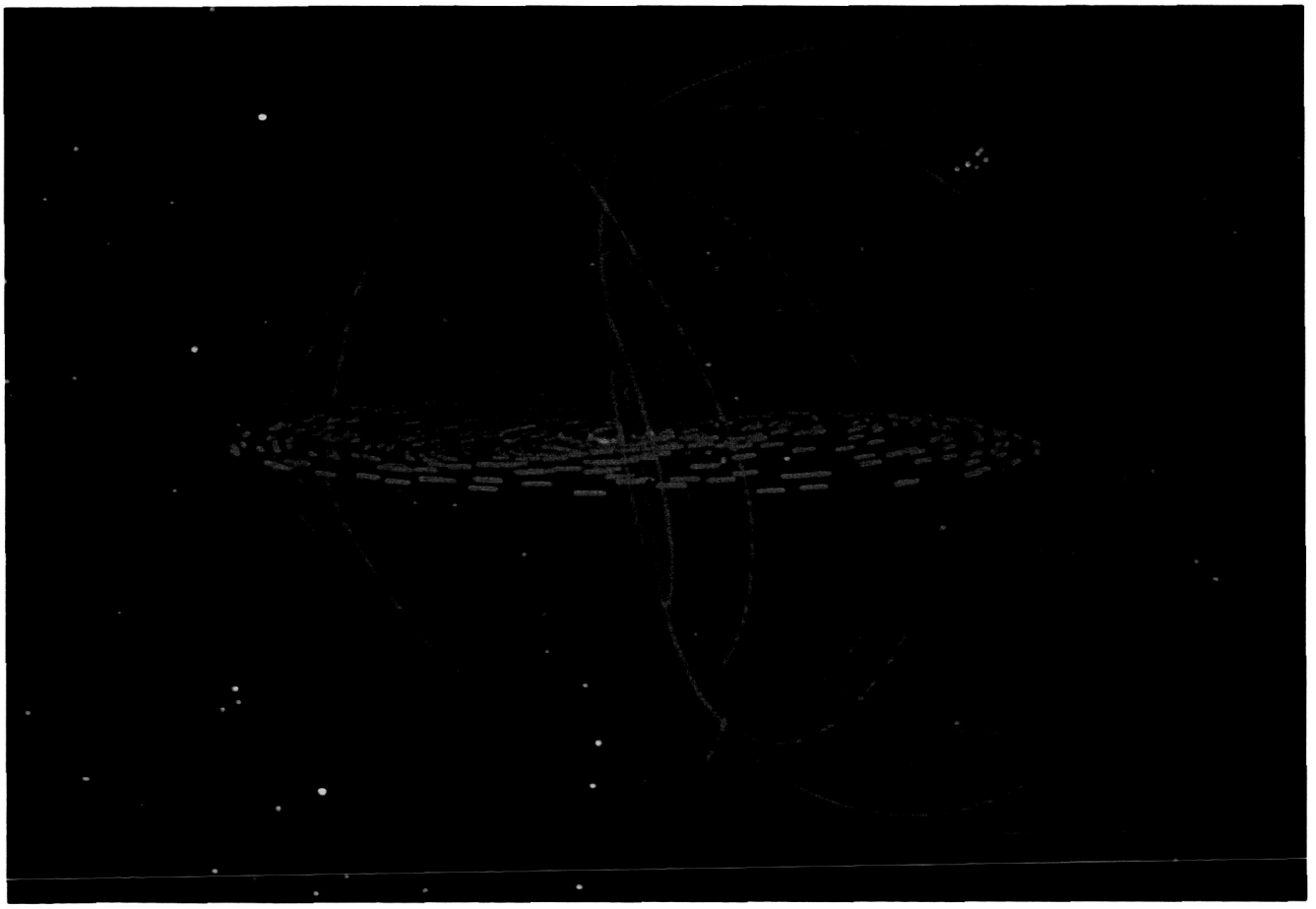

Figure 42. (c) Global view of Jupiter's magnetosphere, from a model generated by R. J. Walker, University of California at Los Angeles.

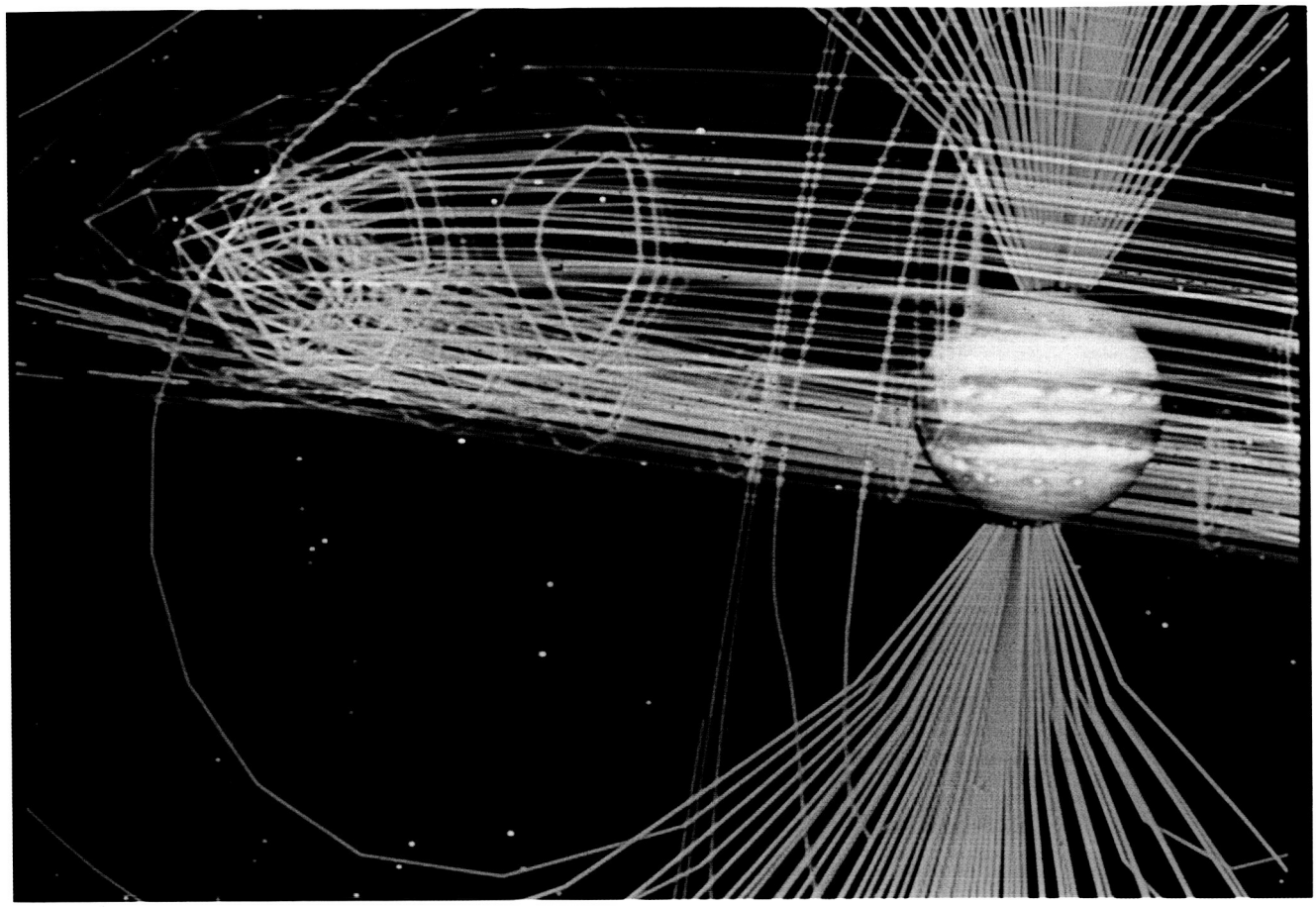

Figure 42. (d) Numerical simulation of an energetic ion (shown in red) spiraling around Jupiter's magnetic field lines near the orbit of Io.

swept back by the solar wind. The field lines shown unconnected here actually connect with the downstream solar wind. This picture is from a numerical simulation performed by J. G. Luhmann using a modified gas dynamic solar wind—magnetosphere model developed by J. R. Spreiter and others in the 1960s and 1970s.

Anticipated Results

For nearly a quarter of a century scientists have been able to use instruments carried by spacecraft to study the properties of Earth's magnetosphere. More recently, they have also been able to study by spacecraft the magnetospheres of all the planets known to the ancients—Mercury, Venus, Mars, Jupiter, and Saturn. Jupiter's magnetosphere is of special interest because it is the largest single object within the solar system and the rapid rotation of Jupiter gives rise to a magnetosphere that is part way between that of Earth and a pulsar. For Earth and Jupiter (fig. 43), which have relatively strong magnetic fields that interact with the magnetic field carried by the solar wind, the magnetic field acts as an obstacle and produces a shock wave much farther from the planet than in the case of bodies such as the Moon and Venus, which have negligible intrinsic magnetic fields.

The advantages of the Galileo mission for investigations of magnetic and electric fields and of charged particles in the jovian magnetosphere are the spinning section of the spacecraft, a flexible

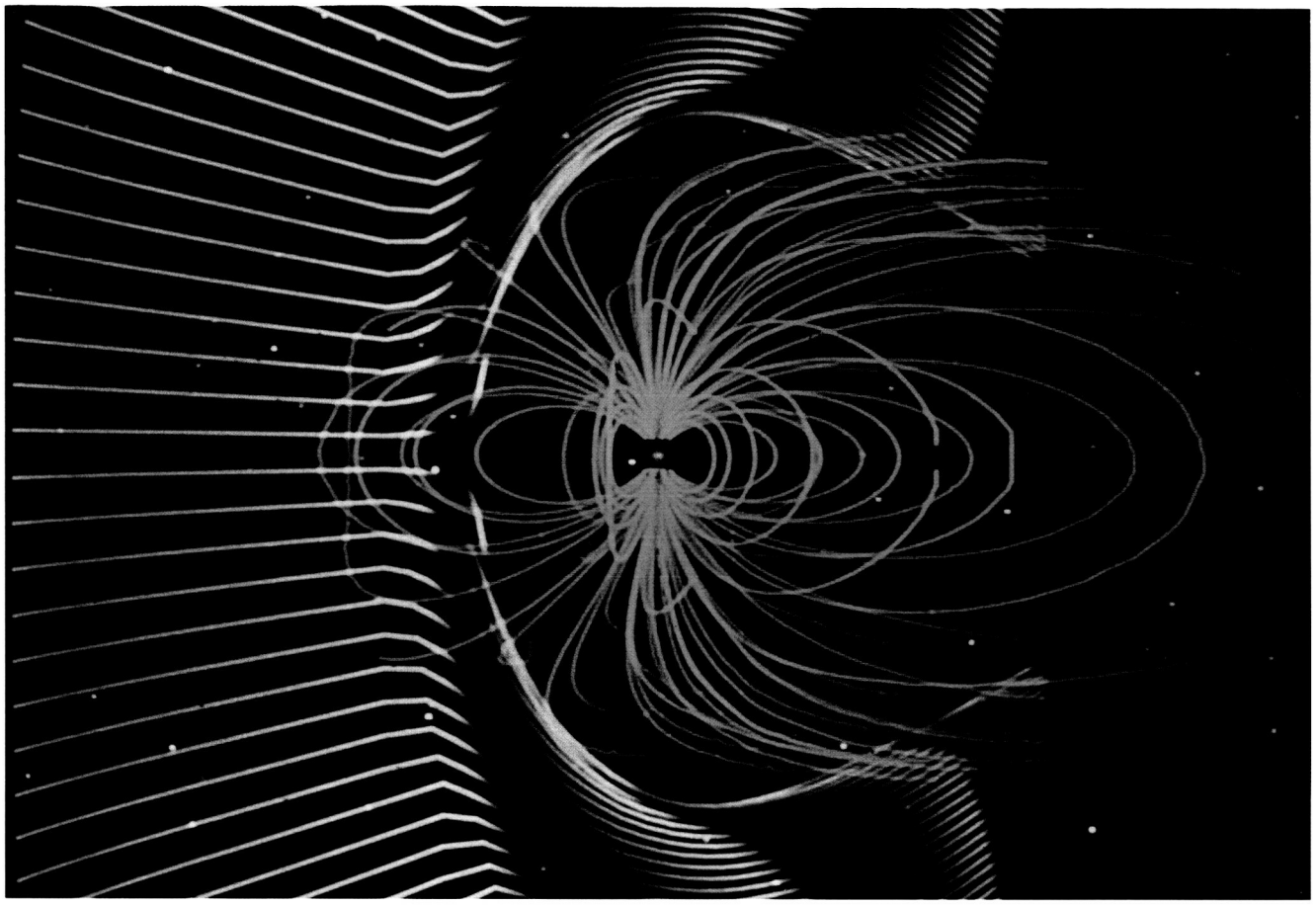

Figure 42. (e) View of the solar wind interaction with Jupiter's magnetosphere. (From *Jupiter's Magnetosphere: The Movie,* by J. F. Blinn and R. S. Wolff)

command system, and a series of orbits that allows close flybys of the Galilean satellites, a survey of the jovian magnetotail, and a subsequent local-time survey of the magnetosphere. The spinning section of the spacecraft gives the important capability for a suitably designed instrument to view all angles for particle velocity vectors at the satellite position. The command system provides the opportunity to tailor the operation of the instruments for the most effective measurements in each of the diverse plasma regimes of the magnetosphere and its environs, for example, magnetosheath, plasma sheet, satellite wake or flux tube, or magnetotail wind. Targeted encounters with the satellites and a tour of the magnetotail during a sustained mission of over a year offer exceptional opportunities for studies of most of the important plasma regions and their temporal responses to Iogenic and solar wind plasmas.

The Pioneer and Voyager missions provided brief glimpses of a structurally complex and time-varying jovian magnetosphere. Major features of this magnetosphere were identified, as summarized in figure 44. The dense plasma torus is centered around Io's orbit and has a thickness equivalent to about 2 Jupiter radii. The disk-like structure, a plasma disk or plasma sheet, extends from the outer boundary of the Io torus. The detailed structures and temporal behaviors of both the torus and plasma disk are currently unknown. The regions of the magnetosphere to be surveyed by the Galileo orbiter during the initial orbit and the tail petal orbit are shown in figure 45. In addition, a specially designed sensor for energetic particles is carried on

the Galileo probe to clarify the features of the extremely high radiation levels at altitudes less than 3 jovian radii above the planet's atmosphere.

As the Galileo spacecraft crosses the plasma sheet in the middle and outer magnetosphere, the magnitudes of field-aligned and cross-field currents will be determined. Their values and location will be correlated with the position of the current sheet as found with the magnetometer. The motions of the plasma sheet will be directly determined from the three-dimensional flow vector, and the azimuthal component will be separated from the radial outflow or inflow component. Angular distributions and ion compositions will be examined to discern the contributions of electrons and ions from the ionosphere, solar wind via the magnetosheath, and the large satellites in the inner magnetosphere. Thus, the formation and dynamics of the plasma sheet, or disk, can be understood.

The substantial periods of time that the Galileo spacecraft will spend in the area of the plasma sheet offer the unique opportunity to view the responses of the jovian magnetosphere to the time-variable source of Iogenic plasmas. If specific Io volcanic eruptions can be identified with temporal fluctuations in densities, composition, and motions of the plasma sheet, we will make remarkable advances in our knowledge of the transport of mass and momentum in the jovian magnetosphere.

The Voyager spacecraft provided an initial survey of plasma wave and radio emission phenomena in the jovian magnetosphere. Galileo will provide further details, relating particularly to

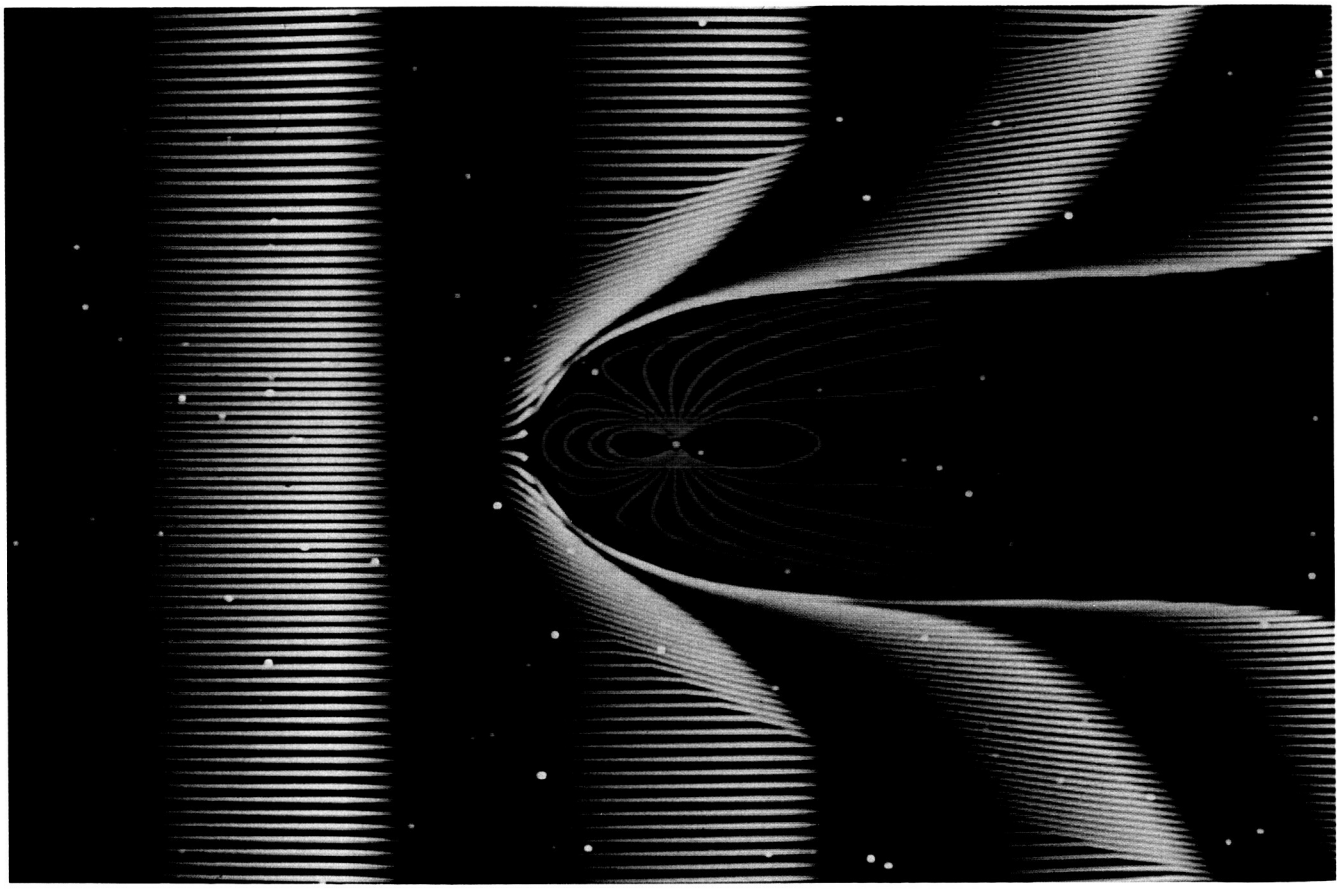

Figure 42. (f) View of the solar wind interaction with Jupiter's magnetosphere. (From *Jupiter's Magnetosphere: The Movie*, by J. F. Blinn and R. S. Wolff)

the free energy source for the particle wave involved and long-term variations. Figure 46 shows the various types of plasma waves and radio emissions detected by the two Voyager spacecraft and where these occur.

Simultaneous observations of three-dimensional particle velocity distributions and plasma waves with the Galileo spacecraft allow the first studies of wave-particle interactions in the wide-ranging types of plasmas in the jovian magnetosphere. For example, the velocity distributions of ions can be examined to determine whether resonant acceleration by ion cyclotron waves is an important mechanism for ion heating in the torus and plasma sheet. Furthermore, the amplitudes of broadband electrostatic noise can be compared with plasma velocity distributions to determine the importance of anomalous resistivity in plasma heating. Free energy sources, for example, ring distributions in the electron distribution function, for the generation of intense electrostatic waves near the upper hybrid resonance frequency are identified and related to the wave amplitudes observed with the plasma wave instrument. In general, the direct measurement of the plasma density and other parameters gives the propagation and resonance conditions for plasma waves in wave-particle interactions. Thus, the mechanisms for providing Jupiter with intense radio sources can be understood.

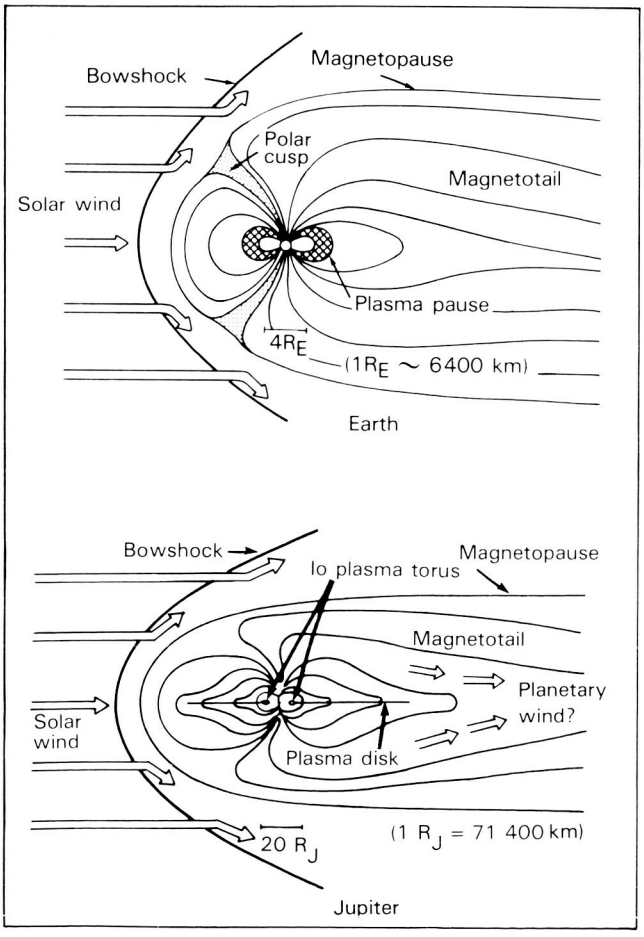

Figure 43. Comparisons of the magnetospheres of Earth and Jupiter. The terrestrial magnetosphere is shown at a scale about 55 times that of the jovian magnetosphere.

Of the plasma waves that occur in the inner regions of the magnetosphere, the main questions that remain have to do with the mechanism by which the waves are produced. For example, electrostatic cyclotron waves occur near the equatorial plane in and near the Io plasma torus. For a full understanding of the plasma instability responsible for these waves, complete measurements of the three-dimensional electron velocity function must be obtained. Such measurements will be available for the first time from the Galileo plasma instrument.

Galileo will also study whistler mode auroral hiss emissions, as discussed earlier.

In addition to locally generated plasma waves, several distinct types of radio emissions were identified by the Voyager spacecraft. These emissions come from the inner region of the magnetosphere. They include decametric radiation known to be associated with Io and two types of kilometric radiation (broadband and narrowband) apparently associated with the Io plasma torus. Although the general spectral characteristics of this kilometric radiation are reasonably well known, considerable uncertainty exists regarding the exact region in which the emissions are generated. Because the Voyager radio astronomy measurements did not include a direction-finding capability, source positions can be inferred only indirectly from ray-tracing models. With Galileo, source positions will be obtained directly from direction-finding measurements that utilize the spin modulation of signals received by the electric dipole antenna on the end of the spun section's magnetometer boom.

The jovian decametric radiation is generally believed to be generated along the Io L shell at a radial distance at which the electron gyrofrequency

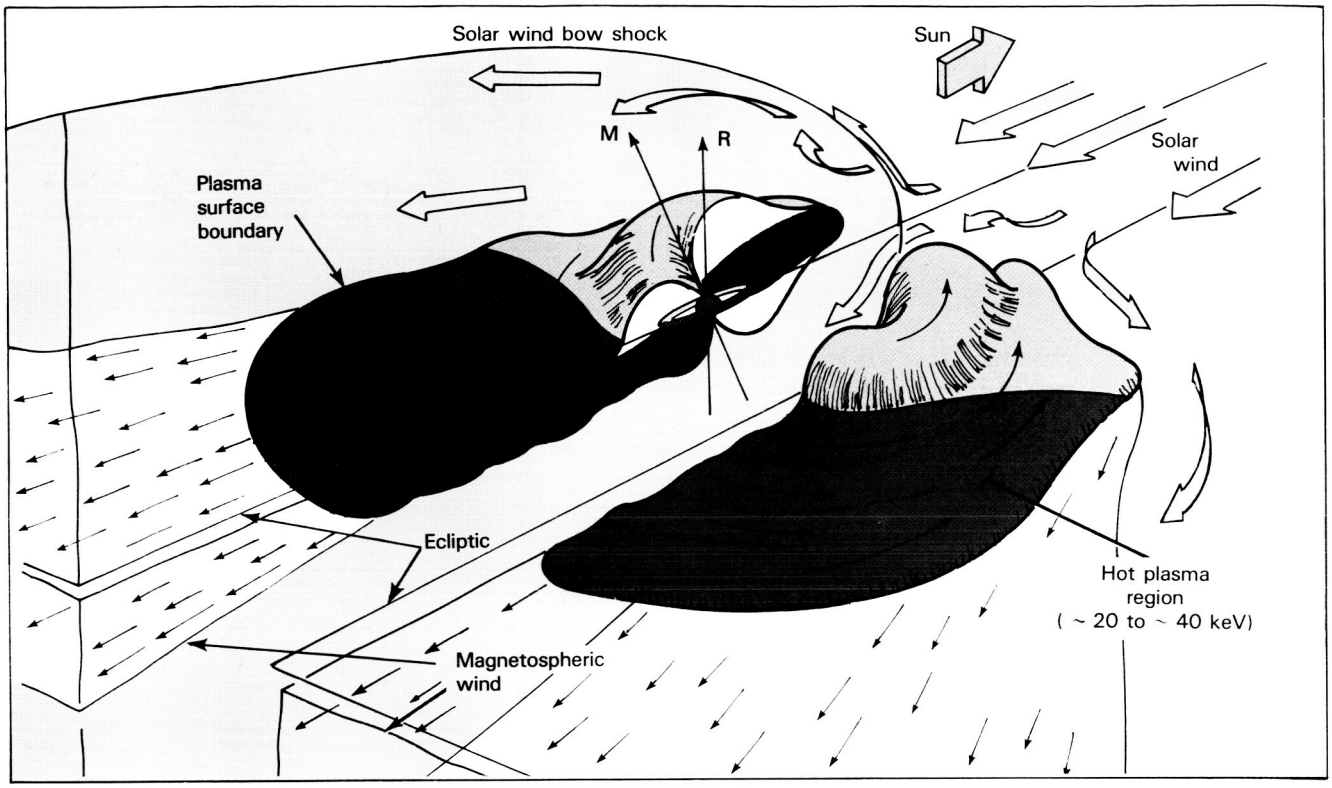

Figure 44. The jovian magnetosphere showing some of its major regions and relationship with the solar wind.

is equal to the wave frequency. The general location of the source for decametric radiation is indicated in figure 47. Although it is unlikely that this basic hypothesis is wrong, the relationship could be verified by direction-finding measurements. More puzzling is the complex decametric arc structure discovered by Voyager. At present, no single theory for the multiplicity of the decametric arc structure of the radio emissions has received broad acceptance. Possible explanations include interference effects produced by multiple ray paths from a single source, unusual magnetic structure at the foot of the Io L shell, and multiple reflections of electromagnetic waves excited by Io. Direction-finding measurements by Galileo should allow us to find the correct explanation by providing information on the relative direction of arrival of the individual arc elements.

Galileo will provide an opportunity to use radio emissions as a remote sensing tool to monitor changes in the inner magnetosphere during the long periods when Galileo is near the apojove of its elliptical orbits. It is clear from both ground-based and Voyager observations that large changes in intensity take place in the radio emissions from Jupiter over times ranging from a few hours to several months. At the present time the exact reasons for these temporal changes are not understood. However, as knowledge of the mechanisms responsible for the jovian emissions increases, it is believed that the spectrum and intensity of the radio emissions can be used to monitor remotely the dynamic processes occurring in the jovian magnetosphere. At Earth, for example, intense radio emissions at kilometric wavelengths are closely correlated with discrete auroral arcs and charged particle precipitation at high latitudes. The terrestrial kilometric radio emissions are therefore a useful remote indicator of global auroral activity. At Jupiter, the radio emissions can be expected to provide a similar remote monitor of temporal changes in the inner regions of the magnetosphere,

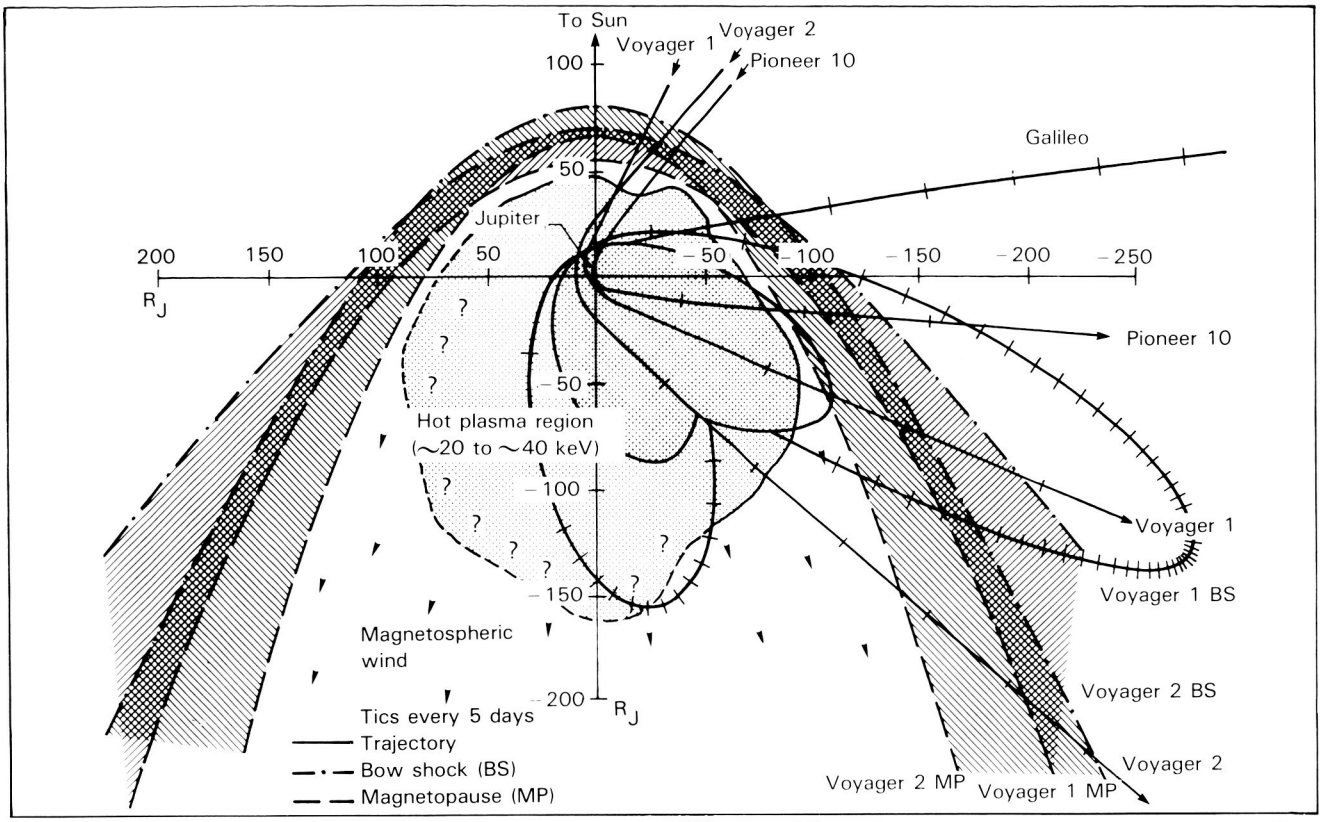

Figure 45. Survey of the jovian magnetosphere during the Galileo tour depicting how the spacecraft will be able to sample the various regions.

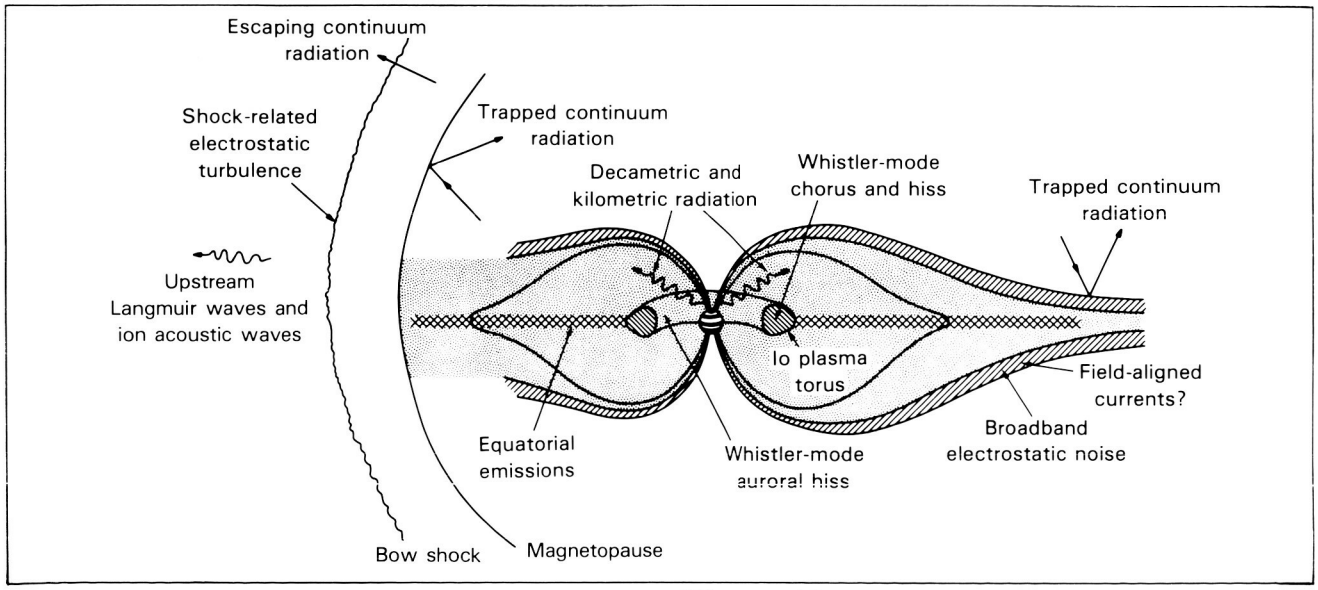

Figure 46. Plasma waves and radio emissions in the jovian environment.

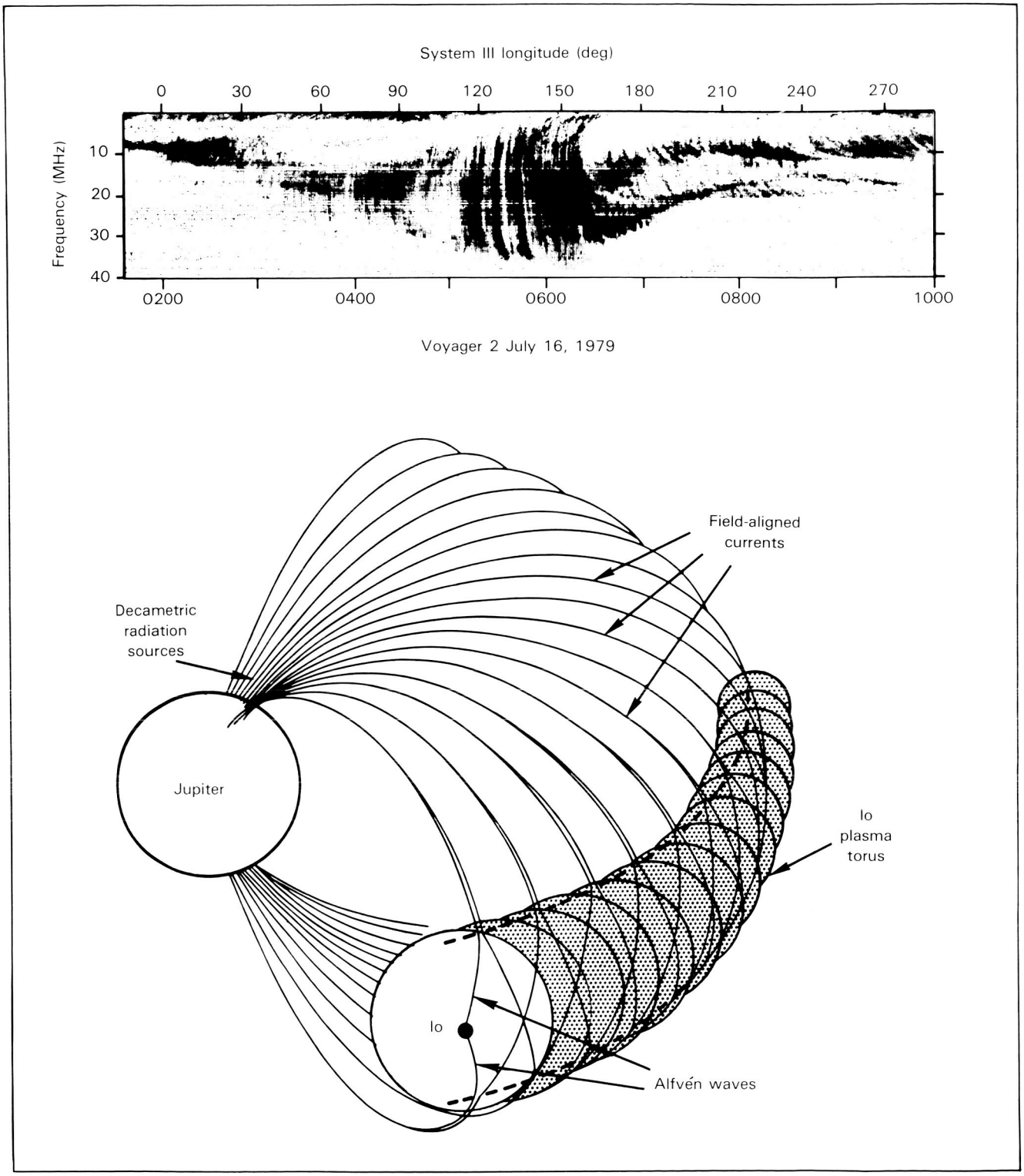

Figure 47. Decametric radiation from Jupiter probably originates from magnetically field-aligned currents from the Io plasma torus.

possibly providing evidence of jovian magnetic storms, if they occur, or evidence of impulsive injection of material into the magnetosphere from volcanic activity on Io.

The encounters with the Galilean satellites offer exciting opportunities for observing fields and particles phenomena and for inferring several physical characteristics of these bodies. The satellites are embedded in Jupiter's magnetosphere, and the interaction between the satellites and the magnetosphere is known to be strong. This interaction is driven by the flow of corotating plasmas and magnetic fields past the satellites (fig. 48). There are two main models for possible scenarios of this fascinating interaction, as shown in figures 49 and 50, respectively. The first supposes that the satellite is magnetized, in which case a magnetopause and a tail current sheet are formed. The second model assumes that the satellite acts as an unmagnetized conductor. These investigations by Galileo are especially significant because they afford an opportunity to investigate interactions that occur when the magnetic field strength in the plasma is quite strong. This situation is in sharp contrast to the interaction of the solar wind with the planets.

As the charged particles corotate with the magnetosphere, they sweep past the Galilean satellites, and "wakes" are created in front of the satellites. By examining the ion velocity distributions in the wakes, we can determine the mechanism for ion loss from these bodies. The effectiveness of ion pick-up by the magnetospheric plasma flow is derived from the signatures in the

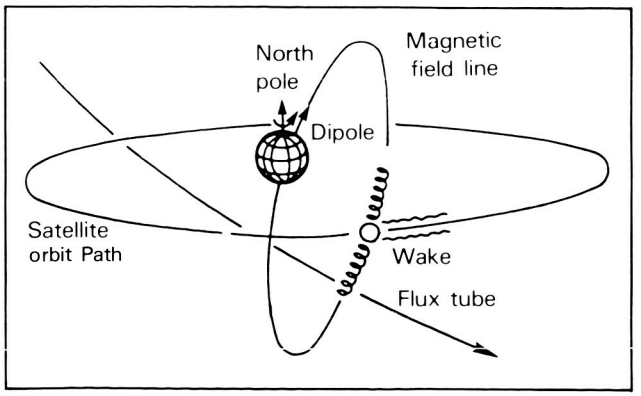

Figure 48. Typical interaction between a satellite and the magnetosphere showing the location of the flux tube and the leading wake.

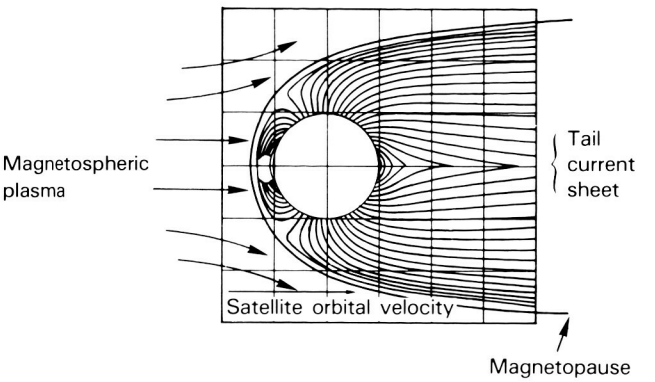

Figure 49. Magnetic field in the vicinity of a Galilean satellite that is assumed to have an intrinsic magnetic field.

velocity distributions of these ions. The mass spectrometers will be used to delineate the major ions produced in the vicinity of the satellite. For Io these ions include S^+, SO^+, and O^+, and for the icy satellites perhaps H_2O^+, OH^+, and O^+ can be found. Such measurements give the rate of mass loss from each satellite. Perturbations of the plasma flow can be identified in terms of the conductivity of the satellite, for example, flow around a conducting cylinder. During the closest satellite

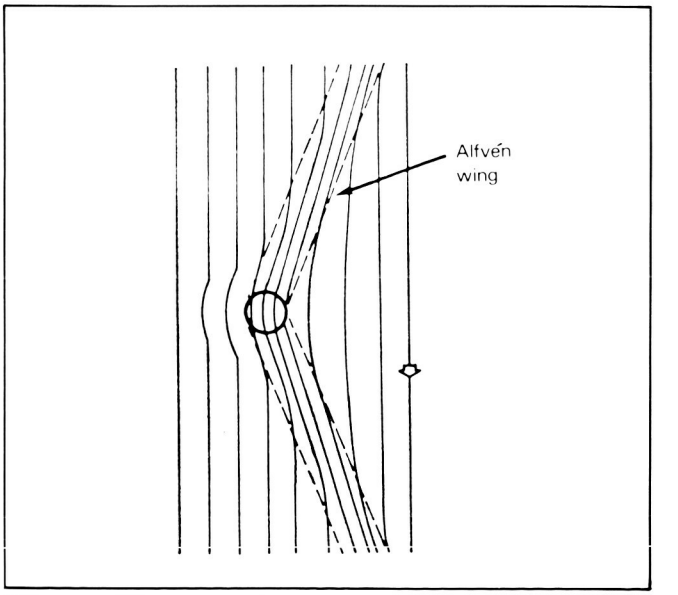

Figure 50. Magnetic field in the vicinity of an icy Galilean satellite that is assumed to be an unmagnetized conductor, as viewed from the "leading-trailing" meridian.

encounters it is possible that a magnetopause or ionopause may be detected, thus providing further information concerning the magnetic and atmospheric properties of that body. If the flyby of the satellite is polar, strong field-aligned currents to and away from the jovian ionosphere, especially in the case of Io, can be expected. Also possible is field-aligned acceleration of ions and electrons by electrostatic double layers or anomalous resistivity. The relative contributions of the ions in the plasma torus and sheet from the various Galilean satellites will be assessed during the encounters.

The Galileo flyby of Io will also uniquely complement Voyager's flyby of that satellite by passing 20 times closer, thereby giving an improved determination of the intrinsic magnetic field, and crossing through the wake near the equatorial plane instead of through the flux tube. Because Io is known to have a very strong interaction with the jovian magnetosphere, accounting for a power input of about 10^{12} W, the Galileo flyby of the satellite should add significantly to our understanding of this interaction.

To determine unambiguously the interactions of the Galilean satellites with the jovian magnetosphere, it is necessary to pass above the polar caps and also through the equatorial wakes of these bodies. For example, the polar cap flybys will be used to search for field-aligned currents to the ionosphere, and the wake intercepts will be employed for identification of mass losses and for the most sensitive determination of intrinsic magnetic moment. Thus, multiple close flybys of the Galilean satellites are a firm requirement for decisive studies of the interaction of these bodies with the magnetospheric plasmas. The interaction of each satellite with Jupiter's magnetic field is expected to be different due to the wide range of the surface and atmospheric properties, ambient magnetospheric plasmas, intrinsic magnetic moments, and conductivities. The Galileo mission offers a unique opportunity to study the interaction of planetary objects with magnetized plasmas.

Voyager sensed the presence of Jupiter's magnetotail at Saturn. The existence of the magnetotail wind at radial distances beyond 130 R_J offers an exciting goal for the tail petal orbit of the

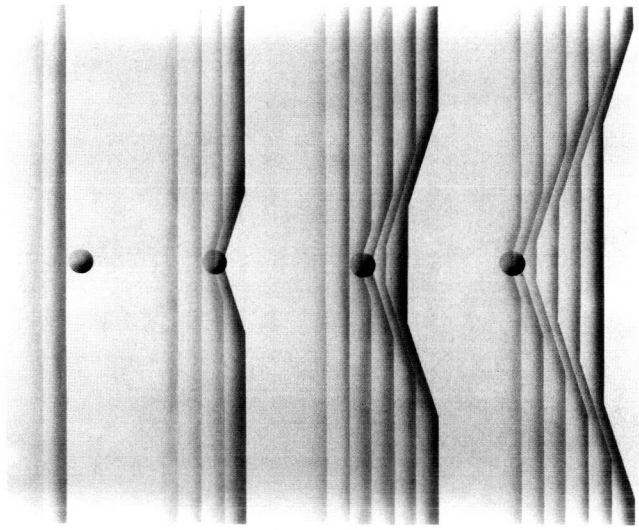

Figure 51. If the corotating energy exceeds the magnetic energy density, Alfvén waves are set up.

Galileo mission. The origins of this wind are unknown. It is possible that the magnetotail wind develops at an Alfvén point (fig. 51), where the corotational energy exceeds the magnetic energy density. Thus, magnetic bubbles could be slung radially outward into the magnetotail. The low pressures in the magnetotail would produce high-speed radial outflow. On the other hand, the outflow wind might be thermally powered by the hot plasmas in the plasma sheet inside the Alfvén point. A third possibility is that the magnetospheric wind is the signature of reconnection of magnetotail field lines with the magnetic fields of the solar wind in a convection pattern controlled by day side magnetic merging rates. Indeed, the responses of the magnetotail to fluctuating internal plasmas, such as Iogenic plasmas, or to varying solar winds are unknown. Is the magnetotail characterized by spectacular, explosive activity or a mere quiescent outflow of plasmas? The exploratory petal orbit into the magnetotail will answer many questions concerning the origins and dynamics of this immense and little understood plasma region.

chapter 5 MISSION DESIGN

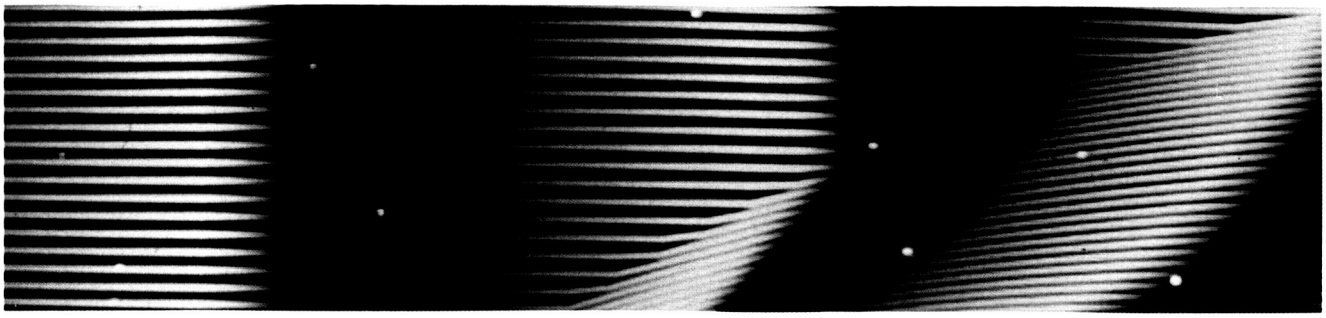

The Galileo spacecraft will be launched in May 1986 on a direct Earth to Jupiter trajectory. Many factors influence the events of the mission, and careful planning is required to ensure success at each stage.

Mission design is the process of developing an operational strategy for the mission that will maximize the science return within the constraints and limitations imposed by the laws of nature and the demands of management. Major variables that influence the mission return are the design and selection of the spacecraft flight path and high-level sequence planning. To permit flexibility in these areas, requirements are levied on spacecraft design, launch vehicle capabilities, ground data system capabilities, and tracking and telemetry coverage. Mission design constraints imposed by project management generally relate to fiscal limitations or to safe and reliable operation of the spacecraft. Nature's constraints pertain to orbital and celestial mechanics that control the set of flight paths and corresponding geometries available to mission design.

The May 1986 launch will utilize a broken-plane trajectory, with arrival at Jupiter in late 1988 (fig. 52). Several months after launch, a plane change maneuver will be required to transfer the spacecraft to a higher heliocentric orbit (fig. 53). Although a ballistic trajectory would be the ideal, low-energy flight path, such a trajectory is not feasible for the 1986 launch opportunity due to Jupiter's position relative to Earth and the capabilities of current launch vehicles.

For the 1986 launch opportunity, the minimum launch energy (C_3) for type I trajectories (transfer angle less than 180°) is about 84 km^2/s^2 (fig. 54). The minimum C_3 for type II trajectories (transfer angle greater than 180°) is only about 81 km^2/s^2, but the time of flight for type II trajectories is almost one and a half years longer. Based on current specifications of Centaur performance and Galileo spacecraft mass, the maximum C_3 capability available is 80 km^2/s^2. Therefore, ballistic trajectories are not possible for the Galileo mission in 1986.

In figure 54, the "ridge" between the type I and type II minima occurs because Jupiter does not lie in the ecliptic plane. The ballistic solution to the Lambert problem for a transfer angle near 180° has a large heliocentric inclination. The ridge is therefore the region of launch/arrival date combinations that have a near-180° transfer. The high C_3 values on the ridge are due to this large heliocentric inclination. In contrast, the high C_3 values for late launch/early arrival and early launch/late arrival combinations are due to the high heliocentric energy requirements of near-ecliptic transfers on those dates.

The theoretical minimum energy transfer to Jupiter could occur if Jupiter were in the ecliptic

plane. In this case, a perihelion to aphelion (Hohmann) transfer would be possible. It would have a 180° transfer in the ecliptic plane, with a transfer time of about two years and nine months and a C_3 of about 78 km^2/s^2. Introduction of a broken-plane maneuver on trajectories with near-180° transfer angles allows the launch C_3 to be used primarily for achieving the heliocentric energy necessary to reach Jupiter's distance from the Sun (as with a Hohmann transfer). The broken-plane maneuver primarily changes the heliocentric inclination and node at the most efficient place.

Ballistic and broken-plane trajectories are shown schematically in figure 53. The first segment of the broken-plane trajectory lies in the ecliptic, and the second segment has the inclination necessary to reach Jupiter. If the maneuver were done at a point 90° from Jupiter, the inclination would equal Jupiter's declination at arrival. However, since the velocity is decreasing outward on the trajectory, the change in velocity (ΔV) required for an inclination change performed closer to Jupiter is lower even though the resulting inclination change is greater.

The characteristics of an optimal broken-plane trajectory are somewhat more complicated than this simplified model. Given the maximum available energy, the trajectory design process finds the optimal plane (not necessarily the ecliptic) from which to perform the minimum plane change necessary to intersect the out-of-the-ecliptic position of Jupiter. For a higher available launch energy, more of the plane change can be done at launch, resulting in a smaller broken-plane maneuver.

As a specific example to illustrate the broken-plane effect, consider the trajectory with a May 21, 1986, launch date and an arrival date at Jupiter of August 27, 1988. The characteristics for the ballistic and optimal broken-plane trajectories are summarized in table 4.

Some of the trajectories in figure 54 that are not near-180° transfers can also be utilized subject to a maximum C_3 constraint. In this case the ballistic trajectory is essentially matched by performing a maneuver as soon after launch as operational considerations will allow. In effect, this maneuver uses the spacecraft propellant system as an additional upper stage on the launch vehicle. These "energy augmentation" maneuvers become larger as the distance of a given trajectory from the ridge increases. For a C_3 capability less than the ballistic C_3 minimum, *all* trajectories will require a maneuver of either the broken-plane type or the energy-augmentation type. For a C_3 capability greater than the ballistic minimum, there exists a

Figure 52. Galileo 1986 Earth to Jupiter trajectory.

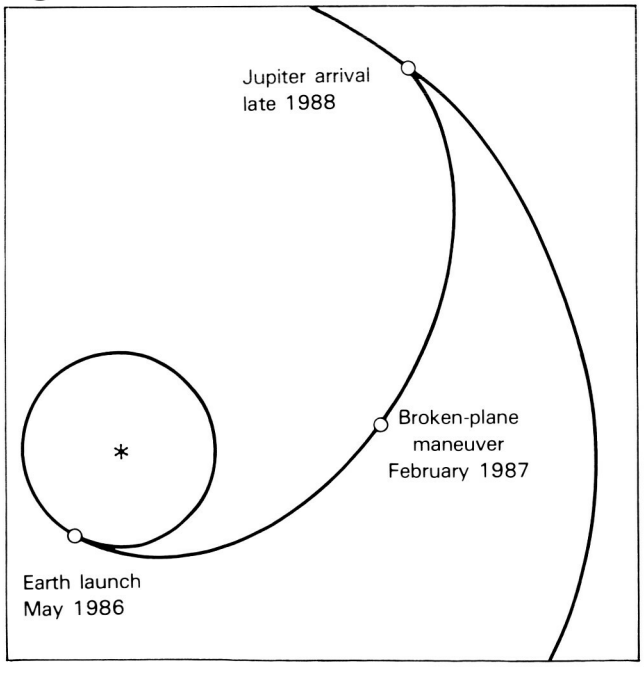

Figure 53. Schematic of broken-plane trajectory.

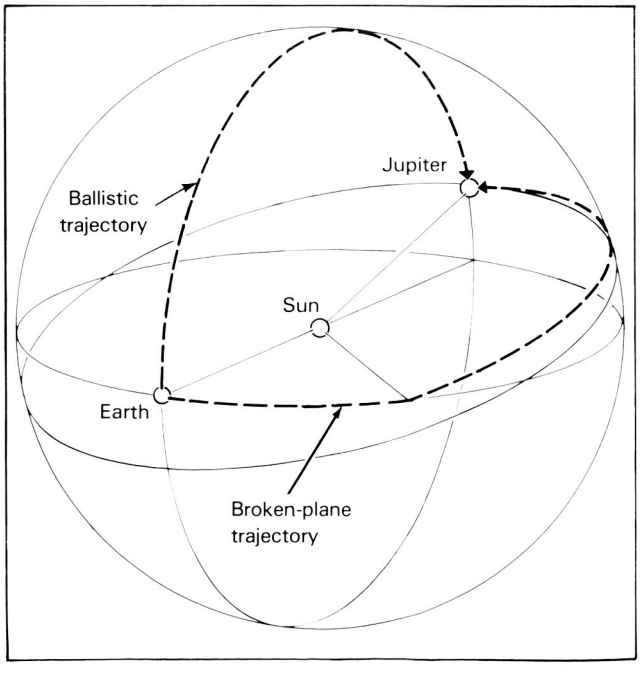

region within which optimal trajectories are ballistic.

Mission Performance

Onboard attitude control and ΔV capability on the Galileo spacecraft are provided by the retropropulsion module, with a total usable propellant capacity of 932 kg. Propellant is required for deterministic maneuvers, navigational maneuvers, and attitude control. Deterministic maneuvers, which are identified in the first stages of mission design, consist of the broken-plane maneuver, the orbiter deflection maneuver after probe release, the Jupiter orbit insertion maneuver (JOI), and the perijove raise maneuver of the first orbit. Navigational maneuvers consist of interplanetary trajectory correction maneuvers, an orbit trim maneuver after insertion, and in-orbit maneuvers for satellite tour navigation.

A common measure of mission performance is propellant margin. Propellant margin, which is a

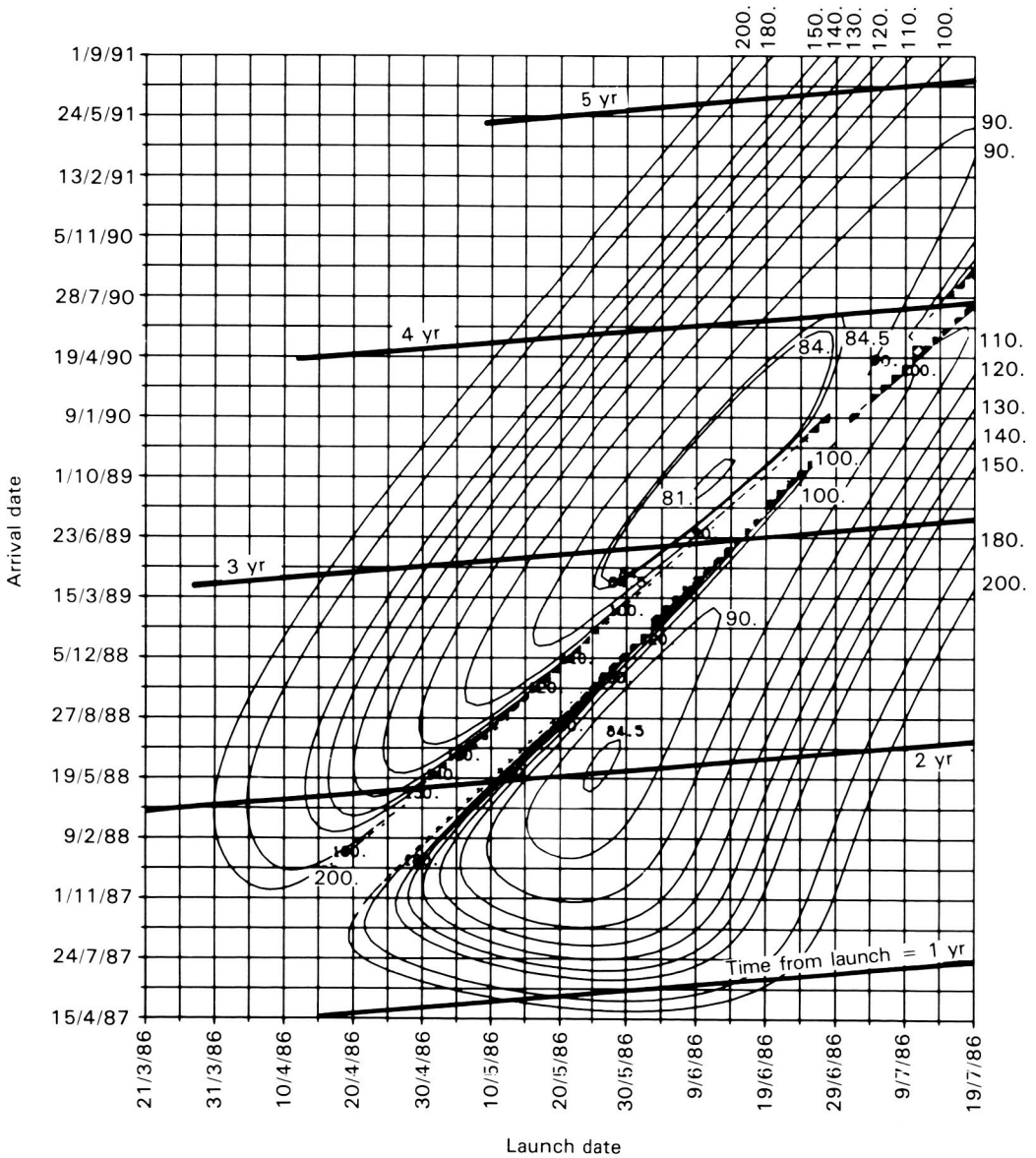

Figure 54. C_3 contours for the 1986 launch opportunity to Jupiter.

function of launch date and arrival date, is defined as the amount of propellant remaining in the retropropulsion module after completion of an eleven-encounter satellite tour with 90 percent probability of success. Any given trajectory with a specified launch date and arrival date is a feasible trajectory if the propellant margin is nonnegative. The region of all feasible trajectories in the launch/arrival space is called the feasible region. Propellant margin contours in the launch/arrival space are shown in figure 55.

Selection of a launch/arrival strategy consists of choosing a launch period and accompanying arrival dates that maximize performance while satisfying mission constraints. The two mission constraints that are relevant to the choice of a launch/arrival strategy for this mission involve the orbiter aspect angle and solar conjunction.

During the probe's descent into Jupiter's atmosphere, the orbiter will relay radio signals from the probe to Earth. The orbiter aspect angle is the angle between the spacecraft roll axis, which points in an anti-Earthline direction, and the line of sight to the probe. To minimize signal interference from rotating spacecraft booms, the orbiter aspect angle is not to exceed 92°. This constrains the arrival date to no earlier than August 4.

In the current nominal mission timeline (table 5) the probe is separated from the orbiter 150 days prior to probe entry into Jupiter's atmosphere. Due

Table 4. Ballistic and Optimal Broken-Plane Trajectory Characteristics for Launch Date 5/21/86 and Arrival Date 8/27/88

Parameter	Trajectory Type	
	Ballistic	Broken Plane
Launch energy (C_3)	118 km²/s²	80 km²/s²
Declination of launch asymptote[a]	−48°	−22°
Heliocentric inclination[b]	11°	3°
Broken-plane maneuver	—	231 m/s
Hyperbolic approach velocity at Jupiter	6.1 km/s	5.8 km/s

[a]Earth equator.
[b]Ecliptic.

Figure 55. Propellant margin (kg) for $C_3 = 80$.

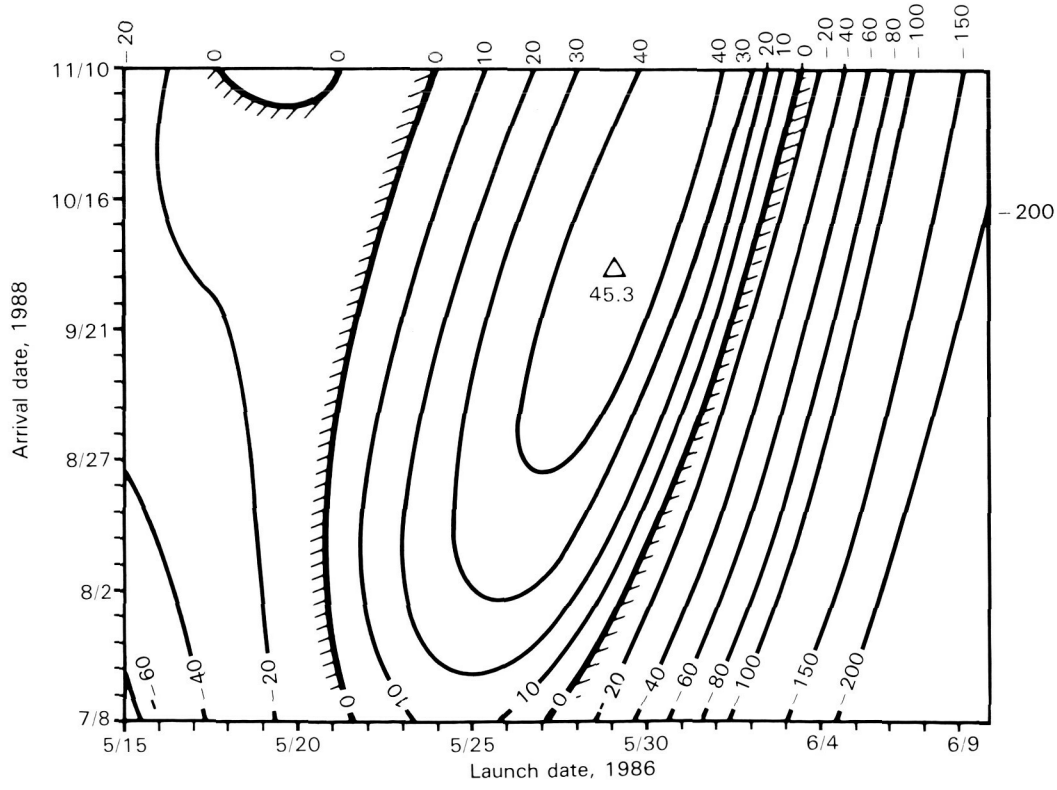

to navigation considerations, separation is constrained to occur no sooner than 14 days after solar conjunction or no later than 20 days before solar conjunction. This requirement excludes arrival dates between September 16 and October 22.

In figure 56 the arrival date constraints are superimposed on the propellant margin contours. The set of usable launch date/arrival date combinations consists of those which lie outside these constraints and within the contour of zero propellant margin.

Approximately 150 days before Jupiter arrival, the spacecraft will be spun up to 10 rpm and the probe released. This spinup will provide the probe with the required spin stability for its five-month solo journey to Jupiter. The probe has no maneuvering capability; therefore, prior to separation the spacecraft must be traveling on the precise ballistic entry trajectory.

Three days after separation, an engine burn

Table 5. Sequence of Events

Event	Times from Jupiter Encounter (perijove)
Probe separation	−150 days
Orbit deflection maneuver	−147 days
Io flyby	−4 hr 7 min
Orbiter perijove	0 hr
Probe entry	10 min
Start of probe relay link	12 min
Orbiter overflight	40 min
End of probe relay link	1 hr 12 min
JOI start	1 hr 42 min
JOI end	2 hr 30 min
Solar occultation entrance	7 hr 25 min
Solar occultation exit	9 hr 55 min
Earth occultation entrance	10 hr 55 min
Earth occultation exit	13 hr 50 min
Perijove raise maneuver	100 days

Figure 56. Arrival date constraints.

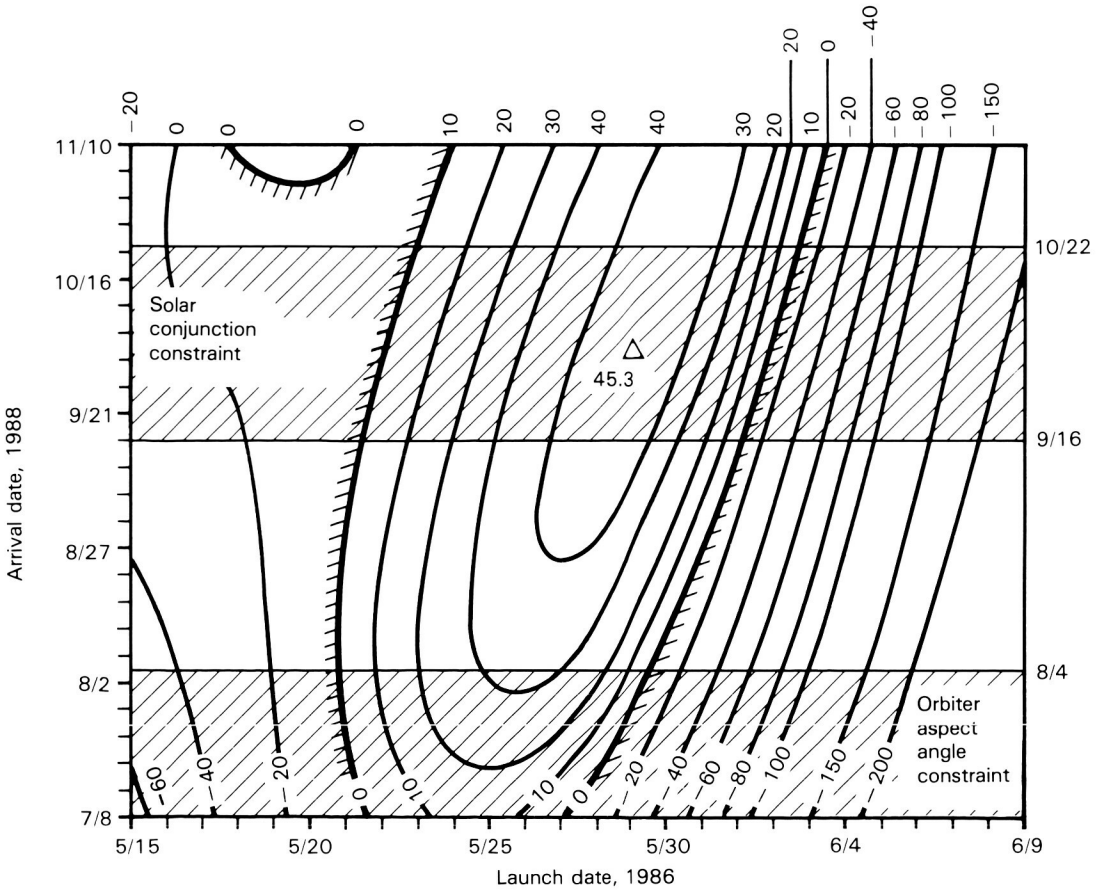

provides a ΔV of about 55 m/s to deflect the orbiter's trajectory so that it will not follow the probe into Jupiter. The orbiter is specifically targeted to encounter the satellite Io about four hours before closest approach. The Io encounter time is selected so that the subsequent radius at closest approach to Jupiter is 4 R_J. In addition, this maneuver establishes the orbiter–probe phasing so that the orbiter is approximately overhead the probe 30 minutes after the probe's entry into the jovian atmosphere.

Figure 57 shows a trajectory pole view of the Io flyby. Performance considerations dictate that this encounter be a close equatorial flyby. The orbiter will pass in front of Io so that the gravitational attraction of Io will slow the orbiter, reducing the Jupiter orbit insertion ΔV requirements by about 150 m/s for a 1000-km flyby altitude at Io. The orbiter will pass through Io's wake, since it will fly by the leading hemisphere of the satellite. The Io flyby also qualifies as a gravity pass, since there is no Earth occultation and the spacecraft's trajectory will be bent as it passes in front of Io. This will be the only close Io flyby during the mission, since the orbiter would probably not be able to withstand a second pass through the harsh jovian radiation environment at the orbit of Io.

Shortly after the orbiter has passed through its 4 R_J perijove, it will begin to receive data from the probe, which will have begun its descent into the jovian atmosphere. The orbiter will transmit the probe data to Earth in real time as well as record the data on its tape recorder. Soon after the probe mission has been completed, the 400-newton engine will be ignited and will burn for almost an hour to achieve the desired 200-day highly elliptical initial orbit about Jupiter. The Io flyby, probe relay, and JOI burn are shown in figure 58.

About seven hours after perijove the orbiter will be occulted by Jupiter from the Sun for two hours. Shortly afterward there will be a three-hour Earth occultation.

Approximately 100 days later, at the first apojove, the perijove raise maneuver will raise perijove to 11.5 R_J so that the orbiter will survive the radiation of eleven more passes through the jovian system.

Probe Mission

Many constraints affect the design of the probe mission: the expected lifetime of the probe battery precludes separating the probe earlier than 150 days before encounter (E – 150 days); separation must occur outside the approximately 30-day

Figure 57. Io flyby.

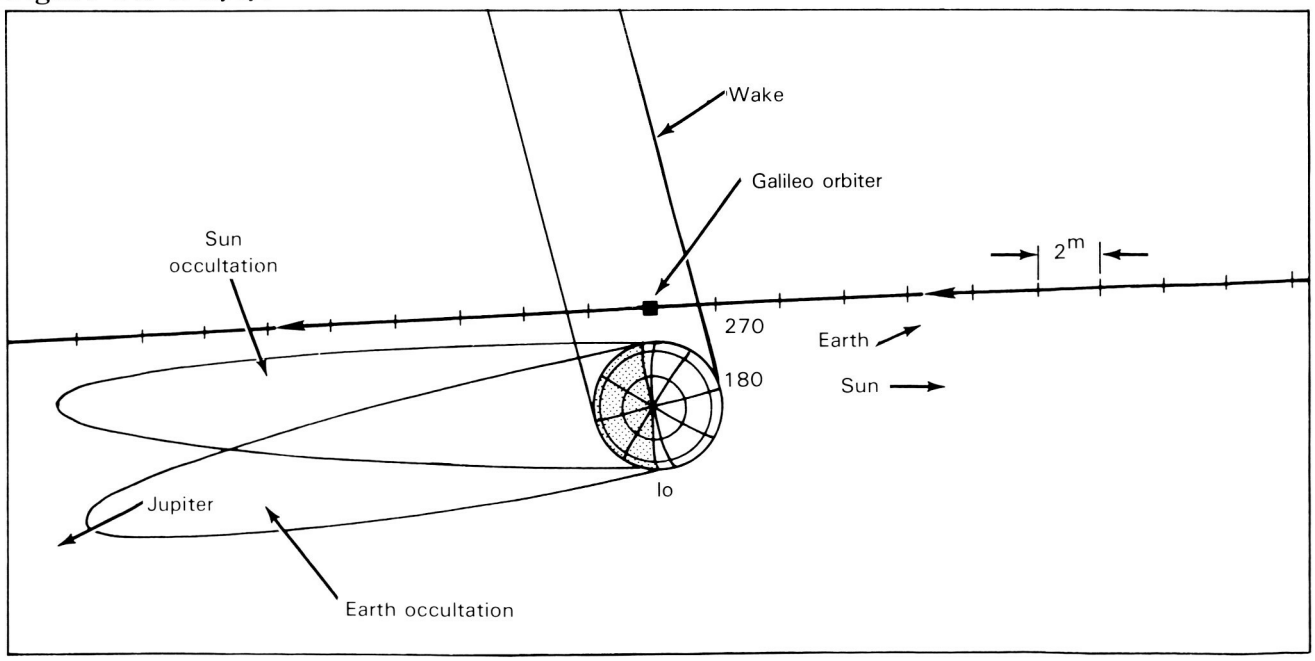

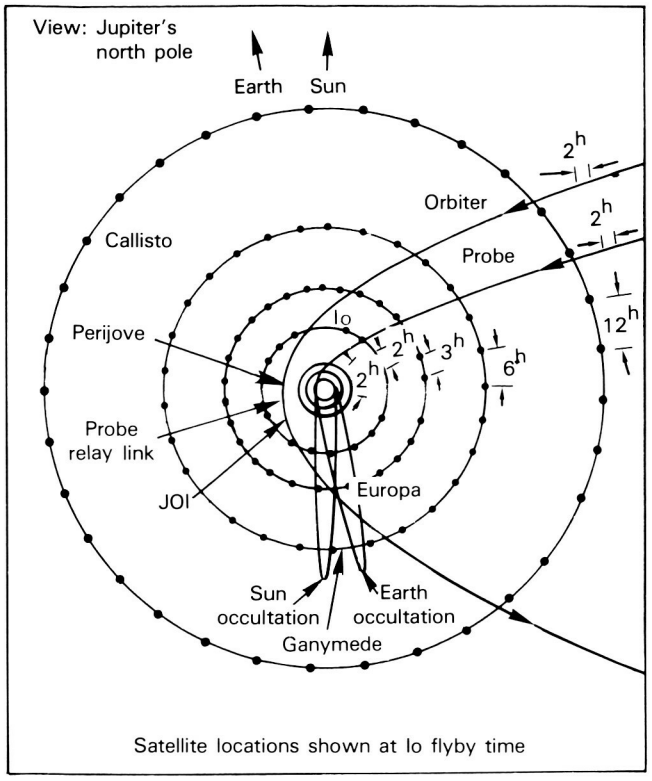

Figure 58. Arrival geometry.

period around solar conjunction; the orbiter aspect angle cannot exceed 92°; for scientific reasons the entry latitude must be between ±5.5° excluding the region between ±1.0°; for safety reasons, the probe cannot cross the ring plane at a distance less than 1.8 R_J; for probe survivability, the entry speed relative to the atmosphere must be less than 47.8 km/s. These constraints must all be considered in adopting the targeting strategy.

A sketch of the basics of probe trajectory geometry is shown in figure 59. The V_∞ vector, the approach velocity of the spacecraft relative to Jupiter, is shown piercing the near side of Jupiter at a declination of δ_∞ from the equator, corresponding to that of the approach velocity vector, measured from the equator. The ground tracks of three possible probe trajectories are shown on the surface of Jupiter, all passing through the V_∞ vector. Also shown on the surface of Jupiter is the locus of points for which the relative flight path at entry (γ_E) is a constant (nominally, $\gamma_E = -8.6$). The trajectories labeled 1 and 2 will have entries in the northern hemisphere. For trajectory 1, the entry latitude (ϕ_E) is equal to the declination of V_∞, and entry occurs long after the nodal crossing point at which the probe flies through the equator. This means that the probe crosses the equator at a high altitude and will fly safely over the particle ring discovered by Voyager. In fact, it can be shown that for all values of δ_∞, if entry is at a latitude equal to or greater than δ_∞, the equatorial crossing is at or above 2.0 Jupiter radii—safely above the visible ring.

In trajectory 2 the probe enters at a low latitude in the northern hemisphere, only shortly after crossing the equator. In this case, the probe will have flown through the equatorial plane at a low altitude and will have penetrated the visible ring.

Trajectory 3, at a much higher inclination, allows entry in the southern hemisphere prior to crossing the equator, and the probe is therefore safe from impact with ring material. However, the relative entry speed of trajectory 3 is higher than for the other trajectories because the direction of the probe's inertial velocity is not so closely aligned with the rotational velocity of Jupiter.

The first probe science instruments will be activated at about six hours from entry (E) and 8.5 R_J from the center of Jupiter. Three lightning and

Figure 59. Probe targeting geometry.

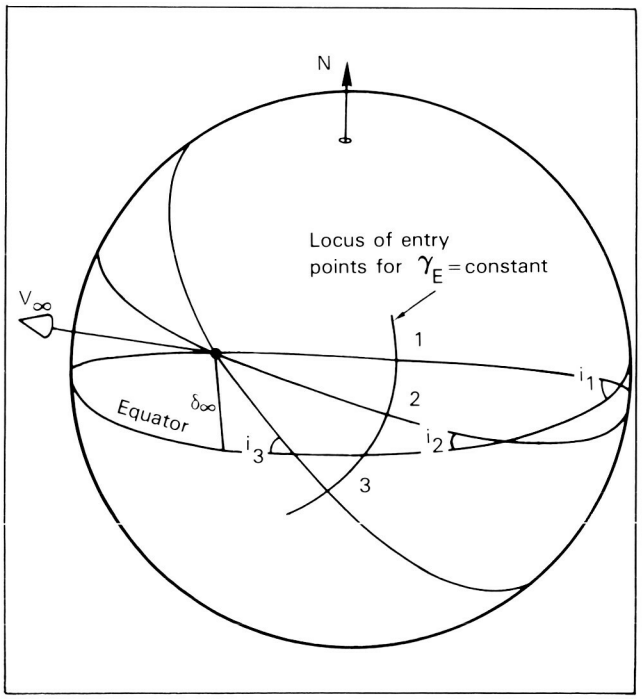

energetic particles samples will be taken between about 5 and 3 R_J (about E − 3 hours to E − 2 hours). At about E − 18 minutes the nephelometer and atmospheric structure instruments will be calibrated. Data taken before the probe transmitter is turned on will be stored for playback to the orbiter during the relay period.

Entry is defined to occur when the probe reaches an altitude of 450 km above the 1-bar atmospheric pressure level. At this point the probe will be moving with an atmosphere-relative speed of about 47.4 km/s and will have a relative flight path angle of −8.6°. Deceleration due to atmospheric drag will build quickly, reaching a maximum of about 2270 m/s^2, or 231 Earth g's, at about E + 58 seconds. Maximum dynamic pressure will be about 5×10^5 N/m^2. By E + 115 seconds, the probe's speed will decrease to Mach 1. Here, at an altitude of about 49 km, the probe will deploy its main parachute and subsequently jettison the ablative aeroshell structure, which will have dissipated the major portion of the entry energy. Atmospheric sample analysis by the probe's scientific instruments and transmission to the orbiter of both stored and real-time data will begin at this point. For the next hour the orbiter will record the probe's data and relay it in real time to Earth. Probe terminator crossing (from day to night) will occur at about 19 minutes past entry. The possible water cloud deck will be traversed between about E + 22 minutes and E + 24 minutes (based on the nominal probe delivery and performance). The 10-bar pressure level will be reached at about E + 38 minutes. The end of the probe data relay period will occur at about E + 62 minutes, when the probe has penetrated to the (approximately) 21-bar pressure level, at an altitude of about −137 km. A representative sequence of events for the probe mission is shown in table 6.

Figure 60 illustrates to scale the typical orbiter/probe arrival geometry from the orbiter's Io flyby through the relay period and JOI. Note that the probe and orbiter trajectories are both nearly in Jupiter's equatorial plane.

Figure 61 (not to scale) illustrates, in a planar approximation, the dynamic behavior of the link geometry as a function of the time past entry. Note that at signal acquisition, the signal enters the relay radio antenna (RRA) to the left of the RRA axis, while 30 minutes later it enters to the right of the

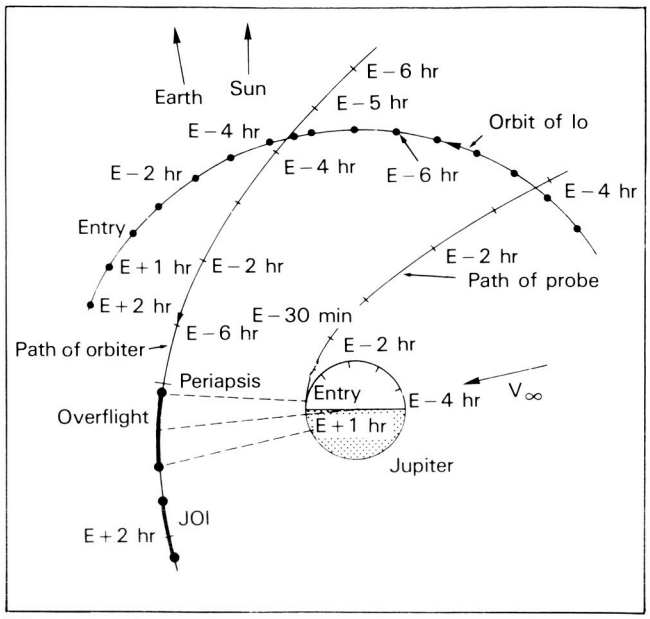

Figure 60. Typical probe arrival geometry.

axis. Therefore, at some point between E + 2 minutes and E + 30 minutes, the signal crosses the RRA axis. At the end of mission (EOM), the signal would arrive far off the RRA axis if the RRA were to remain inertially fixed. The dashed figure of the RRA represents a repointing of the antenna to improve the relay link performance in the later portion of the mission. It may also be inferred that environmental losses will increase during the mission as the probe falls deeper into the atmosphere and penetrates the clouds, resulting in attenuation of the radio signal as the path length increases.

Figure 62 illustrates the probe descent profile for pressure, temperature, and altitude as a function of time.

Satellite Tour Design

The Galileo mission is the first mission to use an orbiting spacecraft to perform an intensive scientific investigation of Jupiter, its environment, and its Galilean satellites—Io, Europa, Ganymede, and Callisto. The orbiter will perform a series of at least eleven highly elliptical revolutions about Jupiter. On each of these revolutions, a close, targeted flyby of one of the Galilean satellites is planned. This series of targeted encounters is termed a "tour."

The influence of the gravity of any of the

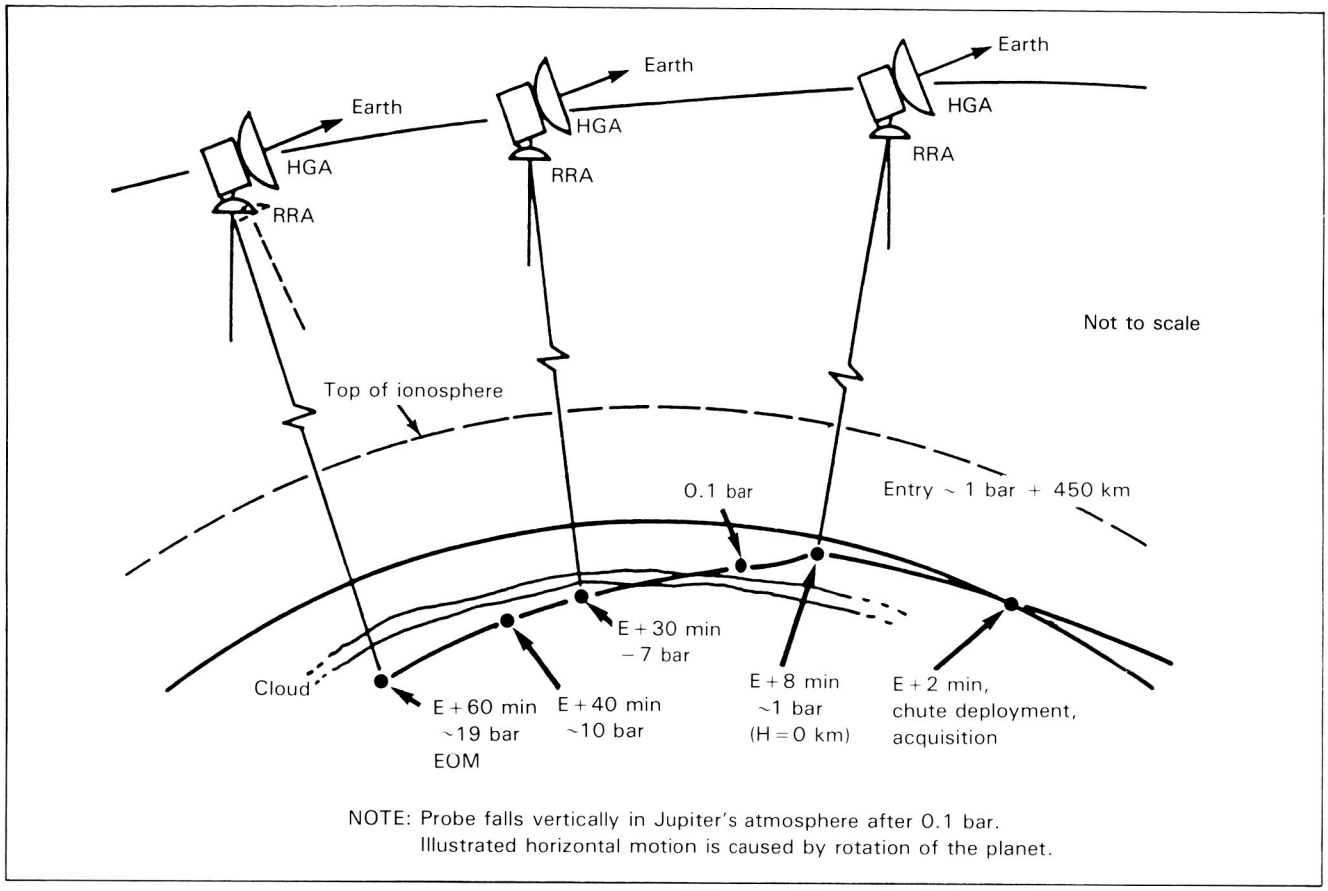

Figure 61. Relay link geometry.

Galilean satellites may be used to shape and control the orbiter's trajectory. Consequently, repeated close flybys with Europa, Ganymede, and Callisto are used to target the orbiter to the next satellite encounter. In this manner, tightly limited orbiter ΔV propellant need only be used for fine tuning navigational purposes.

The design of a successful tour is constrained by other factors in addition to the laws of orbital mechanics. Specifically, budgetary and hardware constraints significantly influence the tour, as well as the need to design encounters that permit the most useful scientific observations to be made. These mission constraints and scientific requirements are described later.

At each satellite encounter, different aimpoints exist that allow the orbiter to return to the same satellite or to encounter a different satellite. Consequently, an abundance of aimpoints at each satellite encounter can result in many possible tours, each of which will satisfy many of the science objectives in different ways. While it is possible to design a tour to satisfy any single science requirement, the tendency for various science desires to be mutually incompatible rules out the possibility that any single tour can satisfy all the science requirements. Therefore, strategies must be developed to maximize the satellite tour science. Tour design strategies and their application to a representative tour are discussed later.

Gravity-Assist Trajectory Design

In the past ten years, several interplanetary missions have utilized the gravity assist of an intermediate planet in order to reach subsequent targets. Most recent have been the Voyager flybys of Jupiter and Saturn in which those planets were used to target the spacecraft's heliocentric trajectories.

Many missions currently in the planning and analysis stage use gravity-assist concepts to reduce performance requirements. Interplanetary trajectory options for Galileo that have been studied include Mars-powered swingbys, Earth–Venus–Earth gravity assists, and Earth–deep space ΔV–Earth gravity assists.

Galileo will use a close flyby of the satellite Io near the orbit insertion maneuver to reduce the orbit insertion ΔV requirements. In addition, the Galilean satellite tour will be possible only by using the gravity assist resulting from the satellite encounters.

The basic mechanism of gravity-assisted flybys is illustrated in figure 63. Flying by the trailing or leading edge of a secondary body (satellite) provides an increase or decrease in the spacecraft's energy with respect to the central body (Jupiter). Note that the spacecraft velocity vector with respect to the central body also rotates. The rules for orbit rotation are shown in table 7.

Each of the Galilean satellites provides unique

Table 6. Probe Mission Sequence of Events

Time from Entry	Probe Altitude	Atmospheric Presssure (bars)	Event
−165 days			Final entry targeting maneuver
−150 days			Probe separation
−147 days			Orbiter deflection maneuver[a]
−140 days			Establish initial relay radio antenna (RRA) cone position[a]
−10 days			Update RRA cone based on latest navigation data[a]
−24 hr			Position stator for relay[a]
−6 hr	7.5 R_J		Initiate probe preentry sequence
−4.5 hr	5.8 R_J		Io encounter[a] (stator movement allowed for Io science)
−3 hr	4.1 R_J		First LRD/EPI sample
−3 hr	4.1 R_J		Fix stator position for remainder of probe mission[a]
−18 min	0.5 R_J		NEP and ASI calibrations
0 s	450 km	10 to 7	Entry (at 450 km altitude, by definition)
57 s	100 km	0.0007	Maximum dynamic pressure
58 s	97 km	0.0008	Maximum deceleration
115 s	49 km	0.09	Deploy main parachute
120 s	46 km	0.10	Nominally at pressure = 0.1 bar
124 s	45 km	0.11	Jettison aeroshell
135 s	42 km	0.12	Turn on transmitter; begin acquisition sequence
185 s	34 km	0.20	Latest time of acquisition[a] (99.5 percent probability)
503 s	0	1.0	Nominally at pressure = 1 bar
17 min	−35 km	2.9	Probe aspect angle minimum
19 min	−42 km	3.5	Cross terminator (for baseline arrival date of 8/25/88)
21 min	−48 km	4.0	Orbiter overflies longitude of probe[a]
22 min	−51 km	4.3	Enter cloud
24 min	−57 km	5.0	Exit cloud (nominal)
32 min	−78 km	7.7	Exit cloud (latest)
32 min	−78 km	7.7	Begin periodic repositioning of RRA[a]
38 min	−92 km	10	Nominally at pressure = 10 bars
62 min	−137 km	21	End of baseline mission

[a]Orbiter/RRH events.

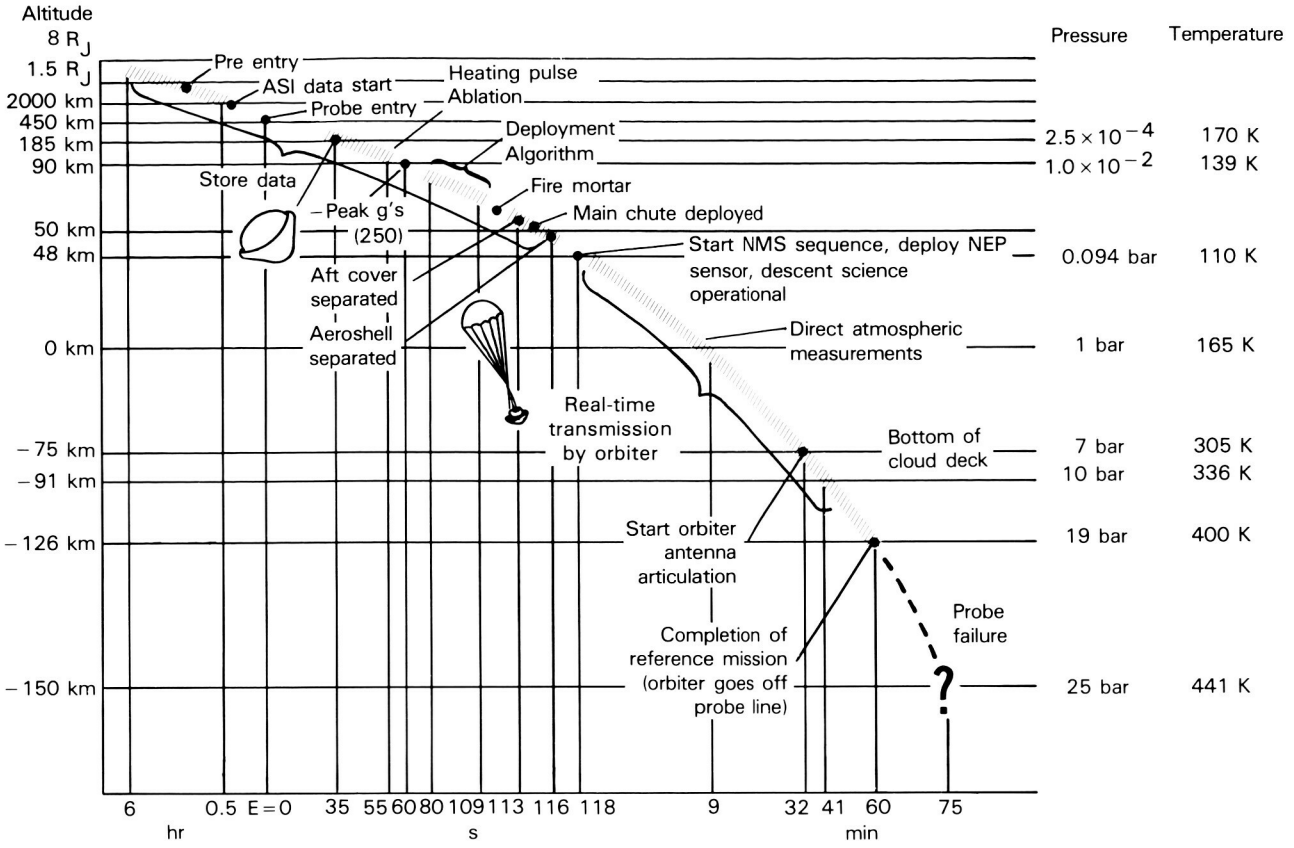

Figure 62. Probe descent profile.

Figure 63. Mechanics of gravity-assisted flybys.

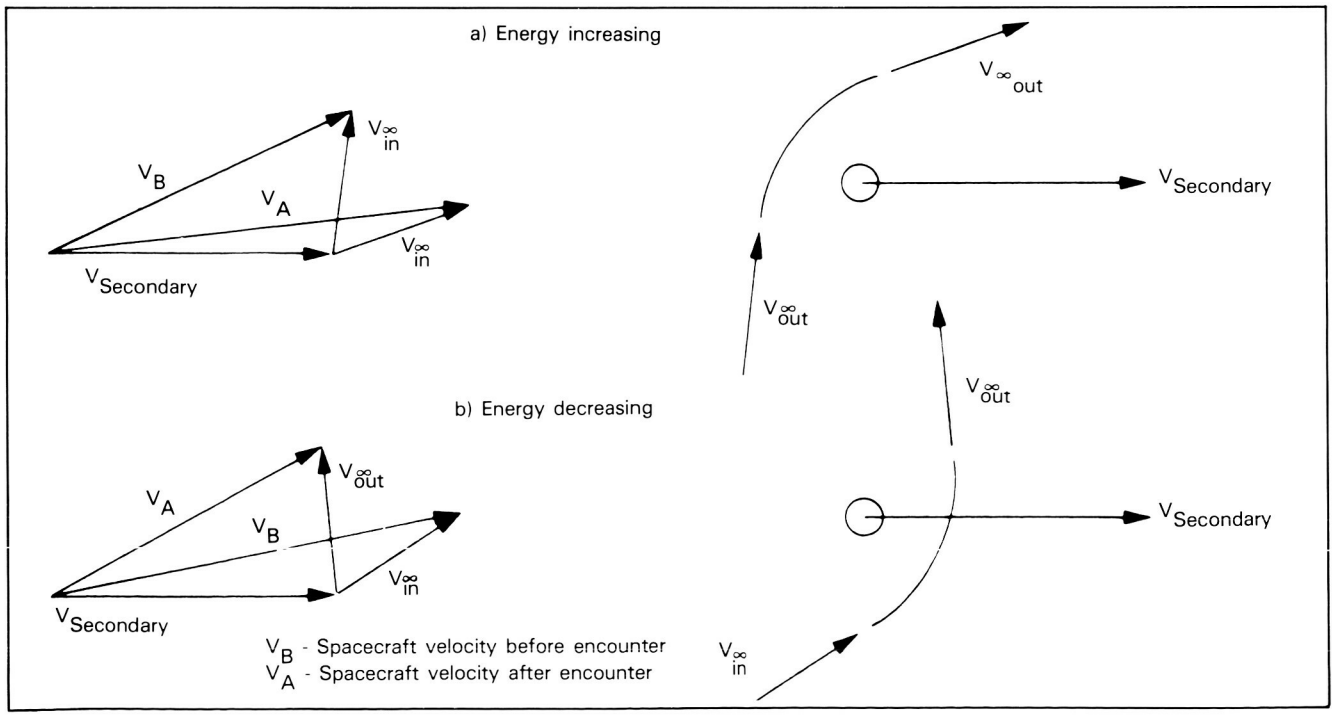

Table 7. Orbit Rotation

Spacecraft velocity with respect to the central body is		reduced	increased
Satellite encounter is	inbound	counter-clockwise	clockwise
	outbound	clockwise	counter-clockwise
		orbit rotation is	

Polar flybys of the secondary body can be used to provide an out-of-plane gravity assist to change orbit inclination.

gravity assist capabilities due to differences in their masses and orbital distances from Jupiter. Table 8 provides a summary of important physical and orbital data for each of the Galilean satellites. These satellites are in near-circular equatorial orbits, and the inner three satellites are locked into a tight resonance (Europa's period is twice Io's period, and Ganymede's period is twice Europa's period).

The most effective satellites for changing the spacecraft's orbital period (equivalent to changing energy) are Io and Ganymede. Because of Io's small orbital radius, the orbiter's encounters with Io are near perijove, making these encounters efficient to change energy. The initial approach to Jupiter utilizes a close Io flyby to remove energy from the spacecraft orbit and thereby reduce the orbit insertion ΔV. However, the orbit of Io is deep within Jupiter's radiation belts, and the orbiter is designed to tolerate only one close pass through that harsh radiation environment. Thus, there is only one close Io encounter in the satellite tour.

Ganymede, the most massive satellite, is effective for changing the spacecraft's orbital period, orbital orientation [through rotation of the orbiter's line of apsides (the line through perijove and apojove of an orbit)], and orbital inclination. Consequently, most tour designs tend to have more encounters with Ganymede than with any other satellite.

Callisto, the outermost Galilean satellite, is slightly more effective than Ganymede for changing orbiter inclination and/or orbiter perijove radius. On the other hand, because it is less massive and located farther from Jupiter than Ganymede, Callisto is less effective than Ganymede for changing orbital period. Its effect in rotating the line of apsides is about the same as that of Ganymede.

Europa, the least massive satellite, is least efficient for changing either orbital period or inclination. Nonetheless, the high science priority to study Europa requires that every tour design include several Europa encounters.

Mission Constraints

Constraints on the orbiter mission are imposed due to concerns about overall mission risk and reliability, operational costs, hardware capabilities, instrument reliability, and navigational accuracy. Project operational budgets dictate that the nominal orbiter mission conclude 20 months after Jupiter orbit insertion.

Hardware capabilities of the space shuttle and

Table 8. Galilean Satellite Physical and Orbital Data

Satellite	GM[a] (km^3/s^2)	Radius (km)	Orbital Radius (10^3 km)	Orbital Radius (Jupiter Radii)	Eccentricity	Inclination (deg)	Period (days)
Io	5934	1820	422.2	5.91	0.003	0.037	1.769
Europa	3196	1533	671.4	9.40	0.009	0.418	3.551
Ganymede	9885	2608	1071.1	15.00	0.001	0.254	7.155
Callisto	7172	2445	1883.4	26.38	0.008	0.163	16.689

[a]GM = Newton's gravitational constant times satellite mass.

the Centaur upper stage restrict the available ΔV (i.e., propellant mass) for tour navigation purposes. Specifically, the total tour ΔV budget (deterministic plus statistical at 90% probability) is only 205 m/s.

Instrument and orbiter reliability concerns impose a maximum accumulated radiation dosage value to which the orbiter may be exposed. Energetic electrons and protons trapped in Jupiter's radiation belts can cause interference and damage in electronic parts in the Galileo orbiter. The measure of radiation dosage adopted is the dose in krad (Si) transmitted through a thickness of 2.2 g/cm^2 of aluminum for a spherical-shell model (the dose that would penetrate to a piece of silicone situated in the center of a spherical shell of aluminum 2.2 g/cm^2 thick). To ensure that such effects do not seriously degrade spacecraft performance, a maximum acceptable dose for the entire mission has been established at 150 krad. To ensure that prohibitive shielding masses are not required to meet this constraint, it is necessary to raise the orbiter perijove above the more intense region of Jupiter's radiation belts.

The requirement to navigate the spacecraft accurately necessitates that no more than one targeted satellite encounter occur on any orbit. Furthermore, the navigation system requires that a minimum of 28 days occurs between targeted encounters on revolutions during which an apoapsis orbit trim maneuver is to be executed or a minimum of 17 days occurs between targeted encounters on revolutions during which no apoapsis orbit trim maneuver is executed.

Navigational constraints also impose a minimum satellite flyby altitude of 200 km for a targeted encounter.

A nontargeted encounter occurs when the spacecraft passes relatively close to one of the Galilean satellites other than the primary targeted satellite on a given orbit. Nontargeted encounters provide important scientific data-gathering opportunities.

Science Requirements. The scientific investigations to be performed by the orbiter can be divided into three areas: investigations of the Galilean satellites (Io, Europa, Ganymede, and Callisto), investigations of Jupiter, and investigation of the fields and particles in Jupiter's magnetosphere.

A list of the major "requirements" that would provide significant scientific information and are physically realizable is provided in the box in chapter 1. Many of these requirements are mutually exclusive. Consequently, while any one particular requirement can be met, it is impossible for any single tour to meet all of these scientific requirements.

For the Galileo orbiter to have a close satellite encounter, two conditions must be satisfied. First, the orbits of the orbiter and the satellite must nearly intersect. Second, the passages of the orbiter and the satellite through the line of nodes (defined by the intersection of their orbital planes) must occur at nearly the same time.

These two conditions are easier to satisfy for the Galilean satellite system if the orbiter is in an equatorial orbit about Jupiter. Since the Galilean satellites are in near-circular equatorial orbits, the first condition is satisfied for orbiter equatorial orbits provided that perijove occurs within the satellite orbit. The second condition is satisfied by adjustment of the orbiter's period from the gravity assist of the previous satellite encounter and/or deterministic maneuvers.

If the orbiter has a jovicentric inclination greater than a few degrees, the orbit intersection requirements to encounter a different satellite necessitate changes to the jovicentric orbit orientation and inclination larger than what can reasonably be achieved from the gravity assist of a satellite encounter. Large deterministic maneuvers would then be required to provide the orbit geometry changes.

For a 1986 launch, the initial hyperbolic approach direction to Jupiter can vary from being in Jupiter's equatorial plane to being a few degrees out of the plane. Since performance considerations dictate a near-perijove, coplanar orbit insertion, the initial orbit about Jupiter may be inclined a few degrees to the Jupiter equatorial plane. To avoid large deterministic maneuvers, the initial encounters of the satellite tour would be with the same satellite at the same location in its orbit. Orbit inclination is reduced with these encounters until the spacecraft orbit is in the equatorial plane, allowing subsequent encounters with other satellites.

Nontargeted Satellite Encounter Strategy. Since the Galileo spacecraft does not have a wide-angle camera, it is necessary to have encounters with flyby altitudes up to 50 000 km to

gain enough time to mosaic the Galilean satellites at a resolution of 1 km with a narrow-angle camera. In addition, distant flybys provide the only means to image large areas of the satellites not previously imaged by Voyager.

Distant targeted satellite encounters are difficult to design because of the limited gravity assistance available to set up the next encounter. On any perijove pass with a close targeted encounter, it may be possible to have additional encounters, known as nontargeted encounters, with the other Galilean satellites. If these nontargeted flyby altitudes are between 25 000 and 50 000 km, they generally can be used to provide 1-km coverage. Because of the close commensurability between the orbit periods of Europa and Ganymede, it is possible to have repeated Europa and Ganymede nontargeted encounters over several orbits. Callisto is not locked in resonance with Europa and Ganymede; thus, nontargeted Callisto encounters are more sporadic and difficult to include in a satellite tour design.

Nontargeted encounters are a function of jovicentric orbit orientation, targeted satellite encounter time, and perijove distance. Since the orbit orientation for all tours is constrained by the interplanetary trajectory and a magnetospheric requirement to achieve a tail petal orbit, orbit periods and perijoves must be designed to take advantage of the nontargeted opportunities that naturally occur.

Typically, Galileo satellite tours will have about three or four nontargeted encounters within a range of 50 000 km. Even then, some of the nontargeted encounters may be dark-side flybys, rendering them useless for satellite imaging.

Satellite Coverage Strategy. Each of the Galilean satellites is in synchronous rotation with Jupiter; that is, the same satellite hemisphere always points toward the planet. Consequently, as illustrated in figure 64, the approach to an outbound satellite encounter (occurring after perijove) allows viewing of the satellite hemisphere toward Jupiter, while the approach to an inbound satellite encounter (occurring before perijove) allows viewing of the satellite hemisphere pointing away from Jupiter. Therefore, good coverage of a satellite requires at least two separate encounters with that satellite: one inbound and one outbound.

Changes to the shapes and size of the jovicentric orbit or changes to the orbit orientation about Jupiter do not appreciably change the "real estate" viewed on approach to or departure from the satellite. However, the surface illumination is different, depending on where the satellite is encountered in its orbit, relative to the Jupiter-Sun line. Figure 64 shows that the approach phase angles, ϕ, are very low for spacecraft orbital angles near 90° (apojove over the jovian dawn terminator). This orientation always occurs early in the mission, whereas late in the mission, due to spacecraft orbit rotation toward the tail, the approach phase angles are about 90°.

We can construct longitudinal coverage plots that illustrate the satellite surface areas that can be observed on approach and exit for inbound and outbound encounters. An example is shown in figure 65 for spacecraft orbital angles of 90° and 180° (orbit apoapsis located in the dawn and tail regions, respectively).

Regions do exist that cannot be observed on approach or exit for any spacecraft orbital orientation. These gaps unfortunately coincide with regions not observed by the Voyager spacecraft, since both Voyager and Galileo trajectories are posigrade, with perijove far beneath the orbits of Ganymede and Callisto.

By taking inbound/outbound encounter pairs for Ganymede and Callisto at any jovicentric orbit orientation, the longitudinal coverage is maximized due to the true anomaly at encounter being $\pm 90°$. However, for Europa, because the spacecraft true anomaly at encounter is small (within $\pm 30°$), an early outbound (dawn) encounter coupled with a late inbound (midnight) encounter is required to maximize the coverage.

The approach phase angle—the angle measured from periapsis to the spacecraft—for early encounters is very low (high Sun angle), whereas for late encounters the approach phase angle is approximately 90° (low Sun angle). By carefully choosing inbound/outbound pairs at different orbit orientations, it is possible to obtain maximum coverage at different Sun angles and therefore choose which science objectives to emphasize.

Figures 64 and 65 show that the gaps in global coverage, centered on longitudes of 90° and 270° on Ganymede and Callisto and 160° on Europa, cannot be filled by a close targeted encounter. These gaps can be partially filled by distant nontargeted encounters early in a tour and completely

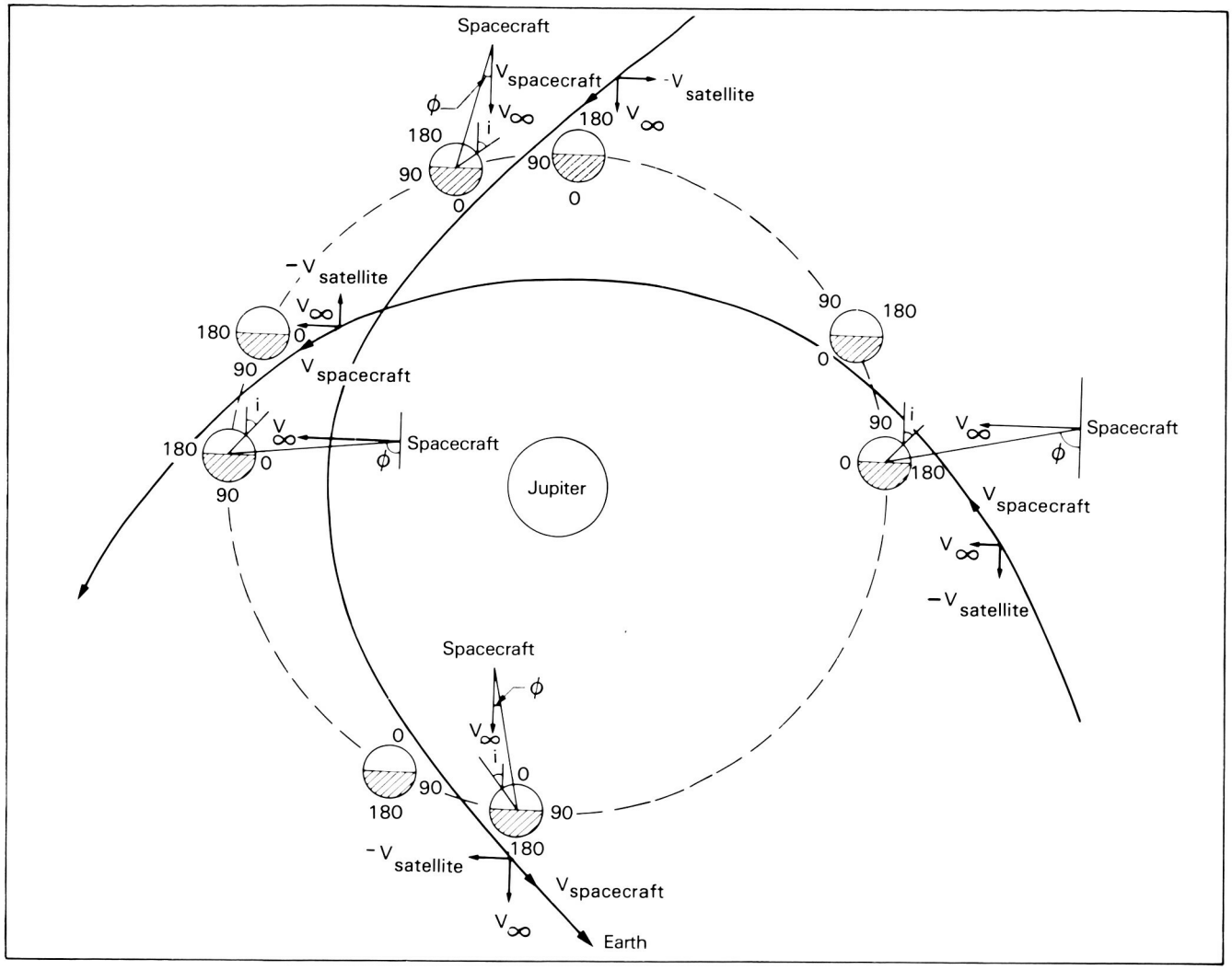

Figure 64. Encounter geometries, satellite longitudes, and phase angles that occur throughout the Galileo orbital tour.

filled by distant light-side nontargeted encounters late in a tour. Distant light-side nontargeted encounters allow mosaics to be taken throughout the entire encounter period, including closest approach. Close targeted encounters do not allow global coverage at closest approach, since the orbiter's velocity is too high to allow enough time to completely mosaic the available surface.

High-resolution coverage can, of course, be obtained only during close encounters. Early encounters feature low-phase approaches, with encounter occurring nearly over the terminator. For close early encounters, therefore, high-resolution coverage at low to moderate Sun angles can be obtained near one terminator. Late encounters feature approach phase angles near 90°. For close, late encounters, high-resolution coverage at low Sun angles can be obtained near one terminator just prior to encounter and near the other terminator just after encounter. The high-resolution low-Sun coverage is thereby doubled, and if the encounter is on the light side, high-resolution high-Sun coverage is also available.

Tail Petal Strategy. A prime magnetospheric requirement is for a tail petal (the pattern of the elliptical orbits resembles a flower; hence,

C-2

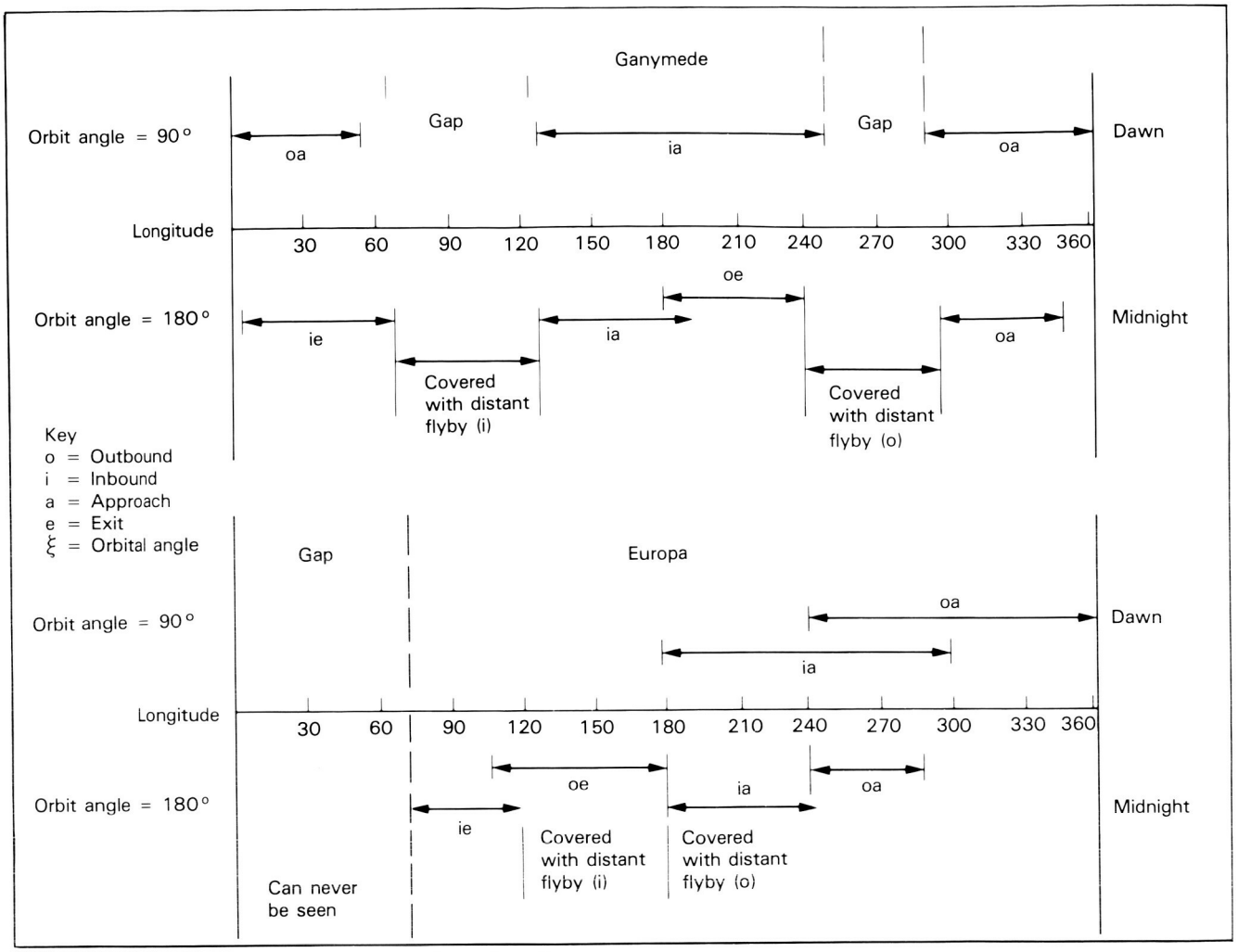

Figure 65. Longitudinal coverage plots for Ganymede and Europa.

the orbits are referred to as petals) orbit (150 R_J apojove located within 15° of the anti-Sun direction) to allow measurements within the jovian magnetotail. Initially, the orbital apojove is located near the dawn petal region. Therefore, it is necessary to utilize satellite gravity assist to help in the rotation of the orbit toward the tail petal region.

To achieve eleven orbits within the nominal 20-month mission, it is not possible to include the large tail petal orbit, with a period of at least 87 days, in the middle of the tour. The strategy, then, is to place the tail petal orbit at the end of the tour. The initial orbit orientation dictates whether it is necessary to rotate the spacecraft orbit immediately toward the tail petal region.

If possible, it is desirable to delay the tail petal rotation for several reasons. First, Jupiter science is enhanced, since longer viewing of the lit hemisphere of Jupiter is allowed. Second, preserving the initial orbit orientation allows high Sun angle approaches to the satellites. Finally, this strategy maximizes the jovicentric orbit orientation difference between Europa encounters, which improves Europa coverage.

Jupiter Occultation Strategy. One of the science requirements in tour design is the inclusion of Jupiter occultations to pass radio signals through the atmosphere (the orbiter is occulted by Jupiter as seen from Earth). Trajectories can be designed to provide Jupiter occultations by delivering the spacecraft to the same point at the same

satellite on successive encounters. Such 360° transfers allow a range of jovicentric inclinations, one of which is selected to provide the most favorable Jupiter occultation. (Transfer trajectories between different satellites require unique jovicentric geometries and cannot be modified for a specific Jupiter occultation.)

For the current mission, Jupiter's equatorial (and satellite orbit) plane is inclined to the Earth–Jupiter line. Consequently, an equatorial satellite tour, required to encounter all of the Galilean satellites, does not yield Jupiter occultations. Inclined orbits, which require 360° transfers, are required to provide the Jupiter occultations.

To design equatorial Jupiter occultations, it is necessary that the orbiter line of nodes (line of intersection between the equatorial plane and the spacecraft's orbital plane) be oriented about 90° from the Earth direction. Then inclined orbits about Jupiter of approximately 2° will provide equatorial Jupiter occultations. For the Galileo mission, this favorable orientation occurs for Callisto inbound encounters and Ganymede inbound and outbound encounters during the middle of the satellite tour.

Perijove Profile Strategy. The satellite tour design begins with the perijove raise maneuver. This maneuver, performed near the first apojove, raises perijove to typically 11.5 R_J, a less harsh radiation environment. The current nominal value is 11.5 R_J, since for a typical tour it holds the accumulated radiation dosage below 150 krad. Values less than 11.5 R_J are permissible provided that the tour's perijove profile is modified so that the 150-krad constraint is not violated.

The initial perijove value affects the timing of the first Europa encounter in the tour. As the orbit period is reduced from its initial 200-day value via satellite encounters, the orbit perijove is also reduced from its initial value. The closer the initial perijove value is to 9.4 R_J (Europa's orbit), the sooner the orbit perijove will be reduced below Europa's orbit.

Representative Satellite Tour

In this section, a representative satellite tour is presented to illustrate the tour design strategies discussed above. This tour satisfies most major science objectives; however, further investigation is required before a final tour is selected.

Table 9 shows pertinent information about each of the satellite encounters in this tour. The jovicentric orbits resulting from these encounters are illustrated in figure 66, which shows the progression of orbits from the initial 200-day orbit to the final tail petal orbit. The coordinate system used in this figure is one in which the direction to the Sun is fixed. Therefore, the total rotation between the initial and final encounters is due to both the satellite encounters and the motion of Jupiter about the Sun. (Note: the number that follows a satellite name indicates orbit number, not flyby number.)

Initial Ganymede Encounters. The Jupiter arrival date for this satellite tour is August 25, 1988. Approximately 100 days later, a maneuver will be executed to raise perijove to 11.5 R_J and to target the orbiter to the first encounter of the satellite tour. Future tour designs will consider values other than 11.5 R_J.

Since the initial tour perijove value is above Europa's orbit, the first satellite encounter must be with either Ganymede or Callisto. For this tour, Ganymede was selected because it is more effective than Callisto for changing orbit period. The initial 200-day orbit period will be reduced to 64 days by this equatorial flyby. The initial tour encounters must be used to reduce orbit period as quickly as possible so that the nominal mission can be completed in the 20 months following orbit insertion. Limited propellant onboard the orbiter rules out using the JOI maneuver to achieve an initial orbit period below 200 days.

The second Ganymede flyby is a polar pass to lower inclination and to place the spacecraft in the equatorial plane. The encounter is used to satisfy the Ganymede gravity experiment, which requires that the tour contain both a close equatorial and a close polar distinction of the principal moments of inertia (measure of satellite mass density distribution, determined from the manner in which the satellite's gravity bends the trajectory) of Ganymede. To achieve sufficient inclination to require the Ganymede 2 flyby to be polar, the Ganymede 1 encounter slightly increases orbit inclination from 2° to 3°. Having an initially inclined jovicentric orbit is desirable because it allows the design of a single Ganymede polar pass in the tour. (Starting from an equatorial orbit usually requires the inclusion of two Ganymede polar passes. The second polar pass is required to reduce the inclination

Table 9. Representative Satellite Tour Summary

Encounter	Date	Satellite/Inbound Satellite/Outbound	Altitude (km)	Latitude (deg)	Objective
1	18 Mar 89	Ganymede/In	834	−20	Reduce period, gravity, magnetic field, wake
2	21 May 89	Ganymede/In	1,146	+89	Reduce inclination, gravity, magnetic field, flux tube
3	22 Jul 89	Callisto/In	494	+5	Reduce perijove, gravity, magnetic field, wake
4	1 Sept 89	Europa/In	1,400	−89	Gravity, magnetic field, flux tube
5	10 Oct 89	Europa/Out	200	+15	Coverage, occultation, wake
6	9 Nov 89	Callisto/Out	6,346	−10	Rotation, occultation, wake
7[a]	2 Dec 89	Europa/In	25,000	+10	Coverage
7	3 Dec 89	Ganymede/Out	3,258	−6	Rotation, occultation, wake
8	21 Dec 89	Ganymede/In	1,722	+7	Rotation, occultation
9	17 Jan 90	Europa/In	472	−2	Coverage, occultation
10[a]	22 Feb 90	Callisto/In	40,630	+12	Coverage
10	23 Feb 90	Ganymede/In	3,680	−13	Increase period, rotation
11	13 Apr 90	Callisto/In	277	+16	Tail petal
11[a]	14 Apr 90	Ganymede/In	45,955	−22	Coverage
	29 May 90	Tail petal apojove (JOI + 21 months)			Magnetosphere

[a]Designates nontargeted encounter.

resulting from the first polar pass. Consecutive polar passes do not maximize satellite coverage, since the satellite is encountered at the same location in its orbit, giving redundant lighting conditions on the same surface area.) For some of the interplanetary transfers in the launch/arrival date space, the initial inclination at Jupiter is sufficiently small that it is possible to encounter other satellites after the Ganymede 1 encounter. For those tours, consecutive Ganymede polar passes may have to be designed if the requirements for a Ganymede gravity experiment are to be satisfied.

The initial Ganymede encounters for this tour were designed to be inbound to prevent the jovicentric orbit from rotating clockwise toward the tail petal region. The period-reducing, inbound encounters rotate the jovicentric orbit clockwise away from the tail petal region. However, due to the motion of Jupiter about the Sun, there is a drift of the jovicentric orbits toward the tail petal region at a rate of about 2.5° per month. This drift during the initial orbits cancels out the rotation away from the tail petal region resulting from the initial inbound Ganymede encounters.

Callisto 3 Encounter. After the initial Ganymede flybys, the orbiter will encounter Callisto on its next passage through the jovian satellite system. Since it is desirable to encounter each of the Galilean satellites as soon as possible, the Callisto flyby is used to reduce perijove below Europa's orbit, thereby allowing a Europa encounter on the next orbit. The Callisto encounter is designed to be inbound to delay rotation toward the tail petal region.

This encounter provides the only opportunity for a close Callisto wake passage. All satellite encounters resulting in a wake passage must necessarily pass the leading side of the satellite, causing a reduction in orbit period and perijove. Because of the large perijove reduction resulting from a close equatorial Callisto flyby, Callisto wake passes must occur early in a tour, when the orbit periods and corresponding perijoves are still relatively high. Callisto wake passages occurring later in a tour, after the orbit period has been reduced to 30 days, would result in low perijove values that would cause excessive radiation dosages to the orbiter.

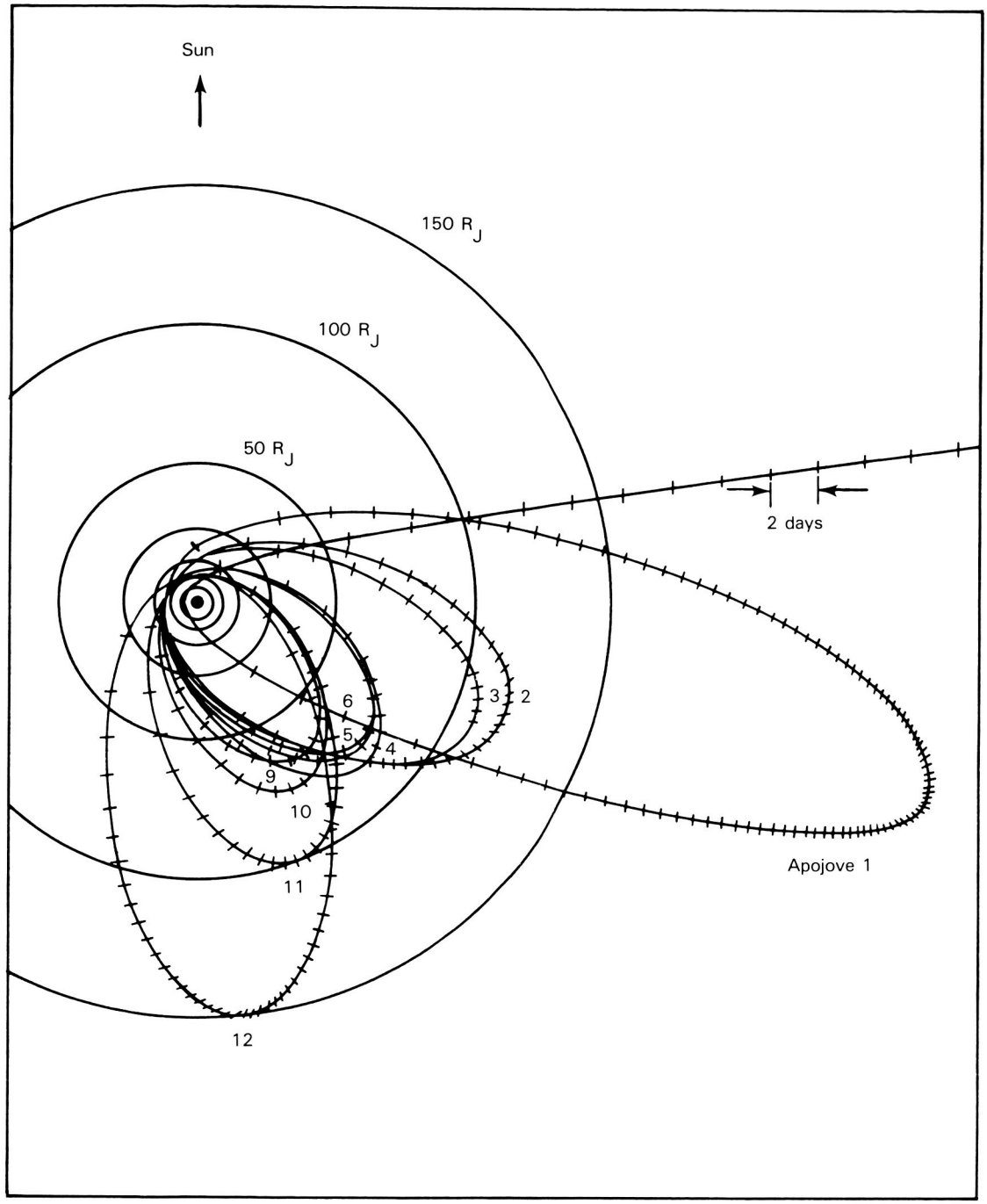

Figure 66. Satellite tour petal plot.

Initial Europa Encounters. The next two satellite encounters in the representative tour are with Europa. The first Europa encounter is inbound, providing high Sun coverage. The second encounter is outbound, as required for achieving the maximum possible Europa coverage.

The Europa 4 flyby is a close polar flyby, enabling the orbiter to pass through the flux tube, a high-priority science objective (see chapter 4). The limited Europa gravity assist allows for the design of Europa polar flybys without using 360° transfer trajectories. In this tour, the Europa polar pass

targets the orbiter from an inbound Europa flyby to an outbound Europa flyby.

Callisto 6 and Ganymede 7 Encounters. At the halfway point of the tour, the following major objectives have not been satisifed: tail petal orbit, inbound/outbound encounters with each satellite, and distant nontargeted encounters with each satellite. The remaining encounters in the tour are designed to satisfy these objectives.

The Callisto 6 and Ganymede 7 encounters are both designed to provide orbit rotation toward the tail petal region. Both encounters are period-decreasing, outbound flybys. These two encounters complete the desired inbound/outbound couplet for each of the satellites.

About one day before the Ganymede 7 encounter, the first nontargeted flyby in the tour, a light-side Europa flyby from 25 000 km, will occur.

Ganymede 8 and Europa 9 Encounters. The next two encounters in the tour are period-increasing, inbound encounters with Ganymede and Europa. Both flybys provide additional rotation to set up a tail petal orbit at the end of the tour.

The Europa encounter, which is the last flyby with that satellite in this tour, is an inbound encounter to maximize coverage.

Ganymede 10 and Callisto 11 Encounters. The final two tour encounters provide orbit rotation and increase orbit period so that the tail petal apojove is moved out to 148 R_J. Usually, the final encounter in a tour design is with Ganymede, since Ganymede is more effective than Callisto for raising orbit apojove. However, reversing the typical sequence of final encounters allows distant nontargeted encounters with Callisto and Ganymede. Both nontargeted encounters are light-side flybys with closest approach altitudes under 50 000 km.

Figure 67 provides trajectory pole views for each of the satellite encounters. Passage of the orbiter through regions of scientific interest such as Earth occultation, Sun occultation, flux tube, and wake, are shown.

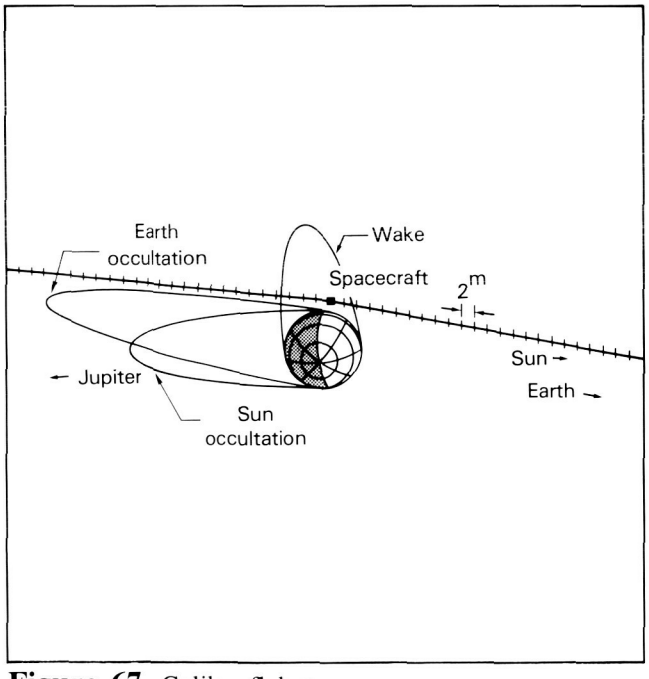

(a) First orbit flyby of Ganymede.

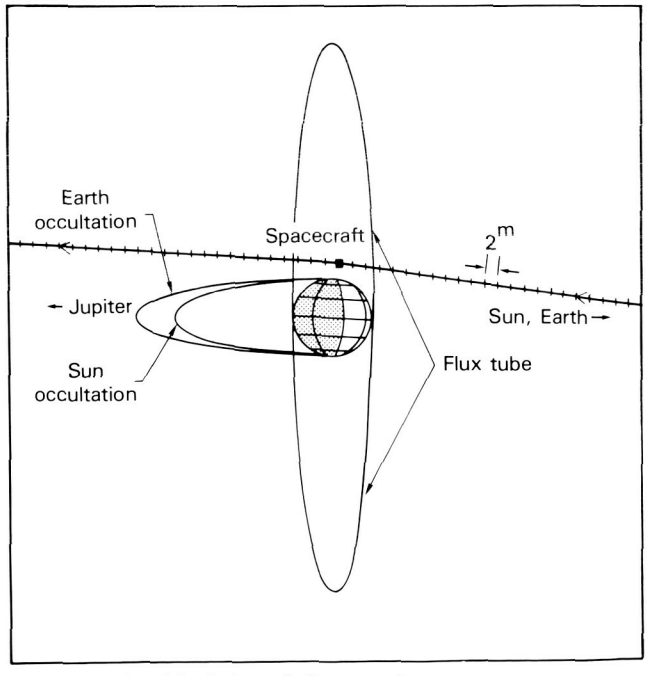

(b) Second orbit flyby of Ganymede.

Figure 67. Galileo flybys.

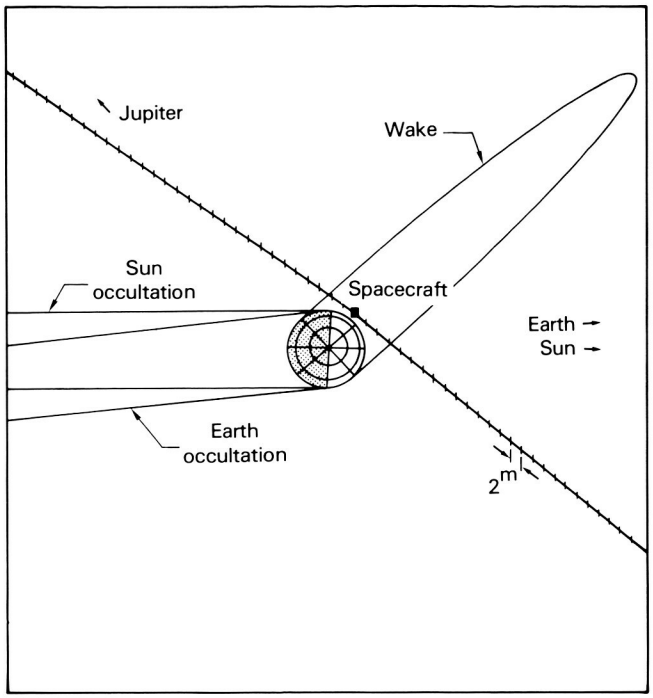

(c) Third orbit flyby of Callisto.

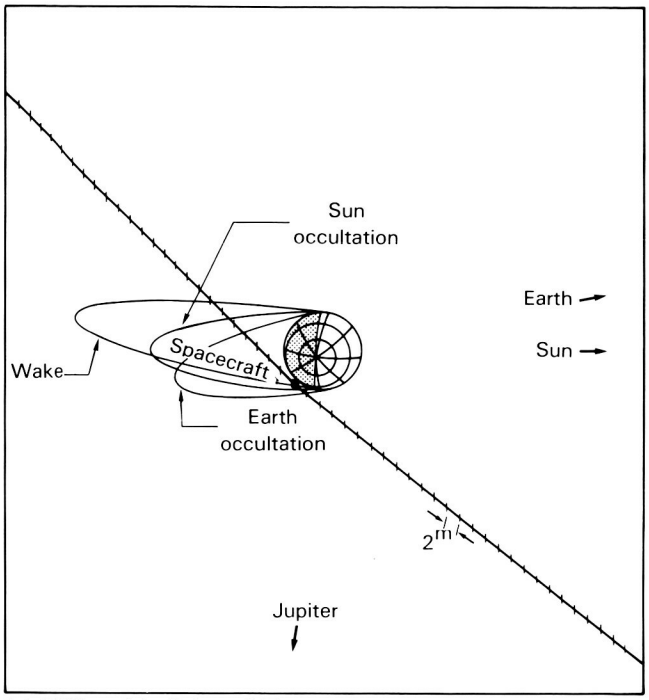

(e) Fifth orbit flyby of Europa.

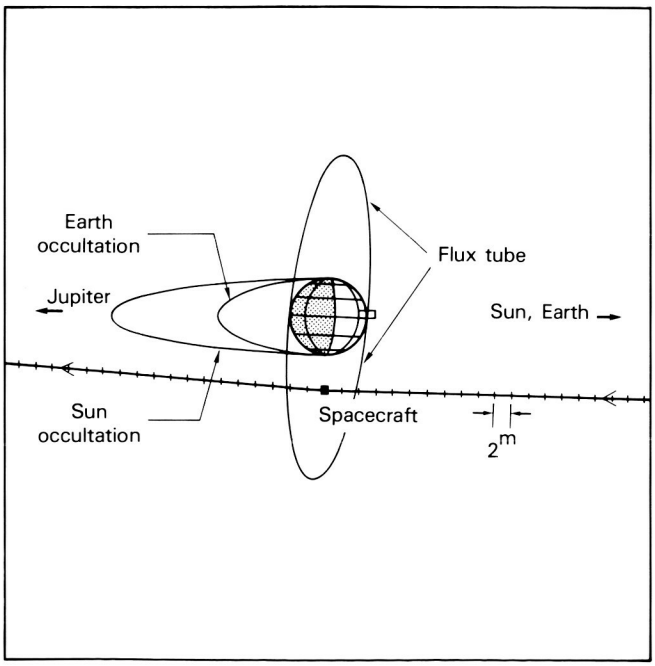

(d) Fourth orbit flyby of Europa.

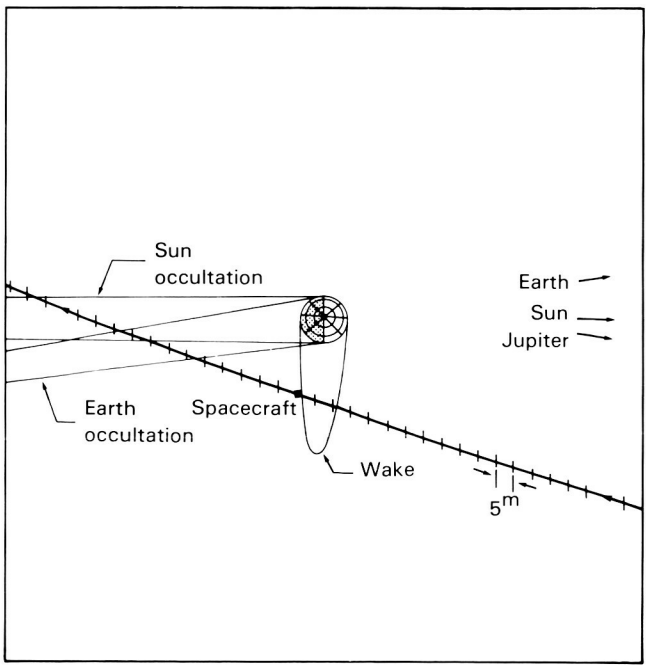

(f) Sixth orbit flyby of Callisto.

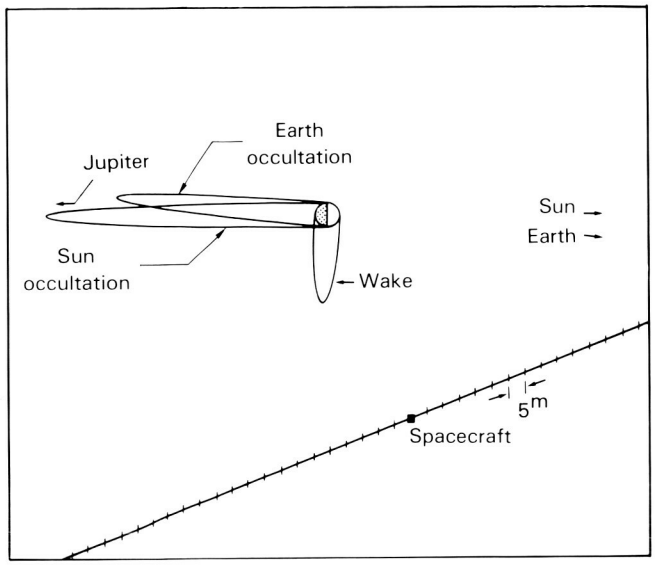

(g) Seventh orbit nontargeted flyby of Europa.

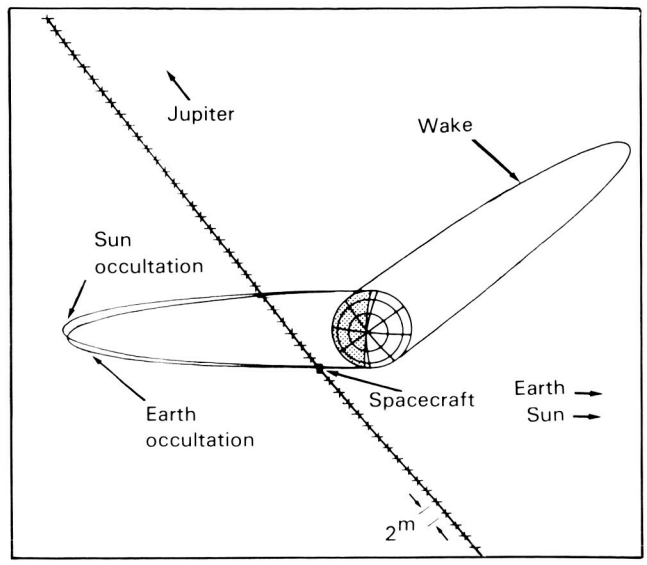

(i) Eighth orbit flyby of Ganymede.

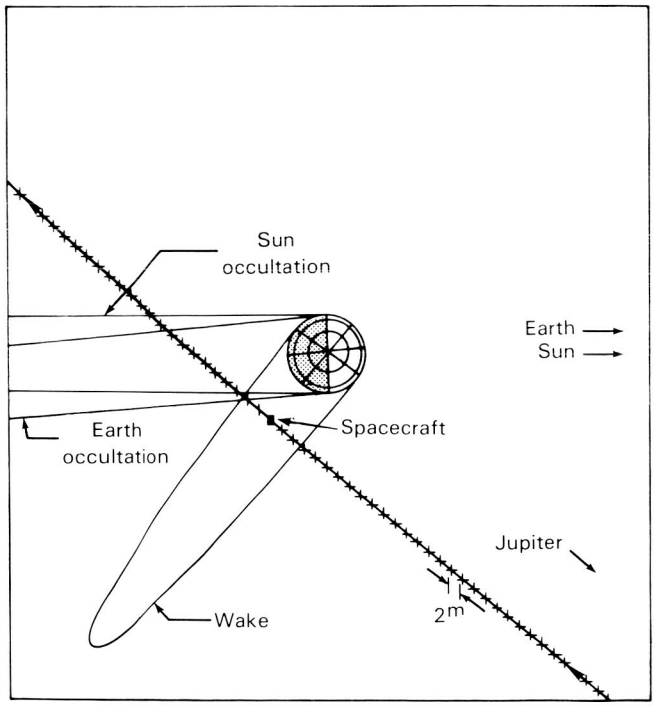

(h) Seventh orbit flyby of Ganymede.

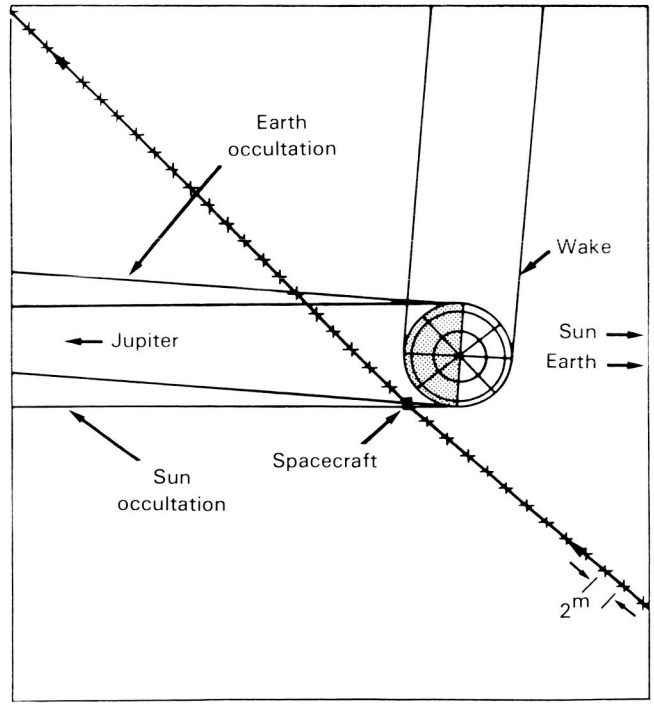

(j) Ninth orbit flyby of Europa.

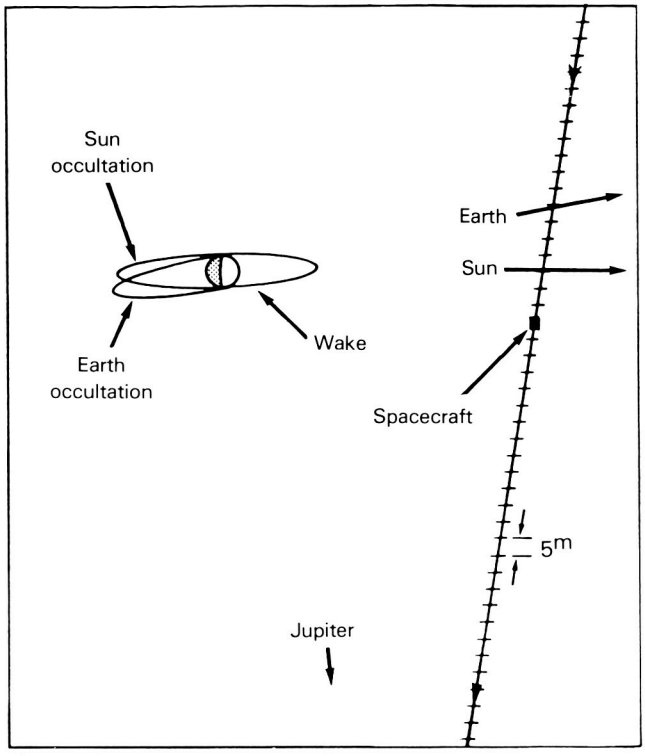

(k) Tenth orbit flyby of Callisto.

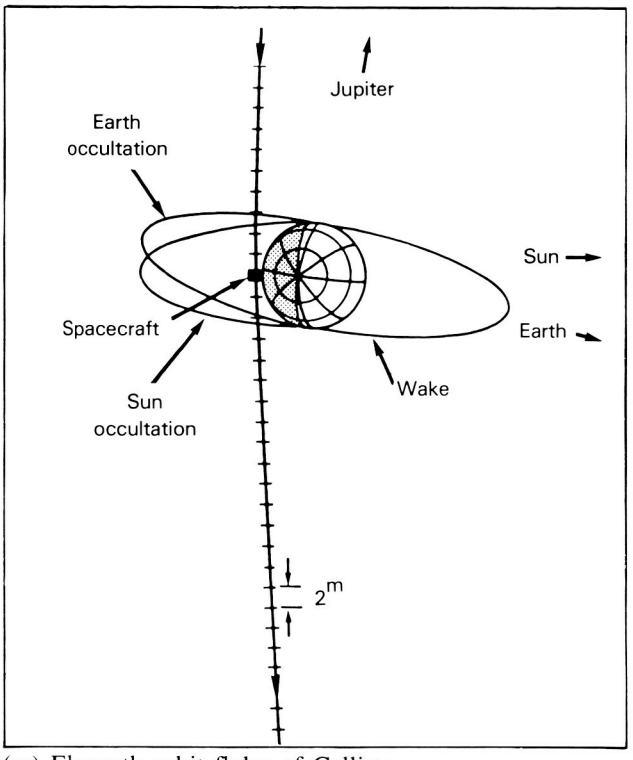

(m) Eleventh orbit flyby of Callisto.

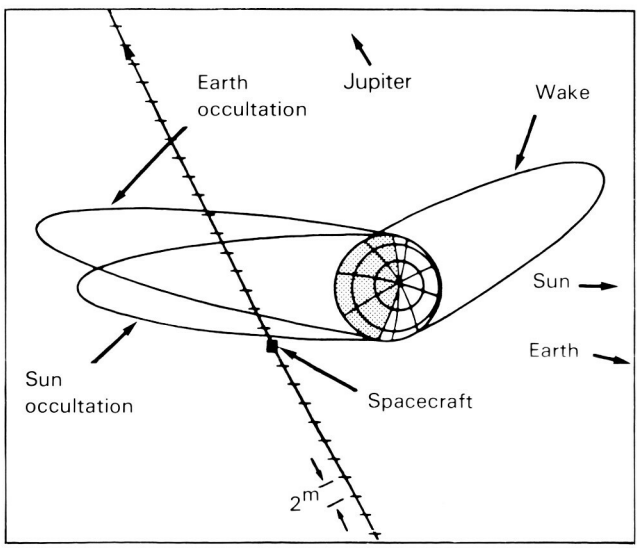

(l) Tenth orbit flyby of Ganymede.

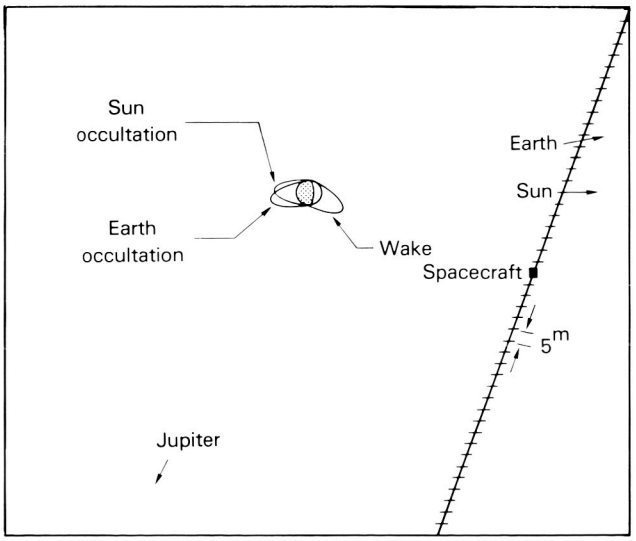

(n) Eleventh orbit nontargeted flyby of Ganymede.

chapter 6 THE GALILEO SPACECRAFT

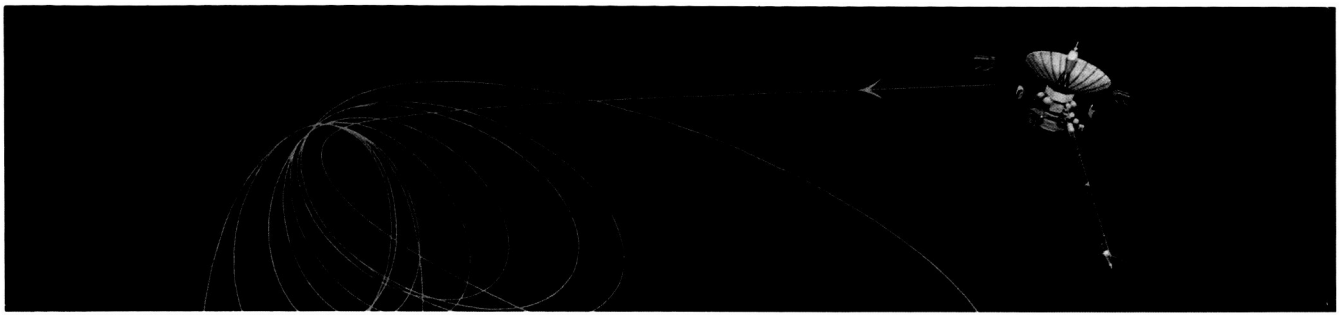

The Galileo spacecraft represents a major design challenge for long-term planetary missions. Like its predecessors, the Galileo system design reflects the influence of mission and science requirements, lifetime considerations, environmental factors, technology readiness, hardware availability, and cost. Additionally, experience gained as part of the Voyager spacecraft design implementation and flight experience, and interfaces with the Space Transportation System, have had profound effects on the design. This chapter presents an overview of the Galileo spacecraft system design within the context of these major considerations.

Spacecraft Design

The spacecraft configuration represents many compromises made to simultaneously satisfy a myriad of different (and sometimes conflicting) requirements. Some of the major Galileo configuration design considerations include requirements to:

- attentuate the intense radiation and thermal environments produced by the radioisotope thermoelectric generators (RTGs). For this reason, the RTGs are mounted some distance away from the bus electronics, and the radiation-sensitive science instruments are mounted on a boom away from the RTGs.
- balance inertial properties for stability and performance. The RTGs and sensitive science instruments are therefore mounted on separate booms whose lengths are compatible with radiation and inertial property requirements while minimizing the use of ballast mass.
- provide unobstructed or nearly unobstructed fields of view for instruments located on the science boom and scan platform.
- provide mounting locations for the bipropellant thrusters where plume exhaust products will not interfere with the operation of any science instrument on the orbiter.
- accommodate the plasma wave subsystem and magnetometer sensors to minimize the effects of orbiter-generated interference.
- provide mounting locations for in-flight calibration targets which are compatible with selected instrument viewing and measurement requirements.
- provide mounting locations for the probe, relay radio receivers, and relay antenna.
- arrange scan platform science instruments and despun electronic equipment bays to minimize products of inertia and use of ballast mass.

- perform critical mission events deep within the harsh jovian radiation environment.
- provide memory "keep alive" power to retain RAM contents indefinitely.
- provide a stable platform for remote sensing instruments and a spinning section for fields and particles instruments.

Galileo also represents a major increase in the application of flight software from previous spacecraft. The emphasis on software is driven by mission and system requirements to:

- control spacecraft attitude and spin rate and meet very precise platform pointing requirements.
- modify control algorithms based on flight performance (hardware idiosyncrasies), spacecraft inertial property changes, and structural dynamics.
- adapt sequence changes based on science and engineering data collection.
- compensate for unexpected operational conditions resulting from our evolving understanding of the jovian environment.
- respond to classes of faults which, if unattended, could result in major mission losses or total spacecraft loss.
- maximize science return based on previous observation and improved understanding.

The Galileo orbiter contains eleven subsystems (including science and the relay radio hardware) that contain nineteen microprocessors with a total of about 320 kbytes of random access memory (RAM) and 41 kbytes of read-only memory (ROM). To provide maximum flexibility in program development and in flight, most subsystem programs are completely reprogrammable. All of the science instrument programs are primarily ROM based; however, provisions have been made in eight science subsystems to allow some instrument program changes. All of these programs run continuously (coordinated with a real-time clock) whenever the subsystem is powered. All accept and interpret commands from the ground, synchronize and control the hardware in their respective subsystems, and acquire engineering and/or science data for telemetry downlink. Portions of these tasks require close cooperation among several processors and depend heavily on data communication across the data system bus. In selected subsystems, a significant amount of data transformation (e.g., compression, expansion, reformatting) and processing (e.g., information extraction, coordinate transformation, and data searching) takes place.

Due to the nature of the phenomena to be measured, fields and particles science requires a spinning section, while the remote sensing science requires very accurate and very stable pointing. Thus, the spacecraft configuration consists of two major sections—spun and despun (fig. 68). The spun section is dominated by a 4.8-m high-gain antenna (HGA), used for transmitting and receiving S-band and X-band signals. Electrical power is provided by two general-purpose heat source RTGs, each mounted on separate 5-m-long booms. Fields and particles science instruments are fixed mounted at distances of 3 m and 11 m along another boom extending from the spacecraft centerline. The majority of the orbiter's electronics are located within an eight-sided spun bus behind the HGA. Also, an integral part of the spun bus is the retropropulsion module (RPM) used for all attitude control and propulsive maneuvers. Six thrusters are mounted on each of two 2-m-long booms on the RPM.

The despun section contains the entry probe, the remote sensing science instruments mounted on an articulable scan platform with 2 degrees of freedom, and the relay radio antenna and hardware. The majority of the support electronics are located within five electronic equipment bays.

A command and data system employing a high-speed data bus interfaces with the total science payload. Elements of this system are located on both the spun and despun sections.

The spun and despun sections are connected by a spin bearing assembly (SBA) containing spin bearings for mechanical interfacing, slip rings for power and grounds, and rotary transformers for data signals. Figure 69 presents a simplified block diagram for the orbiter depicting major functional elements of the spun and despun sections.

Orbiter

The orbiter design accommodates a total of nine scientific instruments (five for fields and particles and four for remote sensing science), each with its own unique demands to maximize data return. The

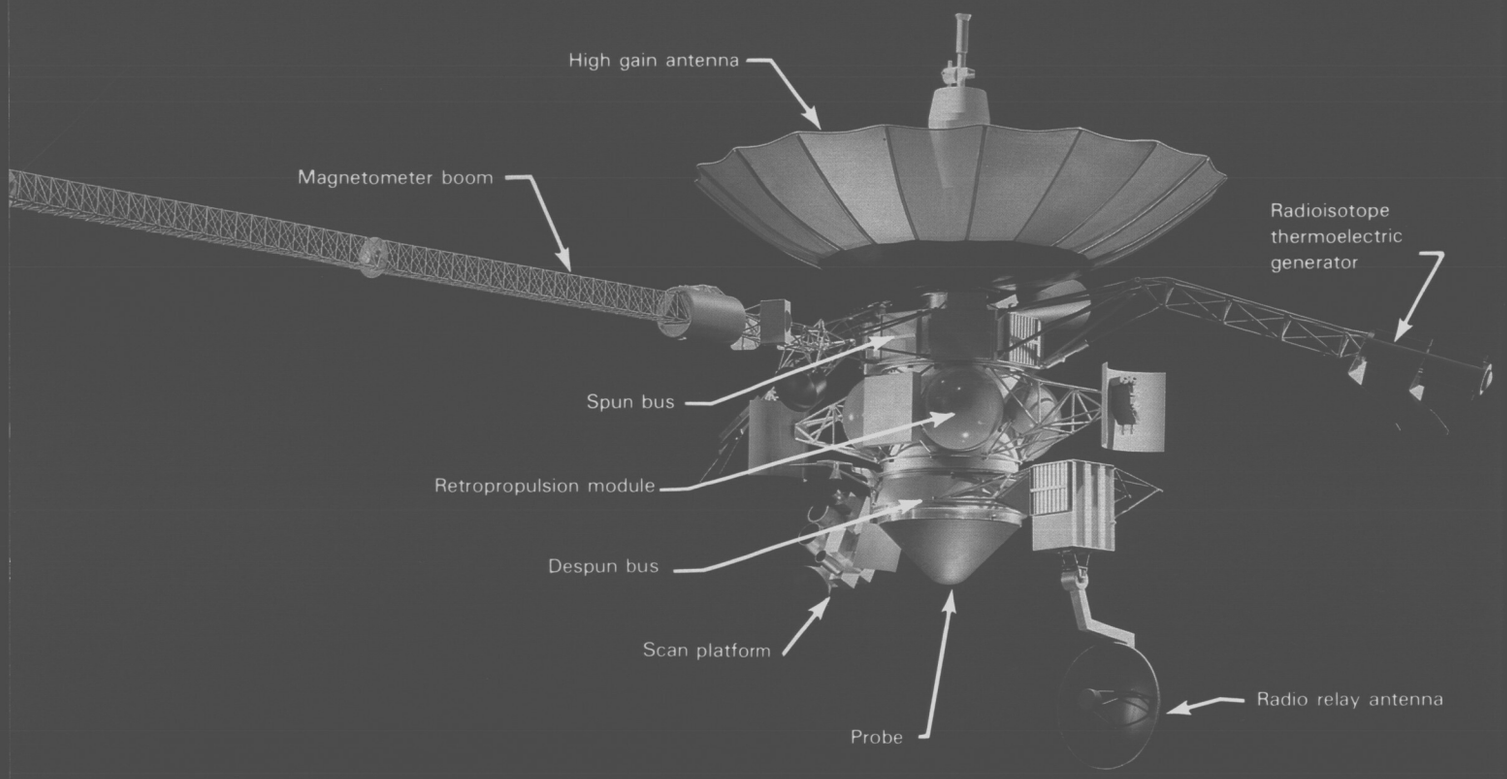

Figure 68. Model of the Galileo orbiter and probe.

orbiter also accommodates the entry probe in both its attached and detached mission phases.

The orbiter contains many elements of advanced technology and new development. The number of new elements is not confined to a single design discipline but is distributed across the total system. The attitude control system contains new high-speed computers, an SBA to interface across the spun and despun sections, a star scanner to establish automatic in-flight attitude determination, and a scan actuator subassembly incorporating a flex capsule wire assembly for electronic interfacing. The data system uses a data bus concept operating at 806 kHz to interface with all science users and some engineering users. The data bus approach is the most effective means of accommodating the requirements of the varied users while simultaneously consolidating data handling and command and sequence functions and is consistent with advances in the state of the art in data systems design.

Other new elements include the furlable 4.8-m high-gain antenna; a charge-coupled device in the imaging subsystem to improve dynamic range, sensitivity, stability, and reliability; and new generation RTGs using improved heat sources and thermocouple design.

The requirement for substantial real-time data return from jovian distances (approximately 5 to 6 AU) is met by the high-performance X-band (8415 MHz) telemetry downlink operating at 115 and 134 kilobits/s. Maintenance of this link requires very accurate pointing of the high-gain antenna simultaneously with many other attitude control

functions, including accurate pointing of the remote sensing science platform at various mission targets.

The orbiter mission and science requirements require a propulsive capability of nearly 1600 m/s for probe delivery, orbit insertion, satellite tour, and other attitude control functions. To meet this need, the orbiter is equipped with a bipropellant propulsion system using oxidizer and fuel pressurized with helium. Usable propellant is limited to 932 kg.

Power is supplied for all electrical loads from the two plutonium-238-fueled RTGs. Output power from the generators degrades with time due to fuel decay and other processes and is limited to 579 W at launch and 486 W at the end of six years. The DC output of the RTGs is regulated and conditioned to provide 30 Vdc and 50 V, 2.4 kHz AC power for the spacecraft systems.

Pyrotechnic elements on the orbiter primarily comprise electroexplosive devices, squibs, and bellow actuators used for separation and deployment events, cable cutter events, and deployment of science instrument and star scanner protective covers. Pyrotechnic events on the despun section include major functions such as spacecraft–launch

Figure 69. Orbiter simplified block diagram.

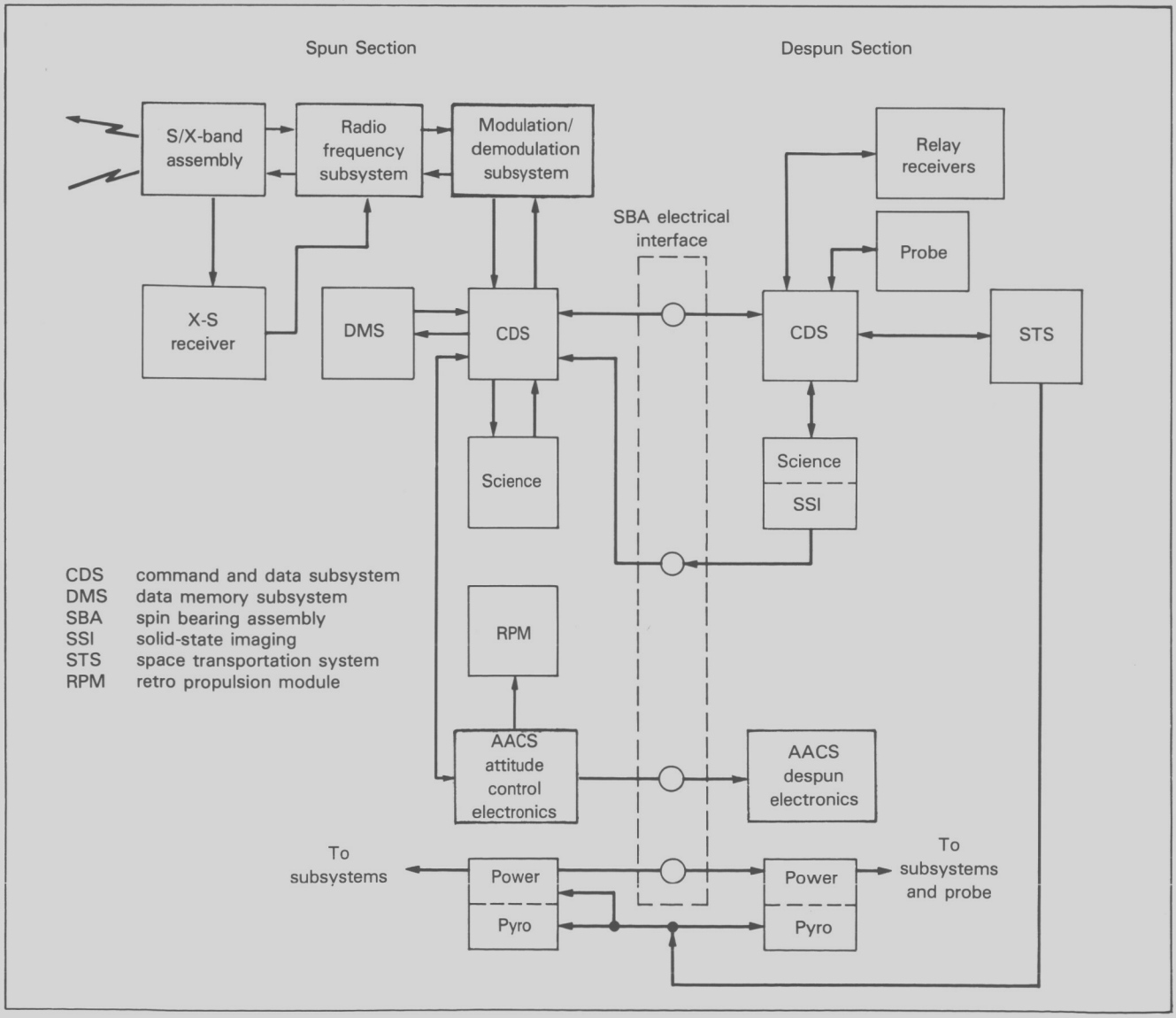

vehicle separation, spun–despun section release, probe separation, RTG and science boom release, relay antenna release, and scan platform science cover deployments. On the spun side, pyrotechnic events include RPM pyrotechnic valve actuation, magnetometer boom deployment, HGA release, and instrument cover deployments.

Orbiter accommodations for the probe are limited to those necessary to deliver the probe and to meet shuttle safety requirements, to monitor and perform health checks during the interplanetary cruise phase, and to perform the critical data reception and Earth relay functions during the probe's jovian atmospheric entry. The orbiter is implemented with probe-dedicated mechanical and electrical interfaces (power, data, and pyrotechnics) as well as special data modes and rates to accommodate the pre- and postprobe separation phases. The probe relay reception function is accommodated via a dedicated movable antenna mounted on the despun section and electrically connected to redundant relay radio receivers.

Launch from the Space Transportation System (STS) results in two major considerations, mass and safety. Galileo is expected to be one of the first of a series of interplanetary missions to utilize the STS. Present shuttle and Centaur upper stage performance estimates limit the spacecraft injected mass to 2550 kg, including adapters. Because the STS is a manned vehicle, special safety features have been incorporated to meet shuttle safety requirements. Special electrical inhibits have been added to elements of the power, pyrotechnic, and radio frequency systems and the probe.

The orbiter must operate reliably and autonomously in the harsh jovian radiation and electrostatic discharge environments during probe relay and orbit insertion (accomplished at 4 R_J). The design of both the hardware and software mechanizations maximizes the probability of success for these major critical mission phases.

The orbiter must also be immune to single faults that could result in the loss of probe delivery, relay data return, orbit insertion, more than one science instrument, or more than 50 percent of all engineering data.

In the launch configuration (figs. 70 and 71) the HGA and all booms must be furled so that the spacecraft fits within the shuttle payload bay. In the flight configuration with probe attached (fig. 68) the RTG booms, science boom, and HGA will be deployed and the magnetometer boom extended. In flight, the HGA will point toward Earth while the spun section spins at a nominal 3.15 rpm and the despun section is stabilized. HGA pointing updates, spin rate control, and small propulsive maneuvers will be accomplished using RPM 10-N thrusters mounted on booms located on opposite sides of the orbiter. Most of the large propulsive maneuvers will be accomplished using the RPM's single 400-N engine with the complete orbiter spinning at a nominal 10 rpm.

Telecommunications System

The telecommunications system located totally on the orbiter's spun section is comprised of elements required for receiving uplink commands and transmitting downlink telemetry. The uplink portion of the system receives the radio frequency carrier signal with command data at 2115 MHz and demodulates, detects, and routes command data to the command and data system, while the downlink portion receives telemetry data from the command and data system and modulates it onto S-band and X-band carriers at 2295 and 8415 MHz, respectively.

The telecommunications system design provides a dual channel downlink. The high-rate channel provides a convolutionally coded, pulse-code-modulated microwave channel, while the low-rate channel data is uncoded. Key elements include the furlable 4.8-m circular parabolic HGA (fig. 72) used for receiving and transmitting both S- and X-band signals, redundant transponders, redundant dual-power S- and X-band power amplifiers, and an S-band low-gain antenna. A late addition to the telecommunications equipment includes the X to S down-converter receiver to implement an X-band uplink receive capability.

Transmission of telemetry data is available at S-band and/or X-band over a wide range of selectable data rates, depending on both spacecraft and ground conditions. The uplink S-band communication data rate is 32 bits/s and can be maintained throughout the mission over the low-gain antenna if the orbiter is pointed toward the Sun.

The diameter of the antenna itself was selected based on mission data return considerations and provides for real-time* imaging from Jupiter at 134

*The term real-time here refers to time at the spacecraft, since radio messages traveling at the speed of light take about 30 minutes to reach Earth.

and 115.2 kilobits/s. A maximum power allocation of approximately 160 W (33 percent of total available) is provided for the combined S-band and X-band communications function. This power is divided among the telecommunications elements based on mission requirements and power amplifier design needs. Dual power level, traveling wave tube amplifier transmitters provide maximum S-band cruise data return and high-rate X-band data return from Jupiter while simultaneously satisfying dual-frequency tracking and radio science requirements.

The combination of an X-band high-rate channel and the HGA provides the key to Galileo's high data rate capability. Intended for use primarily at Jupiter, the combination permits real-time transmission of probe entry data at 28.8 kilobits/s or real-time imaging data with real-time low-rate science at 115.2 kilobits/s as well as real-time imaging, with low-rate science and playback low-rate science at 134.4 kilobits/s. A full-resolution picture read from the imaging camera's charge-coupled device occurs about once every 60 seconds. The capability also exists to read out a high-resolution

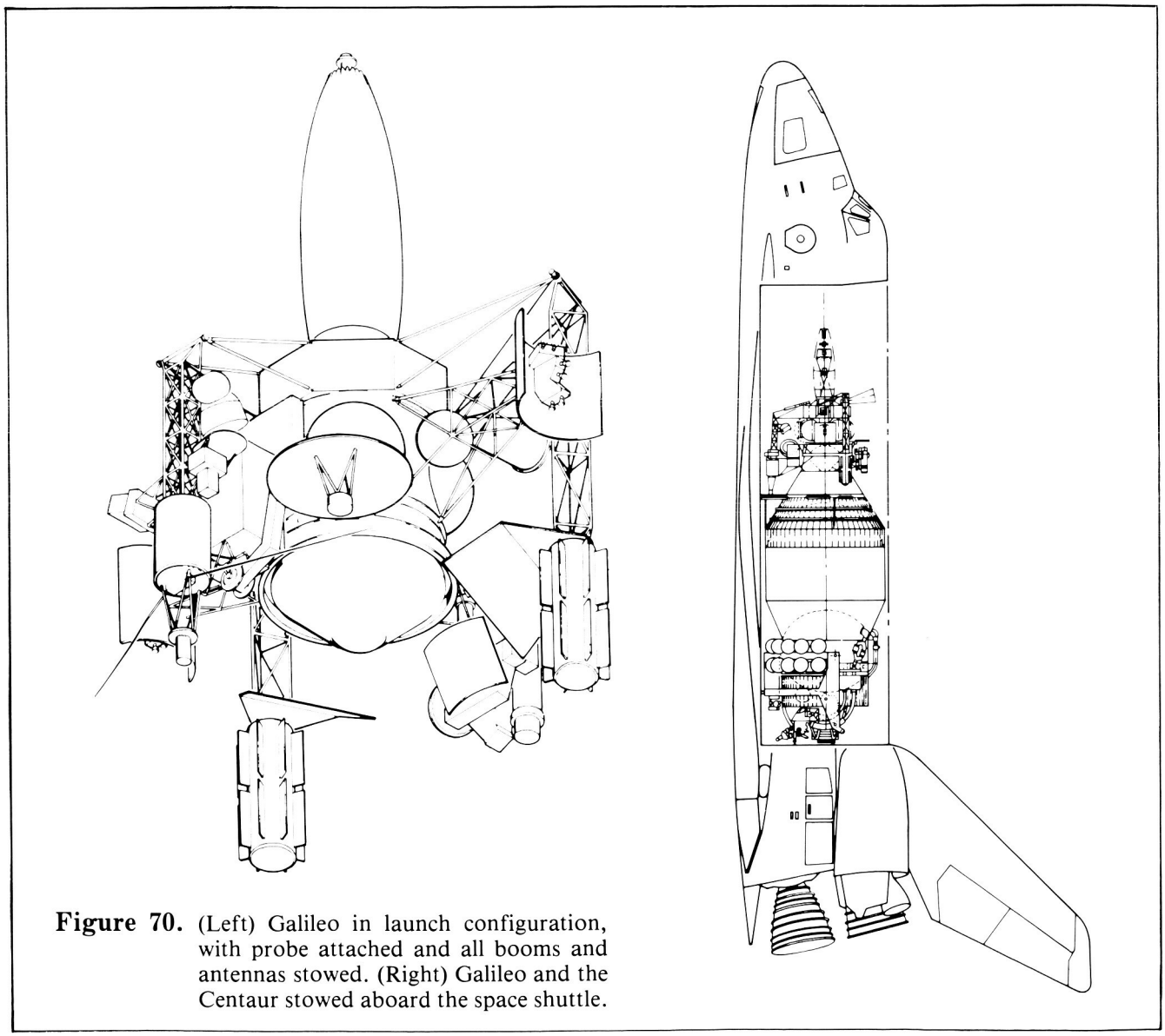

Figure 70. (Left) Galileo in launch configuration, with probe attached and all booms and antennas stowed. (Right) Galileo and the Centaur stowed aboard the space shuttle.

picture in about 2 seconds. A constant 7.68 kilobits stream of low-rate science and engineering data is provided during cruise and Jupiter operations.

Link conditions permitting, however, high-rate channel data at 7.68 kilobits/s, 28.8 kilobits/s (probe), or higher can be transmitted via the HGA and S-band system. The low-rate S-band channel is intended primarily for returning continuous 40 bits/s engineering telemetry throughout the mission. Radio frequency output power is modulated by adjusting S-band (or X-band) modulation indices to balance the needs for carrier tracking against those for data return. Significant performance parameters of the major elements comprising the telecommunications system are shown in table 10.

The telecommunications channels provide two "classes" of data quality to the scientific users—high quality (bit error rates less than 5×10^{-5}) for nonimaging science and a lower quality (bit error rates less than 5×10^{-3}) for imaging. This is achieved by operating the downlink channel at a signal to noise ratio equivalent to an error rate of about 5×10^{-3}, thus maximizing data quantity returned for imaging. Nonimaging science is coded onboard the orbiter using a Golay error-detecting, error-correcting code to allow reconstruction of the data received at Earth to the quality needed for those science users.

Several other features are incorporated in the telecommunications area, mainly to enhance radio science and navigation. A noncoherent tracking

Table 10. Galileo Telecommunications Parameters

Parameter	S-band	X-band
Transmitter output power (dbm)[a]		
Low power	38	41
High power	43	43
HGA peak gain (dbi)[a]		
Transmitting	37.8	49.9
Receiving	37.0	48.3
LGA peak gain (dbi)		
Transmitting	6.8	N/A
Receiving	37.0	N/A
Receiver threshold (dbm)	−153	−148
Modulation index range (deg)	20 to 100	20 to 100

[a]dbi, decibels referenced to isotropic radiator; dbm, decibels referenced to 1 mW.

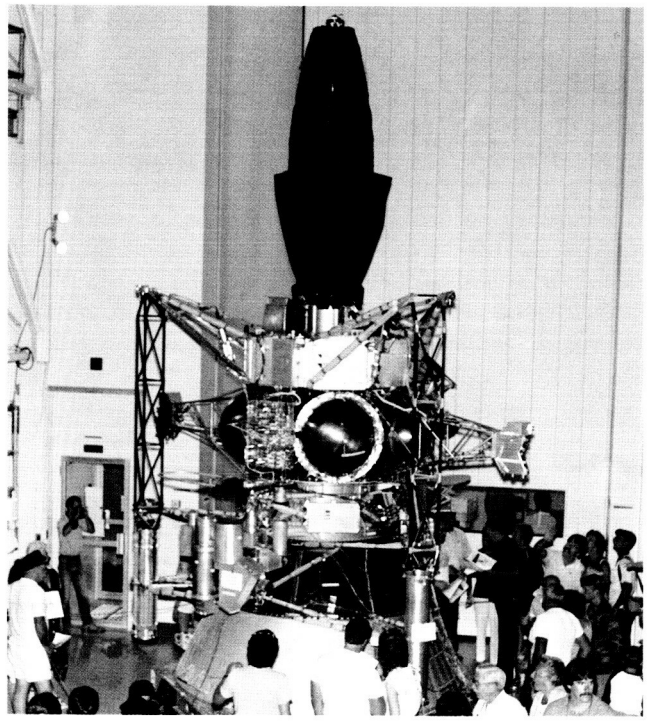

Figure 71. The Galileo development test model, with booms stowed, antenna furled, and spacecraft adaptors attached, in the launch configuration, was on display at the Jet Propulsion Laboratory during an Open House in August 1983.

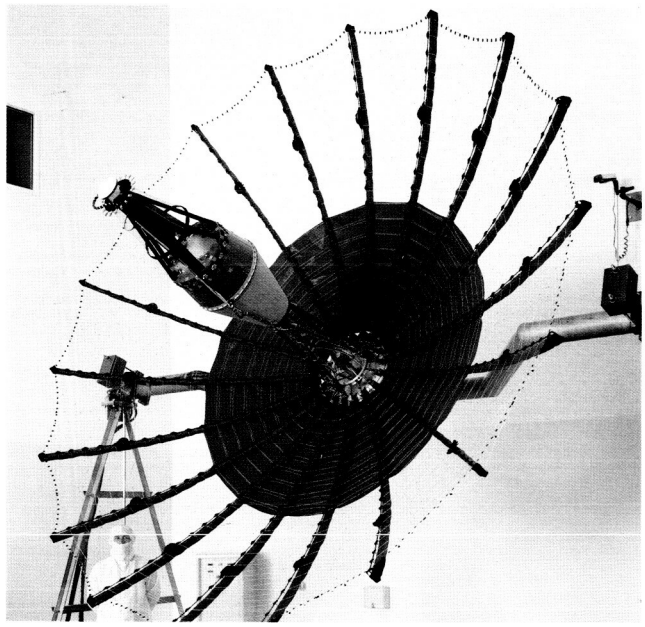

Figure 72. The high-gain antenna during spacecraft integration.

mode is available which permits the orbiter to be commanded while the downlink frequency source is controlled by an auxillary oscillator or an ultrastable oscillator providing short-term frequency stability of better than 5 parts in 10^{12}. A differential downlink-only ranging mode is also available using one S-band and three X-band sine wave tones modulated onto the downlinks to enhance navigational accuracy. A single X-band to S-band down-converter receiver is available for receiving X-band uplink signals to enhance radio science and the search for gravity waves. The capability exists to completely remove all telemetry modulation from the downlink carriers, thus maximizing atmospheric penetration depth during Earth occultations.

Propulsion System

The Galileo RPM system (fig. 73), located on the orbiter spun side and supplied by the Federal Republic of Germany, is based on earlier bipropellant Symphonie designs. The system provides all directed impulse for attitude control, trajectory correction, and Jupiter orbit insertion. The propulsion functions consist of spin rate control, fine turning to point the HGA to Earth, and orienting the spacecraft for propulsive or science maneuvers. The RPM includes four propellant tanks (two fuel tanks containing monomethylhydrazine and two oxidizer tanks containing nitrogen tetroxide), two helium pressurant tanks, twelve 10-N thrusters (six each mounted on separate cantilevered booms), one 400-N engine, and necessary isolation and control elements. At launch, the system is fully loaded with 932 kg of usable propellant and weighs about 1145 kg. Four of the 10-N thrusters are mounted in a direction to provide a functional backup for the 400-N engine. The thrusters are mechanized on two separate branches providing redundancy for spin control, HGA pointing, and trajectory correction. Only three uses of the 400-N engine are planned; all are subsequent to probe separation.

Figure 73. Technicians at Messerschmitt-Bölkow-Blohm inspect the retropropulsion module. The 400-N engine is in the center of the cluster of propellant tanks. (Photo courtesy of Messerschmitt-Bölkow-Blohm GMbH)

Control of propellant to the 10-N thrusters and the 400-N engine is accomplished by opening and closing fuel and oxidizer solenoid latch valves via electrical signals from the attitude control system propulsion drive electronics. The propulsion drive electronics also provide the control signals for opening and closing the thruster and 400-N engine valves.

Command and Data System

The primary responsibility for command, control, and data handling is performed by the actively redundant command and data subsystem (CDS). The major functions of this computer system include processing and issuing real-time commands from Earth and executing sequences of stored commands either as part of a normal preplanned flight activity or in response to the actuation of various fault recovery routines, and controlling and selecting data modes and collecting and formatting science and engineering data for downlink transmission. The CDS employs a new architecture using multiple microprocessors and a high-speed data bus for both internal and user communication, thus taking advantage of the state of the art in data system engineering.

The majority of CDS electronics are located on the orbiter spun side in proximity to the data storage, science, and telecommunication equipment. CDS despun elements are limited to those necessary to support the probe and relay radio hardware equipment, the scan platform-mounted remote science instruments, the launch vehicle, and sequence operations. Six 1802 microprocessors, memory units, and the data bus comprise the "heart" of the CDS. Four of the microprocessors (two high-level modules and two low-level modules) and four memory units contain a total of

144 000 words of random access memory and are located on the spun section along with supporting electronics. The low-level modules of the remaining two microprocessors, each with 16K RAM, are located on the despun section. The data bus comprises three dedicated busses. Two are individually controlled by dedicated bus controller interfaces with each high-level module. The third bus is controlled by the CDS support equipment and is used only for system test operations. The bus interface consists of four separate signals comprising supervisory data at 403.2 kHz, reply data at 403.2 kHz, a synchronization clock at 806.4 kHz, and a real-time interrupt (RTI) at 15 Hz. The bus interface is used by all data users, that is, orbiter science, the attitude and articulation control subsystem, and relay radio hardware receivers.

Interfacing between spun and despun portions of the CDS is accomplished via slip rings and rotary transformers mounted on the spin bearing assembly. Efficient and effective communication with data users is accomplished using a specifically defined protocol structure and real-time interrupt time slicing. The bus and protocol allow users some flexibility in the design of their bus interface. The protocol addressing schemes provide for either a relatively simple bus adapter that employs the user's processor direct memory access capability or a more complex bus adapter with direct memory access capability independent of the user's processor. The protocol allows multiple recipients to be addressed for any given message, although the majority of messages will be to single recipients. Each message consists of a header and a body. The header contains control words which define the message source and recipient via user identification codes and specify the starting address in the user's memory for the message transfer and a filler word for time buffering. The body of the message contains all the data to be transferred from the source to the recipient. Data bus transfers are controlled and conducted during specific RTI intervals during each CDS minor frame (10 RTI intervals). Even-numbered RTIs are used for bus messages to users, while odd-numbered RTIs are used to collect data from users. For at least 10 ms of each RTI frame, internal CDS transactions are accomplished.

Attitude and Articulation Control Subsystem

The attitude and articulation control subsystem (AACS) is responsible for maintaining spun section spin rate; orienting the spin vector; controlling propulsion isolation valves, heaters, 10-N thruster firing, and 400-N engine firing; and controlling the science platform containing the remote sensing instruments on the despun section.

The design of the AACS is profoundly influenced by science requirements and the various spacecraft operational configurations that must be accommodated. In addition to the basic cruise dual-spin configuration (orbiter with probe), the AACS accommodates dual spin without the probe for orbital operations and all spin with and without the probe for trajectory corrections at spin rates from 3 to 10 rpm.

The AACS incorporates many functional elements to meet the demanding performance, lifetime, and reliability requirements. The majority of the AACS functional elements are block redundant and located on the orbiter's spun side. Despun elements include those necessary for controlling the pointing and slewing of the scan platform, pointing the relay antenna, and interfacing with the spun section electronics.

The central element of the AACS is the attitude control electronics (ACE) that control the AACS configuration; monitor its health; perform executive, telemetry, command, and processing functions; provide spun position data to other subsystems; and provide AACS fault recovery. The "heart" of the ACE is a high-speed 2900 ATAC-16 processor and memory containing 31K words times 16-bit RAM and 1K words times 16-bit ROM.

The ROM contents are limited to those functions required to safeguard the science instruments, switch to the low-gain antenna, and Sun point the orbiter to permit ground commanding. Activation of the ROM program occurs only with a detected loss of RAM. The ACE also contains electronics necessary to interface with AACS spun-side peripheral elements, the despun electronics, and the CDS. Interfacing between spun and despun AACS elements is accomplished via rotary transformers located on the SBA.

Other major functional elements of AACS include:

- a radiation-hardened star scanner employing photomultiplier tubes for star field identification for in-flight attitude determination
- linear actuators for raising or lowering the RTG booms to reduce wobble and maintain stability

- acquisition sensors for attitude determination, spin rate data during launch, and Sun acquisition
- propulsion drive electronics to control the RPM latch valve, thrusters, and 400-N engine valves
- spin bearing assembly to provide the mechanical and electrical interfacing between the spun and despun sections of the orbiter as well as to provide despun orientation in clock degree-of-freedom motion
- gyros mounted on the despun scan platform to control platform articulation and stabilization
- accelerometers mounted on the despun side diametrically opposite to each other and aligned parallel to the orbiter spin axis to measure velocity changes during propulsive burns
- scan actuator subassembly to provide the scan platform cone actuation and positioning information. This subassembly contains a flex capsule consisting of 200 printed wire traces for electrical interfacing between the scan platform instruments and the despun electronics.

After launch vehicle separation and RPM pressurization, the AACS enters the all-spin mode, which is utilized many times during the mission. This mode is used primarily for stabilization during all propulsive maneuvers, in which the orbiter spins at roughly 3 rpm for 10-N thruster burns or 10 rpm for 400-N engine burns. This mode is also used during science calibration target observations by the remote sensing science instruments.

For most of the mission, the AACS operates in the cruise mode, in which the orbiter operates in the dual-spin configuration with the spun section inertially fixed. Major functions performed during this mode are wobble control, high-gain antenna pointing, attitude determination, and spin rate control.

The final AACS mode is the inertial mode. Transition to this mode is from the cruise mode with gyros active. While it is in this mode, the AACS performs functions such as closed-loop commanded turns using the RPM thrusters, accurate pointing and slewing of the scan platform, and closed-loop control for wobble angle compensation.

Major AACS performance parameters are summarized in table 11.

Probe

The probe will be carried to Jupiter by the Galileo orbiter and released on an entry trajectory 150 days before entry. A complement of seven science instruments will measure the radiation field near Jupiter and the characteristics of the jovian atmosphere from a distance of about 5 Jupiter radii above the 1-bar level down to levels in the 10 to 20-bar range. Probe data will be transmitted to Earth via the orbiter. This section discusses system requirements and probe design features.

Development of the probe and relay radio hardware (receiver and antenna mounted on the orbiter to receive the probe's radio signal) is managed by Ames Research Center. The Space and Communications Group of the Hughes Aircraft Company is responsible for the design, fabrication, and test of this hardware. The General Electric Company's Re-Entry Systems Division is the principal subcontractor and is responsible for thermal protection up through entry at Jupiter, the structure and heat shields for protection during entry, and the probe separation and parachute systems.

Description

The probe is composed of two major segments, the deceleration module and the descent module (fig. 74). The deceleration module includes the heat shields, the structure that supports the heat shields, and the thermal control hardware for mission phases up through entry. The descent module is the package that descends through the jovian atmosphere by parachute while the prime science data are gathered. It contains the science instruments and the probe subsystems required to support the instruments and transmit the data back to the overflying orbiter, which serves as a relay to Earth. The probe-to-orbiter adapter is supplied with the probe and designed and fabricated by General Electric.

Deceleration Module

Configuration. The entry configuration of the probe is a 45° half-angle cone with a base diameter of about 1.2 m. The radius of the spherically blunted tip is equal to about half the

Table 11. Major AACS Performance Parameters

Parameter	Value (3σ)
Spin rate	3.15 rpm
Spin deadband	0.13 rpm
Scan platform slew rate	0 to 17.5 mrad/s
Scan platform minimum step size	10 μrad/s
Commanded turn rate, maximum	3 mrad/s
Scan platform pointing accuracy	3.4 mrad
HGA antenna pointing accuracy, X-band	
Cruise	1.7 mrad
All spin	2.5 mrad
Total ΔV pointing error (calibrated)	
400 N	5 mrad
10 N	9 mrad
RRH antenna pointing accuracy	35 mrad

base radius. The general shape was selected to provide a minimum-weight probe, primarily because this allows more forward placement of the pressure vessel than do more blunt vehicle shapes, leading to minimum base diameter and minimum ballast required for aerodynamic stability. This shape also has the advantage of being essentially the same as that of the Pioneer Venus probes. This similarity reduced the need for basic aerodynamic testing, since the Pioneer Venus data base was directly applicable. The probe-to-orbiter adapter consists of three bipod assemblies that connect the probe to the orbiter.

Heat Shields. Thermal protection during entry is provided by a carbon phenolic forebody heat shield and a phenolic nylon afterbody heat shield. Although these materials have been used extensively for Earth reentry vehicles, on the Galileo mission they will be subjected to environments never before experienced. For both the forebody and afterbody, radiative transfer is the primary energy transport mechanism. An additional consideration included in the final heat shield design is mechanical erosion (spallation) of heat shield material.

Heat shield performance calculations were done by very large and complex codes which include the detailed physics of the heating/ablation process. These codes include detailed calculations of the radiation from the hot atmospheric shock layer (14 000 K) and the absorption of this radiation (blockage) in the boundary layer gases by

Figure 74. Probe configuration.

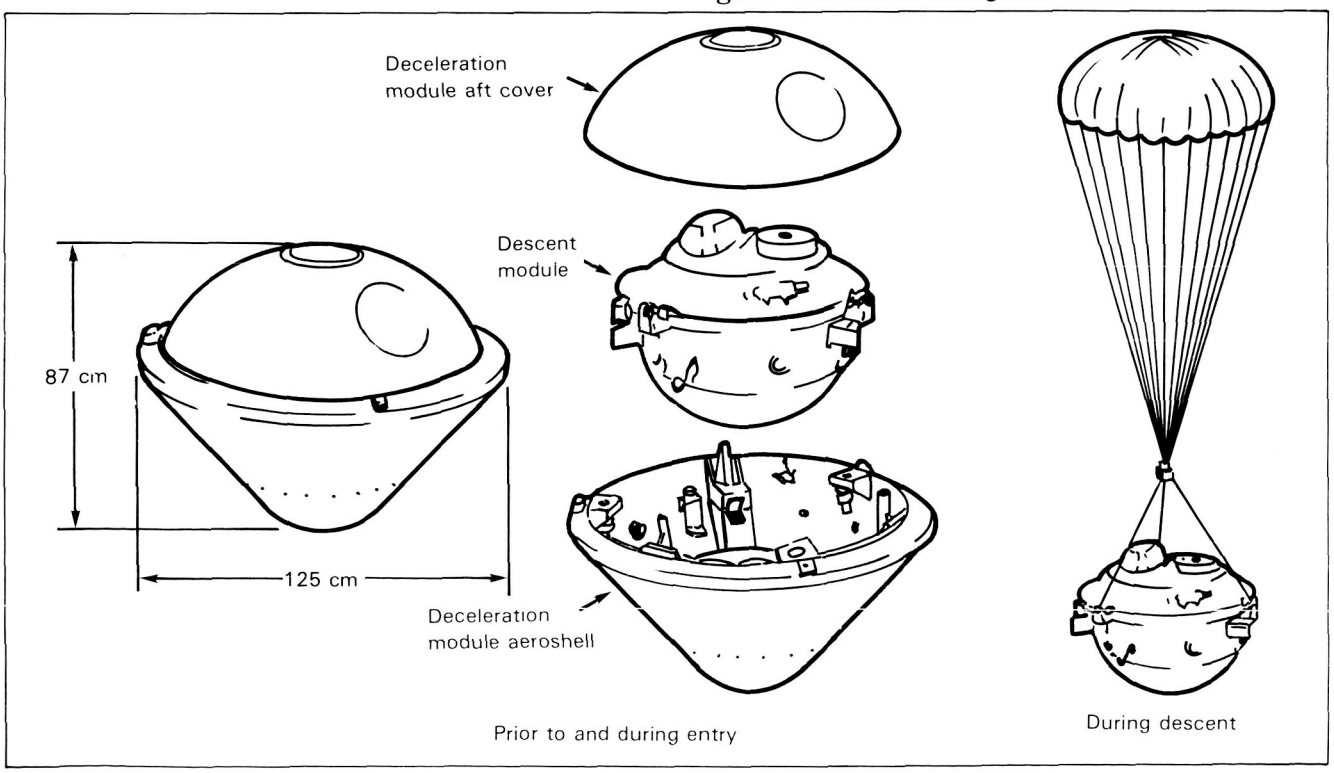

chemical species present. The unblocked heat transfer at the nose of the vehicles at peak heating exceeds 42 kW/cm^2.

The forebody heat shield has two segments: a nosepiece fabricated from a billet of chopped molded carbon phenolic and a tape-wrapped frustum section. These two sections are first bonded together, and then the whole heat shield is bonded to the structure. The final thickness, as shown in figure 75, includes the minimum margins required on the predicted mass loss plus a layer of unablated material which serves as insulation to maintain the bond line below the required limit (approximately 645 K). The margin requirements range from 30 to 45 percent at various stations along the body. These margins are required to cover uncertainties in heat shield performance, entry conditions, and atmospheric composition. The approximate mass of the forebody heat shield is 145 kg, of which about 90 kg is expected to be lost by ablation during entry. This value includes mass loss resulting from spallation of solid heat shield material.

Afterbody heating is also dominated by radiative transport. A detailed calculation of the base heating was made based on the flow-field conditions at the end of the forebody and on a model of the expansion from this corner. Calculated maximum heating rates over the aft end of the vehicle are in the 1 to 2 kW/cm^2 range. The afterbody heat shield consists of two sections: the dome section covering the aft cover and a ring section covering the area between the cover and the edge of the forward cone. Thicknesses were sized to prevent the aft structure from exceeding 477 K, thus maintaining adequate aft cover structural strength at mortar firing and pilot parachute deployment. A margin of over 50 percent on recession has been maintained over the afterbody. The aft heat shield thickness is shown in figure 75.

Thermal Control. Prior to entry, thermal control of the probe is provided by a passive system consisting of multilayer Mylar blankets covering the aft end of the probe and a major portion of the conical forebody, a complement of 1-W radioisotope heaters (RHUs), and partial gold taping of the forebody nose to adjust the heat loss through the unblanketed portion of the heat shield (fig. 76). The design is governed by the requirement that the probe temperatures during the coast phase be maintained in the range of -5 to 10°C. This narrow band results from the requirements to keep operating temperatures for the probe unit and science instruments within the range of -20 to 50°C during descent. For a specific set of thermal blankets, final RHU complement and nose emissivity (gold tape striping) are adjusted to meet the temperature requirements based on thermal vacuum test results. The Probe Thermal Model Test Program resulted in a baseline of 39 RHUs. To minimize charging during passage through the charged-particle environment at Jupiter, surfaces are coated with conducting films and the layers are tied together electrically and grounded to the probe structure.

Structure. The structure of the deceleration module is made of aluminum alloys; the basic assembly technique is riveting. This module consists of the payload support ring, an aft box section ring, three longerons connecting the two rings, and thin skin sections. The descent module entry deceleration loads are reacted primarily through the payload support ring, and the module is held to the payload ring by three bolts passing through bolt catchers mounted in the longerons. At assembly, the interface of the descent and deceleration modules is preloaded to about 5000 kg to prevent relative motion between the modules during launch. The aft cover is an aluminum dome with two longerons and two rings as primary structural elements. The ring at the base of the dome interfaces with the forward aeroshell and is connected through the two longerons to the mortar support ring at the top of the dome. A radio frequency window is cut into the aluminum skin to accommodate the lightning and radio emission experiment. The cover is held in place by three explosive nuts and bolts located 120° apart.

Figure 75. Heat shield design.

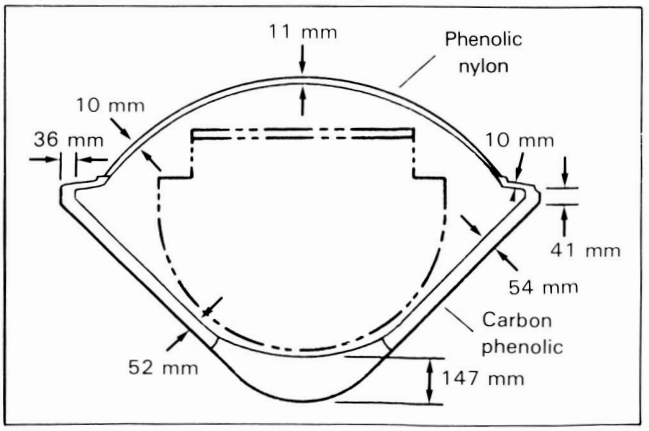

ORIGINAL PAGE
COLOR PHOTOGRAPH

Parachute. The main parachute is used to separate the descent and deceleration modules and to control the rate of descent through the atmosphere. The canopy is a conical ribbon design chosen for its low aerodynamic trim characteristics and low opening shock loads. The material for the canopy and shroud lines is Dacron; Kevlar is used for the riser. The parachute diameter (projected) is 2.5 m, a value selected to guarantee separation of the probe in worst-case conditions, that is, the aeroshell structure without the forebody heat shield. Nominal conditions at parachute deployment are Mach 0.9 and a dynamic pressure of 6000 N/m^2. A swivel is used to decouple probe and parachute spin. The pilot parachute is injected into the wake by a mortar fired at a velocity of 30 m/s. After the pilot chute is established, the separation nuts are fired to release the aft cover. The aft cover, pulled through the wake by the pilot chute, in turn pulls out and strips the bag from the main parachute. The deployment process, from initiation through full opening of the main chute, is designed to take less than 2 seconds.

Descent Module

Figure 77 illustrates the main features of the descent module. Most of the equipment is mounted on a shelf; the aft side of this shelf is used primarily for the science instruments. The probe radio frequency communication subsystem and the pyrotechnic control unit are located in the aft compartment; the main parachute, the lightning and radio emissions detector (LRD) antenna, and energetic particles instrument (EPI) sensor are located on top of this compartment. Note that in contrast to

Figure 76. Probe structural model in its support structure, showing some of the thermal blankets and gold taping.

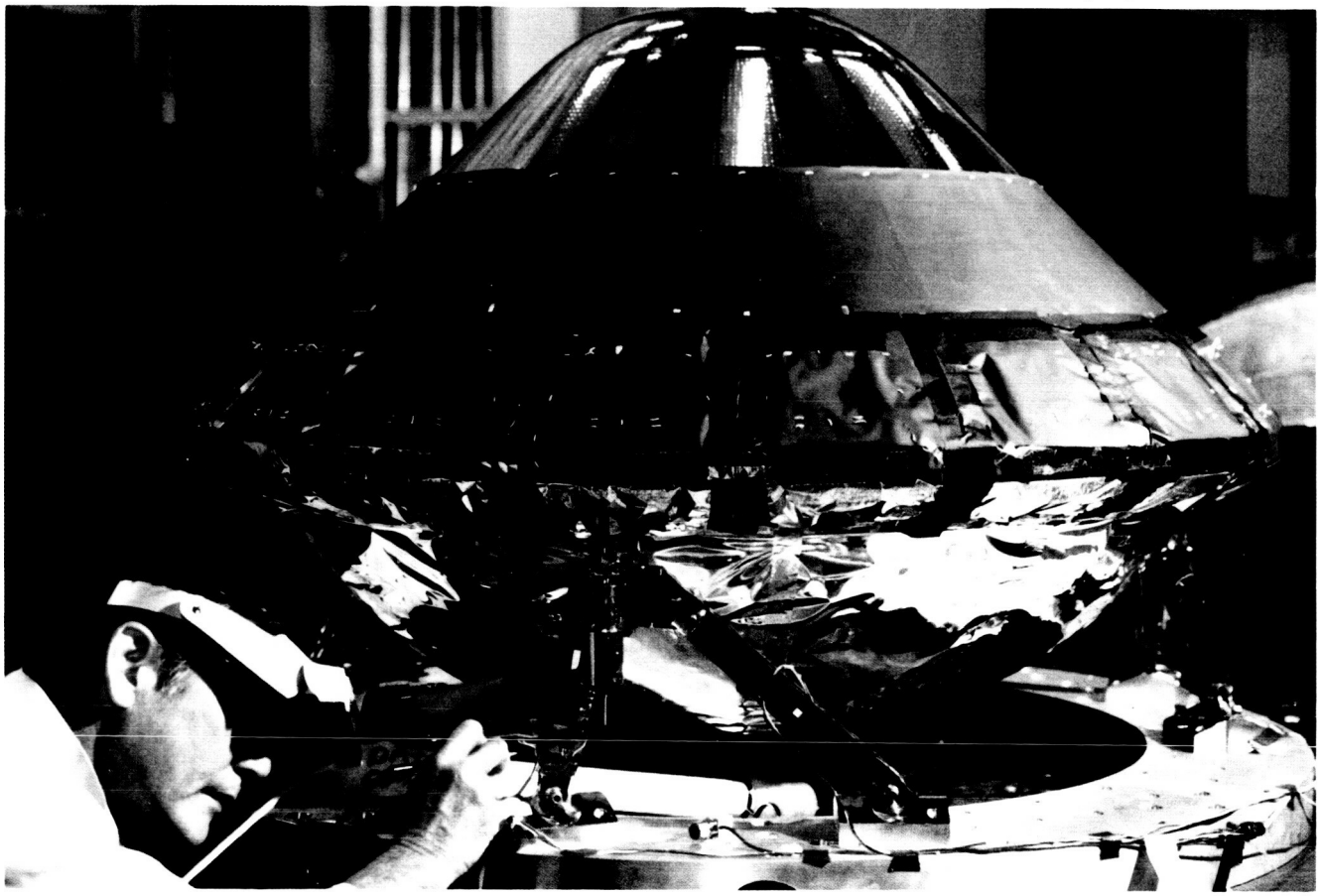

the Pioneer Venus design, which included a sealed pressure vessel, the weight is minimized by venting the Galileo descent module and by protecting individual units as necessary with hermetically sealed housings. The housings are designed for survival to 20 bars and were tested to 16 bars.

Structure. The shelf and its forward interface ring are the primary load-bearing elements between the deceleration and descent modules. The shelf is fabricated as a 66-cm-diameter bonded aluminum honeycomb sandwich; it is 5 cm thick and has 1.6-mm face sheets, a core density of 130 kg/m^3, and a machined z-ring bonded to the periphery of the core to transfer shear loads. A titanium interface ring bolted to the forward surface of the shelf transmits entry loads to the deceleration module. The circular aft compartment is supported by three bipod assemblies that serve as the primary load-carrying structure for parachute deployment and entry loads. This compartment is composed of a 63-cm diameter channel side wall, titanium panels for mounting internal units, an intercostal beam for stiffness, and an aft cover. The aerofairing system consists of a forward dome, six mid-fairing panels, and flexible closeouts around penetrations. The aerofairings are made of titanium sheet, chemically milled to a thickness of 0.2 mm, except in the areas of fasteners. The penetration closeouts are designed as flexible bellows formed in heated molds from Teflon-sintered fiberglass.

Science Instrument Accommodation. The layout of the science instrument packages on the shelf is shown in figure 78. Note that the LRD and EPI share a common set of electronics. The total instrument mass is 28 kg, and the maximum power designated for instrument use is 72 W, with a maximum energy constraint for the probe prime mission of 78 W-h. Each instrument uses one digital line for primary data transfer. In addition, a total of six analog and eight bilevel channels plus nine frame rate and seven clock signals are allocated for use by the instruments. The neutral mass spectrometer is supplied one quantitative command; all other commands are discrete single-pulse signals. Finally, one redundant pyrotechnic pulse is provided for deployment of the nephelometer sensor. Instrument sensors have been placed to meet specific viewing and flow condition requirements.

Thermal Control. Thermal control prior to entry is provided as part of the deceleration module. After entry and probe staging, the descent module provides thermal control for probe descent. Multilayer Kapton blankets are used to isolate the probe interior as much as possible from the external environment. Because the probe is vented, the internal gas temperature essentially follows the atmospheric temperature; however, the blankets do serve to prevent hot (or cold) external structure from affecting the probe's internal temperatures.

Harness. The probe wire harness is fabricated from 30-gauge, high-strength beryllium copper wire to meet severe mass and space constraints, the latter being the most important. All low-level signal wires are shielded to avoid noise problems, and harness bundles are wrapped with aluminized Kapton for protection against buildup of electrostatic charge.

Electronics

To eliminate single-point, catastrophic mission failures, the probe electrical and electronic subsystems, including the radio frequency link with the orbiter and the receiver on the orbiter, are redundant designs. Two parallel and simultaneous data streams go from the instruments to the orbiter.

Communications Subsystem. The communications subsystem provides two L-band microwave channels, one at 1387.0 MHz and one at 1387.1 MHz, each circularly polarized, one with right-hand and the other with left-hand polarization. Each channel consists of an exciter, a power amplifier which puts out 23 W of radio frequency power, and either an ultrastable oscillator or a standard, thermally controlled oscillator. The channel with the ultrastable oscillator will be used for a doppler wind measurement. The transmitter also measures its own output power level. This measurement, along with a measurement of the received signal strength at the orbiter-mounted receiver, is used to determine atmospheric absorption. Both channels are transmitted through a single, passive hybrid and a dual-feed, crossed-dipole antenna. The antenna is a cup dipole consisting of a 25-cm-diameter cylindrical cavity, open at one end and fed by a crossed dipole pair. This design results in an antenna with a 3 dB beamwidth of 56° and a peak gain of 9.8 dB.

Power Subsystem. The power subsystem consists of two electronics units, a lithium/sulfur

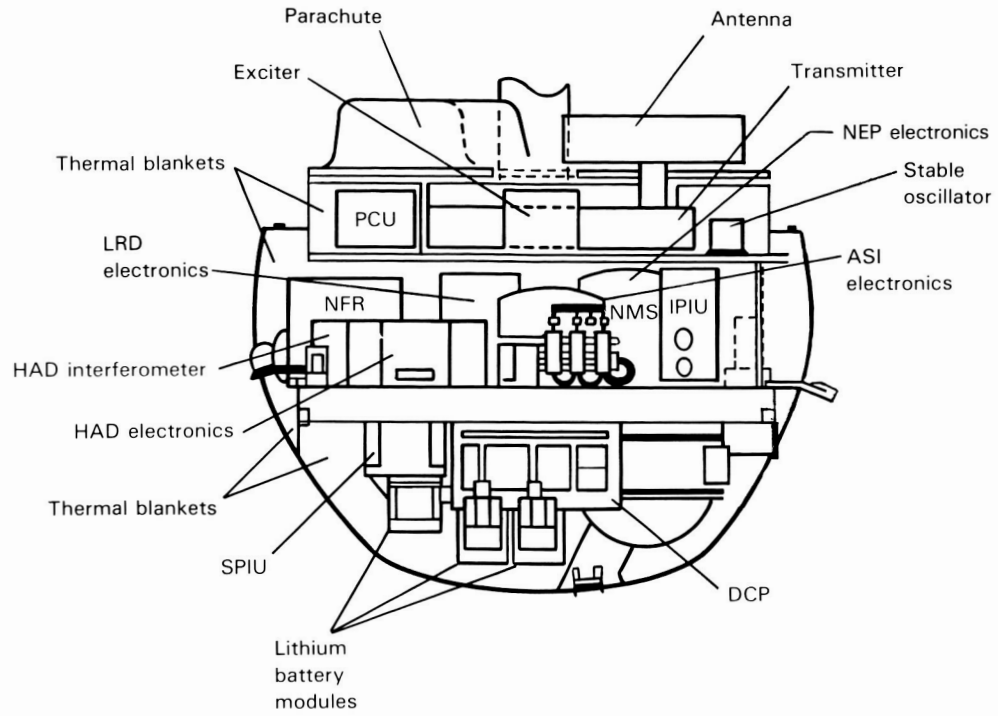

ASI	atmospheric structure instrument	NEP	nephelometer
DCP	data and command processor	NFR	net flux radiometer
HAD	helium abundance detector	NMS	neutral mass spectrometer
IPIU	instrument power interface unit	PCU	pyro control unit
LRD	lightning and radio emissions detector	SPIU	system power interface unit

Figure 77. Descent module internal arrangement.

dioxide ($Li\text{-}SO_2$) battery and a set of thermal batteries. The system power interface unit is the main power distribution unit. It distributes power to the probe subsystems and to the instrument power interface unit from either the probe battery or orbiter power supply. The system power interface unit provides redundant switching for all functions but does not include voltage regulation of the input (voltage regulation is not required for probe units). The instrument power interface unit, in addition to switching, provides both voltage regulation and overvoltage protection for instrument use. The main power supply for the probe mission is the $Li\text{-}SO_2$ battery. This battery is made up of three modules of 13 D-size, high-rate cells. The cells are connected in series with a bypass diode across each cell so that the failure of one cell will not cause the loss of an entire module. Open circuit voltage of the battery is 39 V. The voltage drops to about 34 V with a 6-A load. Total battery capacity at manufacture is expected to be about 21 A-h (about 730 W-h), of which about 2.8 A-h will be used up by ground tests and storage loss (around 5 years). Probe mission requirements are for about 16.3 A-h, leaving a capacity margin at the end of the mission (defined as 48 minutes after entry) of 1.7 A-h. The primary source of energy for pyrotechnic events is a set of four thermal batteries. Pyrotechnic pulses for actuation of these batteries and for neutral mass spectrometer functions later in the descent are provided by a tap on the main battery at the eighth cell.

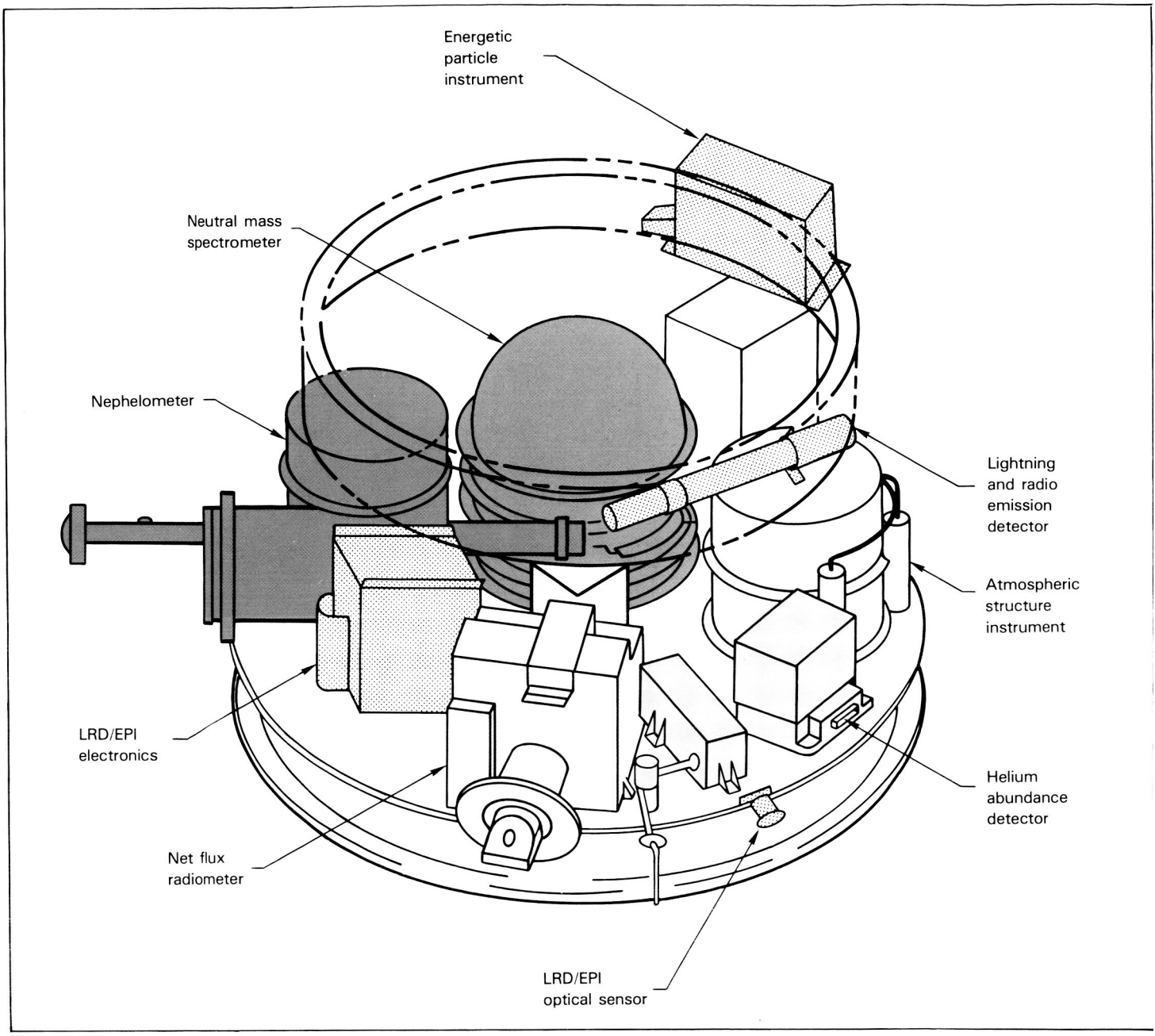

Figure 78. Probe science instrument layout.

Command and Data Handling Subsystem. The command and data handling subsystem consists of the data and command processor, the pyrotechnic control unit, and four acceleration switches (two redundant pairs). The data and command processor is a micro-controller-based unit which provides and controls all system command, telemetry, data storage, and timing functions. The design consists of two basically redundant strings, each controlled by its own microprocessor. All postentry functions, with the exception of some subcommutated engineering data, are contained and are the same on both strings. Preentry command and data functions are divided between the two strings and therefore are not redundant. The self-test function is automatically activated once about 20 minutes before entry; it checks the condition of each string. If a fault is detected on one string that might affect the data on the other string, the faulty string will be turned off and will then remain off.

During the period from separation of the probe and orbiter to the end of the mission, the data and command processor operates in several different modes. For the coast phase, only the coast timer operates. Its purpose is to "wake up" the probe about 6 hours before entry. During the preentry period, one string is used to gather and store LRD and EPI data. Both strings operate starting about 20 minutes before entry through the

end of the mission. The entire sequence from separation to the end of the mission, with the exception of the magnitude of the time for the coast phase, is contained in permanent memory. Entry and descent sequence functions are tied directly to the atmosphere by the acceleration switches. The switches provide an adaptive parachute deployment which removes uncertainties in deployment conditions associated with uncertainties in entry angle and in the characteristics of the atmosphere. The acceleration switches also provide backup initiation of the descent sequence in the event of early or late time-out of the coast timer.

The pyrotechnic control unit provides the pulses for activating all squibs on the probe, except some functions internal to the neutral mass spectrometer. The unit includes arming relays and 48 hybrid drivers. The hybrid drivers are self-contained units which include a command buffer, an active current limiter, and a one-shot circuit, all on a single substrate. They are designed for the NASA standard initiators used on the probe. All probe pyrotechnic functions are implemented with redundant initiators.

Relay Radio Hardware

The relay radio hardware (RRH) receivers, ultrastable oscillators, and antenna (fig. 68) are mounted on the orbiter to receive the probe signal.

The RRH receivers are a key element of the data link between the probe and the orbiter during the probe's descent through the jovian atmosphere and during probe checkout before separation from the orbiter. Each receiver is designed to acquire, coherently track, and process the probe's data along with RRH radio science and engineering data. The receivers also format and buffer the data for transmission to the orbiter command and data system. The acquisition, tracking, and data-handling functions are performed by the microprocessor-controlled section of the receiver. The main functions in the acquisition and tracking process are coarse frequency acquisition through the implementation of a sequential probability radio test; frequency synchronization, using a frequency-lock loop; symbol synchronization, using a symbol-lock loop; ambiguity resolution; and phase synchronization and signal tracking, using a phase-lock loop. Uncertainties and signal perturbations, including uncertainty in probe signal frequency and spin rate, and nonsteady motion of the probe caused by wind shear, wind turbulence, and nonsteady aerodynamics, make the design and test of these functions complex and difficult. The unit must acquire the probe signal within 50 seconds, with an acquisition probability of 0.995 and a false-lock probability of less than 5×10^{-5}. Minimum strength at acquisition is specified as 31 dB-Hz. The unit is required to track a signal strength as low as 26 dB-Hz. In addition to providing probe data, the receiver measures received probe signal strength and doppler rates for radio science use.

The RRH antenna is a 1.1-m parabolic reflector with a dual feed for receiving the two signals from the probe. It is mounted on a deployable mechanism for storage at launch and for pointing during the probe mission. This mechanism is provided by the orbiter. The antenna is mounted on the despun (inertially fixed) part of the orbiter. To eliminate a possible catastrophic failure of the probe mission as a result of failure of the orbiter spin bearing, the antenna mounting mechanism is designed such that the antenna can be pointed along the orbiter's spin axis.

Mass

The total mass of the probe is about 331 kg, that of the probe adapters is 6.8 kg, and that of the RRH equipment is 23.2 kg. Almost half of the total probe mass is dedicated to the heat shield, and the electronic units are considerably heavier than one would expect for standard spacecraft hardware because they include hermetically sealed housing designed to withstand 20 bars.

chapter 7 SCIENTIFIC INSTRUMENTS

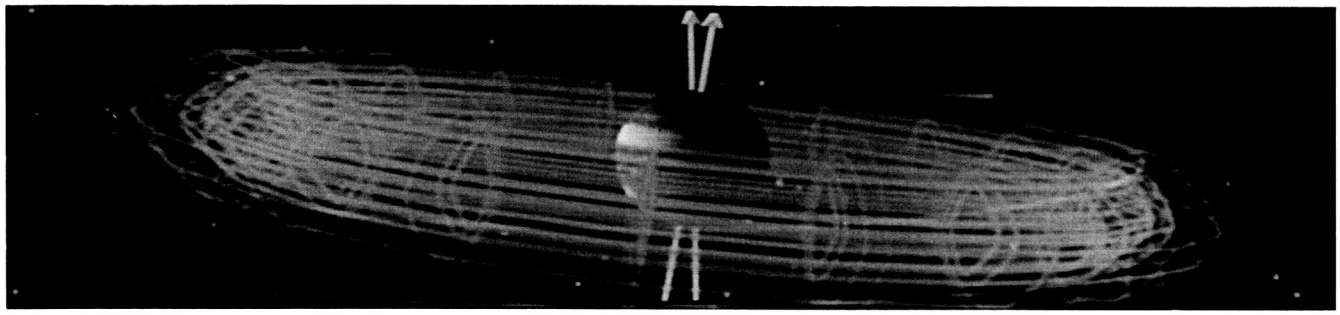

The scientific instruments aboard the Galileo orbiter and probe have been carefully chosen and designed to reap as much knowledge of the Jupiter system as possible. Each will take unique measurements, yet many of their capabilities overlap to provide maximum opportunities to study the planet, its satellites, and the magnetosphere. Galileo's scientific investigations are designed to complement and extend the wealth of knowledge provided by the Pioneers and Voyagers. Along with the members of the science teams, who are specialists in their own fields, interdisciplinary scientists will use the data from several instruments to test new theories and confirm new discoveries. As with all scientific forays, the unexpected finds may be the most exciting, and we will learn to use the instruments in new and different ways to pursue new avenues of inquiry.

Eleven scientific experiments aboard the orbiter will view Jupiter and its satellites for nearly two years (fig. 79). The nonspinning portion of the orbiter provides a stable base for four remote sensing instruments. These optical instruments are mounted on the movable scan platform with their apertures aligned along the same axis so that they view nearly the same areas. The spinning section of the orbiter allows five instruments to view the entire sky to study magnetic fields and particles. The spacecraft's radio equipment will be used to study celestial mechanics and radio propagation.

The remote sensing science instruments and their functions are:

Solid-state imaging camera (SSI)—takes pictures from which horizontal and vertical atmospheric motions are measured and the geology and morphology of the satellites' surfaces can be determined.

Near-infrared mapping spectrometer (NIMS)—measures reflected sunlight and heat emitted from Jupiter's atmosphere to determine composition, cloud structure, and temperature profiles. It is also used to gather data for the study of the chemistry and mineralogy of the satellites' surfaces.

Photopolarimeter-radiometer (PPR)—measures temperature profiles and energy balance of Jupiter's atmosphere and the planet's cloud characteristics and composition. It also measures the brightness, texture, and temperatures of the satellites' surfaces.

Ultraviolet spectrometer (UVS)—investigates the atmosphere of Jupiter above the cloud tops, explores and characterizes the atmosphere of the satellites, and measures Io's torus.

The fields and particles instruments and their functions are:

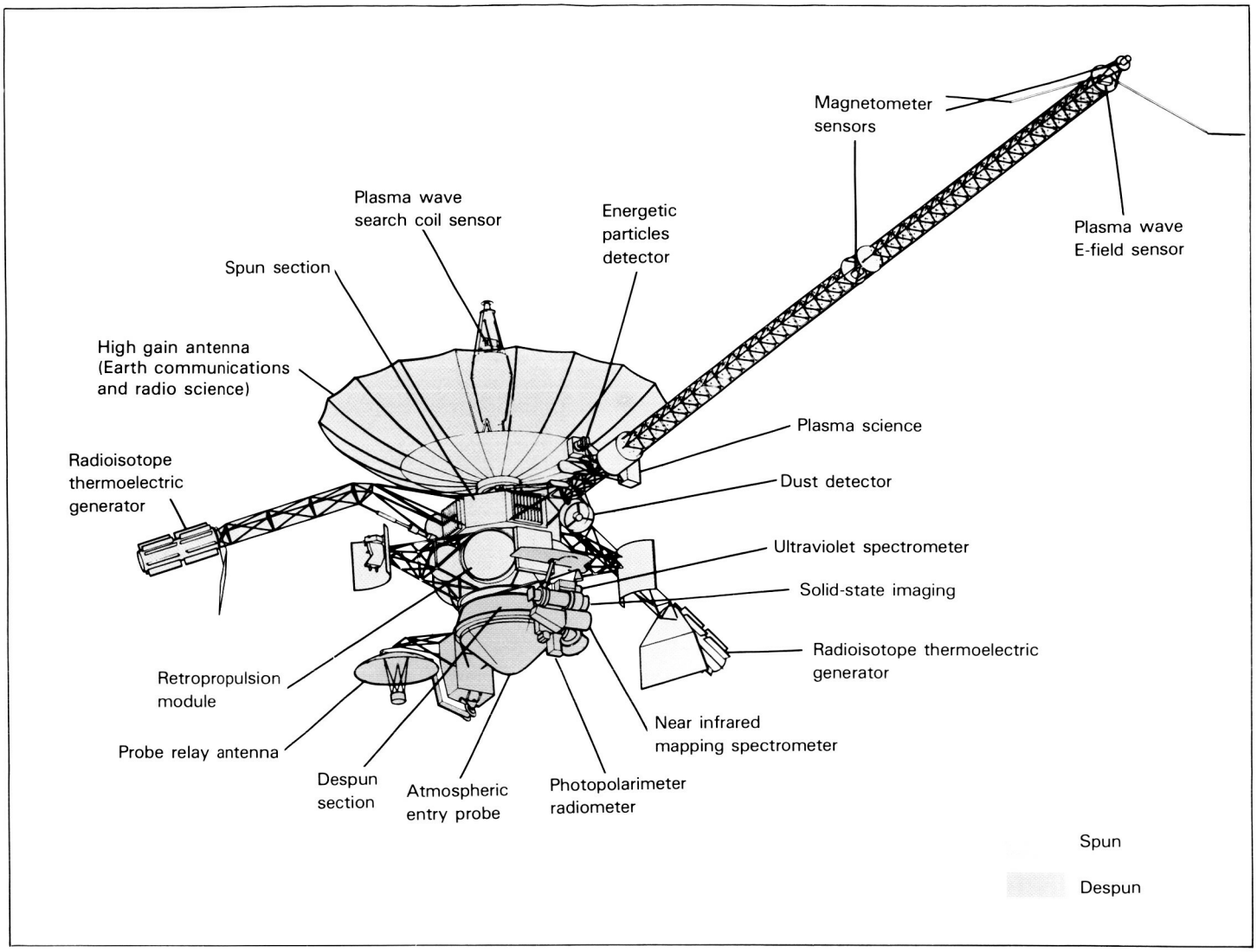

Figure 79. Location of instruments and major elements of the Galileo spacecraft.

Magnetometer (MAG)—measures the magnetic fields associated with Jupiter's magnetic moment and the distortions of these fields due to the presence of plasma and the interaction of the satellites.

Plasma instrument (PLS)—determines the properties of low-energy plasmas throughout the jovian magnetosphere, including their temperatures, densities, bulk motions, and composition.

Energetic particles detector (EPD)—investigates the spatial distributions and temporal fluctuations of ions and electrons, including ion composition, at medium and higher energies in the jovian system with an energy range contiguous to that for the plasma instrument.

Plasma wave instrument (PWS)—provides identification and analysis of the radio and plasma waves in Jupiter's magnetosphere, with the capability of remote sensing of source location.

Dust detection instrument (DDS)—surveys the physical and dynamic properties of small dust particles in the jovian system.

The radio experiments are:

Radio frequency subsystem (RFS)—In conjunction with Earth-based receivers and transmitters, the RFS measures the doppler shift, echo time delay, amplitude, spectrum, and polarization of the radio signals that comprise the Earth-orbit-Earth telecommunications link. These measurements allow study of the gravitational fields of Jupiter, its satellites, and the Sun; the atmosphere, ionosphere, and magnetic field of Jupiter; and gravitational radiation from outside the solar system.

Relay radio hardware (RRH)—measures the amplitude and doppler shift of radio signals from the probe to the orbiter which can then be used to study the atmosphere and ionosphere of Jupiter.

The Galileo probe will plunge at high speed into Jupiter's atmosphere carrying six instruments

designed to discover as much as possible about the atmosphere during the relatively short period of descent. These instruments are:

Atmospheric structure instrument (ASI)—provides information about temperature, density, pressure, and molecular weight.

Neutral mass spectrometer (NMS)—analyzes the composition of gases by measuring their molecular weights.

Nephelometer (NEP)—locates cloud layers in the atmosphere and measures some of the characteristics of the particles making up the clouds.

Energetic particles investigations (EPI)—measures electrons, protons, alpha particles, and heavy ions in the innermost regions of the jovian magnetosphere.

Lightning and radio emission instrument (LRD)—searches and records static generated by lightning flashes on Jupiter.

Helium abundance interferometer (HAD)—determines the important ratio of hydrogen to helium in the atmosphere of Jupiter.

Net flux radiometer (NFR)—senses the differences between the energy flux being radiated inward and outward at each level in the atmosphere.

These instruments are described in detail below.

Orbiter

Remote Sensing Science

Solid-state imaging (SSI). The scientific objectives of the solid-state imaging experiment are to study satellite science, Jupiter atmospheric science, magnetospheric interactions, jovian rings, and targets of opportunity.

For each Galilean satellite we aim to determine the morphology of at least 50 percent of the surface at a scale of 1 km or better and of many selected areas at 100 m or better. Also, the imaging system will map the spatial variation in color and albedo at a scale of 2 km or better and will monitor variations with time. The wavelength range of this camera extends into the infrared. We will also determine the photometric function at several locations and the photometric phenomena resulting from interaction with the magnetosphere. For each Galilean satellite, we hope to find the location of the spin axis, the rate of rotation, and the geometric figure to within 3 km. The scientific objectives for satellite imaging are discussed in detail in chapter 3.

As opportunities arise, we will observe the smaller satellites to obtain information about their surface morphology, color, and albedo and seek small satellites in the vicinity of the jovian rings. All four small inner satellites will be imaged at the highest possible resolution to improve our knowledge of their sizes, shapes, colors, albedos, surface textures, and spin states.

Our objectives at Jupiter are to determine the energetics, structure, motions, and radiative properties of the atmosphere. Atmospheric mass motions can be separated at global scales from atmospheric wave motions. We will investigate the vertical structure of a few specific types of atmospheric features and establish relationships between structure, color, and morphology. Relative cloud motions will help us to determine how winds vary with altitude. This is especially important at the boundaries between belts and zones and at the region of probe entry. The radiative properties of the jovian atmosphere will be investigated by measuring how individual features scatter light at several wavelengths and over a wide range of phase angles. Auroral phenomena in the atmosphere and on the satellites will be mapped and correlated with particle and field observations to determine the nature of interactions of the atmosphere with the magnetosphere.

We will image the rings of Jupiter at the highest possible resolution to find any satellites that may be embedded in the rings. Also, photometric observations will determine color, albedo, column densities, and the size distribution of ring particles.

The imaging experiments will cooperate with other investigations and observe objects such as asteroids, satellites, and comets which are expected to present special target opportunities during the mission. The scientific objectives and the approach are discussed in detail in chapters 2 and 3 (satellite objectives). The team leader for this experiment is Michael Belton of Kitt Peak National Observatory.

The solid-state imaging system is mounted on an articulating scan platform attached to the nonspinning spacecraft bus so that the instrument can be pointed as required.

The instrument (fig. 80) is a single camera

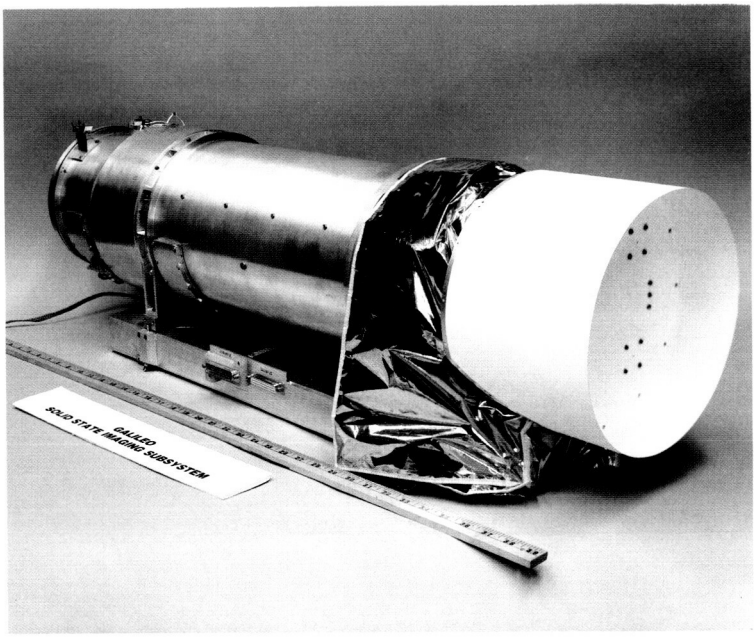

ORIGINAL PAGE
COLOR PHOTOGRAPH

Figure 80. Solid-state imaging (SSI) instrument.

system based on an 800 line by 800 element, solid-state, silicon, image sensor array called a charge-coupled device (CCD). The optics element is an all-spherical catadioptric Cassegrain telescope with a 176.5-mm aperture, a fixed relative aperture of f/8.5, and an effective focal length of 1500 mm. Based on a CCD density of 65.6 elements/mm, the angular resolution is 10.16 microradians per pixel (picture element). This optical system has the ability to reject much off-axis light so that good-quality images of illuminated surfaces of the planet and its satellites will be obtained. A diagram of the optical system is given in figure 81.

The CCD sensor is radiation shielded and radiatively cooled. It is mounted in the camera head together with an electromagnetic focal plane shutter, an eight-position filter wheel, and supporting electronics.

The filter wheel is adapted from the Voyager television subsystem. Photodiodes are uncovered by a pattern of small apertures on the filter wheel which are unique to each filter position. Thus the position of the wheel is accurately encoded for each frame and forms a part of the engineering telemetry from the spacecraft. The filter wheel can be stepped from one to a maximum of seven positions (fig. 82) between exposures.

The shutter (fig. 82) also originated from Voyager technology. It consists of a two-blade focal plane mechanism; each blade is actuated by its own permanent magnet rotary solenoid. The exposure duration is controlled by the time between pulses—an open and close pulse. The first pulse moves a leading blade to cover the aperture. The second moves a trailing blade to close the aperture. Before the next exposure both blades are moved back to their starting positions, traveling together

Figure 81. Solid-state imaging optical system.

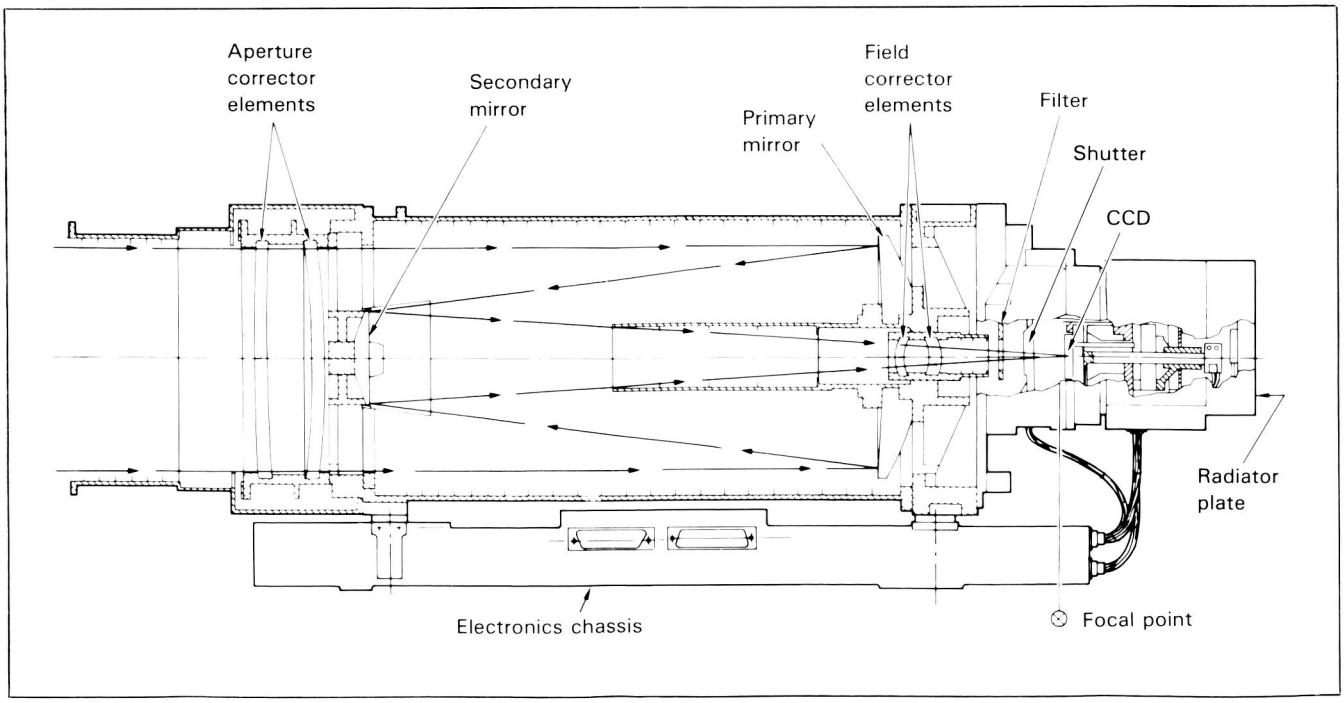

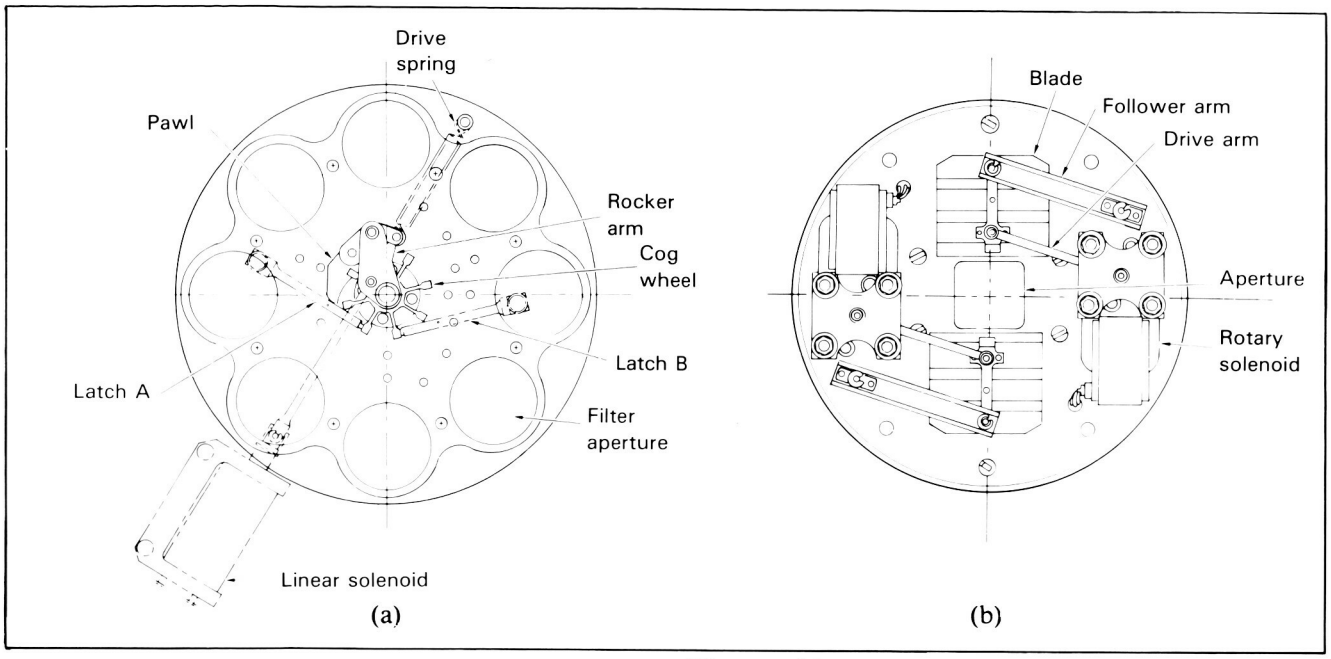

Figure 82. Solid-state imaging instrument filter (a) and shutter (b).

to keep the aperture covered. There are 28 selectable exposure times between $4\frac{1}{6}$ and 51 200 ms.

The image sensor (fig. 83) is a virtual-phase, buried-channel, front-side-illuminated CCD. It uses a polysilicon gate structure with 15.2-μm center-to-center spacing between the photo elements. It has an invariant geometry to ensure fidelity without complex geometric correction, and it requires only simple slope and offset tables for calibration. A very high charge transfer efficiency ensures a uniformly high mean time to failure over the entire array. The device has much greater spectral sensitivity than the vidicon cameras of the Mariner, Viking, and Voyager spacecraft.

Charge is transferred by switching the voltage level of a gate. This is repeated 800 times in the serial direction following each of the 800 transfers in the parallel directions, thereby scanning all the pixel elements in turn. To maintain a wide dynamic range for the slow-scan camera system, thermally induced CCD dark current must be suppressed. This is done by cooling the CCD to 163 K by a closed-loop, heater-modulated, radiatively cooled temperature control system. Analog video data from the CCD are converted to 8 bits for serial output to the telemetry system.

The SSI has four operating modes, characterized by different frame repetition rates: $2\frac{1}{3}$, $8\frac{2}{3}$, $30\frac{1}{3}$, and $60\frac{2}{3}$ seconds. Each sequence consists of a prepare and a readout cycle. In the prepare cycle the shutter is reset, the filter wheel is stepped as required, the sensor is read to reduce dark current, and the shutter is activated to expose the image. The readout cycle converts the image data to digital data, which are placed on the onboard tape recorder or put directly on the telemetry downlink for real-time transmission to Earth. There is also a mode which sums groups of four pixels, thus converting an 800 by 800 image into a 400 by 400 image which can be read out in a quarter of the time and thus be less likely to suffer from the effects of radiation in Jupiter's harsh environment.

Electrons with energies of about 10 MeV, which can be encountered in the inner magnetosphere, will interact with the silicon of the CCD to produce a mean charge of about 2000 electrons concentrated within a few picture elements. To protect the imaging system from radiation damage or the degradation of data during slow-scan readout of the images, 1-cm-thick tantalum shielding surrounds the CCD. The only open area

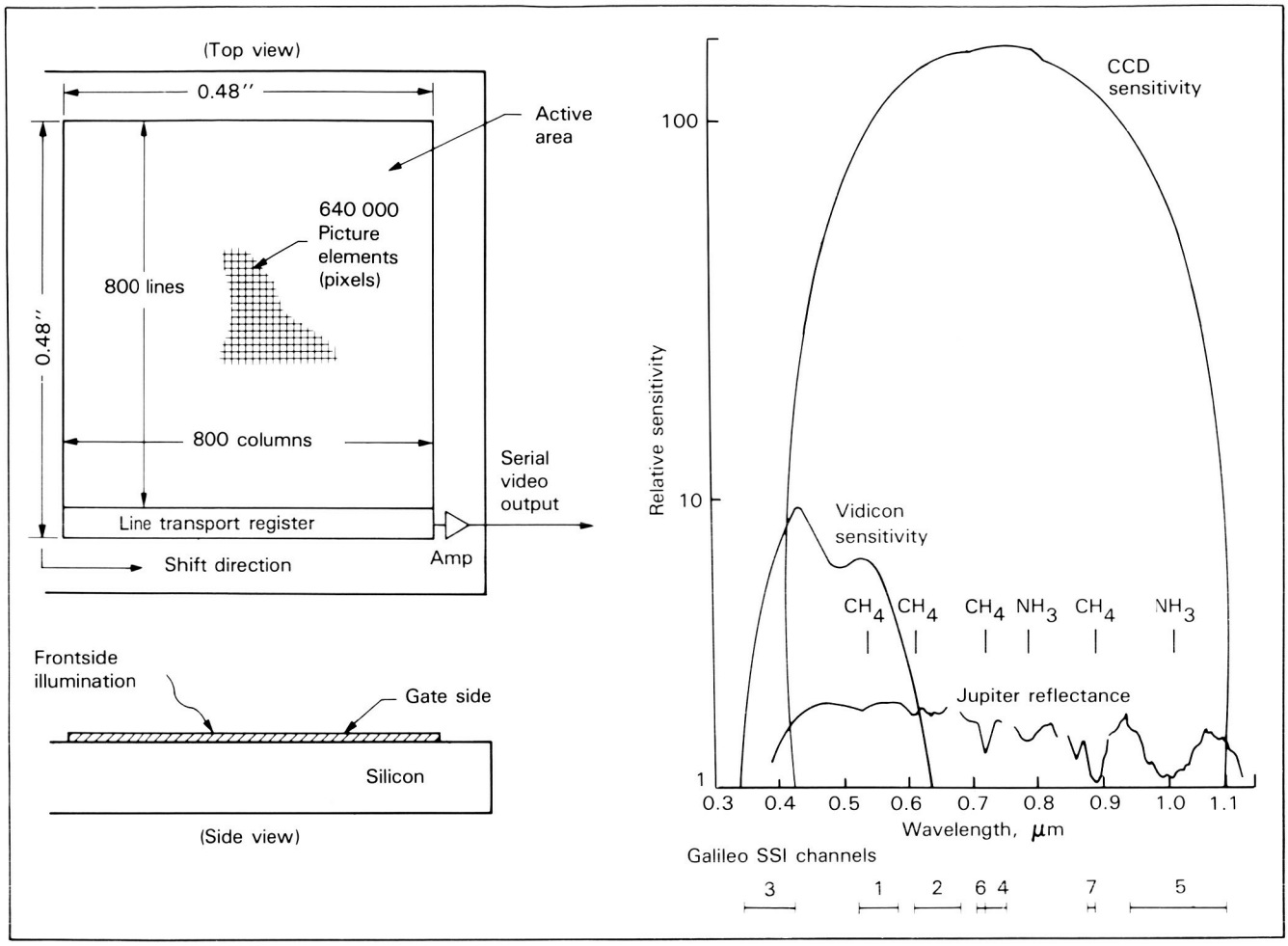

Figure 83. Arrangement of the pixel elements of the charge-coupled device of the solid-state imaging system (left) and graph showing the spectral response at different wavelengths (right) to illustrate the wide spectral coverage of this instrument compared with a vidicon.

is that of the shutter aperture. This shielding, together with the shielding effects of the structure and optical elements, is expected to ensure good image quality for the longest readout of an SSI frame (60⅔ seconds) down to about 15 Jupiter radii from the planet. Inside about 11 Jupiter radii the instrument can be effectively operated only in the 2⅓-second mode.

A microcomputer controls the instrument. This computer receives image parameter words from the spacecraft's command and data subsystem prior to each exposure and issues all the necessary instructions to the filter wheel and shutter drive electronics and other control electronics of the instrument. Backup memories are available, and the operational commands stored in the read-only memory can be transferred to random-access memory with a single command should the read-only memory fail. To enhance the return of image data the SSI has a data compressor and uses a special coder to provide virtually error-free data.

The solid-state imaging system weighs 28 kg and consumes an average power of 17 W.

Near-Infrared Mapping Spectrometer (NIMS). The near-infrared mapping spectrometer (fig. 84) represents a new philosophy and approach in remote sensing experiments for planetary spacecraft by combining spectroscopic and imaging capabilities in one instrument. The infrared

region of the spectrum is extremely useful for investigating the geology of the jovian satellites and for probing the atmosphere of Jupiter. The experiment objectives are to map and determine the mineral content of compositional units on the surfaces of the jovian satellites and to investigate cloud properties and the temporal and spatial variability of minor constituents of the jovian atmosphere. The objectives and approach are discussed in detail in chapters 2 and 3. The principal investigator is R. W. Carlson of the Jet Propulsion Laboratory.

Both spatial coverage derived from a scanning telescope and spectral coverage derived from a spectrometer are important to the goals of satellite and atmospheric studies. The NIMS experiment will spectrally map half of the surface of each of the satellites Europa, Ganymede, and Callisto at a resolution of 25 km or better. In addition, it will obtain spectra of Amalthea, Jupiter's ring, and two of the smaller satellites. In investigating the atmosphere of Jupiter by observing the infrared radiation from it, NIMS will provide information about the chemical composition, the nature of clouds, energy balances, and atmospheric motions.

Species that can be monitored with the NIMS experiment include ammonia, phosphine, water vapor, methane, and germanium. We will also search for other molecules so far undetected. Cloud layering will be studied; for example, ammonia clouds are expected at a level at which the temperature is about 200 K and water clouds are expected at about 270 K (at 2 and 5 bars, respectively). Temperature profiles will also be obtained.

Figure 84. Near-infrared mapping spectrometer (NIMS).

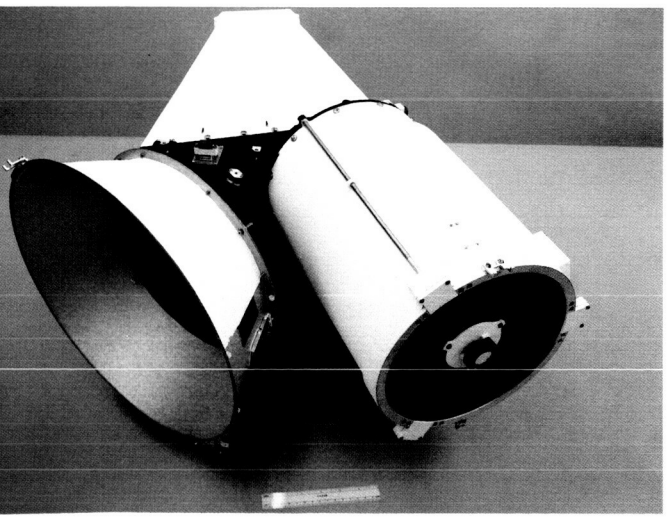

The high photometric sensitivity required of this experiment is achieved by using a relatively large telescope together with the most sensitive detector available for this region of the spectrum, indium antimonide (InSb).

The instrument is shown in figure 85. Major elements are a telescope, an optical chopper, a grating spectrometer, a multidetector focal plane assembly, a passive radiator cooler, and signal chain electronics and controllers for the mechanisms of the unit. Torque drive motors are used for spatial scan and grating motion. Position is controlled by a linear differential transformer which senses the position and controls the torque drive motor accordingly. A microprocessor provides timing, formatting, and operational control over a variety of modes.

The telescope is an all-refractive, 9-inch-aperture Richey-Chretien with a focal length of 800 mm and an aperture of f/3.5. The telescope's field-stop aperture forms the entrance "slit" to the spectrometer section of the instrument. This is an all-refractive system consisting of a Dall-Kirkham type collimator, a plane grating, and a wide-angle, flat-field camera. The collimator has an equivalent focal length of 400 mm and a focal ratio of f/3.5. A dual-blazed replicated grating with 40 lines/mm provides high efficiency over the broad spectral range. The dispersed spectrum is focused on the focal plane assembly detectors by the camera, which has a focal length of 200 mm and operates at f/1.75.

There are 15 indium antimonide detectors and two silicon photodiodes, each placed to sample a specific region of the spectrum. Reflectance losses from the indium antimonide are minimized by an overcoating. Optical filters limit scattered light and background noise. These filters also have gold masks deposited on them to limit the field of view. The detectors are maintained in a hermetically sealed package into which the infrared radiation enters through a sapphire window. They are cooled to approximately 80 K by a passive radiative cooler of aluminum honeycomb which radiates energy into space. Heat input to the assembly is kept very low by supporting it on fiberglass bands and surrounding it with a heat shield.

NIMS forms images from a combination of the motion of its internal scan mirror and the motion of the scan platform upon which it is

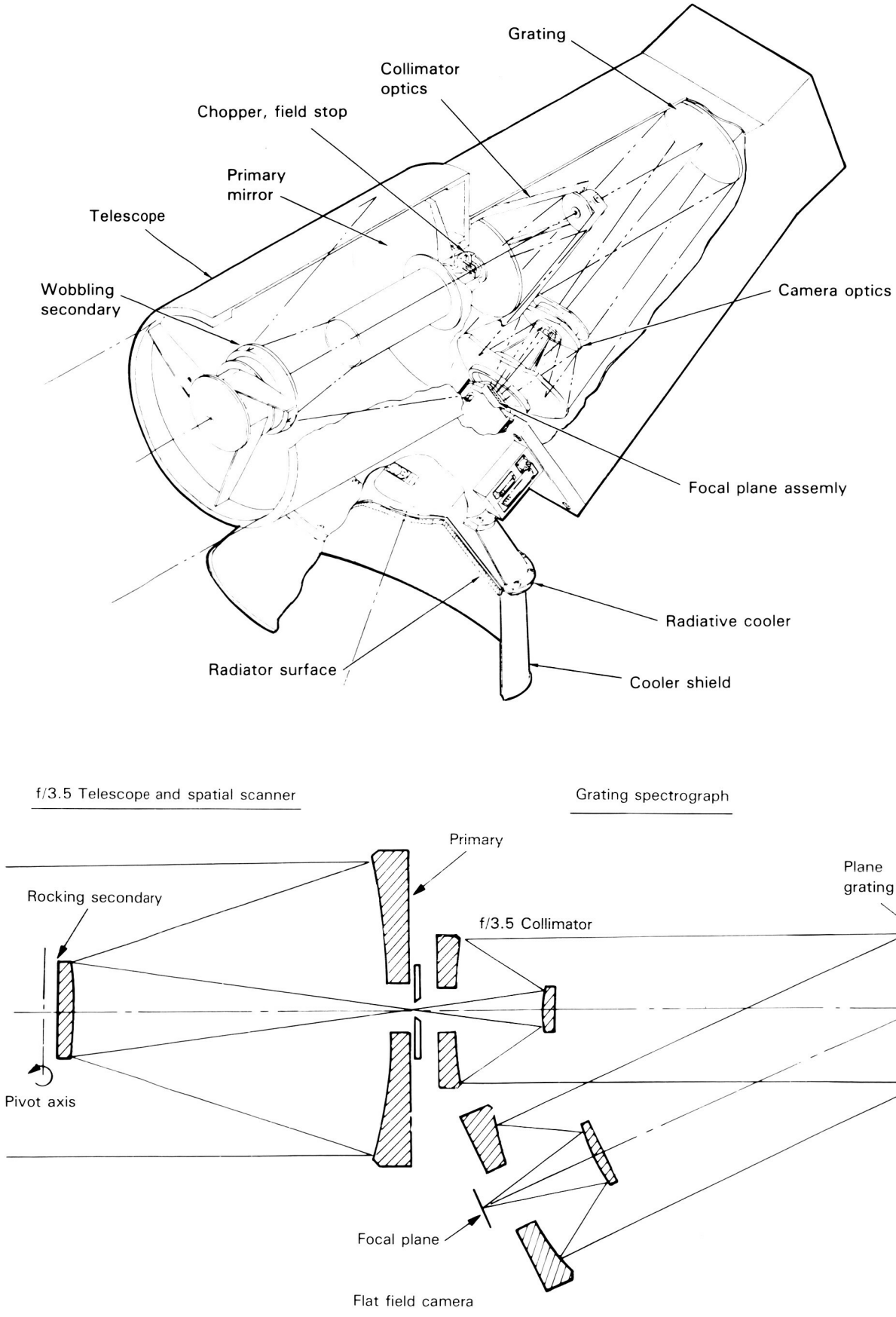

Figure 85. Schematic representation of the NIMS and its optical system.

mounted. Each sample of the detectors (every 1/60 second) gives 17-colocated 0.52-mrad samples evenly spaced throughout the instrument's wavelength range (0.7 to 5 μm). The scan mirror moves to 20 positions in 1/3 second, forming a vertical stripe of samples (the stripe is 0.5 by 10 mrad). The grating steps each 1/3 second to provide another "comb" of wavelengths just adjacent (in wavelength) to the previous comb. A full grating cycle (12 steps) repeats each 4⅓ seconds. Slow, smooth motion of the scan platform is adjusted so that stripes of combs of a given wavelength just overlap spatially. With reference to the image cube (fig. 86), a comb of wavelengths in the upper left corner of the cube is sampled first, the comb just below it on the front face is sampled next, and so on until the vertical stripe is formed. The grating is then stepped. This process continues until all wavelengths extending back from the left column have been sampled. By this time, scan platform

Figure 86. NIMS rim data matrix.

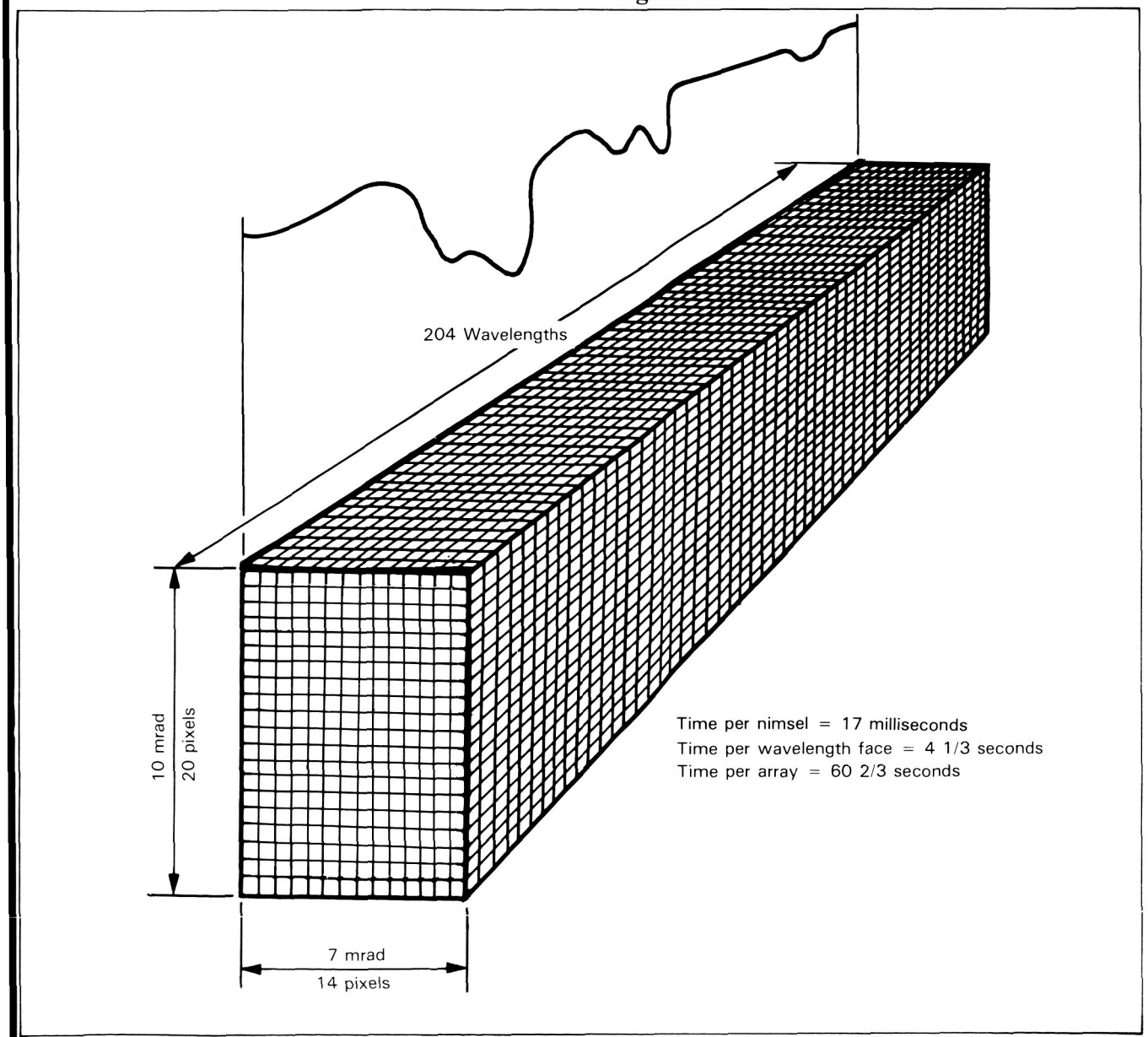

motion has carried the field of view to the second column, where the entire sample procedure repeats. Figure 86 depicts the image(s) formed in 1 minute. During this time, the instrument has sampled an area 20 pixels high by 14 pixels wide (10 by 7 mrad) in 204 colors (wavelength planes). Extracting a "rod" lying behind any of the pixels on the face of the image cube produces a spectrum of a particular spatial area. Extracting a (spatial) face from the cube gives the albedo characteristic of a spatial area at a given wavelength (an image).

The instrument weighs 18 kg and consumes 8 W on the average. It has an angular resolution of 0.5 mrad square and an angular field of 10 mrad (20 pixels) by 0.5 mrad (1 pixel). It covers the spectral range from 0.7 to 5.2 μm and completes a spectral span in 4⅓ seconds.

Photopolarimeter-Radiometer (PPR). The first objective of the photopolarimeter-radiometer experiment is to measure the intensity and polarization in the visible regions of the spectrum of sunlight scattered by Jupiter and the jovian satellites in ten narrow spectral regions. These regions include the locations of the bands in the spectrum where methane and ammonia strongly absorb radiation. In addition, thermal infrared radiation from Jupiter and the satellites will be measured in five broad, contiguous wavelength intervals. Radiation received from the jovian atmosphere consists of solar radiation scattered and reflected by the atmospheric molecules and particles, the thermal radiation emitted from the warmer lower atmosphere, primarily from cloud particles, and collision-induced molecular hydrogen transitions. The final objective is to determine the radiation budget of the planet and satellites by measuring the total reflected solar radiation and the total thermal emission. The principal investigator for this instrument is J. E. Hansen of the Goddard Institute for Space Studies. The scientific objectives for PPR are described in detail in chapters 2 and 3.

The design of the instrument (fig. 87) is an extension of the orbiter cloud photopolarimeter developed for and flown successfully on the Pioneer Venus spacecraft. Reflective optics collect light, which is passed through selective filters and measured by detectors. Figure 88 is an exploded view of the instrument and its housing. The latter has three main parts—a telescope baffle, an aft optics housing, and a stack of plates which provides a mount for the electronics and a base for the instrument. Figure 89 identifies the working components of the instrument's optics.

The primary optical path is a Dall-Kirkham telescope with a 10-cm aperture and 50-cm focal length. Radiation from Jupiter or a satellite passes through a series of baffles, to be reflected by the primary and secondary mirrors through a radiometric stop and a hole in the primary mirror. Radiation can also enter the instrument along an alternate path through two radiometric stops, where it is reflected by a single mirror. The first set of optics is used to gather radiation from an object being surveyed; the other collects radiation from space. These two optical paths meet at a chopper which alternately admits radiation from the planet or a satellite and from space for radiometry measurements. When the instrument is being used for photometry and polarimetry, only radiation coming along the primary path is admitted to the detectors.

Filters for several channels are mounted on a filter wheel. This wheel carries mirrors, which are used in the radiometry mode to reflect light to a lithium tantalate detector. When the instrument is being used for photometry, the beam passes through a filter and enters a Wollaston prism, which diverts the two orthogonal polarizations to two identical silicon photodiodes. By rotating the filter wheel among three adjacent positions with identical filters behind a half-wave retarder for each polarimetry channel, the polarization of the transmitted beam rotates through 90°. Because this effectively changes the roles of the two detectors,

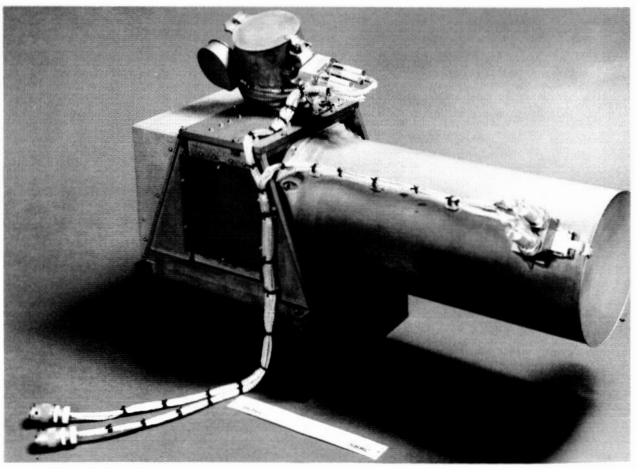

Figure 87. Photopolarimeter-radiometer.

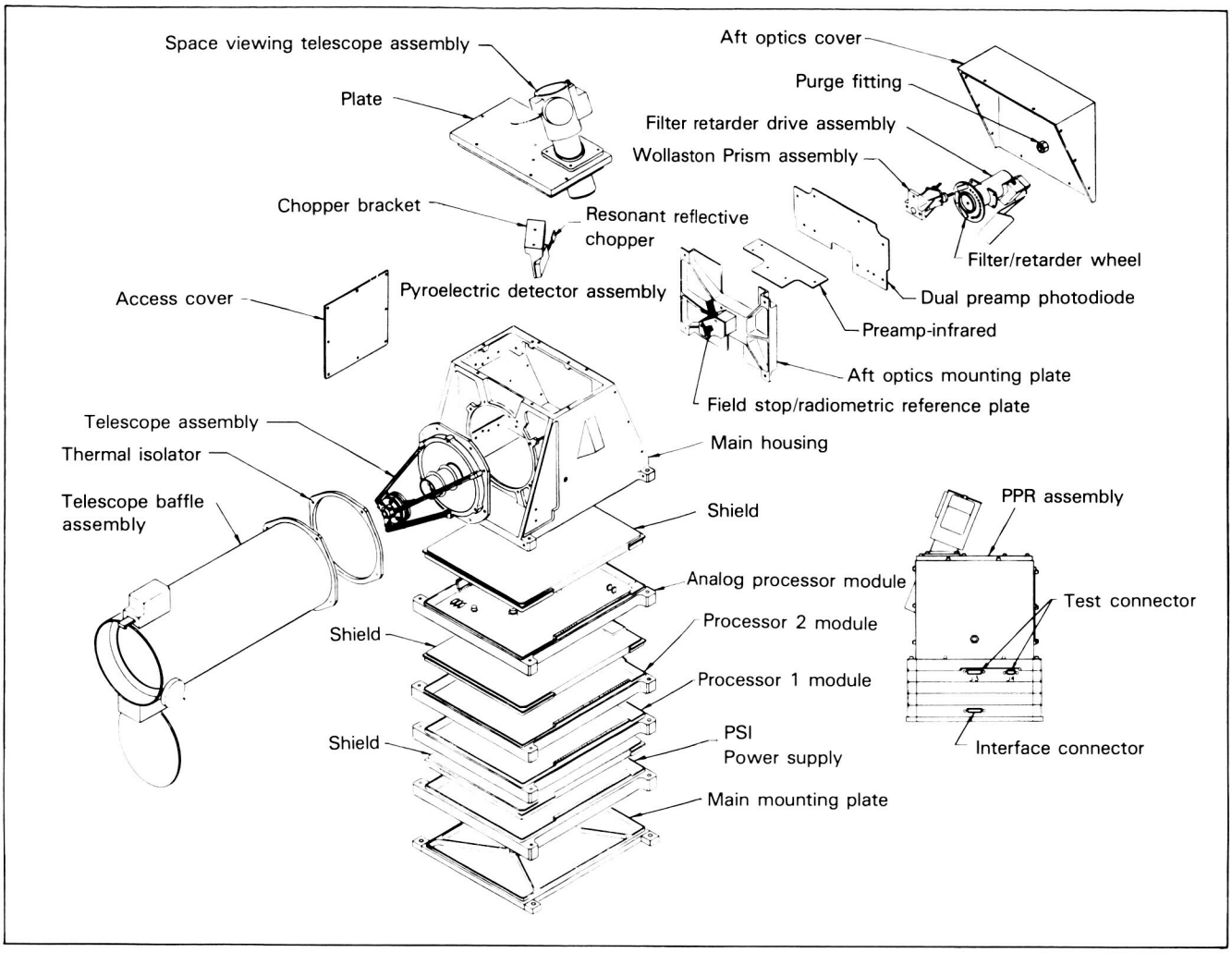

Figure 88. Exploded view of the photopolarimeter-radiometer showing arrangement of the optical system and the sensors.

the orientation of the polarization of the incident beam can be determined.

The polarimetry channels are centered at 4100, 6780, and 9450 angstroms, and the photometry channels are centered at 6180, 6330, 6460, 7980, 8300, 8410, and 8920 angstroms. When the instrument is used for radiometry the infrared channels are centered below 4 μm, at 17, 21, 27.5, and 37 μm, and above 42 μm. Locations and approximate width of all these channels in the electromagnetic spectrum are shown in figure 90.

Modes of operation include a cycle mode which rotates the filter wheel in one direction only so as to transmit each channel at least once every 18 seconds and a radiometry mode which rotates the wheel back and forth among the seven radiometry positions.

The photopolarimeter-radiometer has several safety features. A replacement heater maintains temperature when the power is off. Commandable covers for each optical path protect the optical surfaces when the thrusters of the spacecraft are fired. A sunshade prevents sunlight from entering directly into the optical system.

The instrument weighs 4.8 kg and consumes a peak power of 10 W. When the replacement heater only is operating, the instrument consumes 4.5 W.

Ultraviolet Spectrometer (UVS). The ultraviolet spectrometer (fig. 91) is designed to obtain

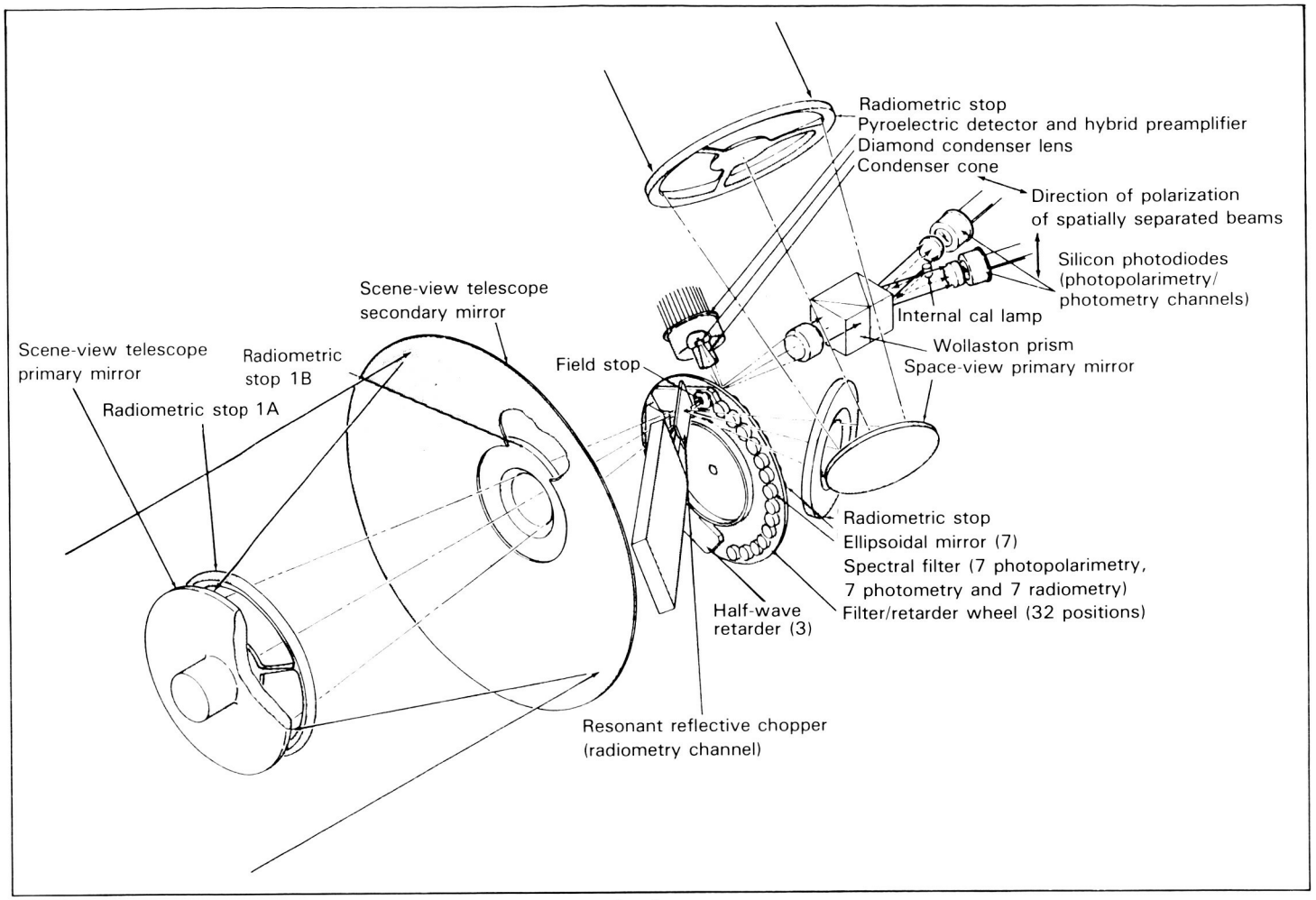

Figure 89. Filter and sensor system of the photopolarimeter-radiometer.

spectra from 1150 to 4300 angstroms to determine the characteristic properties of the jovian atmosphere and the surfaces of the Galilean satellites and to obtain emission spectra to study the plasma torus of Io and aurorae and dayglow in the jovian atmosphere. Properties of the high atmosphere of Jupiter to be determined by the ultraviolet spectrometer include the molecular absorption features that may be characteristic of the colored clouds and auroral zone emissions arising from the bombardment of the high atmosphere by energetic particles. We will also observe airglow emissions from the jovian atmosphere. For the satellites, the instrument will determine the ultraviolet reflective properties of the surface that help to characterize surface materials and their physical state—ice, frost, and size of grains. We will attempt to detect atomic hydrogen, atomic oxygen, and nitrogen from the Galilean satellites to determine how these planet-sized bodies continue to evolve through the loss of volatile gases. To satisfy our third major objective, investigating the plasma torus of Io, we will look for emissions from multiply ionized oxygen and sulfur at wavelengths beyond the capabilities of previous spacecraft. The scientific objectives are discussed in more detail in chapters 2 and 3.

The ultraviolet spectrometer was developed at the Laboratory for Atmospheric and Space Physics (LASP) of the University of Colorado. The principal investigator is C. W. Hord of LASP.

The instrument consists of four sections: a telescope, monochromator, three detectors, and control logic. A cutaway view of the instrument is shown in figure 92.

The 250-mm-aperture Cassegrain telescope coupled with the exit slits to the spectrometer produces a field of view of 0.1 by 1.4° for the 1100 to 1900 and 2800 to 4300 angstrom detectors and a field of view of 0.1 by 0.4° for the 1600 to 3000 angstrom detector. Thus, the telescope can sample ultraviolet radiation coming from a relatively small region of the atmosphere of Jupiter or a satellite surface.

A reflecting diffraction grating of a 125-mm focal length Ebert-Fastie monochromator disperses the ultraviolet light. The position of the grating,

and thus the wavelength of the radiation being measured, is controlled by a programmable grating drive which is directed by the control logic of the instrument. Ruled at 2400 grooves/mm, the grating provides a resolution of 13 angstroms in the first-order spectrum and 7 angstroms in the second-order spectrum.

Three photomultipliers cover the wavelength range from 1100 to 4300 angstroms. Photons striking the photomultipliers produce pulses which are counted, and every 0.0007 second the counters are read and the number of counts is transmitted to Earth.

A microprocessor controls the detectors and the grating drive to give the flexibility of a large variety of data-taking programs. At one extreme the instrument can be programmed to sample one fixed wavelength and look for changes in intensity as the field of view moves across the planetary disk. At the other extreme a program allows the instrument to step to a new wavelength every 0.007 second, producing a spectrum of the planet's radiation in about 4⅓ seconds. Variations between these extremes can be commanded. The instrument consumes 5.33 W at 2.4 kHz and 50 Vac. Its total weight is 5.33 kg.

Particles and Fields Instruments

The major objectives of Galileo's particles and fields instruments are to seek an understanding of the sources of the jovian plasmas and to ascertain which particles originate from the ionosphere, the solar wind, and the satellites alone or in combination; to study the plasma interaction with the satellites; and to investigate the structure and time variability of the Io torus, the jovian radiation belts, the plasma disk, the current sheet, and other structural features of the magnetosphere. In addition, the mission will seek to characterize Jupiter's magnetotail and determine whether a plasma wind flows away from Jupiter there.

These magnetospheric objectives are to be gained by a set of five closely associated instruments—the magnetometer, the plasma instrument, the energetic particles detector, the plasma wave instrument, and the dust detector.

Magnetometer (MAG). The Galileo magnetometer (fig. 93) comprises two sets of ring core sensors. One set of three sensors, which can measure fields over the range of ± 32 to ± 512 nT, is mounted at the end of the magnetometer boom about 10 m from the spin axis of the spacecraft (fig. 79). A second set covering the range from ± 512 to ± 16 384 nT is mounted on the boom about 6.7 m from the spin axis. For a benchmark, the magnitude of the magnetic field at Earth's surface is about 50 000 nT.

The sensor electronics produce an analog voltage that is linearly proportional to the sensed magnetic field. The data system converts this

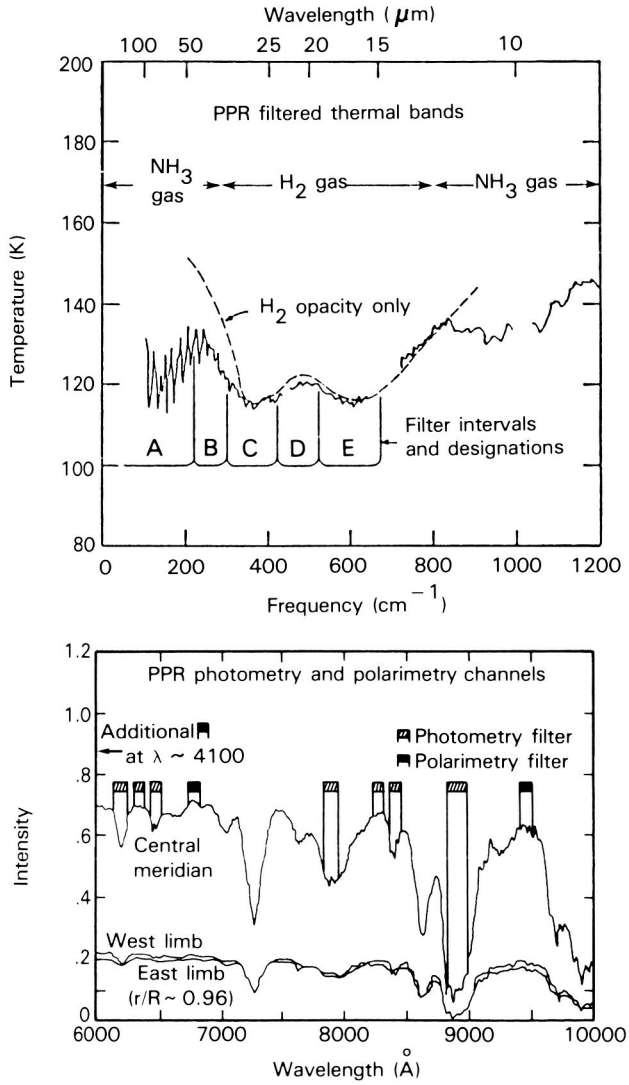

Figure 90. Location of the photopolarimeter-radiometer channels in the spectrum. (Top) The filtered thermal bands. (Bottom) The photometry and polarimetry channels. Both are related to the spectrum of Jupiter.

ORIGINAL PAGE
COLOR PHOTOGRAPH

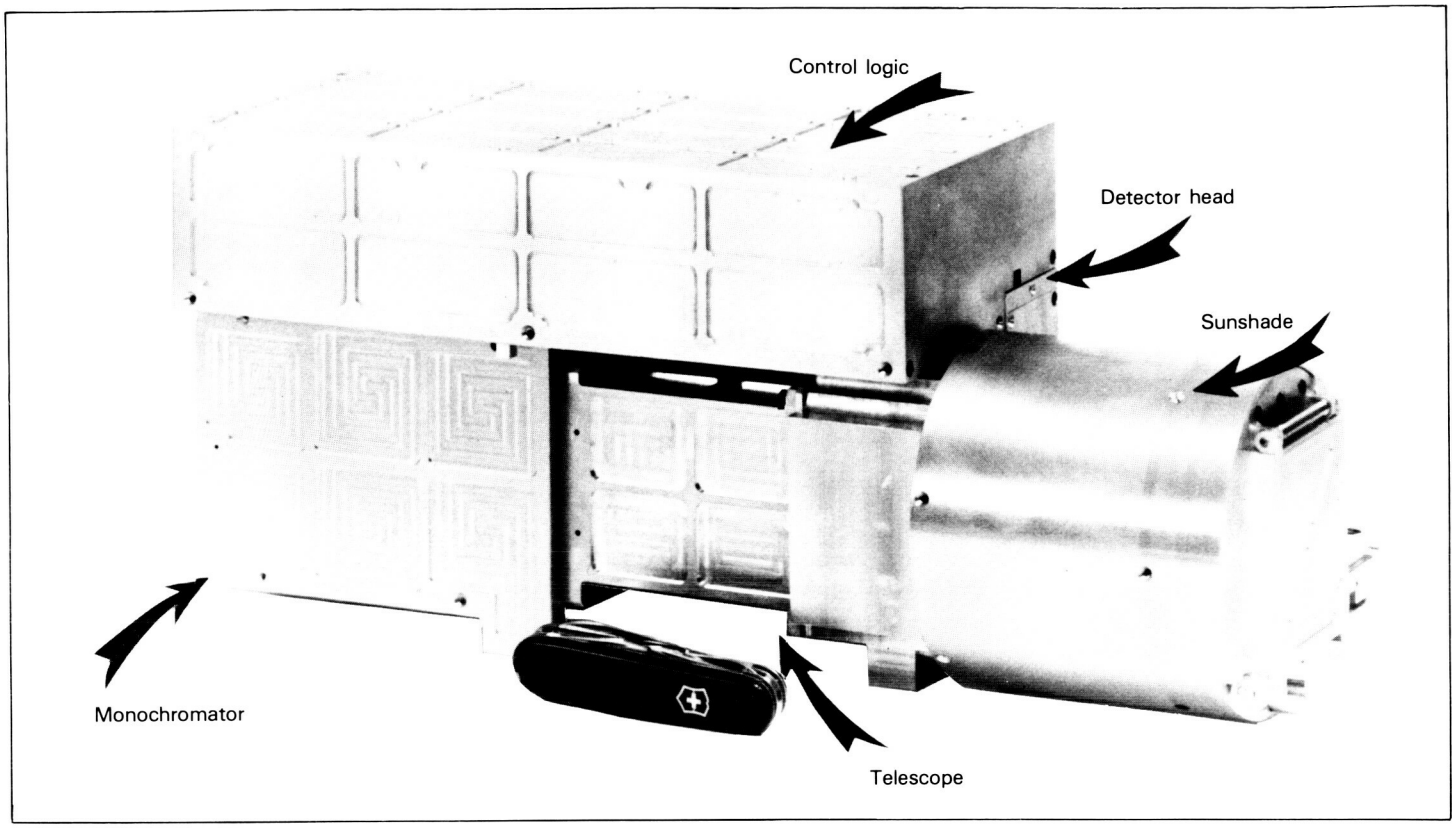

Figure 91. Ultraviolet spectrometer (UVS).

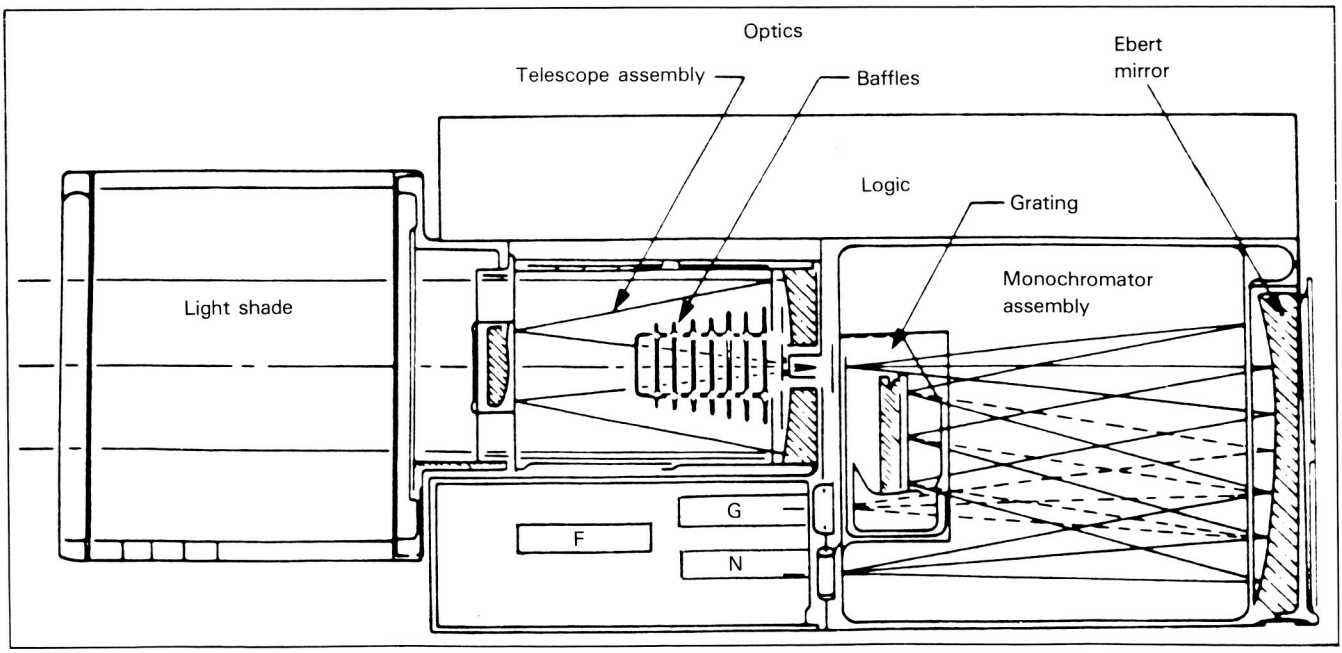

Figure 92. Cutaway section of the ultraviolet spectrometer showing various sections and the optical paths to the detectors.

voltage to a digital signal with 16 bits of resolution. This system is controlled by a microprocessor and provides for data sampling, storage, averaging, and transmittal to the spacecraft system. This microprocessor allows not only great flexibility in selecting instrument modes but also a large improvement for the information telemetered to Earth. The system processes data in two primary modes. In the first, the data processor samples and averages data in even increments of time and stores packets of data in a buffer memory for transfer to the spacecraft system. In the second mode, the data processor spin demodulates the data by resolving it into X, Y, and Z coordinates and then stores the data for transmittal to the spacecraft system. In either mode each packet of data contains three sets of vectors formulated into 16-bit words and one 16-bit subcommutator word. The spin-demodulated data and status information is formulated into a subcommutator word. A third mode, for optimum averaging, averages the spin-demodulated data over long periods and stores them within the instrument. This mode of operation is used when the orbiter is not transmitting or recording data. Short periods of high-speed data may be taken, stored, and read out using the same data buffer used for optimal averaging by putting the instrument into a fourth, snapshot, mode of operation. A fifth, or idle, mode is used to prevent the microprocessor from erroneously using program information while the program portion of random access memory is being changed by command from Earth.

Magnetic field measurements are filtered digitally to increase the resolution of measurements from 12 to 16 bits. The data processor spin demodulates the data from the transverse magnetometers and provides two data words that represent the magnitude of the magnetic field components in phase and in quadrature with the roll angle information provided by the attitude control system of the spacecraft. This provides measurements in two space-fixed directions in the spin plane.

Measurement offsets arising from magnetic fields generated by the spacecraft or the electronics are determined by averaging the magnetometer data over several spin periods. All natural fields being modulated by the spin of the spacecraft will, if measured when the spacecraft has rotated 180°, statistically combine to give zero over many rotations. This can be done for the two sensors mounted in the spin plane but not for the sensor that is mounted parallel to the spin axis. The offset for this sensor is determined by mechanically rotating it into the spin plane, thus interchanging it with one of the others. The dual magnetometer locations, mid-boom and end-of-boom, allow for first-order correction for the simple dipole component of locally generated magnetic fields and how they vary over time or as a result of other spacecraft activities.

Because the magnetometer boom is not rigid and may twist and bend by several degrees, precise alignment of the sensors to the spacecraft coordinate system is determined by a calibration coil mounted rigidly to the spacecraft to provide a known magnetic field of ± 3 nT at the outboard sensor. The principal investigator for this instrument is Margaret G. Kivelson of the University of California at Los Angeles.

Plasma (PLS). The plasma instrument (fig. 94) includes two sets of electrostatic spherical-section analyzers. Almost all the angles for particle velocity vectors at the spacecraft position are sampled. Electrons and positive ions are measured separately and simultaneously. The energy/unit charge range is 1.2 to 50 400 V and is divided into 64 passbands. In addition, three miniature mass spectrometers are positioned at the exit apertures of the electrostatic analyzers to identify the composition of ions. The location of the instrument on the spacecraft is shown in figure 79.

For comparison with previous measurements at Jupiter, the energy/unit charge ranges of the Pioneer and Voyager plasma instruments are 100 to 4800 V and 10 to 5920 V, respectively. The corresponding range of the Galileo plasma analyzer is 1 to 50 000 V. This extended energy range spans the important energy gap between 5920 and 30 000 V in the combined performances for the Voyager plasma instrument and medium-energy particle detectors. Temporal resolutions for obtaining electron and positive ion spectra are about 200 seconds for the Pioneer analyzer (ions only) and about 100 seconds for the Voyager Faraday cups. The corresponding temporal resolution for the Galilean plasma analyzer is 5 seconds; complete three-dimensional velocity distributions for positive ions and electrons can be telemetered once each 20 seconds. These improved temporal resolutions are particularly important during the fast encounters

of the satellites and the traversals of plasma boundaries such as those of the plasma sheet and current sheet in the middle and outer magnetospheres. No ion mass spectrometers were included on the Pioneer or Voyager spacecraft. The Galileo spectrometers will provide the first direct identifications of ion species.

A diagram of the Galileo plasma instrumentation is shown in figure 95. There are two electrostatic analyzers (labeled A and B) for measurements of the energy/unit charge for electron and positive ion intensities, separately and simultaneously. Each electrostatic analyzer comprises three 70° spherical-segment plates. The outer and inner plates are grounded, and the center plate is supplied with a programmed series of voltages to effect analyses of the energy spectra of electron and positive ion intensities. The inner and outer channels between the plates correspond to the positive ion and electron analyzers, respectively. The inner surfaces of the center and outer plates of each analyzer are serrated with sawtooth grooves to decrease scattering of electrons and solar ultraviolet emissions. As shown in figure 95, each electrostatic analyzer is equipped with a set of sensors. There are a total of seven sensors (labeled 1E to 7E) for measurements of electron intensities and similarly a total of seven sensors (labeled 1P to 7P) for positive ion intensities. The direction of the field of view for each sensor is determined by its position at the exit aperture of the electrostatic analyzer. For example, the fields of view for sensors 4P and 4E are directed at 90° to the spin axis of the spacecraft, whereas sensors 7P and 7E view charged particle velocity vectors directed generally antiparallel to the spacecraft spin axis. Three miniature mass spectrometers for positive ions are mounted at the exit apertures of the electrostatic analyzers. Each mass spectrometer comprises an electromagnet, two spiraltrons, and a system of collimating and aperture slits. Two mass spectrometers are positioned at the exit aperture of plasma analyzer B (1MI, 1MD and 3MI, 3MD), and one mass spectrometer (2MI, 2MD) is placed at the exit aperture of plasma analyzer A. The integral sensors, for example, 1MI, are placed along the line of sight through the spectrometer and thus respond to ions not deflected by the gap magnetic field. The differential sensors, for example, 1MD, are displaced from this line of sight to detect the mass/unit charge distribution of the ions passing through the electrostatic analyzer and deflected by the gap magnetic fields. Collimators are included in the spectrometers for defining the mass resolution. A programmed series of currents is supplied to each electromagnet to achieve 64 passbands.

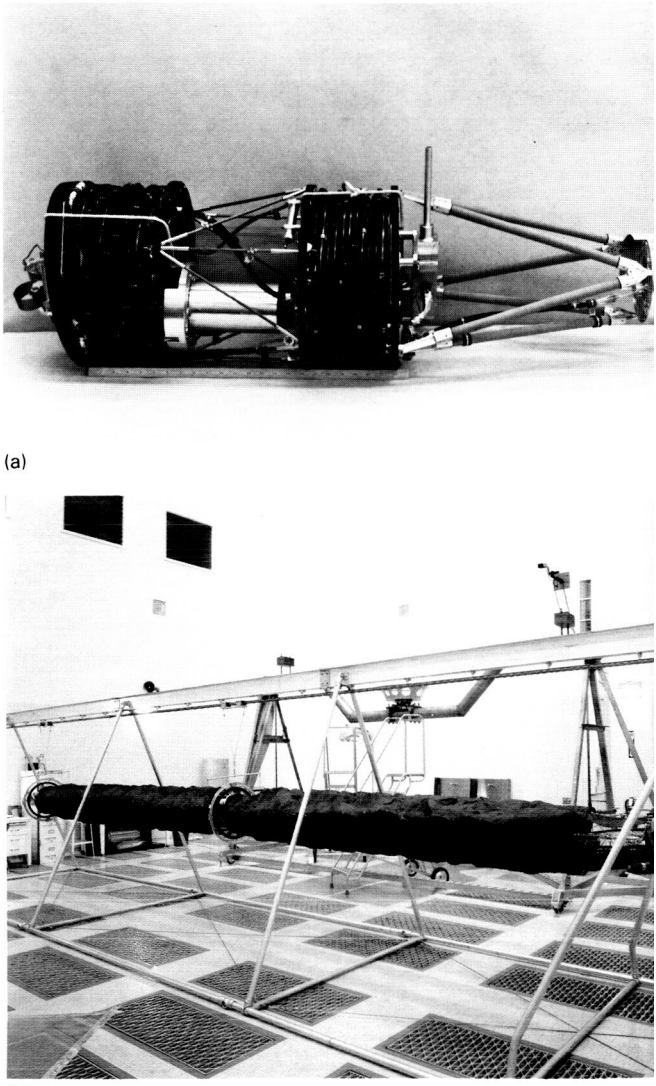

(a)

(b)

Figure 93. Magnetometer sensors (a) on collapsed boom (launch configuration), (b) on boom as it will extend after launch, with thermal blanketing.

The fields of view of the Galileo plasma instrument with respect to the spin axis of the spacecraft are summarized in figure 96. The overall field of view of the plasma instrument is fan shaped. The seven fields of view for the energy/unit charge analyses of positive ion and electron intensities are labeled 1 through 7. Each

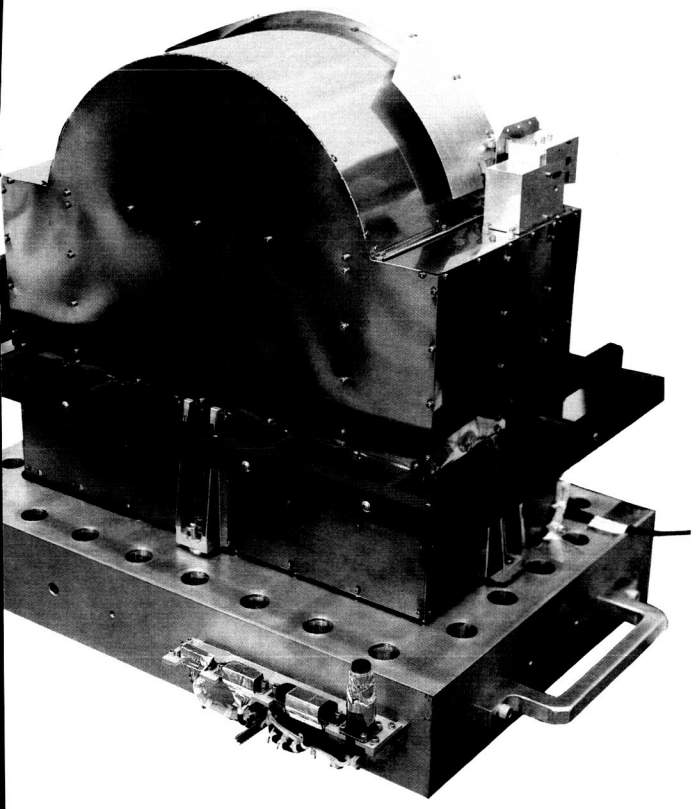

Figure 94. Plasma instrument (PLS).

field of view corresponds to measurements of positive ions and electrons, separately and simultaneously. The seven fields of view are not contiguous in order to attentuate the background rates caused by electron scattering along the plates into the sensors in the high-intensity electron environment of the jovian magnetosphere. The fields of view can be widened by reducing the analyzer angle, but a conservative design reduces scattered-electron background rates. The fields of view for the three miniature mass spectrometers, 1M, 2M, and 3M, are also shown in figure 96. Coverage of the solid angle for particle velocity vectors at the spacecraft position is implemented by the rotation of the fan-shaped field of view about the spacecraft spin axis. This rotation is sectored electronically to provide three-dimensional angular coverage.

Each of the two plasma analyzers, A and B, and their sensors are programmed and powered separately in the instrument. Each plasma analyzer is equipped with an individual analyzer plate high-voltage supply, spiraltron high-voltage bias supply, magnet current supply, and low-voltage power converter. The voltage output of the spiraltron bias supplies can be increased by ground command to optimize the operating lifetime of the sensors. In addition, there are two RCA 1802 microprocessors in the data-handling unit. Only one microprocessor is used to operate the entire instrument at a given time, but a configuration control allows either microprocessor to service the instrument. Sequences of plate voltages, current steps, and sensor read-outs can be tailored from onboard basic software modes by ground command.

Thus the plasma analyzer can be operated flexibly via electronic reconfiguration by ground command. All sequences of energy/unit charge passbands, mass/unit charge passbands, sensors, and angular sectors can be tailored for a specific plasma region. The temporal resolution of a given measurement series can also be selected. The plasma analyzer is also equipped with sufficient onboard hardware and software to implement automatic beam capture modes for ion velocity distributions and for determination of ion composition. The principal investigator is Louis S. Frank of the University of Iowa.

Energetic Particles Detector (EPD). The energetic particles detector (fig. 97) measures the flux and the spectra of ions and electrons with energies exceeding about 20 keV and the composition of ions with energies exceeding about 100 keV per nucleon. Particles arriving from all directions are measured by making use of the sweeping motion of the spacecraft's spin and movement of the instrument on a stepping platform. Recent success in measuring three-dimensional distributions around Earth has shown the importance of sampling the full unit sphere around the spacecraft to understand the dynamics of magnetized plasmas.

The instrument has two separate bidirectional, solid-state detector telescopes mounted on a stepping platform that covers 186.3° in steps of 30.6°. These telescopes form two subsystems: a low-energy magnetospheric measuring system (LEMMS) and a composition measuring system (CMS). These two telescopes are identified in figure 98. The spacecraft location for this instrument is shown in figure 79. Outputs are counting rates and pulse-height analyzer words. Energetic particle rates as a function of time, energy, and particle species are transmitted for 49 separate rate channels, each of which is defined by energy and time-of-flight discriminators and by coincidences between detector elements. A pulse-height analyzer provides high-resolution data from each telescope. The telescope of the composition measurement system transmits 4.5 pulse-height anlyzer events per second. Every 4.6 seconds, the pulse-height

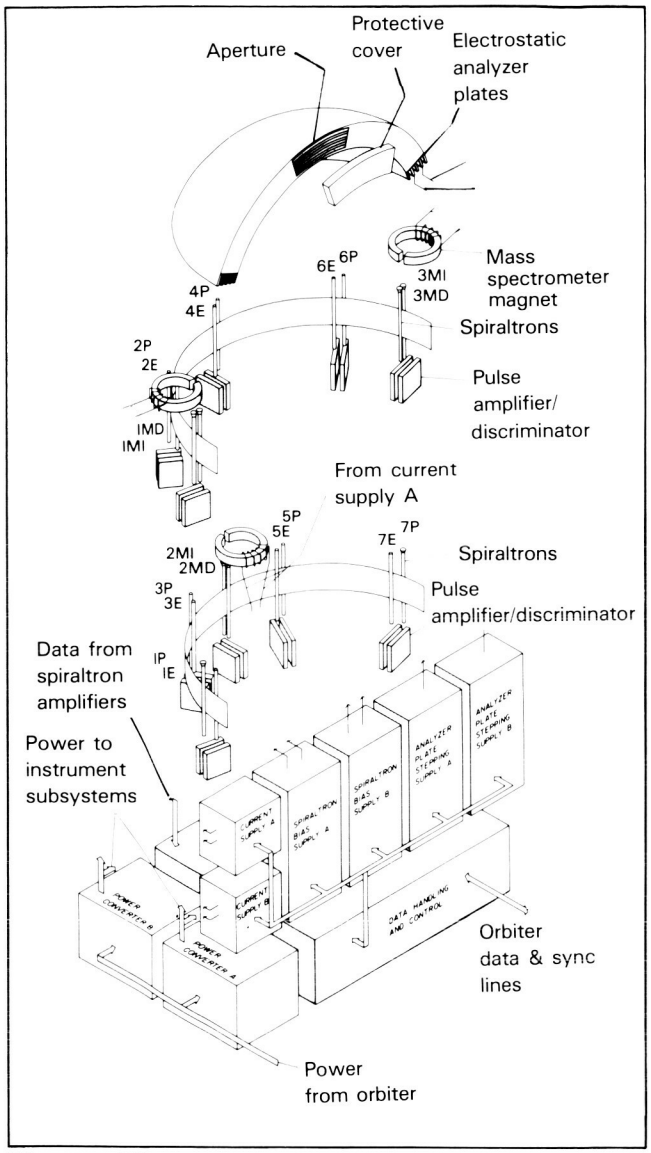

Figure 95. Plasma instrument exploded view.

analyzer is switched to the low-energy magnetospheric measuring system to accumulate a 47-channel ion or electron spectrum.

The low-energy magnetospheric measuring system includes an ion telescope with two solid-state detectors and a magnetic electron spectrometer with two sets of detectors to measure the energy and angular distribution of low-energy particles in the jovian magnetosphere. One detector of the ion telescope covers the energy range 0.02 through 3.4 MeV. This is the primary low-energy ion detector. The other detector used with this telescope, coupled with a 2.7-mm platinum absorber, is used to define additional electron, proton, and alpha particle channels by coincidence and anticoincidence logic circuits. An 800-gauss magnet is used to focus electrons in the range 0.015 through 1.0 MeV into the two detector pairs of the magnetic electron spectrometer. In each pair a back detector provides active anticoincidence shielding. The energy ranges covered are 0.015 through 0.2 MeV and 0.1 through 1.0 MeV. Higher ion and electron energies are covered with a heavily shielded detector pair.

The composition measurement system's telescope has a three-parameter, solid-state detector system consisting of nine detectors which are used to measure with high resolution the composition, energy spectra, and pitch angle distributions of energetic ions in the jovian magnetosphere. At the 180° end of the telescope are three thin (2 and 5 μm) detectors (J_a, J_b, and J_c). Another detector, K, measures the rear total energy and the time of flight of particles between front and rear detectors, thus allowing much more accurate composition measurements in the low-energy range. It also provides a better background rejection, thereby allowing composition measurements to be made much closer to Jupiter. Another detector, L, mounted behind the rear time-of-flight detector is used for anticoincidence detection. The remainder of the detectors on the 0° end form a much larger configuration looking in the direction opposite to the time-of-flight configuration and are identical in type and function to those on the 180° end.

When operating, the instrument is controlled with great flexibility by two microprocessors. In normal operation the data are divided into azimuthal sectors of 6 to 24° at the nominal spin rate of 3 rpm. After each rotation of the spacecraft, the stepping platform rotates the telescope 30.6° in cone angle so that the flux of particles from every direction is covered each 140 seconds, approximately. In low-flux environments within the jovian magnetosphere the low-energy detectors will be active. In the middle magnetosphere the composition measurement system will alternate between low and high energy every 1⅓ seconds, and in very high flux regions only the high-energy range will be active.

The principal investigator for this experiment is Donald J. Williams of the Applied Physics Laboratory, The Johns Hopkins University.

Plasma Wave Subsystem (PWS). The plasma wave experiment provides measurements of the spectral characteristics of electric and magnetic fields in the frequency range 5 Hz to 5.65 MHz. These time-varying fields are called plasma waves and arise from instabilities in the electron and ion populations in the jovian magnetosphere. The instrument uses an electric dipole antenna to determine the electric field spectrum of plasma and radio waves over the frequency range from 5 Hz to 5.6 MHz and two search coil magnetic antennas to determine the magnetic field spectrum from 5 Hz to 160 kHz.

The plasma wave instrument is an improvement over earlier instruments flown in the Earth's magnetosphere and to the outer planets. Nearly simultaneous measurements of the electric and magnetic field spectra allow us to distinguish electrostatic waves from electromagnetic waves. Improvements in receiver technology give better frequency resolution over a wider frequency range. Also, the spinning of the spacecraft permits the use of a radio direction-finding technique to determine the locations of radio sources.

The sensors consist of one 6.6-m tip-to-tip electric dipole antenna for detecting electric fields and two search coil magnetic antennas for detecting magnetic fields. Accommodations on the spacecraft for these antennas are shown in figure 79. The electric antenna consists of two graphite epoxy elements tapering from 2.0 cm in diameter at the base to 0.4 cm at the tip. The elements are mounted at the end of the magnetometer boom perpendicular to it and approximately 10.6 m from the spin axis of the spacecraft. Preamplifiers are contained in a housing at the base of the dipole elements. Differential charging effects are kept low by a 250-megohm resistor connecting the antenna element to the spacecraft ground.

The search coil magnetic antenna consists of two high-permeability rods, 26.6 and 27.5 cm long, mounted on the high-gain antenna feed. One is optimized for the frequency range 10 Hz to 3.5 kHz and the other for 1 to 50 kHz. The winding on the low-frequency search coil is 50 000 turns of 0.07-mm-diameter copper wire; that on the high-frequency coil is 2000 turns of 0.14-mm-diameter copper wire. The two search coils are mounted at right angles to each other to minimize electric coupling between sensors. Both sensors are mounted perpendicular to the spacecraft spin axis;

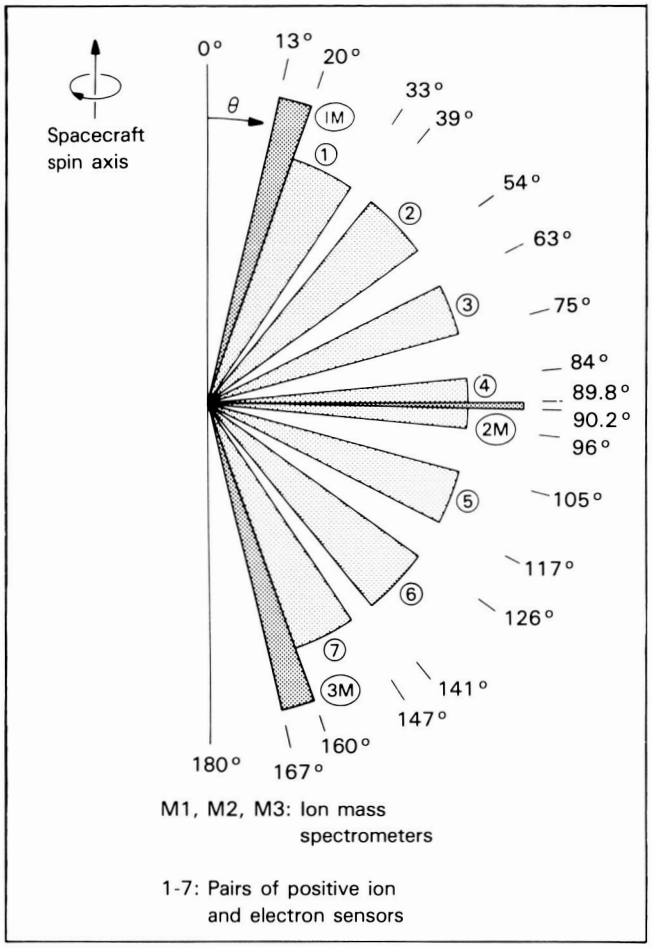

Figure 96. Fields of view for the plasma instrument.

the high-frequency sensor is also perpendicular to the axis of the electric antenna, and the low-frequency sensor is parallel to the electric antenna axis. A preamplifier mounted near the search coil provides a low-impedance signal to the main electronics.

Onboard signal processing takes place within a main electronics package mounted near the base of the magnetometer boom. Signals from the antenna and the search coils are processed by four main elements: a low-frequency spectrum analyzer, a medium-frequency spectrum analyzer, a high-frequency spectrum analyzer, and a wideband waveform receiver.

Several modes of operation and methods of data transfer can be selected by ground command. The high-frequency spectrum analyzer is always connected to the electric antenna; the medium- and

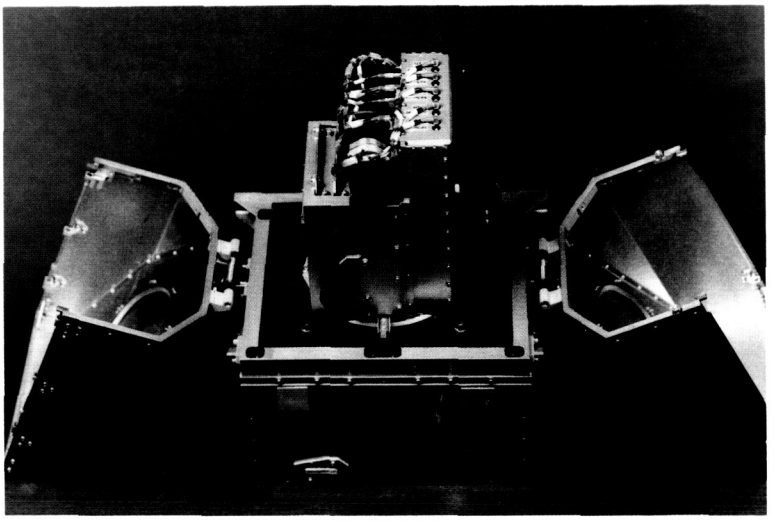

Figure 97. Energetic particles detector (EPD) with protective covers unhinged.

low-frequency spectrum analyzers and the wideband waveform receiver can be connected to either the electric or the magnetic sensors. In normal operation the medium- and low-frequency analyzers are switched back and forth between electric and magnetic antennas so that alternate electric and magnetic spectrums are obtained. The analyzers can also be locked on either sensor to improve time resolution. The wideband waveform receiver provides the most rapid measurements of electric and magnetic field waveforms during periods of special interest, such as satellite encounters.

The principal investigator is Donald A. Gurnett of the University of Iowa.

Dust Detection (DDS). The dust detection experiment (fig. 99) is designed to gain understanding about the physical and dynamic properties of small dust particles in the jovian system. This instrument comprises a set of grids, electron and ion collectors for sensing the impact products of a dust particle, and pulse rise-time circuits to determine the mass and speed of dust particles entering the wide field of view of 140°. The corresponding mass and speed ranges of the dust detector are 10^{-16} to 10^{-6} g and 2 to 50 km/s, respectively.

The main features of the sensor are shown in figure 100. The collecting area of the detector is 1000 cm^2. Positively or negatively charged particles entering the sensor are first detected by the charge (Q_p) that they induce when passing through the entrance grid. This signal is evaluated only when there is a subsequent event recorded by the plasma impact detector, which has a hemispherical gold-plated target. The ions and electrons of the impact plasma are separated by an electric field and accumulated separately by charge-sensitive amplifiers. Two pulses of opposite polarity (Q_E and Q_I) are delivered, from which much information is gathered. The rise time of the voltage pulse (t_{RE} and t_{RI}) is independent of a particle's mass but is a measure of the speed of the particle. The height (greatest polarity) of the pulse represents the total charge and is proportional to the particle's mass multiplied by its velocity. From these data we can derive the mass and speed of the dust particle.

Special design features ensure a positive identification of dust impacts. Some of the positive ions pass through the ion collection grid and are detected by an electron multiplier known as a channeltron. By comparing the channeltron output signal (Q_C) with that from the charge sensitive amplifier, we can separate impact events from any noise. The amplitudes of the positive and negative charge pulses, the channeltron signal, and the corresponding rise time measure the mass and the impact speed of each dust particle in several ways, thereby increasing confidence in the identification of an impact and the measure of the impacting particle's speed and mass.

The location of the dust detection instrument on the spun section of the orbiter allows the experimenters to ascertain the flight direction of the impacting particles for statistical analysis concerning dust streams. It can measure impact rates from 1 particle per 115 days to 100 particles per second.

The principal investigator is Eberhard Grün of the Max-Planck-Institut für Kernphysik, Heidelberg, Federal Republic of Germany.

Radio Science

Galileo's radio telecommunications system will be used by several investigators grouped under the experiment title radio science. There are two groups of experiments: celestial mechanics and relativity, and radio propagation. The celestial mechanics and relativity team is led by John D. Anderson of the Jet Propulsion Laboratory, and the radio propagation team is led by Taylor Howard of Stanford University.

The airborne and ground-based radio communications system of Galileo is more advanced

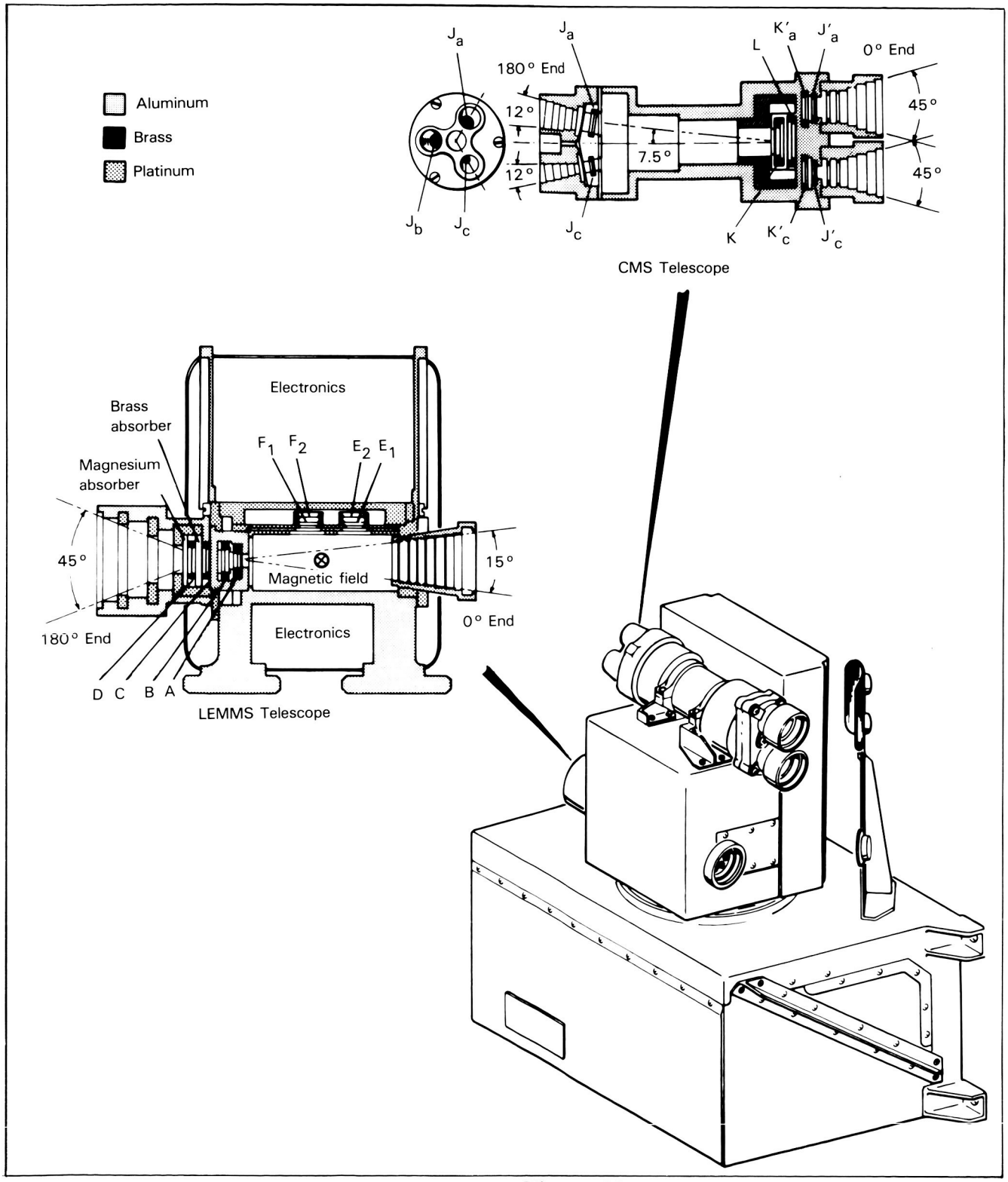

Figure 98. The energetic particles detector showing the two telescopes and an overall view of the instrument.

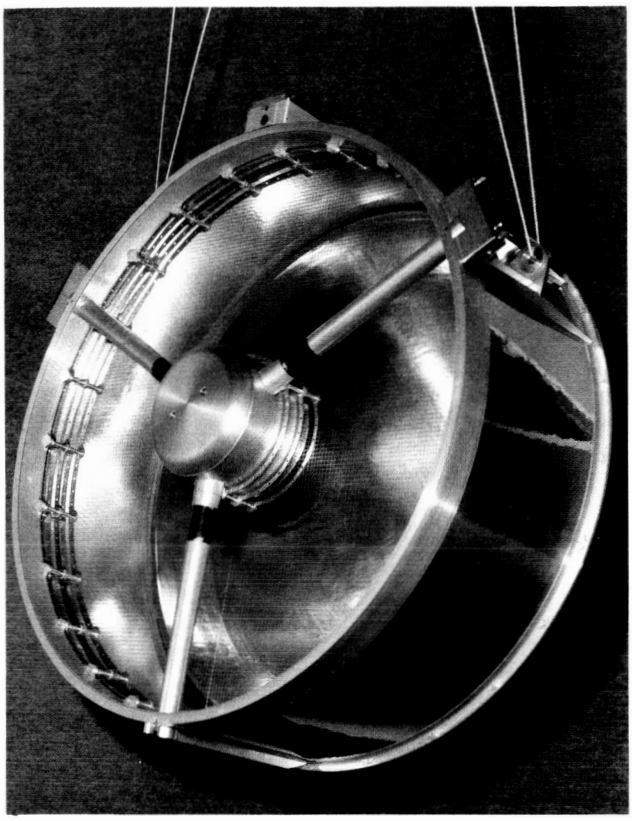

Figure 99. Dust detector (DDS).

than that used on earlier space missions, primarily because communication at higher bit rates was desired. Also, the information about Jupiter obtained from Pioneer and Voyager has suggested improved experiments for the Galileo mission. The system has been improved by designing a larger high-gain antenna with better pointing capability; a higher uplink frequency (7795 versus 2115 MHz); higher power with the same coherent dual-frequency, downlink capability; an ultrastable, onboard oscillator; and linearly polarized waves. The improvements made for communication purposes also benefit radio science; for example, the characteristics of the radio waves have been changed to allow the propagation team to extract more useful information.

The Earth-to-orbiter link consists of either an S-band uplink at 2115 MHz or an X-band uplink at 7795 MHz, from which the orbiter transponder generates coherent, simultaneous downlink signals at 2297 and 8442 MHz. The transponded signals are returned to Earth using transmitter power of up to 20 W and the 5-m high-gain antenna on the spacecraft. The lower-frequency (S-band) signals are linearly polarized, while the higher-frequency (X-band) signals are circularly polarized.

Celestial Mechanics. The celestial mechanics experiments use the radio system to sense small gravitational perturbations on the trajectory which are used to determine the structure of the gravitational fields of Jupiter and the Galilean satellites. The extra round-trip time delay due to the gravity field of the Sun during solar conjunction can be used to constrain theories of general relativity and improve the ephemerides of Jupiter and its satellites. Doppler data using the ultrastable oscillator can be used to measure the general relativistic redshift in the gravitational field of Jupiter. Also, the experimenters will use the 7795-MHz uplink to search for very-low-frequency gravity waves traversing the solar system. If the effects of the spacecraft orbit, the solar wind, and Earth's atmosphere are removed from the doppler data, any remaining deviations can be attributed to gravity waves. The great distance of Galileo from Earth allows very-low-frequency waves to be detected more easily.

A primary aim of the celestial mechanics experiments is to measure the shapes of the gravitational fields of Ganymede, Io, and Europa. The results should allow us to make a better selection of models for the interior of the satellites. The experiment provides data on the central density, differentiation of materials within the satellites, and chemical composition and physical states of the interiors. This is possible because Galileo will approach the satellites much closer than did any earlier spacecraft, so that gravitational effects will be stronger and easier to observe. Changes in Io's mean orbit with time, determined to greater precision, will provide a better measurement of tidal heating and may help solve the question of whether volcanic activity on Io is episodic or continuing.

Radio Propagation. Radio propagation investigations (fig. 101) include studies of the atmosphere, ionosphere, and magnetosphere of Jupiter. Radio occultations of the planet will provide measurements of the pressure, temperature, and density of the atmosphere as a function of height from the apparent doppler shift introduced by atmospheric refraction. Absorption of the radio wave from the orbiter will be used to determine the location of ammonia cloud layers, and measurements of the doppler shift of the probe signal will provide estimates of the horizontal wind velocity as

a function of height. All of these observations will be used to constrain models of the composition, dynamics, and heat flow within Jupiter's atmosphere.

Radio occultation of the planet will also provide measurements of the electron density versus height, electron density irregularities versus height and time, and rotation of the plane of polarization of the orbiter's radio signal by the combination of the magnetic field and plasma (Faraday rotation). Measurements of the amplitude of the probe signal will give further information on electron density irregularities. These observations will constrain models of heat flow and composition within the ionosphere and the direction and magnitude of the magnetic field near to Jupiter.

As Jupiter moves through superior conjunction and passes behind the Sun as seen from Earth, radio transmissions from the spacecraft to Earth pass close to the solar disk (fig. 102). The dual-wavelength signal allows investigation of solar coronal plasma density, spatial distribution, magnetic field, characteristics of turbulence in the plasma, solar wind velocities near the Sun, and characteristics of so-called traveling interplanetary disturbances which consist of large plasma clouds ejected from the Sun.

Probe

Atmospheric Structure Experiment (ASI)

The objective of the atmospheric structure experiment (fig. 103) is to define the thermal structure of the atmosphere of Jupiter starting where the atmosphere first measurably affects the probe's motion and ending at the level at which the descent mission must end because of loss of communications or other reasons. The aim is to define the thermal structure, that is, how temperature, pressure, and density of the upper and the lower atmosphere vary with altitude. Other tasks are to define the temperature and pressure levels at which clouds form, the internal structure of the clouds (which may indicate phase changes or chemical processes), and depths and altitude separations of cloud layers and to help determine the radiative balance in the jovian atmosphere by defining the temperature levels that govern infrared emission. Regions of adiabatic lapse rate and stable lapse rate will be sought to define regions in which convective overturning is occurring—important information relative to the circulation and dynamics of the atmosphere.

Three types of sensors are used to define the atmosphere's structure: temperature sensors, pressure sensors, and a three-axis accelerometer. In principle, three state properties are independently determined by the data. The mean molecular weight can be determined through the equation of state in the absence of significant vertical flow in the atmosphere. Alternatively, given the molecular weight as determined by the companion experiments carried aboard the probe (the neutral mass spectrometer and the helium abundance detector), the three measured properties may be analyzed to determine vertical velocities of atmospheric masses from the difference between the absolute descent rate, defined by the pressure and temperature data, and the velocity of the probe relative to the atmosphere, defined by the accelerometers.

Part of the experiment is also to reconstruct the entry and descent trajectories from the pressure and temperature data and the equation of hydrostatic equilibrium. Altitudes should be defined by this method to within about 1-km accuracy. On the Pioneer Venus probes this method yielded altitude values accurate to within about 0.5 km up to 136 km above the venusian surface.

The principal investigator for the atmospheric structure experiment is Alvin Seiff of the Space Science Division, Ames Research Center.

The essential requirements of a temperature sensor for accurate measurement of local atmospheric temperature on a descending probe are that it be thermally well coupled to the atmosphere and that any heat inputs which are not of local atmospheric origin be kept small. Thermal coupling is obtained by locating the sensor on the probe in a region of high relative flow velocity and by designing the sensing element to have a high heat transfer coefficient and low thermal inertia. Other heat inputs are minimized by selecting support material that has low thermal conductivity, by having a highly reflective sensor surface to reduce radiation input, and by avoiding convection from the probe boundary layer by locating the sensing elements well above this layer. Self-heating is kept low by restricting the current needed to excite the sensor.

The sensor is a dual sensing element, platinum resistance thermometer. Primary and secondary sensors are mounted on a single head. The primary is a free wire, approximately 1.1 m long by 0.1 mm

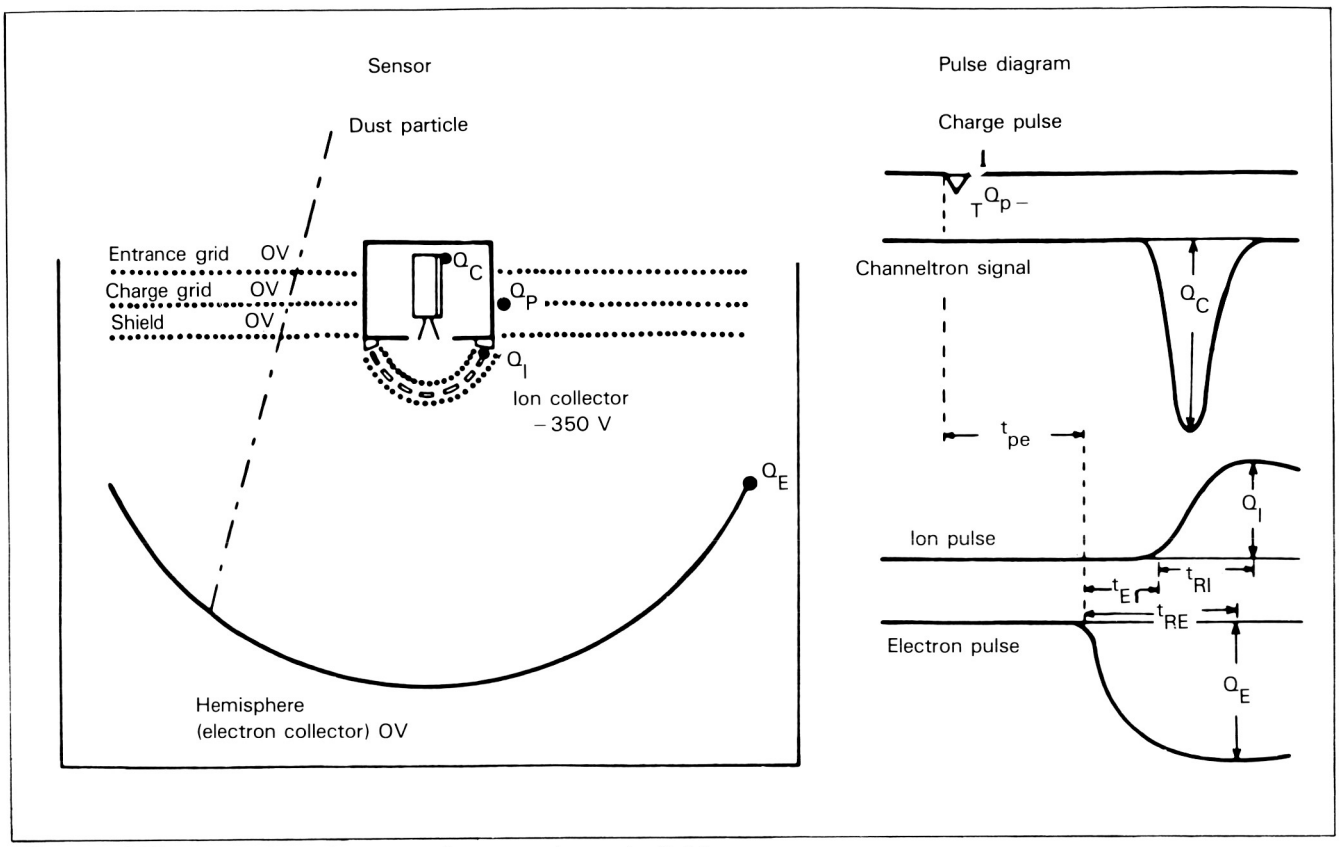

Figure 100. Dust detection experiment: schematic (left) and quantities measured by the instrument (right).

in diameter, wound over glass insulation on a frame of platinum-rhodium alloy. The secondary sensor is a 1-cm-long by 0.25-mm-diameter wire laid down on a raster over a glass film and covered by a glass film on the leading quadrant of the sensor support frame's outer member. The frames are made of platinum-rhodium alloy to match the thermal expansion coefficient of the sensing elements and to avoid resistance changes due to thermal strain. The glass coatings match the thermal expansion coefficient of platinum.

The support stem is a low-conductivity, thin-walled tube of stainless steel which limits conduction from the probe to the sensor.

The temperature range is 0 to 500 K, which permits measurements to continue if the probe's mission extends below the 16-bar level of the nominal mission where the temperature is expected to be 400 K. Response times for the primary sensor range from 16 ms at deployment to 5 ms at the 16-bar level. For the secondary sensor these times range from 0.3 second at deployment to 0.08 second at the lower level. The accuracy is expected to be about 1 K.

The pressure sensor has to cover a wide range from 0.1 to 16 bars by means of several sensors with ranges related approximately geometrically—0.5, 4, and 28 bars. The first two operate during the period in which the probe is descending to a pressure level of 4 bars. They are read alternately for accuracy checks and redundancy of this important data. Below the 4-bar pressure level, only the 28-bar range sensor is used.

Two sensor types were available for use on Galileo: those used earlier on the missions to Mars and Venus, both of which gave excellent results. The Viking type was selected because it demonstrated high reliability by returning data from the martian surface for several years. Pressure is sensed by the deflection of a thin

stainless steel diaphragm which is 1.5 cm in diameter.

The deflection is measured by changes in reluctance of the air gap between the diaphragm and the central pole piece of a magnetic circuit of which the diaphragm is a part.

Two circuits are used, one on either side of the diaphragm, and the inductances which they affect oppositely are coupled to produce a signal proportional to the deflection of the diaphragm. This sensor has high inherent stability. Its measurements are repeatable within 0.1 percent of full scale on each range. Zero offsets will be checked periodically on the trip to Jupiter, and the accuracy goal is 0.5 percent of the reading.

The axial accelerometers are also required to cover a wide range from one-millionth of a g to 400 g and to be accurate within about 100 parts per million to permit accurate reconstruction of the entry trajectory. Sensors developed by industry for the missile program met most requirements but required further development to meet the high-g loads which could result if the entry angle of the probe became steeper than expected in a colder-than-expected jovian atmosphere.

A test mass is free to rotate about a flexural hinge under the action of an imposed acceleration. A coil wound on the test mass carries a current which is proportional to the acceleration and is generated by the sensor servo electronics. This current interacts with the field of a permanent magnet to produce a restoring force to oppose the motion of the test mass. The servo electronics adjusts the current to hold the test mass in a nearly fixed, null

Figure 101. As part of the radio propagation experiments, the scattering and refraction of radio waves from the orbiter will be used to study the atmosphere and ionosphere of Jupiter. Similar experiments will be attempted on satellite atmospheres and waves and the rings of Jupiter. The radio waves from the probe will also be used to study the atmosphere and ionosphere of Jupiter, with the signal source *inside* the atmosphere and the phase and amplitude comparator onboard the orbiter instead of on Earth.

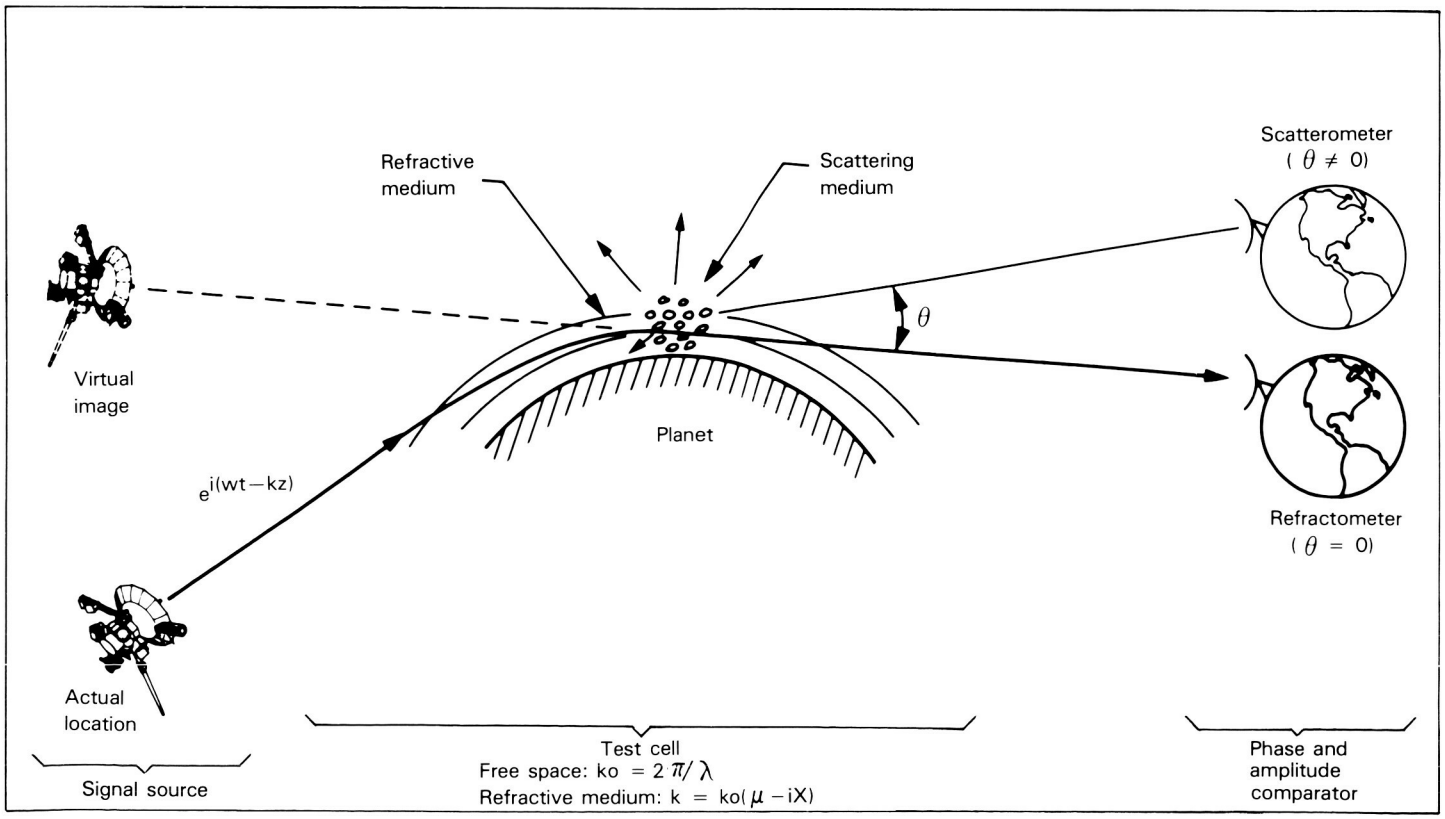

position, thereby permitting the sensor to have an output which is close to perfect linearity. Position is sensed by capacitive pickoffs and is held constant to within a few milliradians. The current in the test mass coil is read to measure the acceleration. The sensor is depicted in figure 104.

There are two axial sensors, each having four ranges with full-scale values of 0.0125, 0.4, 6.4, and 410 g. The sensors are read alternately at intervals of 5/16 second during the entry of the probe into the atmosphere and at 8-second intervals during the descent, when the acceleration is averaged for each sensor over the 16-second interval preceding the reading. There are also two lateral sensors which are vectorially combined to obtain the acceleration normal to the axis of the probe, which is read once each second during probe entry. During descent, three values are read every 16 seconds: the average, the minimum, and the maximum values during the sampling interval.

The acceleration measured by the prime axial sensor and the acceleration normal to the probe's axis are used to measure the statistics of departure from the mean value at plus or minus four levels of departure axially and at four levels in the resultant normal acceleration channel. Such data will be used to analyze the influences of atmospheric turbulence on motion of the probe.

Neutral Mass Spectrometer (NMS)

Despite intense efforts by observers and theoreticians, the gross composition of the jovian atmosphere is not accurately known. The primary objective of the probe's neutral mass spectrometer (fig. 105) is to determine the abundances and isotope ratios of major constituents as a function of altitude to a high degree of accuracy. We will also search for trace constituents. The instrument was developed by the Goddard Space Flight Center, and the principal investigator is H. B. Niemann of Goddard.

To enhance the range of measurements, the basic sample inlet system is supplemented by three selective subsystems: a noble gas purification cell and two enrichment cells for the more complex compounds.

The inlet system, which is shown schematically in figure 106, consists of two fully self-contained units which operate in sequence as the probe descends through the atmosphere. Both units contain a high-pressure flow system with gas inlets placed near the apex of the probe and exit ports placed at the minimum pressure point inside the probe. For design purposes, the ambient pressure at the exit was assumed as the worst condition expected during the mission. The pressure difference

Figure 102. When the spacecraft is on the far side of the Sun from Earth, the radio signals which pass close to the Sun are deflected and provide information about the structure of space. At the same time, the signals pass through the solar corona and provide information about conditions there.

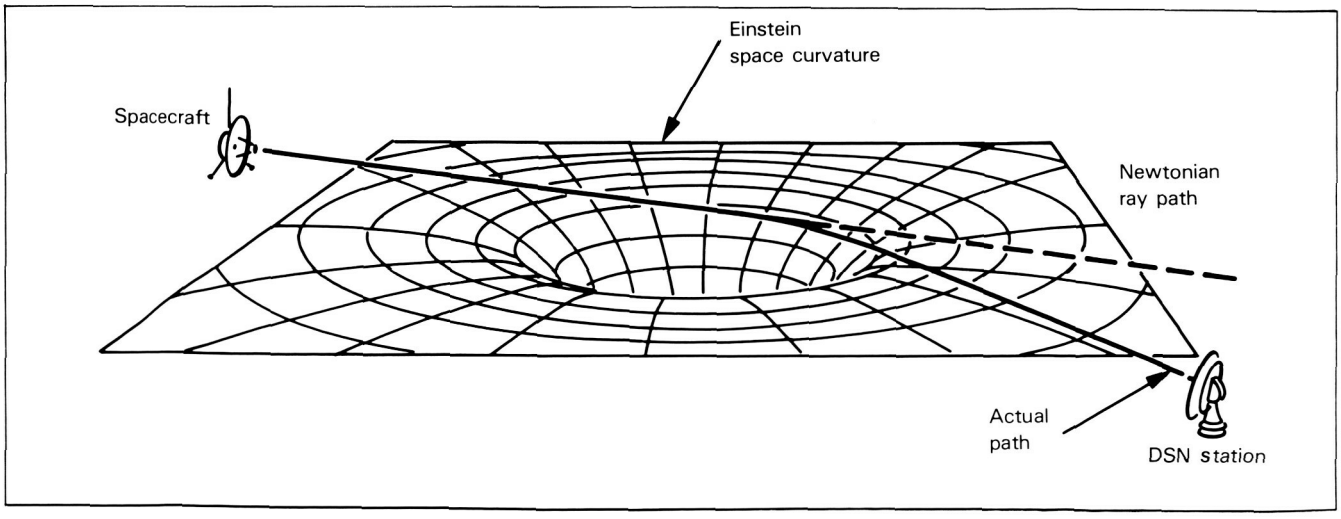

of about 6 mbar between the stagnation point and the low-pressure point causes a flow past the pressure-reducing leaks. Inlet and outlet ports are sealed by metal-ceramic devices and kept under vacuum prior to entry. After entry they are opened in sequence by redundant pyrotechnic actuators.

A small fraction of the gas flowing through the high-pressure flow system is conducted through the pressure-reducing leaks into the ionization region of the ion source. The leaks, which are arrays of micrometer-sized glass capillaries (typically seven capillaries per leak), have conductances chosen so that the pressure in the ion source does not exceed 10^{-4} mbar. The sample enrichment system is an integral part of the high-pressure flow system. Atmospheric gas, after passing by the capillary leak, is also conducted to enrichment cells, which contain getters that, when activated, chemically bind reactive gases during the measurement sequence and thus allow a pure noble gas analysis. The cells are packed with gas-absorbing compounds chosen to absorb trace gases such as hydrogen sulfide, ammonia, and phosphine and complex hydrocarbons. Gases absorbed by the cells are released by a programmed heating cycle during descent of the probe. During these cycles the cells are isolated from the main flow system by solenoid-operated microvalves and are connected through separate capillary leaks to the ionization region.

Two independent leaks are employed for enriching the sample. These, and the first direct leak, can be isolated from the ion source redundant ball closures to prevent the ion source pressure from exceeding its optimum value, and to permit repeated observation of system background pressure after the initial sampling and enrichment sequences are completed. The second independent inlet system is opened to the atmosphere after the first system has been isolated from the ion source. Sample distortion caused by gas–surface interactions is minimized by directing the high-pressure flow against the capillary leak and by so locating the leaks in the ion source that the gas leaves the capillaries on the ion source side directly through the ionizing electron beam. The gas emitted from the capillaries can thus be isolated and analyzed without experiencing surface collisions with the walls of the ion source.

A cross-sectional view of the ion source design is given in figure 107. The gas flow path for the second inlet system near the leak is marked by arrows.

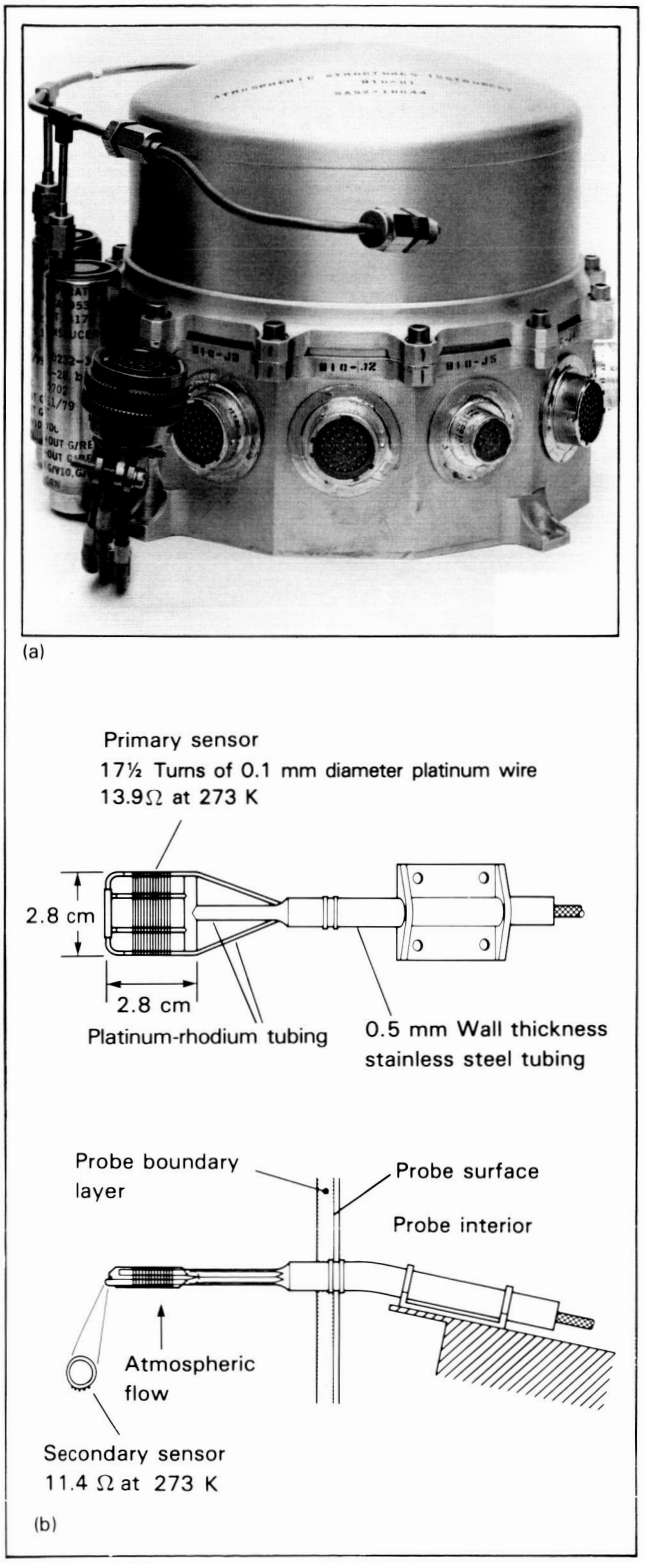

Figure 103. (a) Atmosphere structure electronics with pressure sensors attached. (b) ASI temperature sensor.

Also shown are the positions at which the sample gases enter the ion source from the first leak and the leaks which supply the enriched and purified samples. Three different ionization energies are selected by changing ion source potentials.

Limits of the pumping speed in a flight system do not permit instant removal of the gases from the ion source after they initially pass the ionization region. A component of randomized gas therefore contributes to the measurement. The ratio of direct beaming to the randomized component strongly depends on the geometry of the system. It is most critically affected by the distance between the electron beam and the capillary exit and by the cross-section of the electron beam. A ratio of at least 5:1 is expected based on laboratory tests on an engineering unit.

The high-pressure operation of a mass spectrometer is limited by mean free path considerations leading to losses due to ion–molecule collisions. A higher density in the ionization section can be tolerated as a result of beaming because the ionization volume in which this high density exists is extremely small, having only a small effect on the ion path.

The measurement sequence is as follows. Initially, all microvalves are closed and all ball closures are open. The first inlet breakoff is opened

Figure 104. Four of these accelerometers are used to measure axial and lateral accelerations as part of the ASI experiment on the probe.

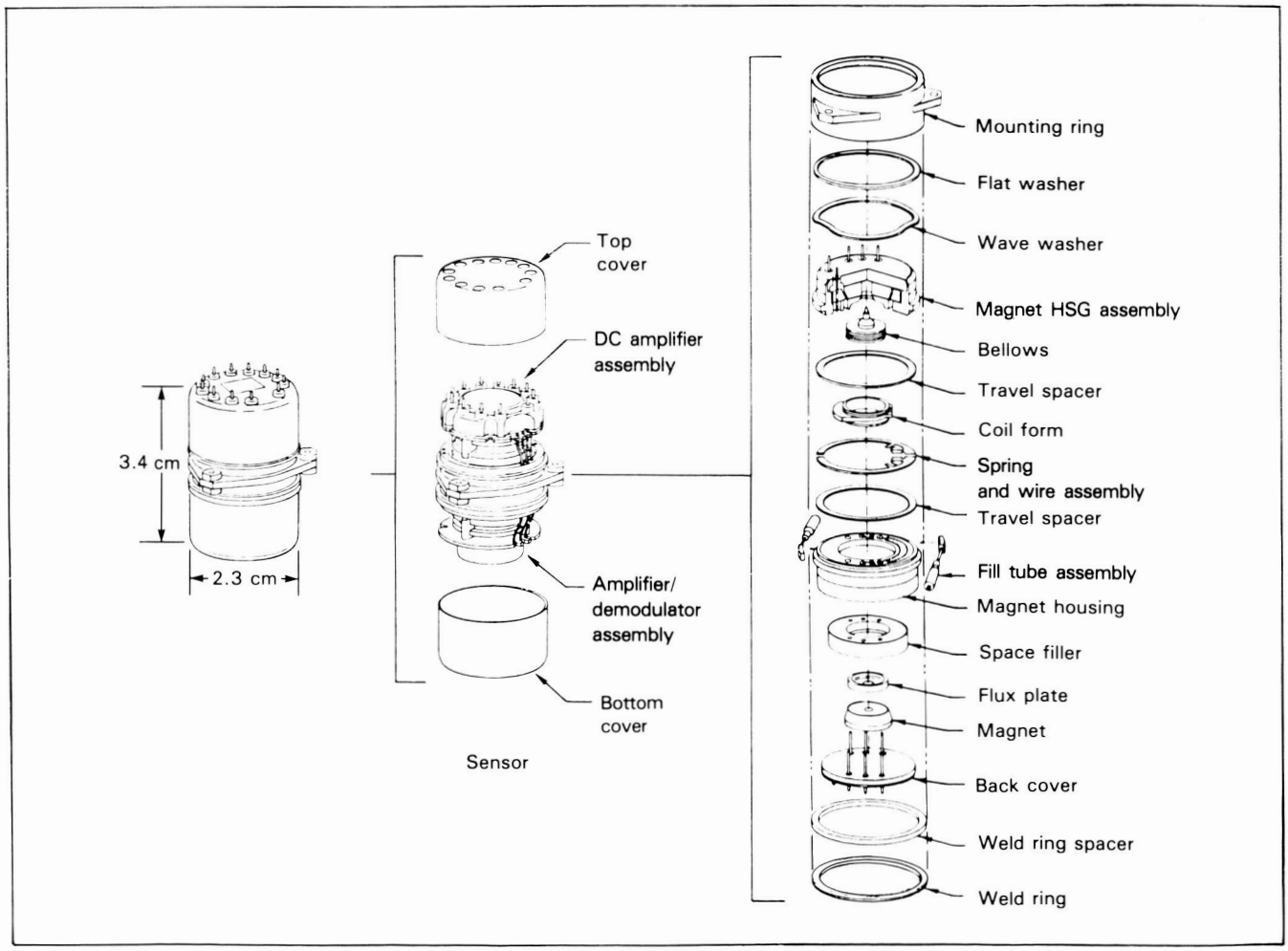

when the probe reaches a pressure level of about 100 mbar. Approximately 1 second later the first outlet breakoff is opened, allowing ambient gas from Jupiter's atmosphere to flow past the capillary leak, through which a small fraction is conducted into the ion source.

While the direct analysis is made other valves are opened for a nominal 2 minutes to allow ambient gas to flow through the enrichment cell until its getter is saturated with hydrogen and the getter housing volume is filled with gas. Next, two of the valves are closed as another valve opens and the remaining gas, mostly hydrogen, is absorbed by another getter. Remaining in the enclosed volume are the noble gases and some hydrogen whose partial pressure is determined by the equilibrium vapor pressure of the hydrogen dissolved in one of the getters. In the third step two valves are closed and the other opened to introduce a fraction of the gas in the volume enclosed by four valves, through a leak into the ion source.

Prior to opening of one of the valves, a ball closure is shut and the ion source and analyzer section of the mass spectrometer are evacuated to background level via two more getters and a sputter ion pump.

Mass spectra are obtained during pump-down time to record the remaining background gases. The noble gases subsequently introduced into the ion source through a leak are analyzed for approximately 1.5 minutes. During this time the enrichment cell is heated, the gases absorbed are desorbed, and, after opening another valve, they are added to the noble gases flowing though the leak into the ion source. After about 1.5 minutes of analysis of these gases the ball closure is shut and the mass spectrometer is pumped once more to background pressure level so that the partial pressure of the background gases can be measured with the mass spectrometer. The first inlet system is now completely isolated from the mass spectrometer, and the sequence is repeated for the second inlet system, for which a separate noble gas cycle is not intended.

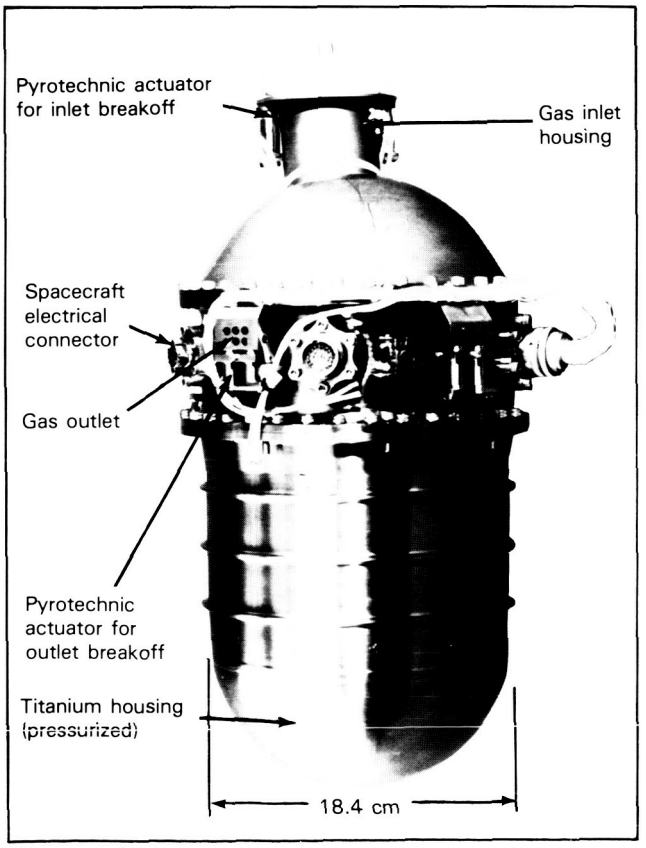

Figure 105. Neutral mass spectrometer (NMS).

The ion source (fig. 107) uses electron impact ionization in a miniature, dual-filament configuration. The second filament is turned on automatically should the first filament burn out or break. A collimated electron beam is directed through the ionization region past the capillary leak. The energy of the beam is varied to permit species to be identified and discriminated by observing spectra of fragmentation patterns at several different electron energies. Chemical reactions of gases on the surface of the hot filament are kept low by isolation through narrow slits and by separate pumping of the filament region. Ions are focused into the mass analyzer for filtering. The importance of minimizing gas-surface interactions in the high vacuum side requires that the ion source be a very compact and integral part of the sample inlet system.

A quadrupole analyzer filters the ion beam produced by the ion source, transmitting ions of a chosen charge-to-mass ratio only. The selected ion beam is focused on a secondary electron multiplier ion detector. The quadrupole mass filter was chosen in preference to a magnetic sector spectrometer because of its light weight, versatility, high resolution, and simplicity. The only dimensionally critical element in the system is the precision rod assembly, whose rigid and compact design has proved to be extremely stable. The normal

mass range covered is from 1 to 52 AMU (atomic mass units) with occasional mass sweeps of 1 to 150 AMU.

The pumping system establishes a flow of sample gas through the ion source at a particular pressure when a sampling device is opened, and after analysis and closure, it removes the sample from the ion source region. Nonevaporable getters and sputter ion pumps are used because of their simple adaptation to spaceflight systems. They depend only on electrical power for their operation and do not have moving parts. The application to the probe mass spectrometer required care, because hydrogen and helium are the major gases in the jovian atmosphere. While hydrogen is absorbed at a very high rate by getter materials, helium absorption is practically nil. Sputter ion pumps also pump hydrogen with high efficiency, but hydrocarbons are synthesized in the pump by reactions of hydrogen ions with carbon trapped on the pump surfaces. The effective pumping speed for helium is usually low because of the low ionization cross-section of helium and the requirement that helium be buried physically in the pump elements since it does not become chemically bound or go into solution as does hydrogen. This requires sputtering of comparatively large amounts of cathode material, which tends to release large quantities of gases previously entrapped in the pump surfaces. Thus, to eliminate the synthesis of hydrocarbons in the sputter pump, a cascaded pump system is used.

The high-capacity getter pump is located ahead of the sputter ion pump. The gas flow from the mass spectrometer into the getter pump is conductance limited to maintain a constant pumping speed during the measurement phase. Hydrogen and all reactive gases are absorbed in the getter before they reach the sputter pump. Helium is the only major gas to be pumped by the sputter pump.

Gases emitted by the pump pass the getter

Figure 106. Inlet systems for atmospheric samples by the neutral mass spectrometer.

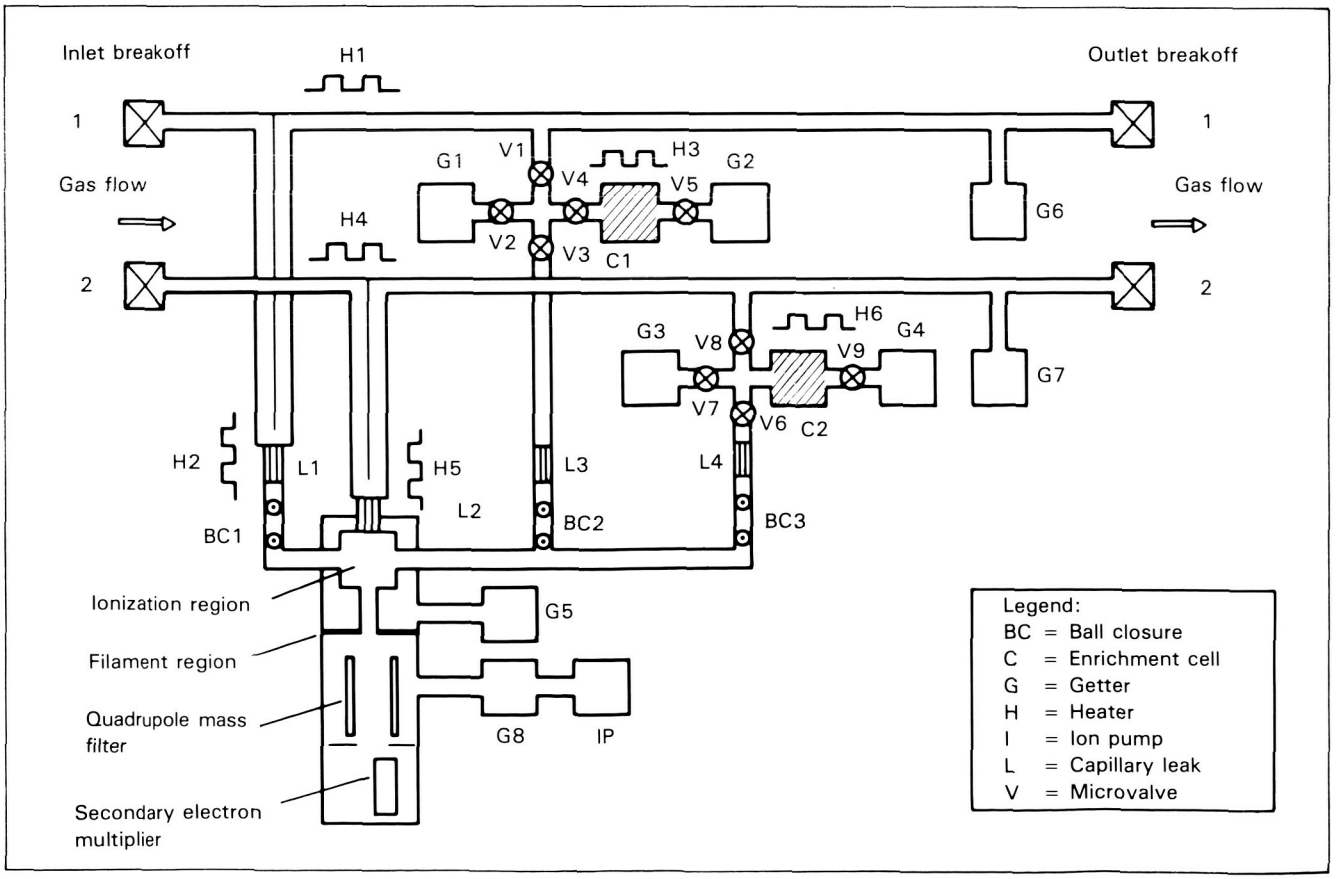

before they can enter the mass spectrometer, and their contribution to the ion source gas is therefore significantly reduced. Small sputter pump instabilities, not fully avoidable with the present state of technology, are buffered by the preceding getter chamber. A drawing of the instrument is shown in figure 108.

The electronic system for the mass spectrometer is based on concepts developed for previous spaceflight applications. Power commands and timing events are accepted and processed by a logic system. The primary measurement is stored in an output register for interrogation by the spacecraft's telemetry system.

The instrument is under the control of a programmer which is an array of read-only memory (ROM) devices. During each of 8192 0.5-second intervals each of six instrument variables, including mass number, ionization energy, and inlet system configuration, can be configured to any allowable state. Mass number selection in a quadrupole is a function of amplitude and frequency of the radio

Figure 107. Ion source for the probe's neutral mass spectrometer.

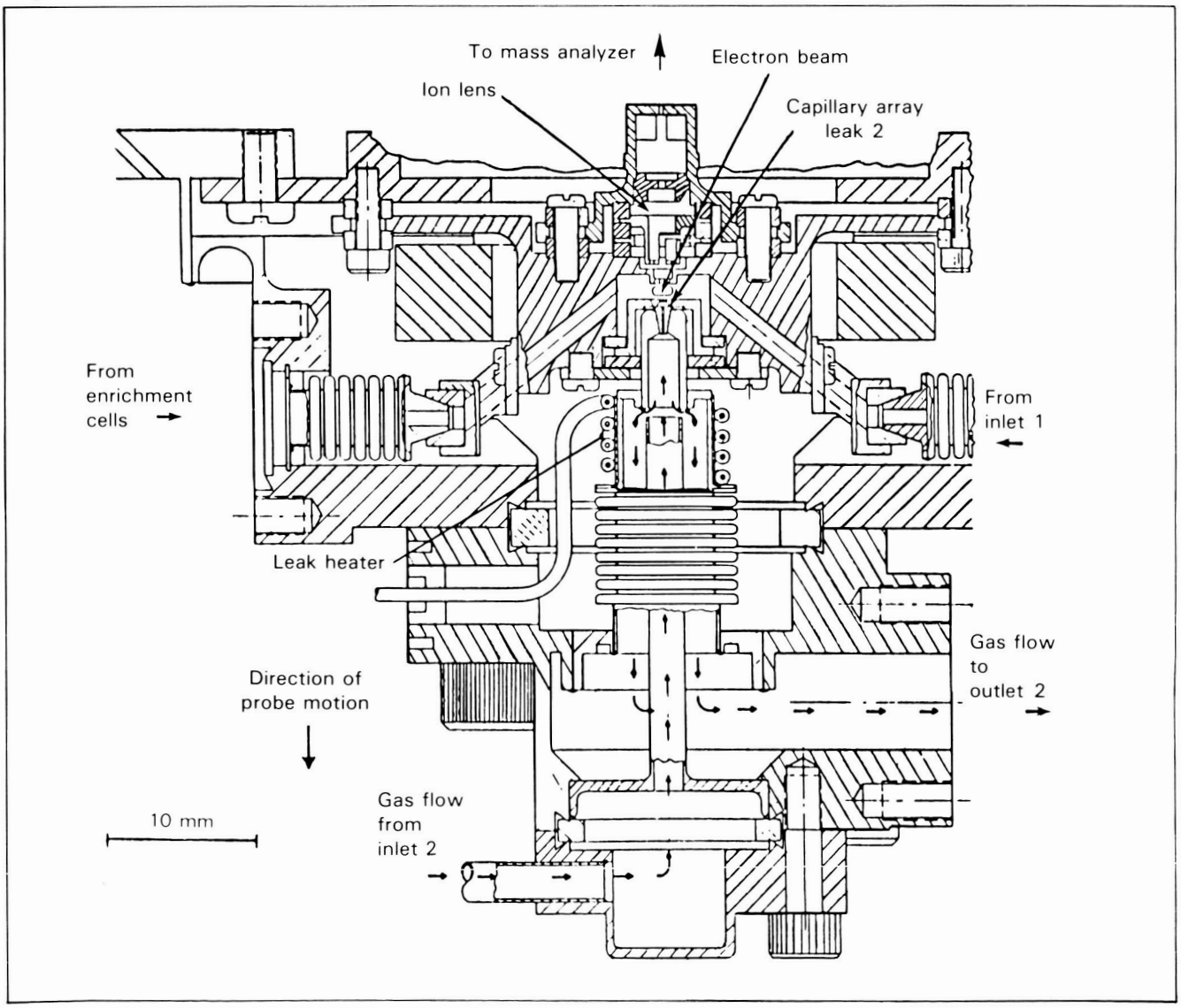

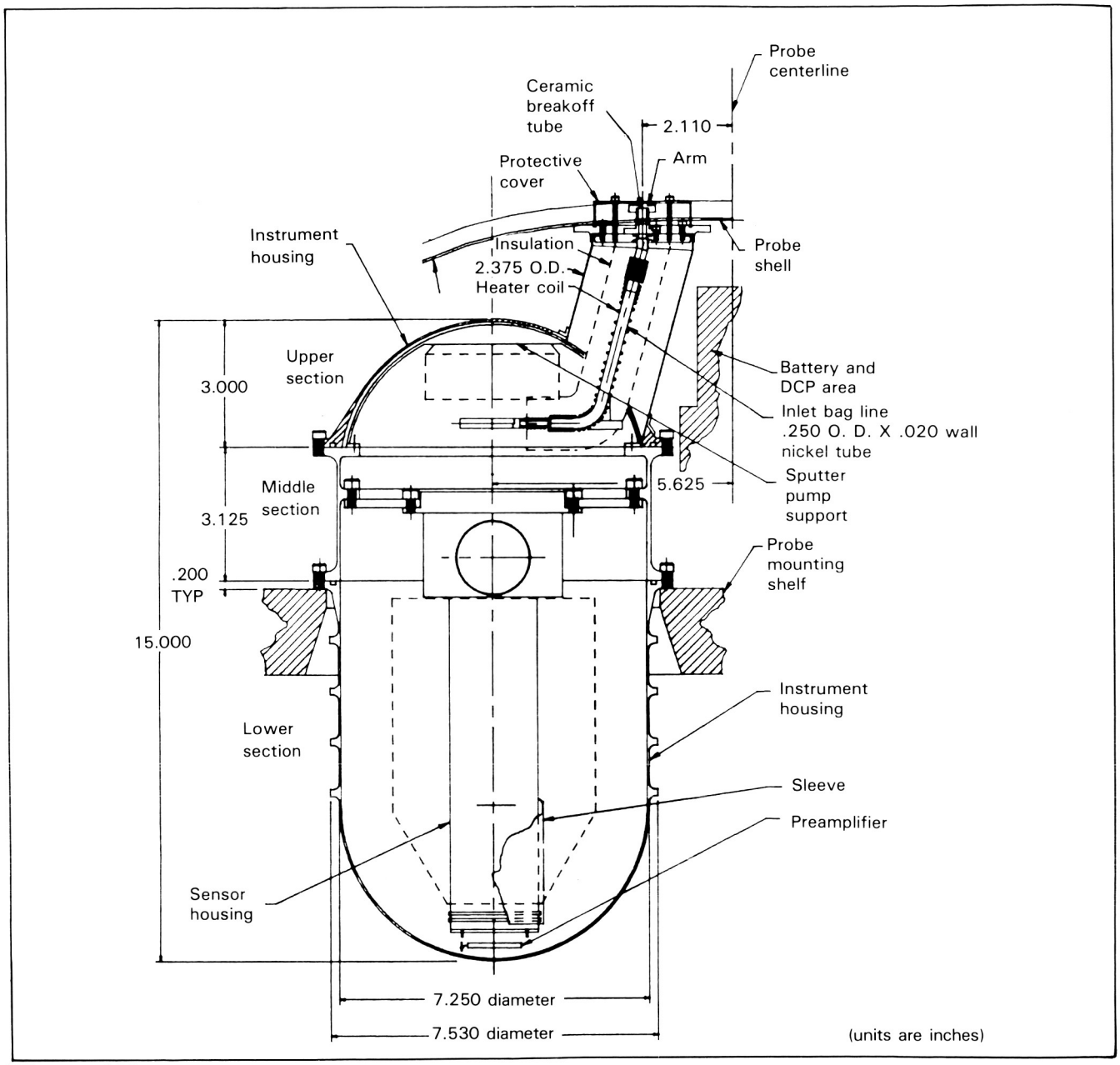

Figure 108. Diagram of the neutral mass spectrometer.

frequency signal applied to the rods. Two frequencies are used: one to cover the mass range 0.5 to 20 AMU and the other to cover the range 20 to 150 AMU. Mass number is proportional to the amplitude of the radio frequency signal. The instrument has constant resolution over the total mass range.

The total weight of the instrument is 11.8 kg. It consumes 25 W on the average, of which 12 W are needed for the pumps and heaters.

Nephelometer (NEP)

The nepholometer experiment (fig. 109) is designed to make in situ measurements of cloud structure and to determine the character of the particles in the main clouds and in the atmosphere of

Jupiter as the probe descends through it. A knowledge of the physical properties of cloud particles, including their size, number density, and optical parameters such as the index of refraction, is essential to an understanding of the energy balance of the planet. Since the interaction of light with the particles is influenced by these properties, the nephelometer experiment, which measures the light-scattering properties of particles, will yield valuable information on the characteristics of the particles.

The NEP experiment has several scientific objectives. At altitudes corresponding to pressures of 0.1 bar to greater than 10 bars, it will determine the presence and vertical extent of the clouds with resolution and at altitude intervals of less than 1 km. At these altitude intervals it will detect clouds containing more than 3 particles/cm^3 in which the particles are about 1 μm in diameter. Also, the experiment will determine the characteristic dimension for particles in the range of 0.5 to 20.0 μm for each altitude interval and determine the particle number densities for clouds containing more than 3 particles/cm^3 of characteristic dimensions between 0.5 and 20.0 μm at each altitude reported. Finally, NEP will determine whether the particles are spherical to find out whether they are liquid or solid (ice). The principal investigator for this experiment is Boris Ragent of Ames Research Center.

The instrument consists of an optical unit and an electronics unit. The optical unit has a forward scatter unit immediately aft of a backward scatter unit. The forward scatter unit protrudes radially from the probe's skin, while the edge of the backward scatter unit is flush with the skin.

The forward scatter unit consists of transmitter, mirror, and receiving assemblies rigidly mounted together on a deployable arm. The protruding arm is extended outside of the probe's skin after removal of the heat shield assembly. It holds the mirror assembly rigidly at its extremity, thus defining the path between the transmitter and receiver assemblies. The arm is designed to allow cloud particles to flow through the instrument's sensitive volume as the probe descends.

The transmitter consists of a solid-state laser diode, source and associated driving electronics, a collimating lens for collecting and focusing the light, and a long collimating tube containing a number of apertures for defining the emitted light beam and minimizing scattered light. A solid-state light detector near to the light source is used to monitor the strength of that source.

The mirror assembly consists of four 90°

Figure 109. Nephelometer (NEP).

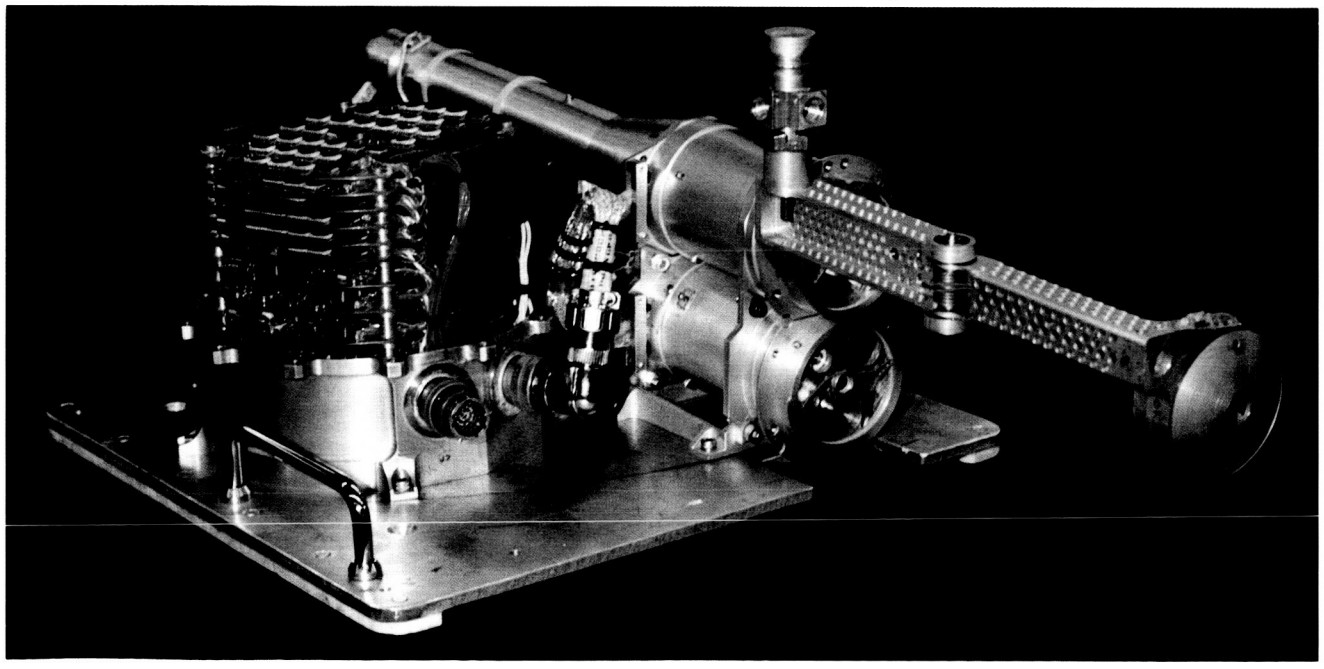

segments of conical mirrors, each of whose axes is coincident with the optical axis of the transmitter assembly. These segments have cone semiangles of approximately 87.25°, 82.5°, 70°, and 55° and are mechanically fastened to form a circular assembly that is rigidly aligned by the deployed mounting arm at a fixed distance from the aperture of the transmitter assembly facing it. The resultant optical axis is coincident with the optical axis of the transmitter assembly.

The transmitted beam passes to the external atmosphere through a hole in the center of the mirror. Light is scattered by atmospheric particles encountered by the beam at scattering angles of approximately 5.8°, 16°, 40°, and 70°. This scattered light is reflected by the appropriate mirror in a direction parallel to the optical axis of the transmitter.

A heater unit is mounted on the back of the mirror assembly to reduce condensation during descent through the jovian atmosphere.

The receiver assembly consists of four subassemblies arranged peripherally around the end of the transmitter's collimator tube. Each consists of a plastic Fresnel lens which focuses incoming light that is parallel to its optic axis onto an aperture behind which is a solid-state silicon detector and an electronic preamplifier. This registers the incoming light. The optic axis of each lens is parallel to that of the transmitter assembly but is displayed radially so that it intersects its opposing conical mirror at the approximate centroid of the projected area of the mirror in the lens plane. The aperture for each subassembly, together with the applicable conical mirror and the dimension of the transmitter beam, defines the angular acceptance function for each channel. A small plane mirror is mounted outboard of the 5.8° mirror quadrant and is used in conjunction with a light source and detector in the backward scatter unit to monitor alignment and surface contamination. A cover plate containing a surface metallic grid covers the entire receiver assembly, and solid-state temperature sensors are used to monitor the temperature of the receiver detector and preamplifier assembly.

The backward scatter unit also contains a transmitter and a receiver unit. The transmitter unit consists of a solid-state laser diode source, driver electronics, source monitoring detector, and a collimating and focusing lens. The receiver assembly is similar to that in the forward scatter unit. No reflecting mirror assembly is used, and the sensitive sampling volume is determined by the overlap of the fields of view of the transmitter and receiver assemblies. A solid-state, light-emitting diode, focusing lens, and source monitor are incorporated in the backward scatter unit so that its beam is directed at the plane mirror mounted outboard of the 5.5° mirror segment of the forward scatter unit. The light reflected from this mirror is focused onto a solid-state detector in the backward scatter unit. The combination is used to monitor both the alignment of the forward scatter unit and the amount of surface contamination of the mirror. The enclosure of the backward scatter unit is similar to that of the forward scatter unit but is much shorter and does not protrude beyond the skin of the probe.

Both the forward scatter and backward scatter units are vented so that the internal pressure essentially matches the internal pressure of the probe.

Although some parts of the electronics and circuitry, especially preamplifiers, biasing circuits, and source driving circuits, are incorporated into the forward and backward scattering optical units, an electronics unit contains the bulk of the electronic components and circuits. These include power conversion from the probe's bus supply to provide power for the instrument, timing and log control circuits, amplifiers, filters, integrators, multiplexors, digitizing equipment, data compression circuits, memory storage, and circuits to interface with the probe's telemetry system.

Data output from the electronics unit to the telemetry system consists primarily of angular scatter measurements. However, calibration and monitoring data are also provided. They include alignment and mirror surface contamination monitor outputs, the source monitor readings for the forward and backward scatter laser diodes and alignment source light-emitting diode, measures of the DC offsets of each of the major scatter channels, outputs of the alignment and contamination detectors, three temperature measurements internal to the scatter units and the electronics box, and a reference voltage reading.

In addition, the gain of the 15° forward scatter channel is indicated four times during each of the integration periods reported for this channel to indicate the presence of any fluctuations in the cloud structure during an integration period.

For typical terrestrial-type aerosols, the channel sensitivity would correspond to visibilities extending from greater than 30 km to less than a few meters. The sampling sequence is such that immediately on removal of the aeroshell and the heat shield, the nephelometer will take ten complete sets of readings, each at 3-second intervals, then ten readings at 4-second intervals, and so on until it requires 120 seconds for ten readings. After that the sample period remains constant at 8 seconds for the remainder of the descent period. These times correspond to less than 1 km altitude resolution at the time the instrument is turned on, to less than ⅓ km at the end of the probe's mission.

The nephelometer weighs 4.4 kg and consumes about 15 W.

Energetic Particles Investigation (EPI)

A major science objective of the energetic particles investigation (fig. 110) is to study the energetic particle populations in the innermost regions of the jovian magnetosphere—within 4 radii of the planet—and into the upper atmosphere. To achieve this objective the energetic particles instrument will make omnidirectional measurements of four different particle species: electrons, protons, alpha particles, and heavy ions (atomic number >2). Intensity profiles with a spatial resolution of about 0.02 Jupiter radii will be recorded. Three different energy range channels are allocated to both electrons and protons to provide a rough estimate of the spectral index of the energy spectra. In addition to the omnidirectional measurements, sectored data will be obtained for electrons, protons, and alpha particles to determine directional anisotropies and particle pitch angle distributions. The principal investigator is H. Fischer of the University of Kiel, Federal Republic of Germany.

The detector's design will hold the counting rates below 3 million counts per second under the most intense flux conditions. The lower threshold for the particle species to be measured is defined by the material thickness of the probe's aft heat shield. Because of budgetary constraints, the thickness of this material within the experiment's acceptance cone could not be reduced. The heat shield consists of layers of aluminum, silicone adhesive, and phenolic nylon. For perpendicularly penetrating particles it has a resulting thickness of about 0.58 cm, which is equivalent to about 0.87 g/cm^2.

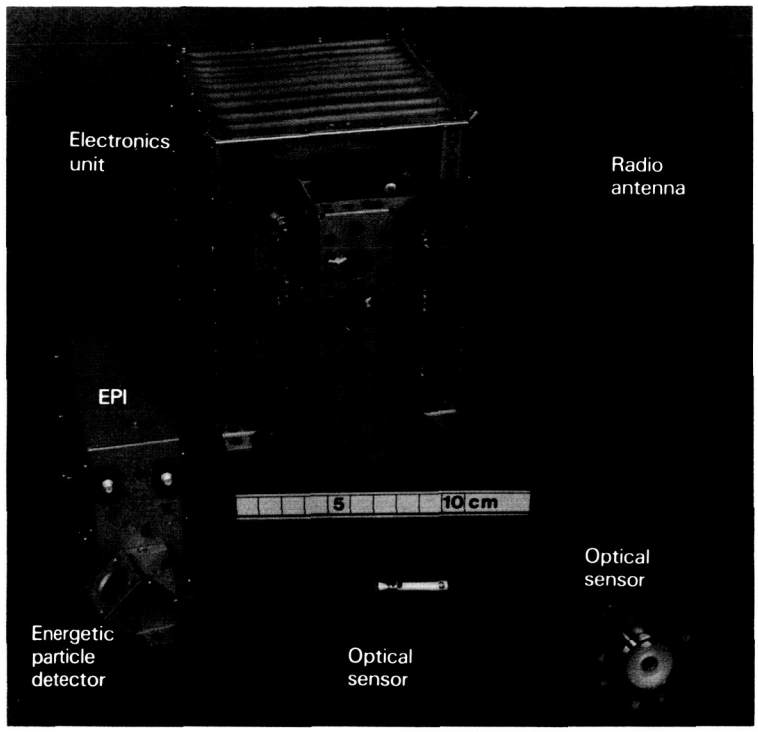

Figure 110. Lightning and radio emission detector/energetic particle instrument (LRD/EPI).

The detector assembly is a two-element telescope using totally depleted, circular, silicon surface barrier detectors. Both detectors have a radius of 0.14 cm with sensitive areas of 0.062 cm^2 and thickness of 0.05 cm. A 0.3-cm-thick (equivalent to 1.55 g/cm^2) brass absorber is inserted between the detectors. The total length of the telescope (upper front detector to lower surface back detector) is 0.6 cm.

The detector assembly is surrounded by tungsten shielding with a cylindrical wall thickness of 0.27 cm (equivalent to 4.86 g/cm^2). The complete probe material, estimated to be equivalent to at least 150 g/cm^2, forms the shielding at the rear of the telescope. A negligible background rate is thus expected from the rear. The tungsten shielding cylinder is elongated beyond the front detector surface and forms an open aperture cone with a length of 0.67 cm and an opening diameter of 0.9 cm. For single particle counting events in the front detector, the aperture opening and the detector area define an opening angle and a geometric factor.

The telescope's axis is mounted at an inclination angle of 41° with respect to the probe's spin

axis. Pitch angle distributions can cover various ranges, depending on the orientation of the spin axis relative to the direction of the ambient magnetic field. Two modes are provided, one for the magnetosphere and one for the atmosphere.

Telescope and analog electronics, the detector bias supply converter, and three housekeeping channels for monitoring leakage currents in detectors are contained in the sensor box. The scaling, data processing, and data formatting are executed with the lightning and radio emission detector data in the central electronics box.

Lightning and Radio Emission Detector (LRD)

The lightning and radio emission detector (fig. 110) carried by the probe is designed to verify the existence of lightning in the atmosphere of Jupiter. The experiment will also provide data on the radio frequency noise spectrum from the jovian atmosphere and will make radio frequency measurements at about 4, 3, 2, and 1 planetary radii above the cloud tops as the probe approaches Jupiter. The principal investigator for the experiment is L. J. Lanzerotti of Bell Laboratories and the University of Florida.

The LRD instrument consists of three basic sensors connected to one electronics box which is shared with the energetic particles instrument. One sensor is a radio frequency antenna, and two of the sensors are photodiodes behind fisheye lenses. The instrument makes measurements in the frequency range from about 10 Hz to 100 kHz, both in the time domain (primarily for deducing from the wave shapes the physical properties of close lightning) and in the frequency domain with three narrowband channels (primarily for deducing the physical properties of distant lightning).

The radar frequency sensor consists of a ferrite core antenna, mounted in a plane perpendicular to the spin axis of the probe, and a linear low-noise preamplifier with a dynamic range of 80 dB. The antenna system responds to the magnetic field in the frequency range from about 10 Hz to 100 kHz. The system is protected from unexpectedly large signals. The voltage induced in the antenna by the spinning probe in the magnetic field in Jupiter is analyzed separately for the magnetic field measurement. The antenna and preamplifier are mounted on the equipment cover under the aft heat shield of the probe.

Two sensitive photodiodes are used as optical sensors to detect lightning flashes. Each is mounted behind a fisheye lens whose optical axis is perpendicular to the spin axis. The sensors are mounted 180° apart to cover a complete spherical field of view. Rapidly varying optical signals are used in coincidence with the radio frequency signals to provide a positive indication of lightning. Steady optical signals provide information on the brightness and opacity of the jovian cloud systems.

The output of the radio frequency sensor is fed in parallel into a time domain analyzer and into a frequency domain analyzer. The time domain measurements use the entire bandwidth of the radio frequency sensor with a sensitivity limited by the broadband noise. The output of the antenna is integrated to provide a signature of field related to time. The resulting waveform signature is then digitized at 4-μs intervals. The broadband noise is measured; the statistics of signal amplitudes, pulse durations, and pulse gap times are accumulated; and selected waveforms are measured according to a preset priority.

Helium Abundance Detector (HAD)

The helium abundance interferometer (fig. 111) will determine precisely the abundance of helium in the jovian atmosphere. Current knowledge suggests that the jovian atmosphere consists almost exclusively of hydrogen and helium, with the abundance of all other gases being less than 0.2 percent of the total. However, the relative proportions of the two major gases are not accurately known. So far, the most accurate information on the helium mixing ratio was obtained by the Voyager 1 experiments, which yielded a value of 11 $\pm$ 3 percent. The Galileo helium interferometer experiment will determine this value to within 0.1 percent. The principal investigator for the experiment is U. von Zahn of the University of Bonn, Federal Republic of Germany.

Due to their large masses and low exospheric temperatures, the giant planets Jupiter and Saturn are presumed to have bulk compositions rather similar to that of the primitive solar nebula from which they formed. We also expect that the observable solar atmospheric composition still resembles closely the composition of this primitive solar nebula. Although a reliable estimate of the solar helium mixing ratio remains elusive, the available

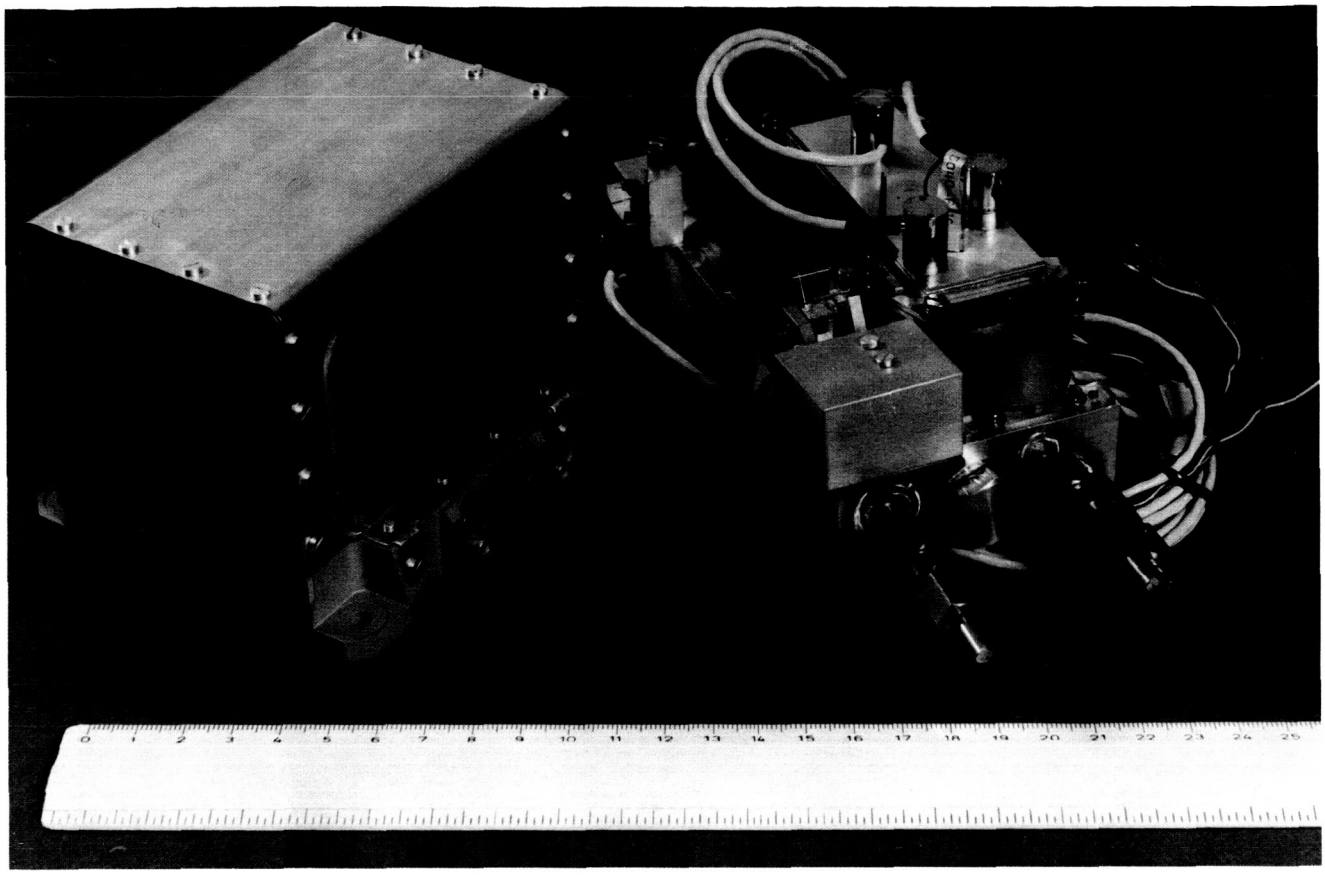

Figure 111. Engineering unit of the Jupiter helium interferometer.

observations indicate that the relative proportions of helium and hydrogen on the Sun closely match those on Jupiter. On the other hand, the latest results of Voyager 1 indicate that the helium mixing ratio in the atmosphere of Saturn amounts to only 6.8 ± 2.5 percent. This seeming deficiency of helium in the saturnian atmosphere may be due to gravitational settling of helium toward the core of Saturn. This mechanism is part of the aging process of the giant planets, which is predicted to proceed faster the less massive the planet. Hence, a precision measurement of the jovian helium abundance by the HAD experiment will be an important step toward a more quantitative understanding of the evolutionary history of the outer planets and the solar system as a whole. The measured helium abundance can also be regarded as a lower limit for the helium abundance in the primitive solar nebula.

Interest in the jovian helium abundance is further enhanced by expectations that it tells us the relative proportions of helium and hydrogen as produced in the cosmologic "Big Bang." Although after the Big Bang some hydrogen was certainly burned in stars to helium, many scientists claim that this in fact is a rather minute effect which has so far changed very little the mean cosmic abundance ratio of helium over hydrogen. If this premise holds true, a precise measurement of the jovian helium abundance in combination with a bit of theory about the evolution of the cosmic hydrogen budget would give us the most accurate value for the abundance ratio He/H_2 right after the Big Bang.

The HAD experiment will accurately measure the relative abundance of helium in the jovian atmosphere by a precision measurement of the refractive indices of the jovian atmosphere over the pressure range from 2.5 to 12 bars. From these data the mixing ratio of helium to hydrogen molecules and the relative abundance of helium can be calculated. Before measurements are made, the trace amounts of methane, ammonia, and water contained in the jovian atmosphere are removed from the jovian gas sample by chemical absorbers.

The instrument is a Jamin-Mascart two-arm, double-pathlength interferometer (fig. 112). As a light source the instrument uses an infrared emitting diode (1) which operates at a wavelength of about 900 nm. An interference filter (2) aids in producing near-monochromatic light. A Jamin plate (3) produces two parallel and coherent light beams (4 and 5). Four chambers 10 cm in length each house the jovian gas (6) and a reference gas (7), and

there is an array of nine photodetectors (8). Additional optical elements are the collimator (9), the inversion prism (10), and the objective (11).

To optimize the accuracy of the method, the refractive index of the jovian gas is measured relative to a reference gas mixture of known refractive index. The reference gas is made up of 28 percent argon and 72 percent neon. This mixture has approximately the same refractive index as one composed of 11 percent He and 89 percent H_2. The reference gas is carried in a small storage vessel within the instrument. During the descent into the jovian atmosphere the reference gas is expanded into its interferometer chambers (7) by means of a membrane valve which keeps the differential pressure between the jovian gas and the reference gas chambers near 50 mbar. This pressure difference is in addition measured with a dedicated sensor to within a few millibars to fully account for the influence of this pressure differential on the observed fringe motion.

The sensor is designed so that, for evacuated chambers, it produces a well-defined interference pattern of consecutive, equidistant bright and dark fringes at the detector array. This pattern does not change if both chambers are filled with gas mixtures having the same refractive index. However, any difference between the refractive indices of the jovian and the reference gas causes a continuous shifting of the pattern with increasing pressure, that is, as the probe penetrates to levels of higher pressure. The detector array allows us to measure the instantaneous position of the fringe pattern to within one-sixteenth of the fringe separation.

The total weight of the instrument is 1.4 kg.

Net Flux Radiometer (NFR)

The net flux radiometer (figs. 113 and 114) experiment of the Galileo probe mission is designed to measure the vertical profile of the difference between the upward and downward radiation (the net flux) in six spectral regions as the probe descends through the jovian atmosphere. The spectral regions were chosen so that the experimental results may contribute to our understanding of the

Figure 112. Schematic of the helium abundance interferometer optics.

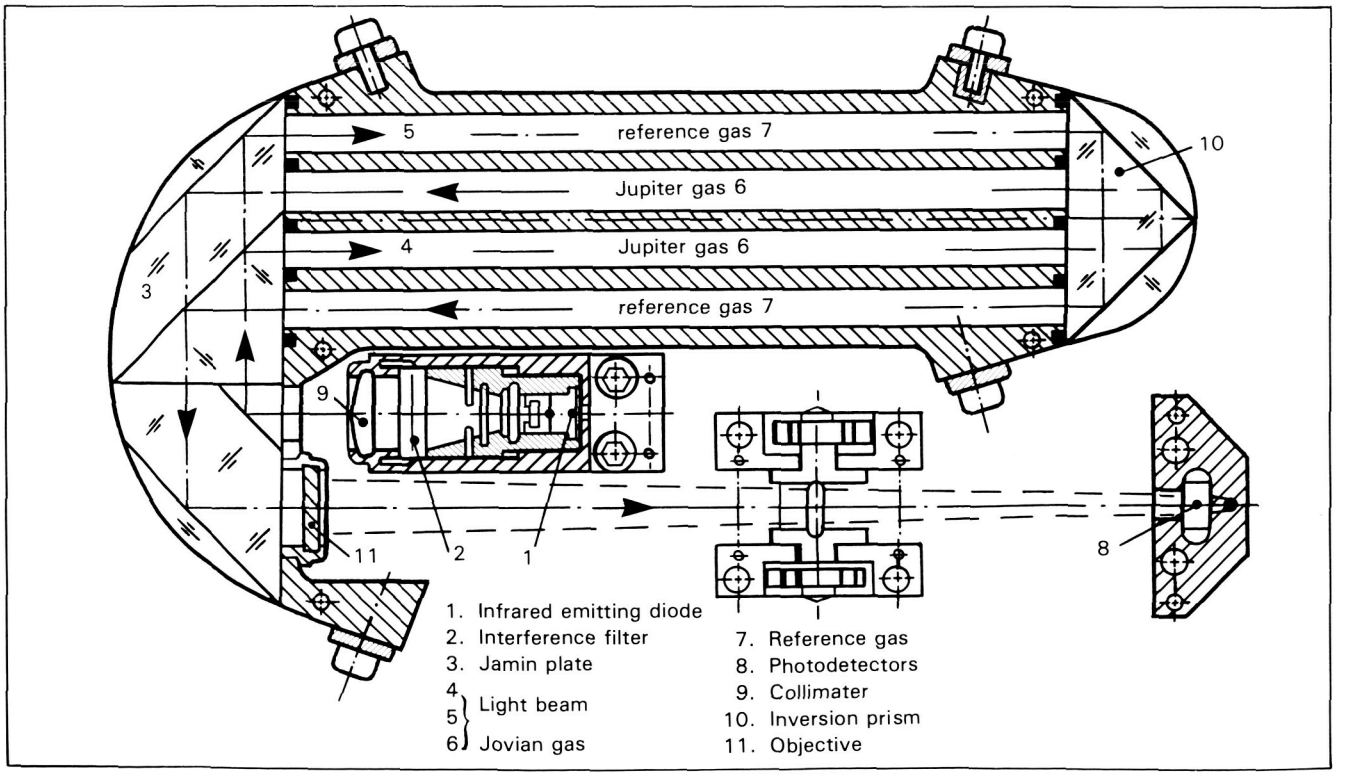

planet's radiation budget and thus to the atmospheric dynamics, to detection of cloud layers in Jupiter's atmosphere and evaluation of their opacity in the visible and thermal regions of the spectrum, and to estimating the abundance of several molecular species which are felt to be important contributors to the atmospheric opacity.

An important part of understanding the radiation balance in the jovian atmosphere is determining the depth of penetration and the location of the deposition of solar radiation. Atmospheric modeling, thus far, can only estimate these parameters. The NFR is the only probe instrument that has the potential for measuring this driving force for atmospheric dynamics.

The principal investigator is R. W. Boese of Ames Research Center.

The technique used to measure the net flux in a planet's atmosphere is to view the upward and downward hemispheres and form the difference $F_{net} = F\uparrow - F\downarrow$. Descending into a planet's atmosphere, the temperature, and therefore the upward-going atmospheric radiation, increase. If the atmosphere is optically thick, as is the case for Jupiter, there will also be an increase in the downward-going radiation. The combined effect is an overall decrease in the net flux. At the 10-bar pressure level, the net flux in Jupiter's atmosphere is predicted to be about 0.1 percent of either one-way flux.

If a planet's atmosphere is structured, for example, cloud layers, perturbations on a smoothly varying net flux profile will result. The magnitude of the perturbation in various spectral regions gives information on the opacity of the layer and therefore on its contribution to the overall radiation budget. The location of the perturbations, correlated with the temperature and pressure levels of the probe's atmospheric structure experiment, allows us to infer the species which caused the perturbation (condensation clouds, for example). Additionally, the shorter wavelength spectral bandpasses of the NFR experiment should yield valuable information on the effectiveness of cloud layers in preventing solar radiation from penetrating Jupiter's atmosphere.

Figure 113. Net flux radiometer (NFR).

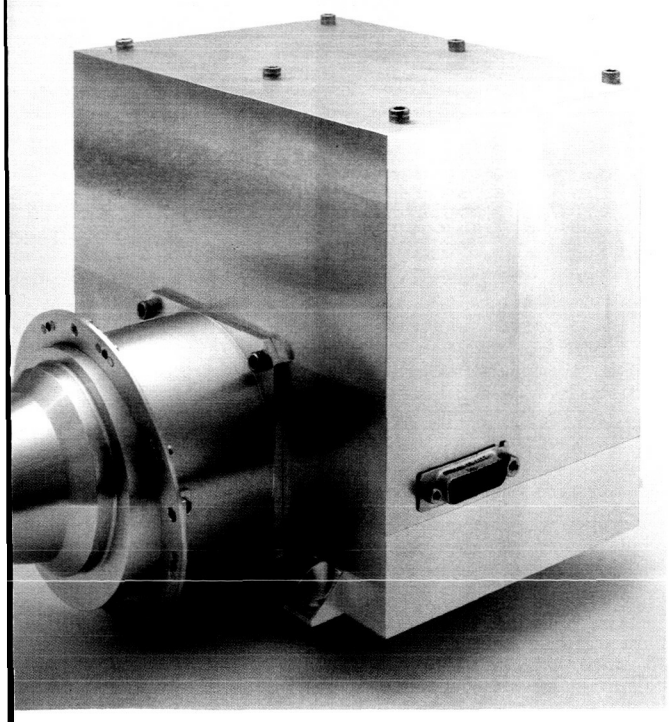

Figure 114. Diagram of net flux radiometer.

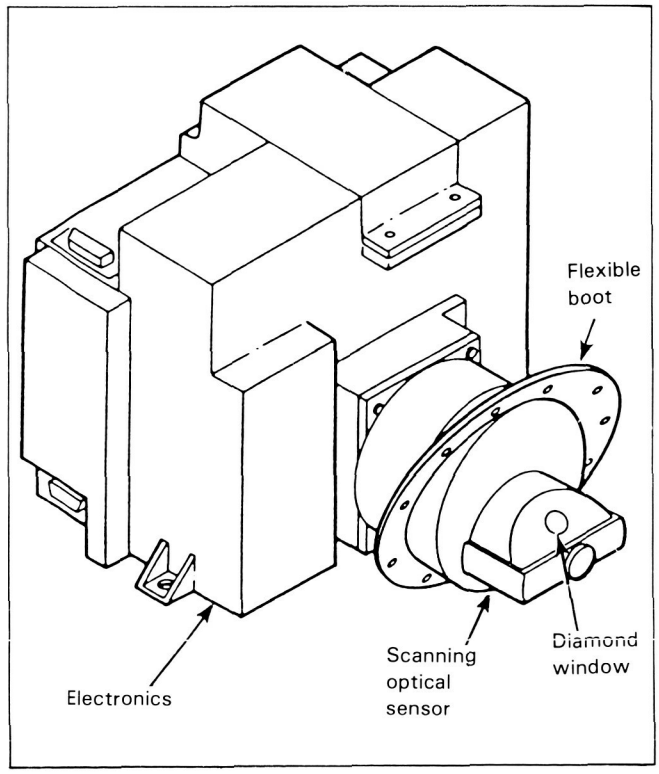

Molecular hydrogen is a major source of gaseous opacity in Jupiter's atmosphere. Methane, ammonia, and water vapor are major contributors to the opacity in a spectral region in which hydrogen is transparent. By measuring the net flux versus altitude in many wavelengths and observing the opacity in the hydrogen windows, it is possible to estimate the abundance of water vapor, methane, and ammonia.

The instrument consists of two units, the optical head and the electronics unit. The vented electronics unit is mounted to the probe instrument shelf. The optical head is fastened to the electronics unit and extends through the probe wall. A flange on the optical head mates with a pliable gasket and becomes part of the probe wall.

The outside of the optics housing is highly reflective to minimize heating or cooling of the optical head. The housing contains apertures for measuring the upward and downward radiation. The direction not being viewed is blocked by a "thermal shroud," which prevents direct atmospheric flow into the optical head and permits thermal control of the components inside of the housing.

Radiation from Jupiter's atmosphere enters the instrument through a diamond window which is sealed with an indium O-ring and is heated to prevent condensation during the probe's descent.

After passing through the diamond window the atmospheric radiation is reflected through a Fabry optical system. The radiation concentration ratio of the condensing cone is less than a factor of 2; its main functions are to shield the detector assembly from unwanted radiation and to permit location of the detector assembly in a relatively benign thermal location.

The detector assembly consists of six spectral bandpass filters, a six-element lithium tantalate detector array, and hybrid preamplifiers. The filter bandpasses are 3 to 500, 0.3 to 3.5, 4.5 to 5.5 , 14 to 35, and 0.7 to 3.5 μm.

The instrument is rotated on precision bearings to each of four "viewing" positions by means of a geared stepper motor. A resolver attached to the gears, along with an LED/detector system, indicates whether the desired optics positioning has been accomplished.

The electronics of the net flux radiometer accomplish the functions of converting and regulating spacecraft power to voltage levels required by the various electronic components. Each channel requires its own amplifiers and integrators. The electronics unit also provides the electronic interface with the probe data handling system. Instrument timing and logic is under microprocessor control. The microprocessor controls the instrument operating mode, packs and formats the data, and shifts the appropriate data to the spacecraft buffer when the NFR read envelope occurs. The data that is packed include the six channels of science data, measurement mode identification, gain select amplifiers status, status of position error, amplifier zero, and housekeeping data.

The NFR utilizes three operational modes: net flux, calibrate, and up flux. In the net flux mode the detector system alternately views upward and downward at a 2-Hz rate. The detector signals are integrated for eleven up-down cycles, digitized, and stored in the microprocessor for packing and transmittal to the probe data handling system.

In the calibrate mode the optics detector system is rotated between the 90° and 270° positions. The blackened inside of the optics housing at the 90° position is instrumented with two temperature sensors which have different, but overlapping, sensitivity ranges. A heated, blackened aluminum block is located at the 270° position. The temperature sensor of this heated blackbody is used with feedback circuitry to actively control the temperature at about 410 K.

In the up flux mode the optics detector rotation is between the 180° position (down view) and the 270° position (controlled temperature blackbody). The measurement will provide an additional, independent check of instrument performance.

The NFR integration period is 6 seconds long; 5.5 seconds are used for measurement and 0.5 second for digitization and setting up for the next measurement.

The 6-second integration period permits a vertical resolution of about 1.2 km at the beginning of the mission and about 0.25 km at the 10-bar level.

Appendix A. Management and Science Teams

Management of a NASA planetary exploration mission requires a complex organizational structure and associated sets of policies and procedures and performance, cost, and time schedules. Achievement of a mission's scientific goals and objectives involves the combined and dedicated efforts of many organizations and individuals. Time commitments for these efforts range from short term to major fractions of the duration of the program (in some cases, more than a decade). The Galileo mission is no exception. The following pages list the major organizations and key individuals associated with the mission. Since it is impossible to acknowledge every participant in a document such as this, we restricted the lists to participants who have long-lasting responsibilities or who have made significant contributions over a short time period. We include those organizations and individuals performing major management or engineering (spacecraft and mission) activities, as well as the scientific participants.

Project Organization

Galileo program management is the responsibility of the Earth and Planetary Division (G. A. Briggs, Chief) of the Office of Space Science and Applications (B. I. Edelson, Director) of the National Aeronautics and Space Administration (J. M. Beggs, Administrator).

Overall project management, orbiter systems development management, spacecraft assembly, experiment integration, probe integration, testing, and tracking and data acquisition management are the responsibility of the Jet Propulsion Laboratory (L. Allen, Jr., Director).

Probe project management and relay radio hardware (orbiter and probe) development are the responsibility of Ames Research Center (W. F. Ballhaus, Jr., Director). Two major U. S. contractors have combined to provide the probe system hardware. The Hughes Aircraft Company is responsible for probe systems design, development, fabrication, and test as well as probe experiment integration. The General Electric Company has general responsibility for probe thermal protection, providing necessary heat shields and structure and, in addition, separation mechanisms and parachute systems.

The "German-NASA," Deutsche Forschungs-und Versuchsanstalt für Luft-und Raumfahrt, e.V., of the Federal Republic of Germany's Federal Ministry for Research and Technology, has responsibility for providing the orbiter retropropulsion module and for cruise-phase tracking support. They have contracted for the module with Messerschmitt-Bölkow-Blohm GMbH (MBB).

The U. S. Department of Energy is responsible for providing the radioisotope thermoelectric generator used to power the orbiter. The General Electric Company is developing the generator under a Department of Energy contract.

Several other NASA centers and organizations have major responsibilities. The Lewis Research Center (A. Stofan, Director) is managing the development of the shuttle/Centaur stage for delivering Galileo from Earth orbit to a Jupiter trajectory. The Kennedy Space Center (R. G. Smith, Director) is responsible for shuttle launch tasks, whereas the Johnson Space Center (G. D. Griffin, Director) is responsible for shuttle launch operations control. Finally, the NASA Spaceflight Tracking and Data Network, Deep Space Network, and NASA Communications Network will combine under the direction of the Jet Propulsion Laboratory to provide the necessary navigation, tracking, and command and data handling operations.

Organizational Participation

In some cases, more than one person may have held a particular position. Where multiple names are listed, they are in chronological sequence.

NASA Earth and Planetary Sciences Division (Headquarters)
- Program Manager
  - R. McCullar
  - A. V. Diaz
  - H. Mannheimer
- Program Scientist
  - R. E. Murphy
  - G. A. Briggs
  - W. L. Quaide

Jet Propulsion Laboratory
- Project Manager, J. R. Casani
- Deputy Project Manager, A. E. Wolfe
- Project Scientist, T. V. Johnson
- Assistant Project Manager for Orbiter Systems, A. E. Wolfe
- Orbiter Development Manager
  - W. S. Shipley
  - R. F. Draper
  - S. G. Jones
- Science and Mission Design Manager
  - J. W. Moore
  - N. R. Haynes
  - W. J. O'Neil
- Science Manager, C. M. Yeates
- Orbiter Science Instruments Manager, W. G. Fawcett
- Mission Operations and Engineering Manager
  - B. G. Lee
  - N. E. Ausman, Jr.
- Flight Systems Integration Manager, R. J. Spehalski
- Assistant Flight Systems Integration Manager, M. J. Cork

Project Engineering Office Manager, B. G. Lee
Probe Spacecraft System Interface Manager, D. H. Kindt
Reliability and Quality Assurance, T. R. Gavin
Software Systems Manager
R. E. Loesch
P. M. Molko
Assistant Orbiter Development Manager, S. G. Jones
Financial Management, R. L. Schieffelin, Jr.
Administration, M. G. Hine

Ames Research Center
Assistant Project Manager for Probe Systems, J. Sperans
Deputy Probe Project Manager, N. Vojvodich
Probe Scientist, L. Colin
Probe Development Manager, J. J. Givens
Systems Engineer, R. W. Schaupp
Experiments Manager, E. Tischler
Operations and Interface Manager, B. Chin

Deutsche Forschungs-und Versuchsanstalt für Luft-und Raumfahrt
K.-O. Pfeiffer
W. Hagenest

German Space Operations Center
Mission Operations Manager, J. Kehr
Software Development Manager, P. Piotrowski

Department of Energy
J. J. Lombardo

Sandia National Laboratories
R. Gregory

Lewis Research Center
W. H. Robbins

Kennedy Space Center
M. Kinnan

Johnson Space Center
H. F. Battaglia

Deep Space Network
Manager, D. J. Mudgway

JPL Flight Projects Support Office
Mission Operations Support Manager, F. Miller

Scientists

Scientific participation in the Galileo mission can be organized in several categories: principal and co-investigators for experiment/instrument teams (eight on the orbiter and six on the probe), team leaders and members for "facility" instruments (imaging, radio science), interdisciplinary scientists,

project scientists, and probe project scientists. The principal participants in each category are given below. It is interesting to note that 115 scientists participate officially in Project Galileo (eliminating multiple-role participation).

Management of the project science activities is coordinated through the Galileo Project Science Group, which is composed of three working groups—Atmospheres, Magnetospheres, and Satellites—to help focus the mission scientific objectives and to hold the membership to a reasonable size (22). Official membership is given below.

Experiments and Investigators

Probe

Atmosphere Structure Instrument (ASI) Investigation

Principal Investigator
A. Seiff, Ames Research Center
Co-investigators
G. Schubert, University of California, Los Angeles
R. C. Blanchard, Langley Research Center
J. D. Mihalov, Ames Research Center
D. B. Kirk, Ames Research Center
S. C. Sommer, Ames Research Center
R. E. Young, Ames Research Center
Science coordinator
E. Tischler, Ames Research Center
Major contractors
Rosemount, Inc.
Tavis Corp.
Bell Aerospace Corp.
Martin Marietta Aerospace

Neutral Mass Spectrometer (NMS) Investigation

Principal Investigator
H. B. Niemann, Goddard Space Flight Center
Co-investigators
S. K. Atreya, University of Michigan
G. R. Carignan, University of Michigan
T. M. Donahue, University of Michigan
R. E. Hartle, Goddard Space Flight Center
N. W. Spencer, Goddard Space Flight Center
D. M. Hunten, University of Arizona
T. C. Owen, State University of New York
Science coordinator
A. Wilhelmi, Ames Research Center
Major contractors
General Electric/Valley Forge
University of Michigan

Helium Abundance Detector (HAD) Investigation

Principal Investigator
U. von Zahn, Bonn University, Federal Republic of Germany
Co-investigator
D. M. Hunten, University of Arizona
Science coordinator
E. Tischler, Ames Research Center
Major contractors
Carl Zeiss
Messerschmitt-Bölkow-Blohm GMbH

Nephelometer (NEP) Investigation

Principal Investigator
Boris Ragent, Ames Research Center
Co-investigators
P. Avrin, Martin Marietta Aerospace
J. E. Blamont, Service D'Aeronomie, CNES, France
J. B. Pollack, Ames Research Center
D. Colburn, Ames Research Center
G. Grams, Georgia Institute of Technology
Science coordinator
E. Tischler, Ames Research Center
Major contractor
Martin Marietta Aerospace

Net Flux Radiometer (NFR) Investigation

Principal Investigator
Robert W. Boese, Ames Research Center
Co-investigators
J. B. Pollack, Ames Research Center
L. A. Sromovsky, University of Wisconsin
P. M. Silvaggio, Craig Research and Technology
Science coordinator
R. Twarowski, Ames Research Center
Major contractor
Martin Marietta Aerospace

Lightning and Radio Emissions Detector and Energetic Particles (LRD/EPI) Investigation

Principal Investigator
L. J. Lanzerotti, Bell Laboratories/University of Florida
Co-investigators
LRD
G. Dehmel, Technische Universität Braunschweig
F. O. Gleim, Technische Universität Braunschweig
E. P. Krider, University of Arizona

K. Rinnert, Max-Planck-Institut für Aeronomie, Lindau
M. A. Uman, University of Florida

EPI

H. M. Fischer, IFKKI, Universität Kiel
G. W. Wibberenz, IFKKI, Universität Kiel
J. D. Mihalov, Ames Research Center

Science coordinator

A. Wilhelmi, Ames Research Center

Major contractor

Dornier Systems GMbH

Orbiter

Plasma Science (PLS) Investigation

Principal Investigator
L. A. Frank, University of Iowa

Co-investigators
F. V. Coroniti, University of California, Los Angeles
V. M. Vasyliunas, Max-Planck-Institut für Aeronomie

Instrument Manager
J. Lee, University of Iowa

Coordinators
Science, R. Wolff, J. Willett, Jet Propulsion Laboratory
Engineering, U. Amundson, R. Gibbs, Jet Propulsion Laboratory

Major contractor/supplier
Ball Aerospace Systems Division

Plasma Wave (PWS) Investigations

Principal Investigator
D. Gurnett, University of Iowa

Co-investigators
S. Shawhan, University of Iowa
C. Kennel, University of California, Los Angeles
F. Scarf, TRW
R. Gendrin, CNET

Instrument Manager
R. Shaw, University of Iowa

Coordinators
Science, R. Wolff, J. Willett, Jet Propulsion Laboratory
Engineering, C. Coppock, Jet Propulsion Laboratory

Major contractors/suppliers
CNET
Able Engineering
Circuit Technology, Inc.

Magnetometer (MAG) Investigation

Principal Investigator
M. G. Kivelson, University of California, Los Angeles

Co-investigators
P. J. Coleman, University of California, Los Angeles

C. F. Kennel, University of California, Los Angeles
R. L. McPherron, University of California, Los Angeles
C. T. Russell, University of California, Los Angeles

Instrument Manager

R. Snare, University of California, Los Angeles

Coordinators

Science, D. Clay, Jet Propulsion Laboratory
Engineering, U. Amundson, J. Farrar, Jet Propulsion Laboratory

Major contractor

Westinghouse

Dust Detector (DDS) Investigation

Principal Investigator

E. Grün, Max-Planck-Institut für Kernphysik

Co-investigators

H. Fechtig, Max-Planck-Institut für Kernphysik
J. Kissel, Max-Planck-Institut für Kernphysik
G. Morfill, Max-Planck-Institut für Kernphysik
M. S. Hanner, Jet Propulsion Laboratory
B. A. Lindblad, Lund Observatory, Sweden
H. A. Zook, Johnson Space Center

Instrument Manager

D. Linkert, Max-Planck-Institut für Kernphysik

Coordinators

Science, M. Hanner, Jet Propulsion Laboratory
Engineering, C. Coppock, Jet Propulsion Laboratory

Major contractor

Messerschmitt-Bölkow-Blohm GMbH

Energetic Particle Detector (EPD) Investigation

Principal Investigator

D. J. Williams, Applied Physics Laboratory, The Johns Hopkins University

Co-investigators

S. M. Krimigis, Applied Physics Laboratory, The Johns Hopkins University
R. W. McEntire, Applied Physics Laboratory, The Johns Hopkins University
E. C. Roelof, Applied Physics Laboratory, The Johns Hopkins University
T. P. Armstrong, University of Kansas
L. J. Lanzerotti, Bell Laboratories
J. G. Roederer, University of Alaska
W. Studeman, Max-Planck-Institut für Aeronomie
B. Wilkin, Max-Planck-Institut für Aeronomie
T. A. Fritz, Los Alamos National Observatory

Instrument Manager

B. Tossman, Applied Physics Laboratory, The Johns Hopkins University

Instrument Coordinators

Science, J. Willett, Jet Propulsion Laboratory

Engineering, R. Parrish, R. Gibbs, Jet Propulsion Laboratory
Major contractors/suppliers
Max-Planck-Institut für Aeronomie
Poly-Scientific
Schaeffer Magnetics

Near-Infrared Mapping Spectrometer (NIMS) Investigation

Principal Investigator
R. W. Carlson, Jet Propulsion Laboratory
Co-investigators
G. E. Danielson, California Institute of Technology
Th. Encrenaz, Observatoire de Paris
F. P. Fanale, University of Hawaii
T. B. McCord, University of Hawaii
T. V. Johnson, Jet Propulsion Laboratory
D. L. Matson, Jet Propulsion Laboratory
J. S. Lewis, University of Arizona
H. Masursky, U.S. Geological Survey
L. A. Soderblom, U.S. Geological Survey
H. H. Kieffer, U. S. Geological Survey
F. W. Taylor, Oxford University
Instrument Manager
I. Aptaker, Jet Propulsion Laboratory
Instrument Coordinators
Science, W. Smythe and P. Weissman, Jet Propulsion Laboratory
Engineering, W. Sleigh, Jet Propulsion Laboratory
Major contractors/suppliers
Cincinnati Electronics
Perkin Elmer
Santa Barbara Research Center

Photopolarimeter-Radiometer (PPR) Investigation

Principal Investigator
J. E. Hansen, Goddard Institute for Space Studies
Co-investigators
P. H. Stone, Massachusetts Institute of Technology
A. A. Lacis, Goddard Institute for Space Studies
L. D. Travis, Goddard Institute for Space Studies
W.-C. Wang, Goddard Institute for Space Studies
G. Orton, Jet Propulsion Laboratory
Y.-L. Yung, California Institute of Technology
Instrument Manager
A. Peterson, Goddard Space Flight Center
Instrument Coordinators
Science, N. Divine, T. Martin, Jet Propulsion Laboratory
Engineering, D. Griffith, J. Farrar, Jet Propulsion Laboratory
Major contractor
Santa Barbara Research Center

Ultraviolet Spectrometer (UVS) Investigation

Principal Investigator
C. E. Hord, University of Colorado
Co-investigators
C. A. Barth, University of Colorado
G. E. Thomas, University of Colorado
A. I. Stewart, University of Colorado
A. L. Lane, Jet Propulsion Laboratory
Instrument Manager
G. McNutt, University of Colorado
Instrument Coordinators
Science, J. Ajello, Jet Propulsion Laboratory
Engineering, D. Griffith, J. Farrar, Jet Propulsion Laboratory

Solid-State Imaging (SSI) Investigation

Team Leader
M. J. S. Belton, National Optical Astronomy Observatories
Team members
C. D. Anger, University of Calgary
M. H. Carr, U. S. Geological Survey
C. R. Chapman, Planetary Science Institute
R. Greenberg, Planetary Science Institute
M. E. Davis, Rand Corporation
R. Greeley, Arizona State University
J. W. Head, Brown University
G. Neukum, Deutsche Forschungs-und Versuchsanstalt für Luft-und Raumfahrt, e.V.
C. B. Pilcher, University of Hawaii
J. Veverka, Cornell University
Instrument Manager
M. Clary, Jet Propulsion Laboratory
Instrument Coordinators
Science, K. Klaasen, Jet Propulsion Laboratory
Engineering, J. R. Locke, Jet Propulsion Laboratory
Major contractor
Texas Instruments

Radio Science

Celestial Mechanics and Relativity
Team Leader
J. D. Anderson, Jet Propulsion Laboratory
Team member
F. Estabrook, Jet Propulsion Laboratory
Science coordinator
J. Brenkle, Jet Propulsion Laboratory

Galileo Project Science Group

Project Scientist, Chairman
Torrence Johnson, Jet Propulsion Laboratory
Project Scientist
Lawrence Colin, Ames Research Center
Atmospheres Working Group Chairman
Donald Hunten, University of Arizona
Satellites Working Group Chairman
Fraser Fanale, University of Hawaii
Magnetospheres Working Group Chairman
Louis Frank, University of Iowa
ASI Principal Investigator
Alvin Seiff, Ames Research Center
NMS Principal Investigator
Hasso Neimann, Goddard Space Flight Center
HAD Principal Investigator
Ulf von Zahn, University of Bonn
NEP Principal Investigator
Boris Ragent, Ames Research Center
NFR Principal Investigator
Robert Boese, Ames Research Center
LRD Principal Investigator
Louis Lanzerotti, Bell Labs
PLS Principal Investigator
Louis Frank, University of Iowa
PWS Principal Investigator
Donald Gurnett, University of Iowa
MAG Principal Investigator
Margaret Kivelson, University of California, Los Angeles
DDS Principal Investigator
Eberhard Grün, Max-Planck-Institut für Kernphysik
EPD Principal Investigator
Donald Williams, Applied Physics Laboratory, The Johns Hopkins University
NIMS Principal Investigator
Robert Carlson, Jet Propulsion Laboratory
PPR Principal Investigator
James Hansen, Goddard Institute for Space Studies
UVS Principal Investigator
Charles Hord, University of Colorado
SSI Team Leader
Michael Belton, Kitt Peak National Observatory
Celestial Mechanics Team Leader
John Anderson, Jet Propulsion Laboratory
Radio Propagation Team Leader
H. Taylor Howard, Stanford University

Radio Propagation Team
Team Leaders
H. T. Howard, Stanford University
V. Eshleman, Stanford University
Team members
A. Kliore, Jet Propulsion Laboratory
G. Lindal, Jet Propulsion Laboratory
R. Woo, Jet Propulsion Laboratory
Science coordinator
J. Briedenthal, Jet Propulsion Laboratory

Interdisciplinary Investigators

Formation and Evolution of the Galilean Satellites
Fraser P. Fanale, University of Hawaii
Jovian Atmospheric Dynamics
Peter Gierasch, Cornell University
Structure and Aeronomy of the Atmospheres of Jupiter and its Satellites
Donald M. Hunten, University of Arizona
Jovian Atmospheric Dynamics
Andrew P. Ingersoll, California Institute of Technology
Geology of the Galilean Satellites
Harold Masursky, U. S. Geological Survey
Ground-Truth Analysis of Radiative Transfer in the Atmosphere of Jupiter
Glenn S. Orton, Jet Propulsion Laboratory
Composition of the Jovian Atmosphere
Tobias Owen, State University of New York
Thermal and Dynamical Properties of the Jovian Atmosphere and Evolution of the Jovian System
James B. Pollack, Ames Research Center
Jupiter Magnetosphere and Satellites—Magnetosphere Interactions
Christopher T. Russell, University of California, Los Angeles
Organic Chemistry of the Jovian Atmosphere
Carl Sagan, Cornell University
Wave Particle Interaction Phenomena at Jupiter
Frederick L. Scarf, TRW
Physical Processes in the Atmosphere of Jupiter and on the Surfaces of the Galilean Satellites
Gerald Schubert, University of California, Los Angeles
Physical Properties of the Galilean Satellites
David Morrison, University of Hawaii
Investigation of the Jovian Upper Atmosphere and of Satellite Atmospheres
Michael McElroy, Harvard University
Magnetospheric Dynamics
James Van Allen, University of Iowa

Appendix B.
Acronyms and Abbreviations

AACS	attitude and articulation control system (orbiter)
ACE	attitude control electronics (AACS)
AMU	atomic mass unit
ASI	atmospheric structure instrument (probe)
AU	astronomical unit (150 million km)
BPM	broken plane maneuver
BS	bow shock
C_3	minimum launch energy
CCD	charge-coupled device (solid-state imaging instrument)
CDS	command and data system (orbiter)
CMS	composition measuring system (EPD)
CRC	critical controller (orbiter AACS)
DCP	data and command processor (probe)
DDS	dust detector (orbiter spun)
DEUCE	despun electronics (orbiter AACS)
DMA	direct memory access
DMS	data memory subsystem (orbiter)
E	encounter; entry
EOM	end of mission
EPD	energetic particles detector (orbiter spun)
ET	external tank
FOV	field of view
GPHS	general purpose heat source
HAD	helium abundance detector (probe)
HCD	hardware command decoder (orbiter AACS)
HGA	high-gain antenna (orbiter spun)
HLM	high-level module (CDS)
Hz	hertz (cycles per second)
I/O	input/output
IM	injection module
IPIU	instrument power interface unit (probe)
IR	infrared
IUE	International Ultraviolet Explorer
IUS	inertial upper stage
JOI	Jupiter orbit insertion
K	kelvin
km	kilometer
LBA	linear boom actuator (orbiter)
LEMMS	low energy magnetospheric measuring system (EPD)
LGA	low-gain antenna (orbiter)
LLM	low-level module (CDS)
LRD/EPI	lightning and energetic particles (probe)
MAG	magnetometer (orbiter spun)
MDS	modulation/demodulation subsystem (orbiter)
MES	main engine start

MLI	multilayer insulation
MP	magnetopause
N	newton
NEP	nephelometer (probe)
NFR	net flux radiometer (probe)
NIMS	near-infrared mapping spectrometer (orbiter despun)
NMS	neutral mass spectrometer (probe)
ODM	orbit deflection maneuver
OTM	orbit trim maneuver
PCU	pyrotechnic control unit (probe)
PDE	propulsion drive electronics (orbiter AACS)
PJR	perijove raise maneuver
PLS	plasma detector (orbiter spun)
PPR	photopolarimeter-radiometer (orbiter despun)
PWS	plasma wave spectrometer (orbiter spun)
R_E	Earth radius
R_J	Jupiter radius
RAM	random access memory
RF	radio frequency
RFS	radio frequency subsystem (orbiter)
RHU	radiosotope heater unit (probe)
ROM	read-only memory
RPM	retropropulsion module (orbiter spun)
RRA	relay radio antenna (orbiter despun)
RRH	relay radio hardware (orbiter despun)
RS	radio science (orbiter spun)
RTG	radioisotope thermoelectric generator (orbiter spun)
RTI	real-time interrupt
rpm	revolutions per minute
SAS	scan actuator assembly
SBA	spin bearing assembly (orbiter)
SPIU	system power interface unit (probe)
SRM	solid rocket motor
SS	star scanner (orbiter spun)
SSI	solid-state imaging (orbiter despun)
STS	Space Transportation System
T	Tesla; time
TCM	trajectory correction maneuver
TWTA	traveling wave tube amplifiers (orbiter)
UVS	ultraviolet spectrometer (orbiter despun)
VEGA	Earth-Venus-Earth gravity assists
Δ-V	velocity change
Δ-VEGA	Earth-deep space ΔV-Earth gravity assists

Appendix C.
Characteristics of Jupiter and the Jovian System

Characteristics of Jupiter, Earth, and Moon

	Jupiter	Earth	Moon
Reciprocal mass[1]	1,047.355	328,900	27,069,000
Mass[2] (Earth = 1)	317.893	1.0000	0.01230
Mass[2] (kg)	1.900×10^{27}	5.975×10^{24}	7.350×10^{22}
Equatorial radius (Earth = 1)	11.27	1.00	0.2725
Equatorial radius (km)	71,398	6,378	1,738
Ellipticity[3]	0.0637	0.0034	0.002
Mean density (g/cm^3)	1.314	5.52	3.34
Equatorial surface gravity (m/s^2)	22.88	9.78	1.62
Equatorial escape velocity (km/s)	59.5	11.2	2.38
Sidereal rotation period	9.841 hours[4,5]	23.9345 hours	27.322 days
Inclination of equator to orbit	3°.08	23°.44	6°.68

Characteristics of Planetary Orbits

	Sidereal period				Synodic period	Mean orbital velocity	Eccentricity	Inclination to the ecliptic
	(AU)	(10^6 km)	(years)	(days)	(days)	(km/s)		(degrees)
Earth	1.000000	149.6	1.00004	365.256	---	29.79	0.0167	---
Jupiter	5.202561	778.3	11.8623	4332.71	398.88	13.06	0.0485	1.30

Satellites of Jupiter

Number	Name	Discoverer	Year of discovery	Mean distance from Jupiter (km)	Sidereal period (days)	Orbital inclination (degrees)	Orbital eccentricity	Radius (km)	Mass (kg)	Mean density (g/cm)
(J16)	(Metis)	S. Synnott	1979–1980	127,960	0.295	(0)	(0)	(20)	?	?
(J15)	(Adrastea)	D. Jewitt, E. Danielson	1979	128,980	0.298	(0)	(0)	12 10 8	?	?
JV	Amalthea	E. Barnard	1892	181,300	0.498	0.45	0.003	135 85 73	?	?
JXIV	Thebe	S. Synnott	1979–1980	221,900	0.675	(0.9)	0.013	55 ? 45	?	?
JI	Io	S. Marius, Galileo	1610	421,600	1.769	0.04	0.004	1815	8.916×10^{22}	3.55
JII	Europa	S. Marius, Galileo	1610	670,900	3.551	0.47	0.009	1569	4.873×10^{22}	3.04
JIII	Ganymede	S. Marius, Galileo	1610	1,070,000	7.155	0.21	0.002	2631	1.490×10^{23}	1.93
JIV	Callisto	S. Marius, Galileo	1610	1,880,000	16.689	0.51	0.007	2400	1.064×10^{23}	1.81
JXIII	Leda	C. Kowal	1974	11,094,000	238.7	26.1	0.148	(5)	?	?
JVI	Himalia	C. D. Perrine	1904–1905	11,480,000	250.6	27.6	0.158	(90)	?	?
JX	Lysithea	S. B. Nicholson	1938	11,720,000	259.2	29.0	0.107	(10)	?	?
JVII	Elara	C. D. Perrine	1904–1905	11,737,000	259.7	24.8	0.207	(40)	?	?
JXII	Ananke	S. B. Nicholson	1951	21,200,000	631	147	0.17	(10)	?	?
JXI	Carme	S. B. Nicholson	1938	22,600,000	692	164	0.21	(15)	?	?
JVIII	Pasiphae	P. Mellote	1908	23,500,000	735	145	0.38	(20)	?	?
JIX	Sinope	S. B. Nicholson	1914	23,700,000	758	153	0.28	(15)	?	?

Source: *The New Solar System,* Kelly Beatty, ed., and *Sky and Telescope*, Nov. 83, p. 405.

Parenthetic names and satellite numbers await approval by the International Astronomical Union. Parenthetic values are uncertain by at least 10 percent. Inclinations and eccentricities are the total values; "forced" components are important for the eccentricities of the satellites Io and Europa. Inclinations are with respect to planetary equators for inner satellites and to orbital planes for outer ones. Compound radii are the values for the "best-fit" triaxial ellipsoid.

[1]The mass of the Sun divided by the mass of the planet (including its atmosphere and satellites). [2]Satellite masses not included. [3]The ellipticity is $(R_e - R_p)$. R_e and R_p are the planet's equatorial and polar radii. [4]Jupiter's internal (System III) rotation period is 9.925 hours. [5]At equator.

References

D'Amario, L. A., and D. V. Byrnes. Interplanetary Trajectory Design for the Galileo Mission. Proceedings of the AIAA 21st Aerospace Sciences Meeting, January 10-13, 1983, Reno, Nevada.

Diehl, R. E., D. I. Kaplan, and P. A. Penzo. Satellite Tour Design for the Galileo Mission. Proceedings of the AIAA 21st Aerospace Sciences Meeting, January 10-13, 1983, Reno, Nevada.

Givens, J. J., L. J. Nolte, and L. R. Pochettino. Galileo Atmospheric Entry Probe System: Design, Development and Test. Proceedings of the AIAA 21st Aerospace Sciences Meeting, January 10-13, 1983, Reno, Nevada.

Johnson, T. V., and C. M. Yeates. Return to Jupiter: Project Galileo, *Sky and Telescope*, vol. 66, no. 2, August 1983, pp. 99-106.

Landano, M. R., and C. P. Jones. The Galileo Spacecraft System Design. Proceedings of the AIAA 21st Aerospace Sciences Meeting, January 10-13, 1983, Reno, Nevada.

O'Neil, W. J., and R. T. Mitchell. Galileo Mission Overview. Proceedings of the AIAA 21st Aerospace Sciences Meeting, January 10-13, 1983, Reno, Nevada.

Yeates, C. M. and T. C. Clarke. Galileo: The Mission to Jupiter. *Astronomy*, February 1982, pp. 6-22.